



Swansea University  
Prifysgol Abertawe



## Swansea University E-Theses

---

# An examination of the corrosion resistance of zinc-magnesium and zinc-aluminium-magnesium coated steels.

Weirman, Chris

### How to cite:

---

Weirman, Chris (2011) *An examination of the corrosion resistance of zinc-magnesium and zinc-aluminium-magnesium coated steels..* thesis, Swansea University.

<http://cronfa.swan.ac.uk/Record/cronfa43111>

### Use policy:

---

This item is brought to you by Swansea University. Any person downloading material is agreeing to abide by the terms of the repository licence: copies of full text items may be used or reproduced in any format or medium, without prior permission for personal research or study, educational or non-commercial purposes only. The copyright for any work remains with the original author unless otherwise specified. The full-text must not be sold in any format or medium without the formal permission of the copyright holder. Permission for multiple reproductions should be obtained from the original author.

Authors are personally responsible for adhering to copyright and publisher restrictions when uploading content to the repository.

Please link to the metadata record in the Swansea University repository, Cronfa (link given in the citation reference above.)

<http://www.swansea.ac.uk/library/researchsupport/ris-support/>



**Swansea University**  
**Prifysgol Abertawe**

An examination of the corrosion resistance  
of Zinc-Magnesium and Zinc-Aluminium-  
Magnesium coated steels

**Chris Weirman**

EPSRC Engineering Doctorate Centre for Steel Technology

*Submitted for the degree of Engineering Doctorate (EngD)*

**2011**

ProQuest Number: 10821503

All rights reserved

INFORMATION TO ALL USERS

The quality of this reproduction is dependent upon the quality of the copy submitted.

In the unlikely event that the author did not send a complete manuscript and there are missing pages, these will be noted. Also, if material had to be removed, a note will indicate the deletion.



ProQuest 10821503

Published by ProQuest LLC (2018). Copyright of the Dissertation is held by the Author.

All rights reserved.

This work is protected against unauthorized copying under Title 17, United States Code  
Microform Edition © ProQuest LLC.

ProQuest LLC.  
789 East Eisenhower Parkway  
P.O. Box 1346  
Ann Arbor, MI 48106 – 1346



## ACKNOWLEDGEMENTS

It has been many years since I left the world of academia after completing my first degree in Chemistry. Since then I have matured and changed, experienced much of life's ups and thankfully not too many downs, the grey hairs are surely winning the battle, but I've always had the desire to improve myself and get the change in title from Mr. to Dr., though I must confess this is so that, should the opportunity arise, I can say yes to the question, "Is there a Doctor on board?", I think I may have watched 'Airplane' too many times.

Leaving the world of work and returning to fulfil that desire was a bit of a gamble to say the least. The daunting prospect of several Masters level examinations to someone who hasn't sat an examination for 11 years just added fear to trepidation, but all went surprisingly smoothly those early days.

I had some low points in the course of this study, namely the desert that was my sample repertoire during year 2 which, through the support of the people I'm leading up to thanking, I've hopefully pulled this around.

So big thank-yous go out to Bryan Jones or TBJ for short who has always been in my corner, Tony Jones, who was there to help when things went off track, Dr. James Sullivan, Jim, for tireless support and SVET diagnoses.

My parents deserve special mention, my Mum, always there for me in many ways, my Dad for his understanding and faith in me, my new In-laws for help in solving my IT issues in writing this, and last but definitely not least my new wife, Mari, my soul mate and sounding board with whom, together, we've got a great future.

Many other people have helped me, supported me, and entertained me during the four years on the scheme. My fellow EngDocs can't go without mention, our intake year was one of the best.

This is Cweirman signing off.

## **Abstract**

This project has investigated the development of the optimum combination levels and processing conditions for zinc and magnesium coatings deposited by a Physical Vapour Deposition (PVD) process under investigation by Tata Steel Europe Ltd.

Temperatures in the range of 100°C to 350°C and times ranges of 2-10 hours and 30 – 300 seconds were investigated and the coatings characterised by optical microscopy, scanning electron microscopy (SEM) with energy dispersive x-ray analysis, (EDX), also known as electron probe microanalysis (EPMA), glow discharge optical emission spectrophotometry (GDOES) and x-ray diffraction (XRD), and examined for corrosion resistance using the scanning vibrating electrode technique (SVET) and accelerated weathering cabinet tests; cohesion and salt spray.

The work has shown that the initial zinc magnesium coatings prepared via the developing Tata Steel Europe PVD process did not perform as well as the current and developing hot dipped zinc-aluminium or zinc-aluminium-magnesium alloys in continuously submerged sodium chloride solutions.

In support of this work, and to contrast the coatings prepared via the PVD process the project investigated changes to the coating composition and substrate gauge of a range of conventionally prepared hot dip galvanised samples. This part of the project has looked at variations in the alloying additions to zinc using magnesium in the range of 0-2wt% and aluminium in the range of 0-5wt%.

Changing coating composition and/or changing processing conditions produced coatings with dendrites per mm<sup>2</sup> (dendrite number) ranging from 350 to 7600. Primary zinc% has also been found to vary in the range of 29% to 95% and the relative corrosion rates have been found to vary between 49% and 477% that of benchmark samples of conventional hot-dip galvanised steel of 275g/m<sup>2</sup>.

Conventional and more recently developed coatings have been studied in mildly alkaline environments by immersion mass loss and SVET testing, as part of a study to investigate if Tata Steel Europe can substitute a lower coating weight, newly developed MagiZinc metallic coating into construction industry in the UK. It was found that both conventional and the new alloy chemistries were seen to have sufficient coating weight after the 28 days, the total cement curing time, to allow the substitution.



# Contents

Introduction and Literature Review .....	1
Introduction.....	2
1.0 Literature Review.....	4
1.1 The Steel Industry in Wales .....	4
1.1.1 Steel solutions for construction.....	4
1.1.2 Metallic coated steels.....	6
1.1.3 Passivation systems.....	7
1.1.4 Organically coated steels .....	8
1.2 Corrosion.....	10
1.2.1 Coating requirements? Why coat? .....	10
1.2.2 What is corrosion? .....	11
1.2.3 Corrosion mechanisms for Iron.....	11
1.2.4 Galvanic corrosion .....	13
1.2.5 Galvanic series .....	14
1.2.6 Pourbaix diagrams .....	15
1.2.7 Evans diagrams and Tafel lines .....	17
1.2.8 Evans diagrams, Polarisation, and the rate of corrosion .....	18
1.2.9 Mechanical effects on corrosion .....	20
1.2.10 Cut edge corrosion .....	21
1.2.11 Surface or uniform corrosion .....	22
1.2.12 Pitting.....	22

1.2.13	Crevice corrosion.....	23
1.2.14	Differential aeration.....	24
1.3	Metallic coatings.....	25
1.3.1	Hot dip galvanising.....	25
1.3.1.1	Production of metallic coated steels.....	26
1.3.1.2	Alloying chemistries used in metallic coatings.....	26
1.3.1.3	Galvannealing.....	31
1.3.1.4	Hot dip coating drawbacks.....	32
1.3.2	Hot-dip coating solidification.....	33
1.3.3	Processing conditions.....	36
1.3.3.1	Substrate gauge.....	37
1.3.4	Physical vapour deposition.....	37
1.3.4.1	Industrialised processes.....	40
1.3.4.2	PVD Process Steps.....	41
1.3.4.3	Evaporation and EML-PVD.....	41
1.3.4.4	Possible benefits.....	44
1.3.4.5	Possible problems.....	44
1.3.4.6	Channelling the vapour.....	45
1.3.4.7	Condensation.....	46
1.3.4.8	Surface preparation.....	47
1.3.4.9	Surface roughness.....	48
1.3.4.10	Surface temperature.....	48
1.3.4.11	Zinc-Magnesium.....	49

1.3.4.11.1	The corrosion chemistry of Zinc-Magnesium .....	50
1.4	Areas of research.....	52
2.0	Introduction.....	55
2.1	Scanning Vibrating Electrode Technique .....	55
2.1.1	Equipment Set-up.....	56
2.1.2	Experimental Theory.....	57
2.1.3	Theoretical assumptions and limitations.....	60
2.1.4	Equipment Calibration .....	61
2.1.5	Sample Preparation .....	64
2.1.5.1	Height Scanning and Planar Interpolated modes .....	65
2.1.6	Interpretation of data.....	66
2.1.6.1	Mass loss data .....	68
2.1.6.2	Residual anode analysis .....	69
2.2	Cabinet testing .....	71
2.3	GDOES .....	71
2.3.1	Interpretation of results .....	72
2.4	Depth profiling.....	72
2.4.1	Preparation of depth profiling samples .....	76
2.4.2	Original method .....	77
2.4.3	Improvements in the methodology .....	77
2.4.4	Etchant development.....	79
2.4.5	Image analysis & data processing .....	80
2.4.6	Measurement of primary zinc %.....	82

2.4.7	Average number of dendrites per mm <sup>2</sup> .....	83
2.4.8	Average dendrite size.....	84
2.5	Hot Dip Simulator.....	84
2.6	Immersed Mass Loss.....	87
3.0	Introduction.....	90
3.1	Samples and sample quality.....	90
3.2	Metallography of reactive samples .....	93
3.3	Microstructural investigation .....	94
3.4	SEM & EPMA .....	95
3.5	Diffusion Annealing Investigation.....	97
3.5.1	Microstructural changes.....	100
3.6	X-ray Diffraction .....	103
3.7	Coating Hardness .....	107
3.8	Erichsen dome testing .....	107
3.9	GDOES Analysis .....	110
3.10	Corrosion testing.....	114
3.10.1	Surface Corrosion .....	115
3.10.2	Cut-edge corrosion.....	119
3.11	Cabinet Testing .....	121
3.12	Discussion and conclusions .....	123
4.0	Introduction.....	126
4.1	Experimental .....	127
4.1.1	Materials .....	127

4.1.2	Metallographic investigation.....	129
4.1.3	Corrosion testing of Zn-4.8wt% Al and HDG coated steels .....	129
4.1.4	Weight loss.....	129
4.1.5	Scanning Vibrating Electrode Technique (SVET) investigation into cut edge corrosion behaviour .....	129
4.1.5.1	SVET sample preparation .....	129
4.2	Results and discussion .....	130
4.2.1	Solidification of the Zn-4.8wt% Al alloys. ....	130
4.2.1.1	Effect of steel gauge on the microstructure of Zn-4.8wt% Al alloy coatings. ....	133
4.2.1.2	Microstructure of HDG coated materials.....	137
4.2.1.3	Cut edge corrosion of Zn-4.8wt% Al alloy and HDG coatings on various gauges of steel.....	138
4.3	Conclusions.....	149
5.0	Introduction.....	152
5.1	Comparison table .....	154
5.2	Dendrite analysis.....	155
5.3	Growth curve analysis.....	158
5.4	Corrosion performance .....	159
5.5	Comparison 1 – Low alloying additions .....	163
5.5.1	Microstructural characterisation .....	164
5.5.2	Corrosion performance .....	165
5.5.3	Comparison 1 results.....	167
5.6	Comparison 2 – Low magnesium MagiZinc type coatings.....	167

5.6.1	Microstructural characterisation .....	168
5.6.2	Corrosion performance .....	170
5.6.3	Comparison 2 Results .....	174
5.7	Comparison 3 – High alloying additions .....	175
5.7.1	Microstructural characterisation .....	175
5.7.2	Corrosion Performance .....	176
5.8	Comparison 7 – Fast Cooled Sample Comparison .....	179
5.8.1	Corrosion performance .....	182
5.9	Comparison 8 – Slow Cooled Samples.....	185
5.9.1	Corrosion performance .....	187
5.10	Overall Comparisons and Relationships – Comparisons 9-12.....	188
5.11	Results and discussion .....	191
6.0	Introduction.....	194
6.1	Experimental Investigation .....	197
6.2	Sample Matrix.....	199
6.3	Passivation Systems .....	199
6.4	Corrosion Test Results.....	200
6.5	Results and Discussion .....	212
7.0	Discussion.....	214
8.0	Conclusions.....	217
9.0	Further work.....	220
9.1	ZnMg PVD.....	220
9.1.1	MGZ development .....	221

9.1.2	High pH testing .....	221
9.1.3	Residual anodes analysis.....	221
	References.....	223

### Figure List

Figure 1 - HPS200 Layers.....	3
Figure 2 – Schematic of a) Composite floor decking and b) Angle Bead systems.....	5
Figure 3 - Recent price trends in zinc base price .....	6
Figure 4 - A typical organic coating line .....	9
Figure 5 - Corrosion as a change in Gibbs free energy.....	13
Figure 6 - Typical galvanic corrosion.....	14
Figure 7 - Pourbaix diagram for Iron.....	17
Figure 8 - Evans diagram.....	19
Figure 9 - Cathodic inhibited Evans diagram .....	20
Figure 10 - Pitting Corrosion of a 304L Stainless Steel Surface .....	23
Figure 11 - Crevice corrosion steps.....	24
Figure 12 - Water droplet corrosion mechanism.....	25
Figure 13 - Cross section micrograph of Hot Dip Galv.....	28
Figure 14 - The microstructure of Galfan .....	28
Figure 15 - Microstructural changes in the addition of Mg to GI a) GI and b) Mg doped GI.....	29
Figure 16 - Coating Microstructure of Galvalume.....	31
Figure 17 - The microstructure of Galvanneal.....	32
Figure 18 - Binary Phase Diagram for Zn/Al.....	34
Figure 19 - Zn Rich Area of Zn/Al Phase Diagram.....	34
Figure 20 - Graphical representation of PVD benefits.....	39

Figure 21 - Schematic of PPL200 .....	40
Figure 22 – Schematic Model of Tata RD&T's Evaporation Droplet .....	42
Figure 23 - Vapour pressure curves for some metallic elements .....	43
Figure 24 - VDB with heating elements .....	46
Figure 25 - The Binary Phase Diagram of Zinc & Magnesium.....	51
Figure 26 - SVET System Schematic .....	57
Figure 27 - SVET Microprobe.....	57
Figure 28 - SVET scan over a point current source .....	59
Figure 29 - Corrosion Cell Current Schematic .....	61
Figure 30 - Schematic of Charge Localisation Calibration Step .....	62
Figure 31 - A typical SVET calibration plot.....	63
Figure 32 - Schematic of a Wheatstone Bridge .....	66
Figure 33 - Representative 2D cut-edge corrosion map.....	69
Figure 34 - 3D Surface Plot of Corrosion Activity.....	69
Figure 35 - GDOES analysis of 1.0Mg annealed at 250°C for 300secs.....	72
Figure 36 – Microhardness testing indenters .....	74
Figure 37 – Angles between faces on a Vickers Indenter .....	74
Figure 38 - Vickers pyramidal indent in Zn-Mg-Al metallic coating.....	75
Figure 39 – a) domed and b) cupped depth samples.....	79
Figure 40 - polished & etched Galvalloy (ZA), 3 secs Nitpic etch.....	80
Figure 41 - original ZA image.....	82
Figure 42 - dendrites coloured in... ..	82
Figure 43 - Sigmascan detection.....	82
Figure 44 - Sigmascan data.....	82
Figure 45 - example primary zinc depth profile.....	83
Figure 46 - MGZ42 Dendrite Count Image .....	84
Figure 47 - IR heating/annealing furnace of the Rhesca Hot-Dip Simulator.....	86
Figure 48 - Mass loss test tube.....	88
Figure 49 - Mass loss test specimen.....	88
Figure 50 - Schematic of EML-PVD .....	92
Figure 51 - Typical sections from a)1.5Mg and b) 1.0Mg.....	92



Figure 52 - zinc droplet rolled flat during production.....	93
Figure 53 - finger mark from reactions with Mg on surface of 1.0Mg.....	94
Figure 54 - As received 1.5Mg sample microstructure.....	95
Figure 55 – Secondary Electron Image (SEM) of annealed 1.5Mg coating .....	96
Figure 56 – SEM Linescan analysis of annealed 1.5Mg from coating surface into substrate .....	96
Figure 57 - Example lab diffusion annealing profile .....	99
Figure 58 - Typical HDS annealing profile .....	100
Figure 59 – a) 1.5Mg as received and b) after 300°C for 120 mins.....	101
Figure 60 – a) 1.0Mg as received and b) after 300°C for 120 mins.....	101
Figure 61 – 1.5Mg, a) 100°C for 600 mins and b) 150°C for 480 mins.....	102
Figure 62- 1.5Mg, a) 200°C for 360mins and b) 250°C for 240 mins .....	102
Figure 63 - 1.0Mg, a) 100°C for 600 mins and b) 150°C for 480 mins .....	102
Figure 64 - 1.0Mg, a) 200°C for 360 mins and b) 250°C for 240 mins .....	103
Figure 65 - X-ray diffraction data for all Mg1.0 samples .....	105
Figure 66 - X-ray diffraction data of Mg1.5 samples .....	106
Figure 67 - hardness changes of 1.0Mg with annealing.....	107
Figure 70 1.5Mg a) bottom, b) side and c) top .....	109
Figure 68 - MZ140 a) bottom, b) side and c) top.....	109
Figure 69 1.0Mg a) bottom, b) side and c) top .....	109
Figure 71 - GDOES analysis of 1.0Mg sample annealed at 250oC for 300 seconds.....	111
Figure 72 - Free Mg in 1.0Mg Annealed Samples.....	111
Figure 73 - MgZn <sub>2</sub> Content in 1.0Mg Annealed Samples.....	112
Figure 74 - Zn & Fe-Zn in 1.0Mg Annealed Samples .....	112
Figure 75- Free Mg in 1.5Mg Annealed Samples.....	113
Figure 76 - MgZn <sub>2</sub> Content in 1.5Mg Annealed Samples.....	113
Figure 77 - Zn & Fe-Zn in 1.5Mg Annealed Samples .....	114
Figure 78 - Mg mass loss 1.5Mg (surface) .....	115
Figure 79 -1.5Mg surface SVET scans a) 975secs and b) 1755 secs.....	116
Figure 80 - Surface mass loss - 1.0Mg Samples .....	117
Figure 81 - Surface mass loss - 1.5Mg Samples .....	117

Figure 82 - PVD Samples Surface Mass Loss .....	118
Figure 83 - Cut-edge losses from 1.0Mg Annealed Samples.....	120
Figure 84 - Cut-edge losses from 1.5Mg Annealed Samples.....	120
Figure 85 - %Red Rust PVD annealed Samples .....	122
Figure 86 - %Red Rust PVD Samples (zoomed).....	123
Figure 87 - Portion of the Zn/Al phase diagram showing the 4.8wt%Al region .....	131
Figure 88 - Variation in volume fraction of primary Zn with depth with varying gauge	132
Figure 89 - Microstructural changes in Zn-4.8wt% Al alloys with increasing substrate gauge (all images taken at 6µm through the coatings).....	134
Figure 90 - Number of primary Zn dendrites per unit area with varying gauge .....	135
Figure 91- Microstructure of HDG on 0.85mm steel gauge (image taken at a depth of 6µm).....	138
Figure 92- Results obtained from mass loss experiments in 0.1% NaCl over 144 hours	140
Figure 93- Representative SVET iso-current corrosion obtained by scanning the cut-edge of the Zn4.8wt% Al samples (the maps are hour 12 of the 24 hour test in 0.1% NaCl). 141	141
Figure 94- Average SVET obtained metal losses (ug) from the Zn-4.8wt% Al alloy and HDG coatings on varying steel gauge after 24 hours .....	142
Figure 95 - Representative ribbon plots showing the anodes against time and anode intensity for Zn-4.8wt% Al alloy samples with 0.38mm and 1.0mm gauge.....	144
Figure 96 - Average intensity over the 24h experiment against their lifetime for a) HDG and b) Zn4.8wt% Al materials with varying gauge .....	145
Figure 97 - Percentage of anodes that are active for defined time frames for HDG coated steel with various steel gauges .....	146
Figure 98 - Percentage of anodes that are active for defined time frames for Zn4.8wt% Al coated steel with various gauges.....	147
Figure 99 - Comparison of the average size of primary zinc dendrites observed for the steel gauges against SVET measured zinc loss (µg) for Zn-4.8wt% Al coated steels....	149
Figure 100 - Primary zinc% as a function of alloying level .....	157
Figure 101 - Effect of alloying on dendrite number .....	157
Figure 102 - Effect of Alloying Level on Dendrite Volume.....	158
Figure 103 - Mass loss v Alloying Level Comparison .....	159
Figure 104 - Total SVET Mass Loss vs. Primary Zinc% .....	160
Figure 105 - Average Anode Intensities - MGZ Samples.....	160
Figure 106 - Residual Anode Analysis MGZ Samples.....	162
Figure 107 - Immersion mass loss comparison.....	163

Figure 108 - MGZ19 micrograph	Figure 109 - MGZ20 micrograph.....	164
Figure 110 - Surface appearance of a) MGZ19 and b) MGZ20.....		165
Figure 111 - Total Mass Loss - Comparison 1.....		165
Figure 112 - Cumulative average mass loss per scan - Comparison 1.....		166
Figure 113 - Residual anode analysis data - Comparison 1 .....		166
Figure 114 - MGZ41 Microstructure .....		168
Figure 115 - MGZ42 Microstructure .....		168
Figure 116 - MGZ41 near substrate interface.....		169
Figure 117 - SEM Image of MagiZinc alloy cross section .....		170
Figure 118 - Comparison 2 Primary Zinc% curves .....		170
Figure 119 - Total mass loss Comparison 2.....		171
Figure 120 – Residual anode analysis at 1.0amps/m <sup>2</sup> threshold .....		172
Figure 121 – Residual anode analysis at 0.5amps/m <sup>2</sup> threshold .....		172
Figure 122 - Anodes >0.5amps/m <sup>2</sup> Average Intensity.....		173
Figure 123 - SVET Scans after 22hours for a) MGZ41, b) MGZ42 and c) 0.55mm HDG .....		174
Figure 124 - MGZ43 Microstructure.....		176
Figure 125 - MGZ44 Microstructure.....		176
Figure 126 - Depth profile - Comparison 3.....		176
Figure 127 - Comparison 3 Mass Loss .....		178
Figure 128 - Comparison 3 Residual Anode Analysis.....		178
Figure 129 - Average anode intensity .....		179
Figure 130 - Elemental partitioning in the phases of MagiZinc <sup>®</sup> .....		179
Figure 131 - Effect of Alloying Level on Primary Zinc%.....		181
Figure 132 - Alloying effect on Dendrite Number.....		181
Figure 133 - MGZ45 microstructure .....		182
Figure 134 - MGZ66 microstructure.....		182
Figure 135 - MGZ48 microstructure.....		182
Figure 136 - SVET Mass Loss v Alloying Level.....		183
Figure 137 - Residual Anode Analysis .....		184
Figure 138 - Average anode intensity .....		184

Figure 139 - Effect of Alloying Level on Primary Zinc .....	185
Figure 140 - MGZ46 Microstructure.....	186
Figure 141 - MGZ47 Microstructure.....	186
Figure 142 - MGZ69 Microstructure .....	187
Figure 143 - Mass Loss Comparison 8 .....	187
Figure 144 - Mass loss to Alloying Level.....	189
Figure 145- Dendrite number vs. Mass loss .....	190
Figure 146 - Scatter graph of primary zinc% v alloying level.....	191
Figure 147 - Scatter graph of Mass Loss v Alloying Level .....	191
Figure 148 - Pourbaix diagram for Zinc.....	196
Figure 149 - Pourbaix Diagram of Mg.....	196
Figure 150 - Overall Comparison - Geographical Passivation Treatments .....	201
Figure 151 - 24 hours SVET Mass Loss Data – Arranged In Passivation Order.....	202
Figure 152 - Immersion Mass Loss Analysis.....	204
Figure 153 - Immersion Mass Loss Data - 3 Days Immersion .....	205
Figure 154 - Immersion Mass Loss Data - 28 Days Losses.....	206
Figure 155 - Comparison of SVET Prediction to Immersion Mass Loss Data.....	208
Figure 156 - SVET Data Comparison of HDG to MZ140.....	209
Figure 157 - Residual Anode Analysis .....	210
Figure 158 - Average Anode Intensity.....	211

### **Table List**

Table 1 - The Galvanic Series (reduced) .....	15
Table 2 - Commercially available Zn-Mg coatings .....	30
Table 3 - ZnMg Intermetallic compositions .....	52
Table 4 - Coating composition determined by optical microscopy .....	91
Table 5 - Initial diffusion annealing parameters .....	98
Table 6 - Initial sample annealing cycles.....	99
Table 7 – XRD Determination of Intermetallic Phases .....	103
Table 8 – intermetallic phases detected after diffusion.....	104
Table 9 - Lifetimes for best performing coatings .....	119

Table 10 - Cut edge corrosion rates for PVD Samples .....	121
Table 11 - PVD Salt Spray Samples .....	121
Table 12 - Zn-4.8wt% Al alloy coated steel sample details.....	128
Table 13 - HDG reference materials .....	128
Table 14 - Average volume fraction of primary Zn and microstructural characteristics	133
Table 15 - Comparison table for the MGZ Sample Set .....	155
Table 16 - Dendrite analysis information MGZ samples.....	156
Table 17 - MGZ Growth Curve Coefficients.....	158
Table 18 – microstructural characterisation of MGZ43 and MGZ44 .....	175
Table 19 - Sample Matrix High pH Investigation.....	199

## **Chapter 1**

### **Introduction and Literature Review**

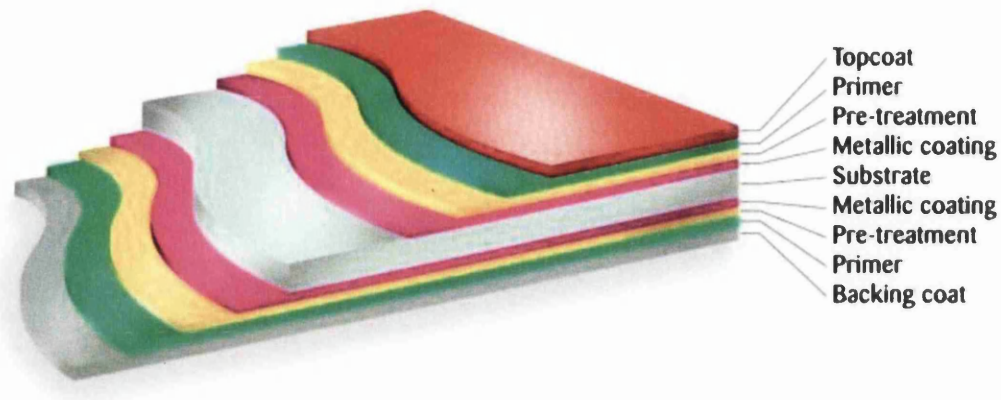
## Introduction

Metallic coatings and their development are continuing to be of tremendous interest to research establishments and to private sector manufacturers. Extensive literature is continually being published both as academic papers[1-3] and as company brochures[4, 5], many depicting investigations into current commercially available metallic and alloy coatings, and some taking conventional coatings into unexplored areas with changes in alloy compositions and processing conditions.

Tata Steel Europe Ltd's (TSE) (formally Corus Ltd.) commercially available metallic coatings are currently all based on hot dip galvanising of steel sheets. They have coating facilities across Europe[6] providing coated steel products mainly for the construction and automotive markets. Their product offering includes flagship coatings include Galvalloy® and the newer MagiZinc®, the former being a ~5% aluminium alloyed zinc layer and the latter a ternary alloy typically comprising 1.6% Magnesium and 1.6% Aluminium alloying levels in the zinc. Galvalloy® is a well established product and forms part of Tata Colors Ltd's prestige building envelope product HPS200®, an organically coated Galvalloy steel strip that finds uses as roof and wall panels and profiles [7], see figure 1. Magizinc® is currently produced only in Tata Steel Europe Ltd's IJmuiden plant in the Netherlands but has found limited use in the automotive market though there are moves to use the coating technology as a construction solution.

For many years there has been a close relationship between the steel industry in Wales and Swansea University. Many thesis submissions, journal publications and conference presentations have emanated from the Materials Research Centre in Swansea University, working in conjunction with Tata Steel's coating and new product divisions, and many have investigated changes to the behaviour of the prepared coatings when processing conditions such as cooling rate have changed[2, 8, 9]. These areas of research continue to be of academic interest and, where the outcome of the research delivers increased coating

performance, or faster production rates, of commercial interest to Tata Steel, especially in the current economic climate where any potential cost saving is greatly appreciated.



**Figure 1 - HPS200 Layers [1, 4]**

To this end this project has investigated Galvalloy® and MagiZinc® type coatings, where, in the case of Galvalloy® the processing conditions experienced by the coating are modified; by the increase in gauge of the coated strip, and in MagiZinc® by varying the alloying levels of Aluminium and Magnesium and investigating the effect on the corrosion properties.

Some focus is given on the opportunities for Physical Vapour Deposition (PVD) coatings with a clear focus on the development of Zinc and Magnesium (ZnMg) based coatings and their associated corrosion resistance. Some work has been reported from the Corus-Posco joint development agreement of PVD ZnMg [10]. TSE Research Development and Technology's (CRD&T) sequential deposition of Magnesium onto previously deposited Zinc on a coil of strip steel. Further work has been carried out into how these coatings form corrosion resistant alloys when diffusion annealed.



## **1.0 Literature Review**

### **1.1 The Steel Industry in Wales**

Production of steel at the Port Talbot site commenced, in a similar context to how we see it now, in 1947 [11] when the Abbey Works of the Steel Company of Wales was built although steel production had been evident since 1717 [11]. Since then production in Wales has seen many changes and continues to experience many challenges from competitors and changes in the economic climate. Recent developments to the industry in the UK, from privatisation under Mrs. Thatcher's Prime Ministerial governance through to the recent purchase by an Indian global, yet family owned corporation, have all brought changes to the business, each with its own benefits and drawbacks.

#### **1.1.1 Steel solutions for construction**

In this modern age of green political policy and agendas steel is increasingly being seen as possible alternative for the traditional construction materials of brick, block and timber. During steel production scrap steel is used to help cool the molten steel during carbon removal in the BOS<sup>1</sup> process and hence is completely recyclable.

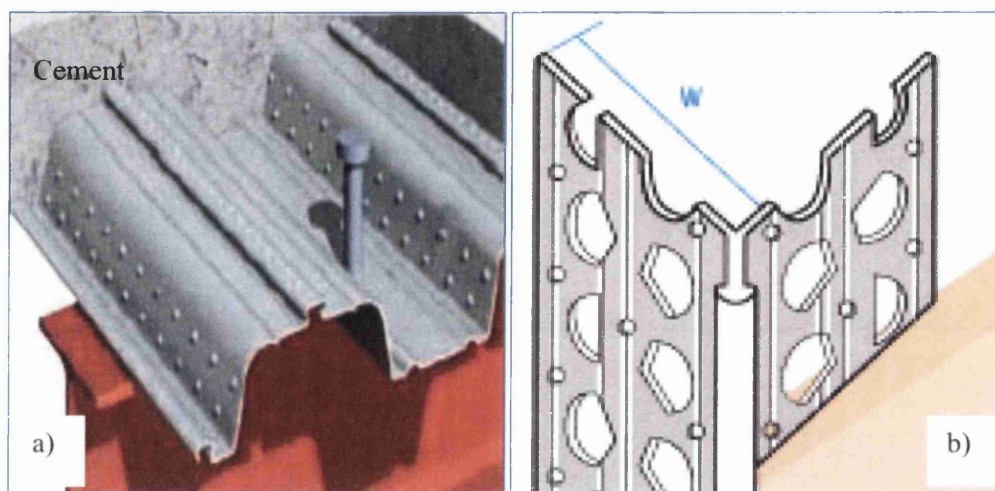
Steel products currently in use in the market place include structural I beams and reinforcement bars which are either primed and then painted after construction, if left uncovered, or immersed in concrete. Other common products intended for external applications such as roof and wall panels and profiles and internal construction components such as lintels, perlins, nail plates, composite floor decking and angle beads. The product design uses metallic and organically coated steels, usually in external applications requiring high levels of corrosion resistance and bare metallic coated steels for internal products. Metallic coatings are designed for long term corrosion protection

---

<sup>1</sup> Basic Oxygen Steelmaking – blowing O<sub>2</sub> into molten 'pig' iron (blast furnace product)

and the products are passivated for short term corrosion protection, intended to inhibit the corrosion of the zinc coating to maintain visual appearance before use. In the case of composite floor decking and some other internal parts like A-beads they eventually become immersed in cement or plaster, see Figure 2.

Part of this project was focussed on the behaviour of a new metallic coating for construction steels, to be sold as a 'bare' material, i.e. without any organic coating, into the UK construction market. The current UK market for such products is approximately 140kt, in gauges ranging from 0.5mm to 2.0mm [12].



**Figure 2 – Schematic of a) Composite floor decking and b) Angle Bead systems [13]**

The construction market is very competitive and even with having a base in the UK, Tata Steel Europe is under competition to maintain its majority share in this market. Product offerings such as MagiZinc® can be seen to deliver a competitive edge if expectations on the coating's corrosion performance can be delivered. The product technology allows the production of thinner metallic coatings that perform comparatively with the thicker

coated, traditional, zinc only<sup>2</sup> counterparts such as Galvatite™, Tata Steel's hot dip galvanized steel product.

Another issue for the manufacture of metallic coated steels is the fluctuations in the price of raw materials. Recent fluctuations in the price of zinc, see Figure 3 - Recent price trends in zinc base price can add significant amounts onto the cost of manufacture, over very short timescales, and with the steel industry's unavoidable reaction times to pass on these production price increases to the customer it can lead to reduced profit margins for the steel producer.



Figure 3 - Recent price trends in zinc base price [14]

## 1.1.2 Metallic coated steels

Many of us will have experienced the effect the atmosphere has on steel or iron, from childhood days playing next to rusty park railings where paint layers have broken and peeled off to rusted stone chips on vehicles for those more experienced. In either instance

<sup>2</sup> Galvatite is actually prepared with ~0.15% Aluminium addition.

this is due to the inherent driving force that is within the material to return to its natural state, more on this later.

In order to prolong the lifetime of the material in its intended, designed, and probably more visually appealing state<sup>3</sup> manufacturers of steel systems often coat their products with a metallic coating. Metallic coatings can be seen to be sacrificial coatings or barrier coatings. Sacrificial coatings exhibit properties where the elements comprising the metallic coating oxidise, or corrode, preferentially to the steel substrate for a certain lifetime depending on the amount of sacrificial coating available for protection. Barrier coatings are prepared from elements are not likely to corrode selectively before the substrate but that inhibit the corrosion of the steel substrate by removing one of the factors required to initiate the corrosion. The choice of the metallic coating elements is covered in detail in section 1.3, Metallic Coatings.

### **1.1.3 Passivation systems**

It is rarely seen that the production of metallic coated steel and its end user are geographically close to each other. One example of close production and end use was the modular construction business unit of Corus Living Solutions that resided within Corus' Shotton works. This is rare and so inevitably the coiled product will require transportation before reaching the end user. TSE makes every effort to keep the product away from factors that can initiate corrosion though this is not always said of the end-user, for instance the products in the construction market would require significant warehousing at or near a construction site in order to keep them dry and retain their visual appearance in the 'as-delivered' state.

---

<sup>3</sup> Shiny, as produced Galvitite can be annealed to produce Galvanneal, a matt grey (dull) metallic coating, with its own attractive properties.

In order to temporarily retain the product in the as manufactured state, i.e. with no evidence of surface corrosion initiation steel strips are usually coated with a thin layer of a passivation system. These systems usually take the form of a thin organic binder or resin layer in which there are additives that inhibit any surface corrosion [15, 16]. These systems are intended for short term protection i.e. during transport, and are not intended to be the backbone of the corrosion resistance system.

#### **1.1.4 Organically coated steels**

The addition of an organic coating to a bare or metallic coated steel system can increase the corrosion protection through the barrier properties of the organic coating [17]. No organic coating is fully impermeable to oxygen and water, though they can restrict the exposure of the substrate to corrosive environments [18]. Organic coated strip steels are usually prepared via a line production process, see Figure 4, where a series of rollers are set with a standard 'gap' so that they can transfer a controlled amount of paint uniformly onto the strip.

Tata Steels Colors can produce many different coloured painted steel finishes and satisfies markets such as construction but also the domestic appliance market for items such as washing machines and fridges [15].

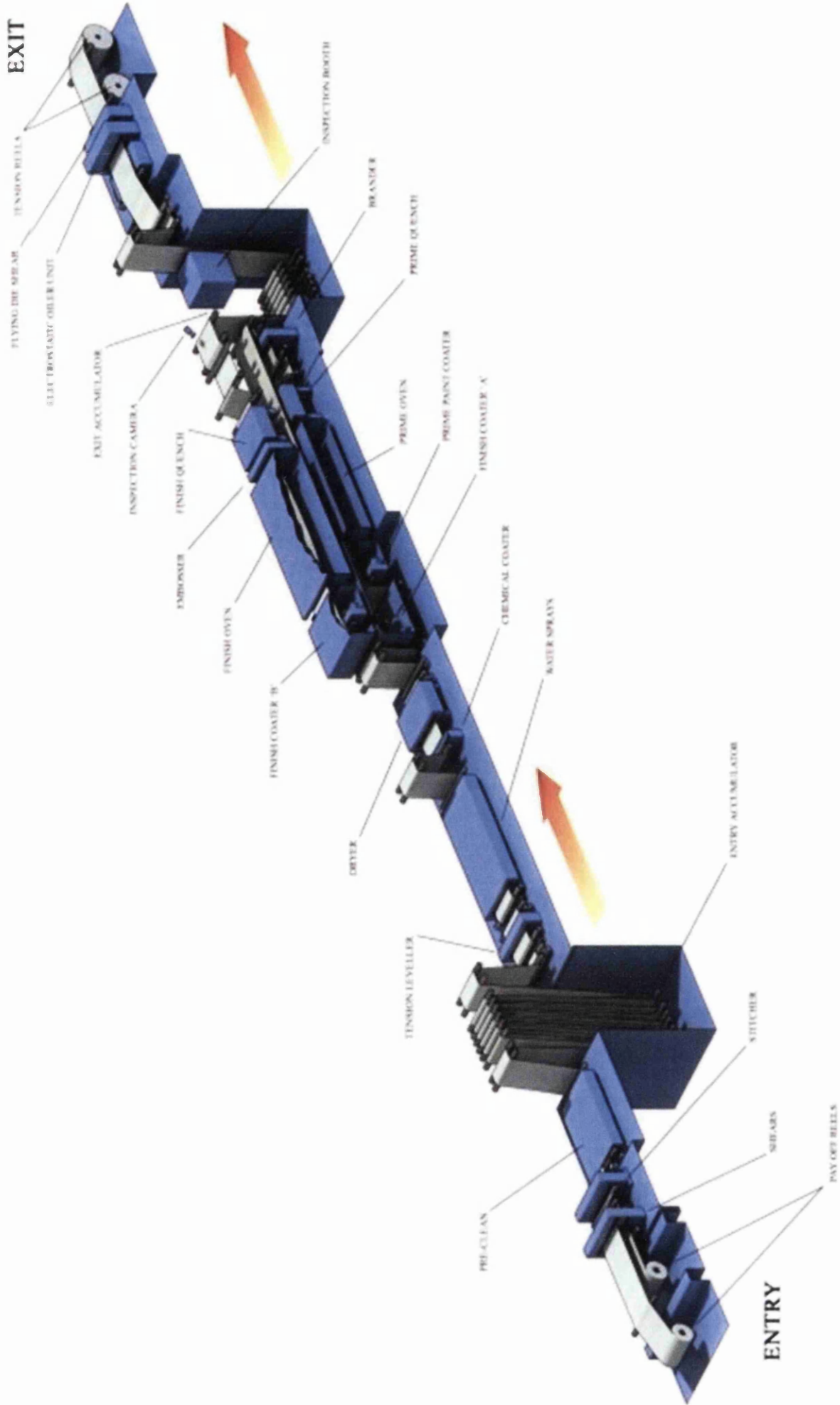


Figure 4 - A typical organic coating line [1]

## 1.2 Corrosion

Apart from stainless steel, where significant alloying additions<sup>4</sup> of chromium enable the formation of a cohesive chromium oxide protective layer [19], the alloying additions in mainstream and even newer, advanced steels is typically <3% [20], and are not intended to protect the steel from corrosive attack.

Most people have experienced the effect the everyday environment has on steel products. From a child encountering rusty park railings to the elderly gentleman watching his classic car turn to rust it is painfully evident that steel is a reactive metal, and once corrosion has started it is difficult to stop.

### 1.2.1 Coating requirements? Why coat?

Historically the simplest method to slow corrosion is to apply paint to the surface of the steel. The painting process usually results in the formation of an organic polymer adhered to the surface which has been engineered to prevent the steel surface from encountering the atmosphere.

Difficulties arise when areas of the surface are not covered with the paint, or if the paint layer is damaged exposing the steel surface. Some of the more sophisticated paint technologies have chemical additions which can slow down the rate of corrosion if the layer is broken, but generally corrosion will initiate upon exposure to the atmosphere.

Corrosion is now more definitively understood and coatings have become more sophisticated in their capabilities in maintaining the steel substrate and the load bearing properties it is so good at delivering.

---

<sup>4</sup> 11% is the minimum alloying addition of chromium required to make a chromium-iron alloy 'stainless'.

### 1.2.2 What is corrosion?

Corrosion is defined as “physicochemical interactions between a metal and its environment which results in changes in the properties of the metal and which may often lead to impairment of the function of the metal, the environment, or the technical system” [21].

Unlike gold most of the metals we see in everyday life are not found in the environment in their metallic forms. Metals have to be chemically removed from the elements they are deposited with, commonly oxygen, in their ores. The ores are the stable ground states for the reactive metals.

The reactivity of the metal can be regarded as a measure of its affinity for the oxygen it is combined with and it is not hard to imagine that the higher the affinity the more difficult it would be to extract the metal. This is one of the reasons why aluminium has comparably, only recently been extracted.

Once extracted there remains a driving force; the metal’s affinity for oxygen, for the return to the stable oxide found in the ore. The atmosphere contains sufficient oxygen and humidity to initiate the oxidation reactions of most metals.

### 1.2.3 Corrosion mechanisms for Iron

In most uses iron, or steel, as an engineering material will come into contact with a corrosive environment. A lay-man may consider a corrosive atmosphere to be an acid cloud or other toxic environment, but the corrosive level depends on the reactivity of the species being considered.

To highlight this point it is worth considering the extremes of elemental reactivity. Gold for instance is so non-reactive that it exists in nature in elemental form (nuggets, gold dust etc.) whereas a very reactive metal such as sodium can only exist as an oxide as it



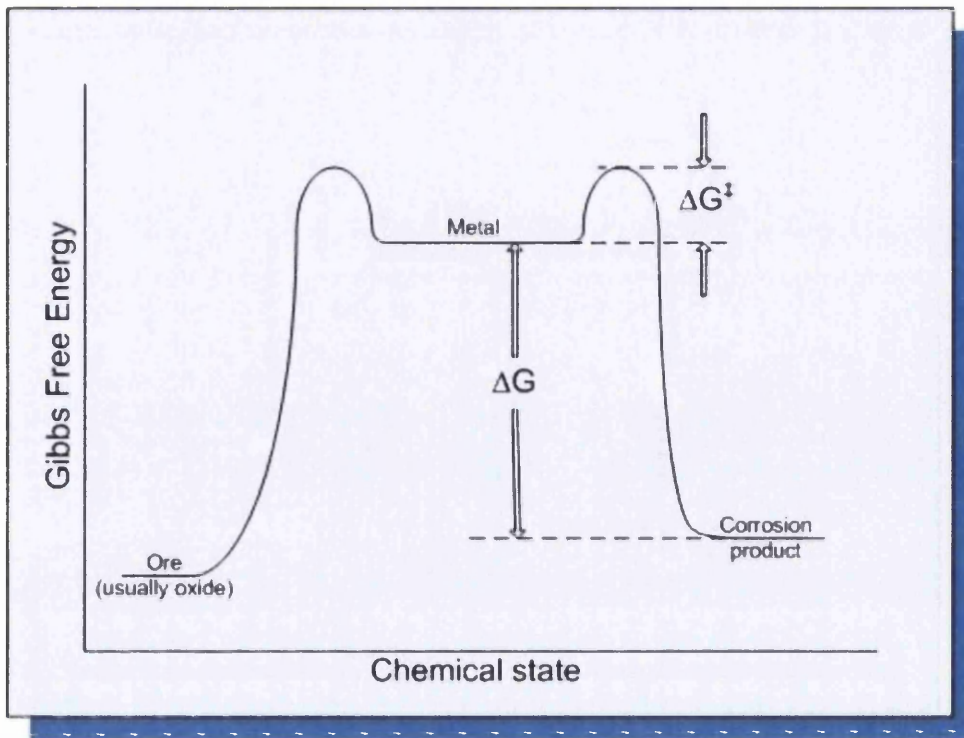
reacts immediately on contact with the air<sup>5</sup>. In the case of steel, immediate contact with the air will not promote corrosion, in fact prolonged contact with very dry air will retain the metal in elemental form. However, when the air has sufficient humidity the conditions are favourable for oxidation to occur, typical atmospheric relative humidity values of >65%RH will be sufficient for the condensation of water onto cold surfaces. Surface salt contamination can lower the %RH level required for the initiation of corrosion due to the hygroscopic nature of salt particles and the deliquescence into corrosion promoting electrolytes.

The mechanism for this corrosion is a change in Gibbs free energy of the metal species, Figure 5. In any chemical reaction the driving force is to lower the overall free energy. Free energy can be considered to be a measure of the stress the system is under to stay in its particular state. Every system strives to be under the minimum amount of stress (just like humans!) and so will undergo reactions to achieve this.

Oxidation is one such reaction, the amount of energy imparted to the system to obtain the metal from its ore is a good indication of the level of strain the metal is under to maintain its metallic state. Until recently (last 100 years) the extraction of aluminium from its ore has been impossible due to the vast amounts of electrical energy required to drive off the oxygen, upon exposure to air aluminium rapidly returns to its oxide to relieve this stress and reduce Gibbs free energy. It is only the oxide's ability to prevent further oxidation of the inner metal atoms that enables aluminium to exist in a metallic form. It is a misconception that aluminium products do not oxidise, it is that the oxide layer is transparent that makes us think the metal has not oxidised.

---

<sup>5</sup> Metallic sodium is available although its storage is carefully controlled (usually kept covered with a suitable hydrocarbon such as paraffin).



**Figure 5 - Corrosion as a change in Gibbs free energy [22]**

In the case of iron, or steel the amount of energy to reduce the ore is considerably less and so the change in free energy is lower and the oxidation (rusting) reaction proceeds slowly (can be observed over a matter of hours).

The rate of the reaction is also dependent on the amount of energy required to initiate the reaction. Called the activation energy;  $\Delta G^\ddagger$  can be regarded as a barrier to oxidation. Barriers to oxidation can be the energies required to transport of oxygen through an already formed oxide layer, the breaking the metallic bonds, the adsorption of oxygen and water from the environment onto the surface, or the formation of temporary species in the breakdown of oxygen and water.

#### **1.2.4 Galvanic corrosion**

Galvanic corrosion takes place when two dissimilar metals are brought into electrical contact with each other, as can be seen in Figure 6 this results in one metal being oxidised, the other reduced. Electrical contact can be via a conducting circuit or an

electrolyte. The corrosion can be predicted by looking at the reactivity of the metals relative to each other; the Galvanic Series.

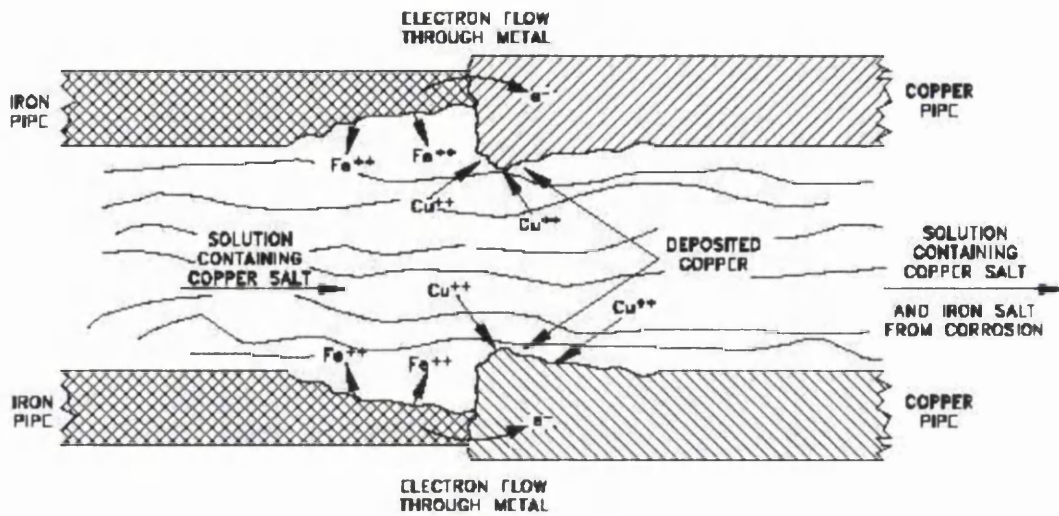
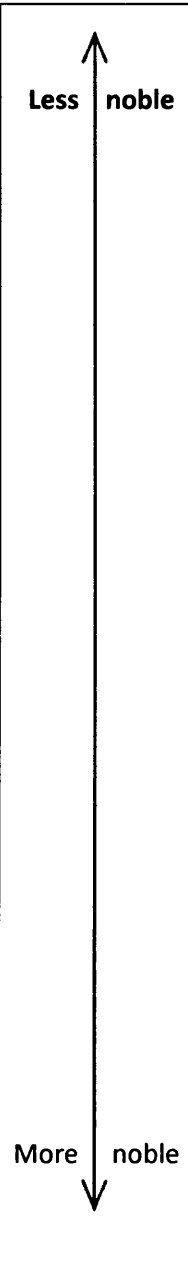


Figure 6 - Typical galvanic corrosion [23]

### 1.2.5 Galvanic series

The Galvanic series (or electropotential series) is a listing, in order, of the reactivity of metals towards corrosion. Table 1 shows some selected metals from the series. The series can be used to predict which one of two metals, when electrically connected, will corrode preferentially. The flow of electrons will be from the less noble to the more noble as the less noble metal corrodes into solution, the more noble metal initiates cathodic reactions; usually the reduction of dissolved oxygen to hydroxide, in the presence of water. The galvanic series is the foundation of battery manufacture as selecting the right combination of metals can give systems to deliver the required voltage for the system, i.e. in common cases 1.5, or 9V.

Magnesium	
Magnesium Alloys	
Zinc	
Aluminium	
Mild Steel	
Cast Iron	
Stainless Steel	
Lead	
Tin	
Brasses	
Copper	
Silver	
Titanium	
Graphite	
Zirconium	
Gold	
Platinum	

**Table 1 - The Galvanic Series (reduced) [24]**

### 1.2.6 Pourbaix diagrams

A Pourbaix diagram, or Potential-pH diagram, is a graphical representation of what corrosion products are expected over a range of potentials and pH conditions. The Pourbaix diagram for any metal can be obtained from reference texts and they can be interpreted to predict if and what corrosion products will form in an electrochemical

system. In Figure 7 it can be seen that at a  $\text{pH} < 9$  and an applied  $E^\circ$  of  $< -0.8\text{V}$  the metal is inert as no corrosion products are predicted, this behaviour is called immune.

The areas where solid corrosion products are predicted are called passive corrosion areas. Although corrosion is predicted in passive regions the corrosion product deposits itself onto the corroding metal surface providing some barrier protection towards further corrosion. The regions notated with values 0 to -6 are regions where the concentration of the soluble species ( $1 \times 10^{\text{value}} \text{mol dm}^{-3}$ ) is required to provide the predicted corrosion deposit.

Areas which predict soluble species are the troublesome areas. In these regions the species will readily dissolve into the electrolyte and be carried away exposing more fresh anodic sites for rapid metal loss.

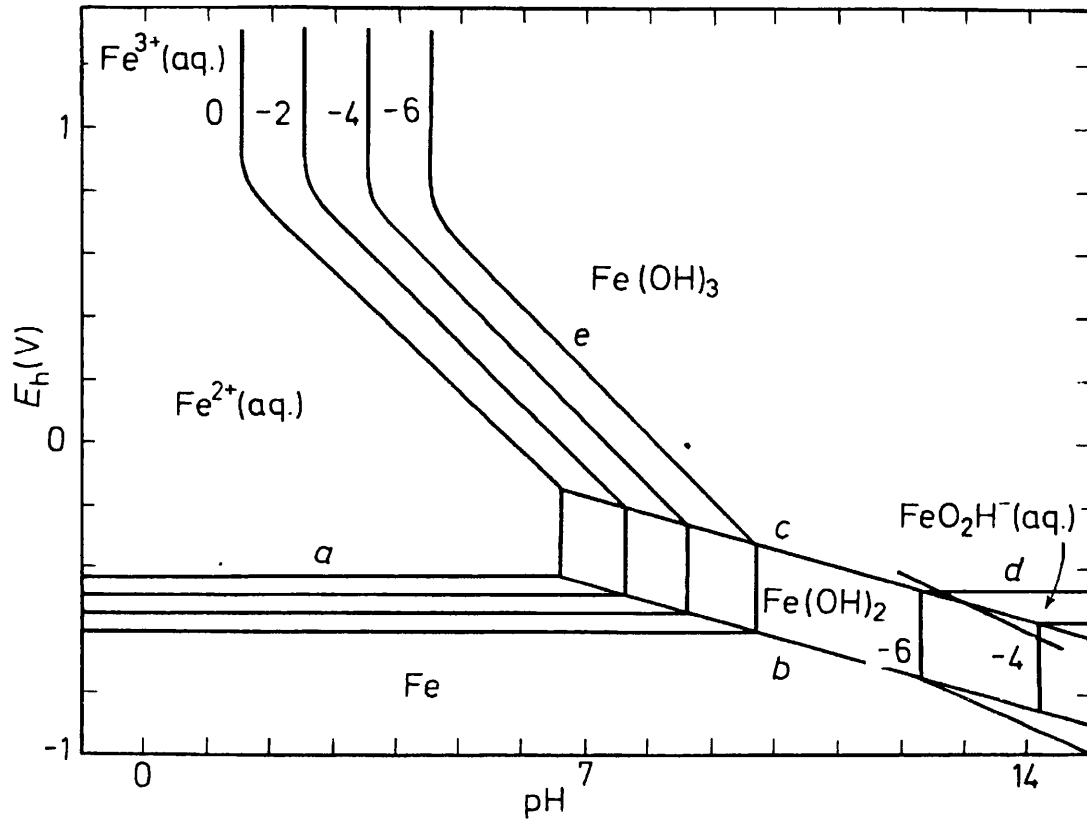


Figure 7 - Pourbaix diagram for Iron [22]

Pourbaix diagrams are useful in engineering systems which take advantage of the immune and passive areas. If the electrode potential or pH can be tailored to give the predicted conditions then corrosion can be slowed, or stopped, as desired.

### 1.2.7 Evans diagrams and Tafel lines

Tafel first determined the relationship between current and electrode potential [25, 26], where;

$$i_{anodic} \propto \exp(E)$$

and, 
$$i_{cathodic} \propto \exp(-E)$$

a plot of these relationships can give straight lines called Tafel lines, on a plot called an Evans diagram, see Figure 8.

### 1.2.8 Evans diagrams, Polarisation, and the rate of corrosion

Usually engineers are interested in the rate of corrosion for prediction of system failure, or possibly the planning for remedial action. According to Faraday's 1<sup>st</sup> Law of Electrolysis, "the mass of a substance produced at an electrode during electrolysis is proportional to the number of moles of electrons transferred at that electron" [27]. So, if we monitor the amount of electrons moving; the current density, then we can determine the rate of corrosion losses at anodic sites.

In a simple galvanic cell reaction if the corrosion current density<sup>6</sup>, is monitored then a slowing of the corrosion reaction will be seen from the initial contact current,  $I_{init}$ . This is due to a phenomenon called polarisation.

Polarisation effectively changes the electrode potential from the initial contact potential of  $E^{\circ}_C$  (cathode, Copper) and  $E^{\circ}_A$  (anode, Zinc) where the initial current is predicted by Ohm's law,  $I = V/R$ ;

$$i_{init} = \frac{E_C^{\circ} - E_A^{\circ}}{R}$$

To  $E_C$  and  $E_A$  which are the effective potentials of the electrodes, giving;

$$I = \frac{E_C - E_A}{R}$$

Where R is the resistance of the couple material to electron movement, also called the Ohmic resistance.

---

<sup>6</sup> The current per unit of surface area

The nature of polarisation is such that the transport of electrons in a corrosion reaction is faster than the reactions of the ionic species at the electrodes [28]. The rate limiting electron reactions at the cathode are reduction or precipitation reactions (sometimes gaseous evolution), and at the anode are the diffusion rates of ionic species into the electrolyte.

An Evans diagram; see Figure 8, displays the polarisation effects for the electron reactions; this can be seen as the curvature, as a plot of  $E$ ; electrode potential, against the current;  $I$ .

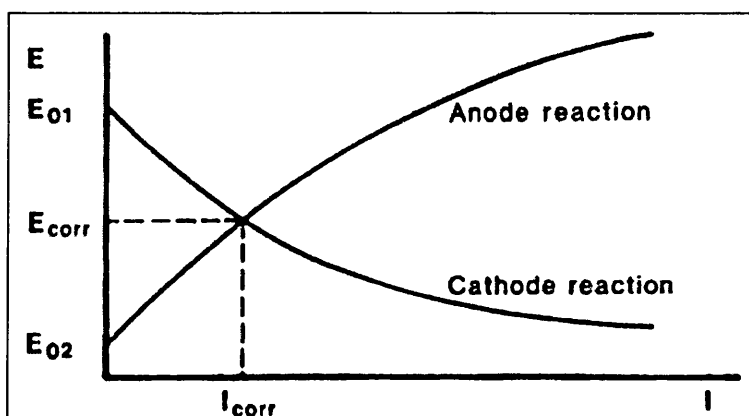


Figure 8 - Evans diagram [21]

The intersection of the anodic and cathodic polarisation curves gives the points  $E_{corr}$  and  $I_{corr}$ .  $E_{corr}$  is called the free corrosion potential and  $I_{corr}$  is the corrosion current and so the rate of corrosion can be predicted.

The amount of polarisation can be affected by anodic or cathodic inhibition; i.e. increasing the amount of retardation of the electrode sites. When this occurs the point of intersection of the anode and cathode polarisation curves changes and the rate of corrosion is changed.

In the case of cathodic inhibition the polarisation curve for the cathode is shifted to lower potentials and the point of intersection is moved relative to the original, non-polarised position, see Figure 9.  $E_{corr}$  is then moved to lower potentials; reducing the



thermodynamic driving force for the reaction, and  $I_{\text{corr}}$  is decreased, slowing the rate of the reaction if initiated.

Anodic control is also possible which has the effect of increasing  $E_{\text{corr}}$ , requiring the system to be able to reach stronger oxidising conditions, and  $I_{\text{corr}}$  is again reduced slowing the rate of corrosion.

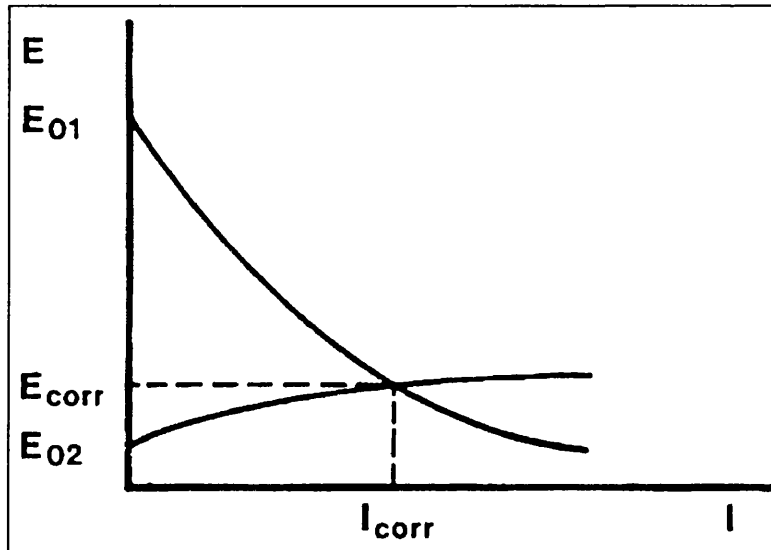


Figure 9 - Cathodic inhibited Evans diagram [21]

### 1.2.9 Mechanical effects on corrosion

We have seen that corrosion takes place wherever it is thermodynamically favourable. In metallic systems the corrosion location can be affected by slight changes in localised chemistry or microstructural effects. These effects can be the areas of grain boundaries, where two neighbouring grains meet they form an area on non-optimal alignment of the atoms in the system. This leaves atoms without the right number of 'nearest neighbours' for the complete unit cell and so not so stable, this can result in the increase in the potential compared to the bulk material and can focus corrosion initiation [20].

The corrosion can also be affected by mechanical implications or physical defects to the engineering system. Simple engineering issues such as cut-edge burrs can lead to the localised holding of a water droplet leading to an environment suitable for corrosion initiation, it is also seen that design of components, particularly those in automotive structures can have ledges where wet, poultice matter can congregate and provide conditions suitable to promote corrosion [29, 30].

### 1.2.10 Cut edge corrosion

There is no way to eliminate the driving force for Fe to convert into its oxides in the presence of a corrosive atmosphere. One way to stop corrosion from occurring is to eliminate the contact of the corrosive atmosphere on the iron atoms. This is most often called a barrier coating and usually takes the form of a painted layer. These are usually a polymeric resin, e.g. polyester, which exclude water from contacting the steel surface (they are usually porous to oxygen).

This is not the best coating process for the protection of the steel, as once the barrier layer is broken, i.e. in the case of an automotive panel a simple stone chip can break the layer, the protection is lost and corrosion can proceed. The most common system for steel protection is to use sacrificial corrosion protection. This system operates by utilising an element, usually zinc, which has a greater affinity to release electrons than the steel substrate, so when a corrosive environment is encountered the zinc is preferentially oxidised in favour of the steel, polarising the steel surface to lower potentials and therefore offering protection from the oxidation potential of dissolved oxygen.

A further benefit of the zinc coating, or galvanised coating, is that some of the relatively thick (~40µm) zinc layer will be drawn over the exposed steel edge on cutting. Even so it is only a matter of time before the sacrificial nature of the zinc coating is exhausted and

the steel will start to corrode. This type of corrosive attack is called cut-edge corrosion and leads to delamination and peel back of outer layers.

### **1.2.11 Surface or uniform corrosion**

Surface, or uniform corrosion, results in material loss from the entire exposed surface. The amount of metal loss is usually expressed in mass per unit area, or by averaging the corrosion depth. The uniformity of loss is a function of the lack of clearly defined anodic or cathodic sites [21], and results in the slow degradation of the technical system, being predictable from average corrosion depth per unit time studies.

### **1.2.12 Pitting**

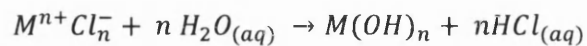
Pitting corrosion can be the most destructive type of corrosion as it can quickly render an engineering system ineffective (e.g. rapid corrosion through a pipe wall). The initiation of pitting corrosion can be the result of many factors, most notably the initiation of corrosive attack through breaks in a passivation layer, or attack of a passivation layer by the presence of certain anions such as chloride. Pitting can also be initiated from inclusions in a metal surface, such as MnS inclusions in steel, or through the initiation of a differential aeration cell, described later.

The effect of pitting corrosion in a stainless steel surface can be seen in Figure 10. Inclusions and small passivation layer breaks can result in a localised area of the metal surface being made anodic. The anodic area of the metal surface is oxidised and metal is lost to the electrolyte, and electrons are liberated to the metal, or inclusion cathodic areas.

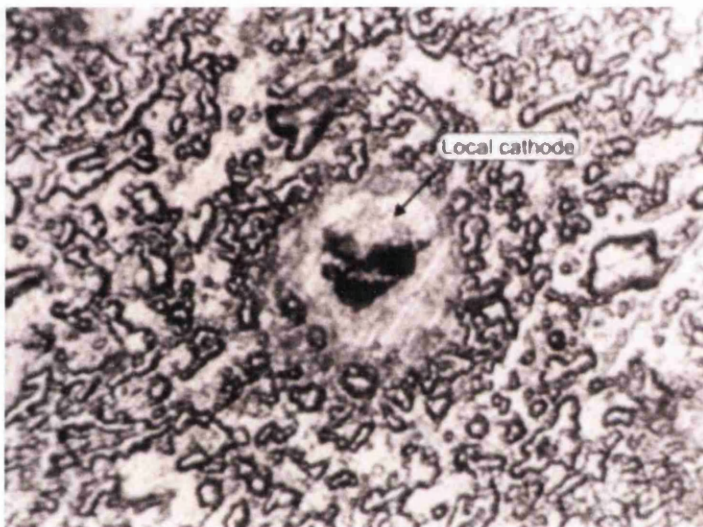
Cathodic polarisation protects the area around the hole from removal and so the corrosion does not spread across the surface of the metal. Very destructive corrosive activity is promoted when the pit becomes covered with corrosion product. This sets up a

differential aeration system as the corrosion product provides a barrier for oxygen transport.

In the presence of certain cations, e.g. halides, the system becomes autocatalytic; the localised increase in metal anions attracts cations to resulting in the creation of acidic conditions via the following reaction;



The subsequent decrease in pH will accelerate the metal dissolution reactions.



**Figure 10 - Pitting Corrosion of a 304L Stainless Steel Surface [31]**

### **1.2.13 Crevice corrosion**

This is a very similar system to pitting corrosion and if at all, is separated by the initiation mechanism. Crevice corrosion is also a differential aeration corrosion mechanism with the same resultant destructive capabilities as pitting corrosion. Instead of a barrier to oxygen transport created by corrosion product the differential aeration system is set up by a stagnant electrolyte in the crevice restricting the transport of oxygen to the crevice depths.

Oxygen is required for the cathodic site reaction and so the reaction rate is proportional to oxygen concentration. Oxygen is replaced much faster outside of the crevice and so the cathodic site migrates from the crevice (potential initiation site) to the exterior surface, see Figure 11. Again, as in pitting corrosion, negatively charged species are attracted into the crevice and possible acidic conditions develop.

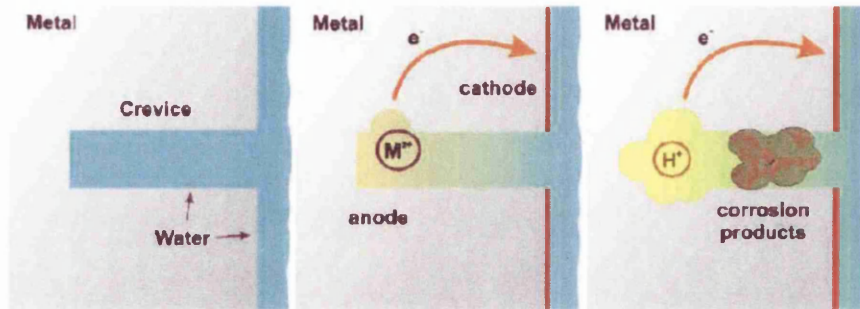


Figure 11 - Crevice corrosion steps [30]

#### 1.2.14 Differential aeration

This is the process by which a barrier to oxygen movement, whether this be a mechanical function, e.g. crevice/crack structure, and the electrolyte distance to travel, or the presence of a barrier layer or corrosion by-product, exists and sets up a cathodic site where the replacement of oxygen can proceed. This also dictates where the anodic site is located. The classic example of a differential aeration system is the water droplet corrosion system, see Figure 12.

Here the barrier to oxygen transport is the thickness of the electrolyte layer. Oxygen is non-polar and therefore the highly polar electrolyte offers resistance to transport. This resistance locates the cathodic sites to the minimum distance for the oxygen to travel and also locates the anodic sites into the centre of the water droplet. The continued corrosion activity results in a ring of corrosion product surrounding an area of metal removal when viewed from above.

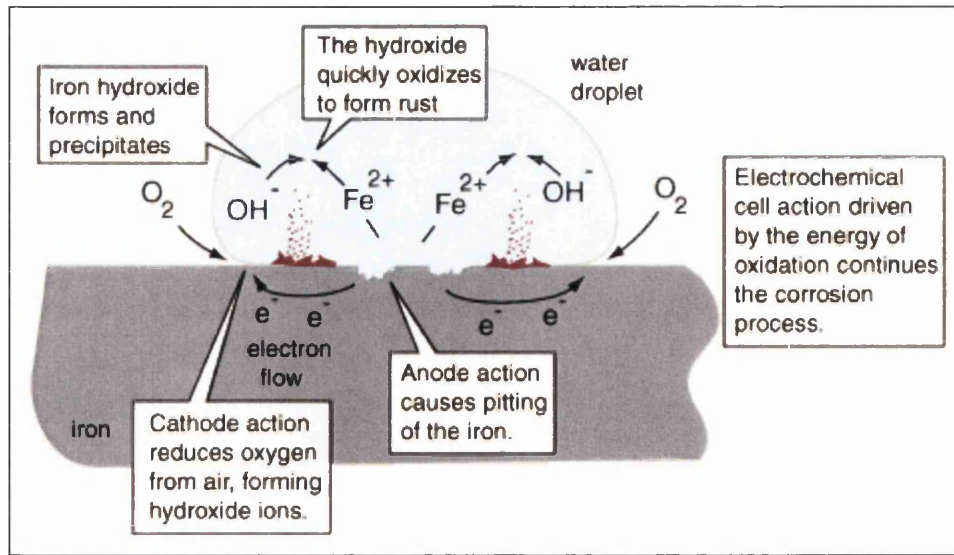


Figure 12 - Water droplet corrosion mechanism [30]

### 1.3 Metallic coatings

Considering the information detailed above it is not hard to see why considerable effort is made to provide mechanisms for the protection of the expensive steel engineering system from the detrimental effects of corrosive attack.

One tried and tested method for the protection of steel is galvanising. Named after the Italian scientist Luigi Galvani who identified the generation of an electric current from the connection of two dissimilar metals, albeit whilst dissecting frogs [32, 33].

Metallic coatings can be sacrificial corrosion protection systems or barrier protection systems and this classification is ultimately due to their position in the electrochemical series, or similarly to their standard electrode potential relative to the protected substrate, i.e. iron or steel.

#### 1.3.1 Hot dip galvanising

Metallic coatings, certainly in the steel industry, are overwhelmingly prepared by immersing the steel strip through a bath containing the liquid metal of the intended coating alloy.

Other preparations methods exist such as electrogalvanising, where a zinc surface can be formed on steel through the passing of an electric current through the steel substrate and a conductive electrolyte and into a zinc anode. The zinc is liberated into solution from local anodic activity and is attracted to the steel cathode to electrically neutralise itself and re-deposit itself as metallic zinc. This tends to be a much more expensive coating technology than hot dip galvanising but can offer some benefits compared to the hot-dip coating technology [34].

### **1.3.1.1 Production of metallic coated steels**

Metallic coated steels are produced throughout Europe [6] with each of the main steel producers tailoring their coated product lines for the intended product or market. In 2005 Corus Colors produced approximately 1 million tonnes of pre-finished steel, with metallic, metallic and organic, or organic only coatings.

### **1.3.1.2 Alloying chemistries used in metallic coatings**

Many coatings for steel exist in the market place, some offer sacrificial corrosion protection for the steel substrate, some offer barrier protection, whilst higher specification coatings offer combinations of both. The simplest of coatings is hot dip galv, TSE's offer in this market is Galvitite<sup>®</sup> (GI) and with processing changes GI can make an iron-zinc intermetallic alloy coating called galvanneal, (GA) that we will discuss later. Zinc-aluminium coatings contain the Galfan<sup>®</sup>, or TSE's Galvalloy<sup>®</sup> (ZA) varieties, and Galvalume<sup>®</sup> (AZ), a zinc-4.8wt%Al coating. Additions of magnesium to the ZA type alloy has been a recent development in the steel industry and has resulted in a range of new hot dip coatings with TSE's offer into the market called MagiZinc<sup>®</sup>. Hot dip

coatings are prepared with no zinc, for intermetallic control aluminium-silicon coatings are used in products similar to TSE's Aludip®.

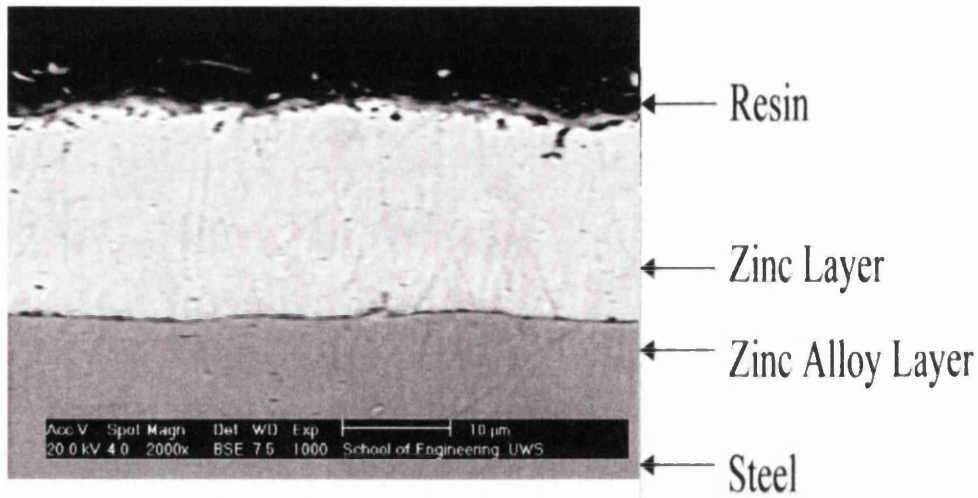
Metallic coatings that require sacrificial corrosion resistance usually contain zinc in the coating formulation as zinc is electrochemically more active than iron in the electrochemical series. Zinc can have limitations in use as the melting point of zinc is 419.6°C, prohibiting its simple use in high temperature applications. For applications such as exhausts aluminium based coatings are used as they give an increased useful temperature range, up to approximately 590°C.

TSE's GI product is the rudimentary zinc coating with very low alloying additions to the zinc bath. If left unalloyed the molten applied zinc will have sufficient heat to promote the formation of iron/zinc intermetallic compounds with the steel substrate by reaction diffusion.

The alloying addition of 0.15% aluminium to the bath inhibits the formation of iron/zinc intermetallics as the formation of iron/aluminium intermetallics is energetically preferred. 0.15% aluminium is sufficient to produce a continuous thin film and restrict the reaction diffusion of iron into the zinc coating.

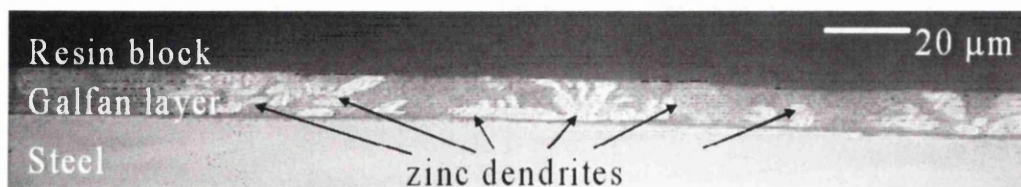
Once cooled the coating can be seen as a homogeneous zinc layer with a thin Fe-Al intermetallic on top of the steel substrate, see Figure 13. The surface of the coating can, by the additional of lead (<0.2%) be made to form a 'spangled' surface where flowered grains form from the cooling nucleation effects. Increasing the amount of nucleation decreases the size of the spangles. Ultra-smooth coatings can be created with the combination of the effects of spangle minimisation (zinc dusting, or steam or diammonium phosphate solution blowing) and temper rolling [35].





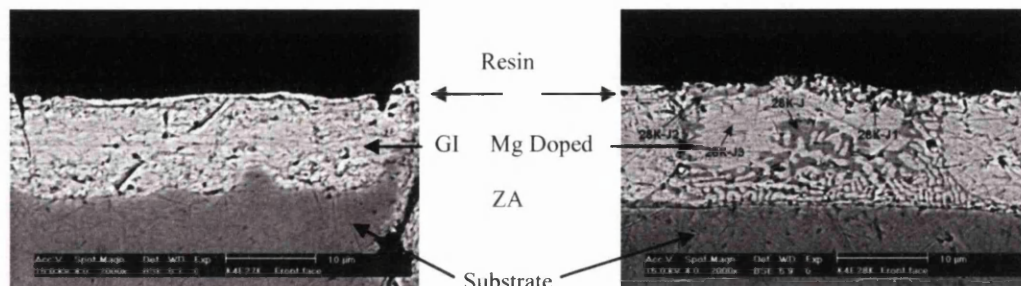
**Figure 13 - Cross section micrograph of Hot Dip Galv [36]**

Aluminium additions to the zinc galvanising bath have been known for many years with the development of Galfan<sup>®</sup> about 30 years ago by the International Lead Zinc Research Organisation. Galfan<sup>®</sup> is based on the alloying of Aluminium and Zinc with controlling additions of Misch metal (a mixture of rare earth metals) to aid wetting and improve flow characteristics. Galvan<sup>®</sup> stimulated the development of Galvalloy<sup>®</sup> (ZA) by Corus Colors Ltd. In Galvalloy<sup>®</sup> aluminium is alloyed at a level of 4.6 – 5% which results in a hypereutectic alloy of aluminium and zinc with no additions. Once cooled the coating microstructure is seen as a series of large domains in which a lamellar structure of pure zinc crystals exists in an Al/Zn eutectic mix, see Figure 14. Depending on the rate of cooling small amounts of primary zinc can be formed on the steel substrate due to the slight excess of Zinc above the eutectic composition being liberated offering a detrimental effect to coating delamination resistance at cut edges [9, 37].



**Figure 14 - The microstructure of Galfan [38]**

It has been seen that the addition of magnesium at levels of 0.01-0.05% in the formation of the Galvalloy® coating has an increase in the resistance of organic coating delamination, but a reduction in the cut edge corrosion performance, see Figure 15a) and b).







**Figure 15 - Microstructural changes in the addition of Mg to GI a) GI and b) Mg doped GI [2, 22]**

Magnesium has a higher affinity for oxygen than zinc and also is limited in its solubility in a zinc matrix due to the vast differences in atomic size; zinc's atomic size is 0.131nm and magnesium's atomic size is 0.16nm. This partitions magnesium away from zinc in the microstructure of the coating which will enable the magnesium to act as a sacrificial corrosion inhibitor for the zinc layer, both enabling zinc to delay its corrosion activity and allowing time to build up a passivation layer of deposited zinc oxides and; depending on environmental conditions, magnesium oxides, hydroxides and simonkolleite,  $Zn_5(OH)_8Cl_2 \cdot (H_2O)$ .

Within the microstructure of galvanised coatings the magnesium acts to promote the formation of a finer grained primary zinc phase while also depressing the amount of zinc rich intermetallic present, see Figure 15. This increased amount of primary zinc is the reason the cut edge corrosion resistance is decreased with increasing alloying additions of magnesium [39-43].

Tata Steel Europe has developed a Zn-1.6wt%Mg-1.6wt%Al coating called MagiZinc<sup>®</sup> (MZ) that has been proven to have superior corrosion performance characteristics over conventional hot-dip galvanised coatings in salt spray testing. Thinner coatings are offered to provide the same corrosion performance as conventional hot dip galv that are both price and environmentally beneficial [44]. This coating chemistry fits into a range of Zn-Al-Mg coatings that are currently available in the market place, see Table 2.

Competitor	Product(s)	Composition	Process	Coating Range [g/m <sup>2</sup> ]	Market / Application
	ZMg EcoProtect	Zn -1.0Mg-0.5Al	HDG	60 – 350	Automotive
	ZE- Mg	Zn + 1micron Mg	EZ	35 - 75	
	Corrender, ZM	Zn-2.0Mg-2.0Al	HDG	90 - 200	Construction
<b>Nippon Steel</b>	SuperDyma <sup>®</sup>	Zn-3Mg-11Al-0.2Si	HDG	90 - 565	Construction, highways
	DymaZinc <sup>™</sup>	Zn-0.5Mg-0.2Al	HDG	> 225	Engineering, Petrochemical
	ZAM <sup>®</sup>	Zn-3Mg-6Al	HDG	60 - 500	Construction, DA
	SuperZinc <sup>*</sup>	Zn-0.1Mg-5Al	EZ	-	Automotive
	MagiZinc <sup>®</sup>	Zn-1.6Mg-1.6Al	HDG	140	Construction, Automotive

**Table 2 - Commercially available Zn-Mg coatings [45]**

Galvalume<sup>®</sup> (AZ) is a more highly alloyed zinc coating compared to ZA with 55% aluminium and 1.6% silicon. The composition offers the highest alloying levels of Aluminium that still offers the sacrificial corrosion protection offered by the zinc's presence whilst also offering the barrier resistance from the aluminium.

The typical AZ coating microstructure consists of primary aluminium dendrites surrounded by the remaining zinc rich inter-dendritic eutectic material; in which are found small silicon rich particles, above an Fe/Si/Al intermetallic layer, see Figure 16.

AZ has been shown to offer superior corrosion protection [46]. It has been shown that the inter-dendritic zinc is the first of the microstructural components to be lost though

sacrificial protection of the steel substrate. Once corrosion initiates the corrosion rate is reduced compared to traditional zinc coatings as the zinc rich inter-dendritic regions sacrificially corrode leaving corrosion products in the channels, reducing transport of oxygen to the deeper zinc rich sites. AZ products typically exhibit lifetimes of 4x that of traditional hot dipped galvanised coatings, leading to their use in the construction market as roof and wall claddings, particularly when subsequently coated with corrosion treating primers and organic based paints or coatings.

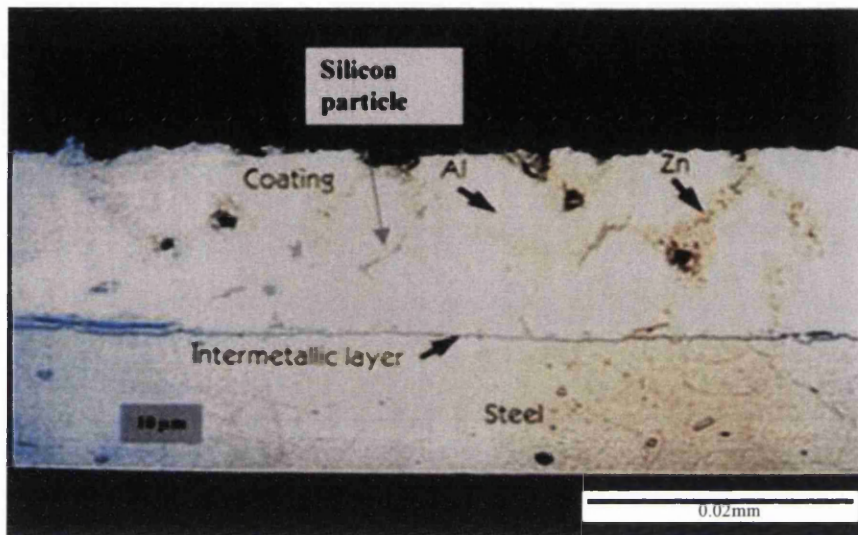


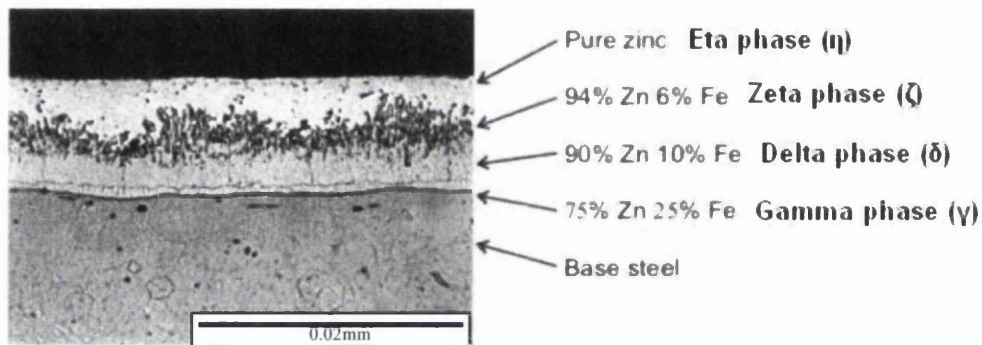
Figure 16 - Coating Microstructure of Galvalume [5]

### 1.3.1.3 Galvannealing

Secondary heating of the GI product allows controlled use of the reaction diffusion intermetallic formation mechanism. Applying additional heating the strip (temperatures ranging from 475 – 500°C) immediately after dipping will breakdown the Fe-Al intermetallic coating allowing reaction diffusion to proceed. The resulting coating contains  $\delta$  phase intermetallic,  $\text{FeZn}_7$ , which forms a columnar structure, the grain boundaries run from the steel substrate to the coating surface vertically, see Figure 17. Other phases are also present depending on the amount of Fe diffusion.

This coating has good powdering resistance when formed as the coating will crack along the columnar grains significantly reducing the likelihood of shear stresses to delaminate the coating, plus offers excellent paintability due to the increases keying points. The coating still offers sacrificial corrosion protection and as such is a widely used product for the automotive body panel market.

Time and temperature dependencies control the coating alloying level with successful galvanneal coating chemistries consisting of four discrete iron-zinc phases.



**Figure 17 - The microstructure of Galvanneal [47]**

### 1.3.1.4 Hot dip coating drawbacks

Along with expensive additions of intermetallic controlling, or oxygen reducing elements to the bath chemistries, some of which can give negative effects (excess silicon in AZ with precipitate as silicon rich hard particles which can lead to internal cracks when formed), there are other factors which limit hot dipping production lines.

All the products mentioned above have a microstructure developed from the cooling of the coating to ambient. Until solid, the coating surface will be sensitive to any contact and as such hot dipped lines have a distance from the bath surface to the first roll in which cooling takes place; other factors such as coating thickness (air blow velocities) and spangle size control (dusting etc.) do, or can, take place in this region also. Therefore, without having unlimited equipment footprints the strip speed is governed by

the ability to cool the strip, with the required coating thickness, before the contact is made with the first post-bath guiding roller.

With the temperatures of the hot dipping process reaction diffusion can also allow the increase of Fe composition in the bath. The same affinity for intermetallic formation, which governs the amount of reaction diffusion in the coated strip, makes formation of intermetallic compounds in the bath spontaneous. The intermetallic compounds form what is called dross, which needs to be skimmed off the bath surface before it becomes entrapped in the formed coating.

### **1.3.2 Hot-dip coating solidification**

Coating solidification occurs under pre-determined rules governed by the equilibrium phase diagram for the alloy composition. Figure 18 and 19 show the binary phase diagram for zinc and aluminium and can be used to predict the phases present for a set composition at a certain temperature. Under equilibrium cooling conditions the phase diagram can be used to predict the amount of primary zinc and eutectic phase that should form. At the eutectic composition and at equilibrium cooling the phase diagram predicts the alloy will instantaneously freeze as eutectic phase only.

The solidification of zinc aluminium has been studied in depth [48] and it has been seen that hypereutectic zinc aluminium coatings solidify by the nucleation of a cell of zinc primary phase, at a rate and dispersion associated with the process

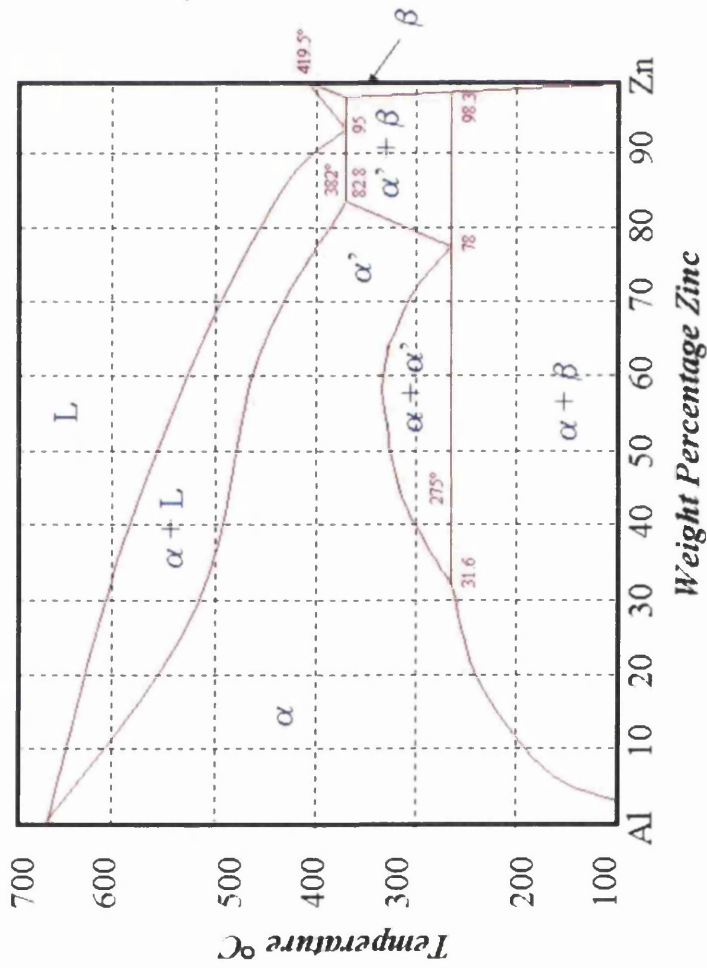


Figure 18 - Binary Phase Diagram for Zn/Al [2]

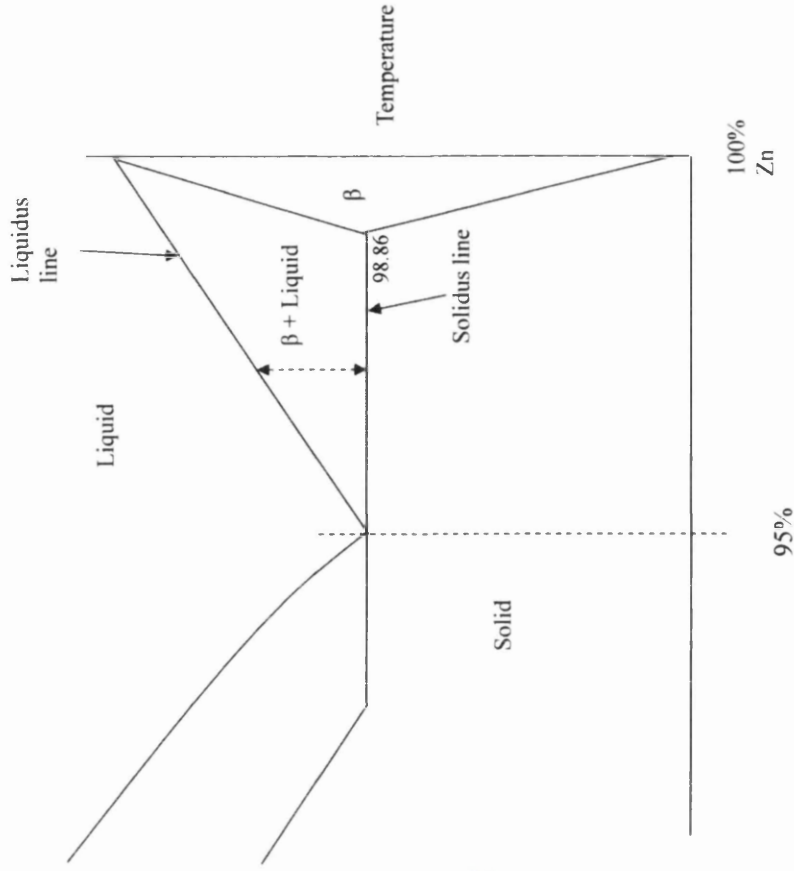


Figure 19 - Zn Rich Area of Zn/Al Phase Diagram [2]

cooling condition at the surface of the substrate at a degree of undercooling from the eutectic temperature [49, 50], followed by dendritic growth governed by the rejection of solute atoms from the solidification front of the primary phase. At a second stage of under cooling the eutectic phase nucleates around the primary zinc dendrites, on the surface of the primary zinc.

Nucleation at the surface of the primary zinc phase provides a reduction in the concentration gradient for primary zinc towards the surface with the surface being comprised entirely of eutectic phase. The nucleation and growth of primary zinc dendrites, combined with a volume reduction from the cooling and solidification results in depressions between the eutectic cells. Some elements may also be incorporated into the bath chemistry such as antimony<sup>7</sup> and lead, as these elements can be found in zinc ores as impurities. These elements can be segregated to the eutectic cell boundaries where they can cause issues such as cracking and corrosion site initiation.

Hypoeutectic alloys of zinc and aluminium have been seen to nucleate primary aluminium dendrites where haloes of eutectic are nucleated. It has been seen in studies of zinc aluminium alloys of near eutectic compositions that the nucleation of the eutectic phase in hypoeutectic alloys occurs at lower levels of undercooling than in hypereutectic alloys, where the nucleation of eutectic phase is seen at higher undercooling levels on primary zinc dendrites [51]. It is therefore concluded that aluminium is a greater nucleation site for the binary zinc aluminium eutectic.

The eutectic structure solidifies in cells of lamellar structured zinc and zinc aluminium phases that separate by diffusion controlled mechanisms ahead of the solidification front. Localised concentration differences can result in the second minor phase being encapsulated within the continuous phase as rod shaped minor phase components.

---

<sup>7</sup> Antimony used to be intentionally added as a grain refiner to the bath chemistries.



Incorporation of magnesium in the alloy results in a depression of the eutectic temperature. This will have the effect of increasing the percentage of primary zinc. The effects of magnesium additions has been studied by Nippon Steel and seen to improve the surface inter-granular corrosion resistance overcoming detrimental effects on tramp elements such as lead and tin [1].

Other elements such as lead, tin, silicon, beryllium and cadmium additions into zinc aluminium binary alloys can also give benefits to the coating. Lead, tin and cadmium can help with the coating appearance as they help with reducing the interfacial energy of the coating and promote spangle formation. As in AZ coatings, silicon can help in the reduction of iron diffusion into the coating by the formation of an intermetallic boundary layer.

Microstructural changes have also been investigated when the coating thickness is increased for the same steel gauge, resulting in changes to the amount of primary zinc dendrites detected in the coating for the same original composition of molten bath alloy with decreasing coating thickness, and an increase in corrosion losses from the thinner coatings [38].

### **1.3.3 Processing conditions**

It can be shown theoretically that the degree of undercooling,  $\Delta T$ , has a marked influence on the solidification of the coating. Undercooling is the temperature of a liquid below its phase transformation temperature before the phase transformation takes place, i.e. a liquid could be 5°C below the temperature of the expected phase transformation,  $\Delta T$  then equals 5. During strip steel galvanising the cooling rate can be varied by the increase or decrease of cooling steam spray volume or gas jets flows onto the molten zinc surface.

In the case of zinc galvanising, heterogeneous nucleation of a primary zinc cell will result in growth of a new dendrite if the free energy change associated with the growth of the

dendrite is greater than that associated with the cell's re-dissolution into the bulk liquid. The balance of whether the cell re-dissolves or whether the dendrite propagates is due to the initial size of the dendrite, according to the equation;

$$r^* = \frac{2\gamma_{SL}}{\Delta G_v}$$

Where,  $r^*$  = critical radius size

$\gamma_{SL}$  = interfacial energy between cell and liquid, and

$\Delta G_v$  = free energy change per unit volume

when at temperature  $T_e$ ,  $\Delta G = 0$ , or isothermally;

$$r^* = \frac{2\gamma_{SL}T_e}{L\Delta T}$$

Therefore for increased undercooling the critical cell size,  $r^*$  will decrease, which will promote the growth of the dendrites from smaller nucleation cells, and increase the overall number of dendrites.

### 1.3.3.1 Substrate gauge

The heat stored in the substrate has the effect of slowing the cooling mechanism of the coated product, so with consistent process conditions it is expected that the coating microstructure will be affected due to the smaller values of  $\Delta T$  associated with the reduction in cooling gradient over the thicker profile.

### 1.3.4 Physical vapour deposition

Physical Vapour Deposition encompasses many different techniques for depositing a coating or film onto a surface [52]. The most commonly operated processes are those relating to the production of packaging material such as foil coating of polymer films as used in crisp packets, to the building of silicon chips and even the coating of reflective

layers in office-type fluorescent light fittings. The deposition technology tends to be slower, or more energy demanding than hot dip coating technologies and therefore is targeted to manufacture thin films or coatings, of the order of a few microns, as opposed to hot dip coatings which can produce coatings up to many 10's of microns.

Each variation of the technology shares common principles and techniques to ensure the finished product has the desired properties and characteristics. A basic understanding of these principles is important in understanding the peculiar design of the equipment, and how this will affect the industrialisation of the technology. The desired characteristics of the product are also wholly dependent on the operational processes of the equipment, and it is important to determine the correct parameters to deliver a satisfactorily functioning product to the customer.

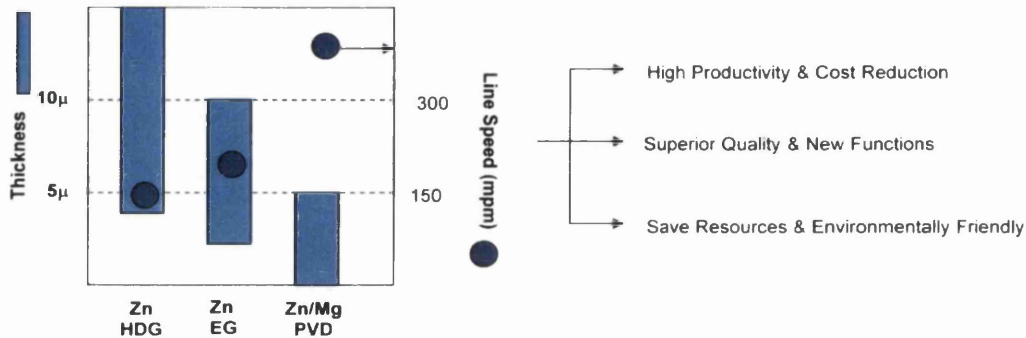
Tata Steel Strip Products Ltd. is currently investing in the development of new technology to produce a new product initially for the construction market, and possibly into the automotive sector later [53].

The technology involves the controlled evaporation of a metal, or metals, from a levitated molten droplet, and the containment and channelling of the vapour towards an awaiting strip steel surface. The technology is called Electromagnetic Levitation (EML), and the process is called EML-PVD, or EMELY.

The vision of the development team is to deliver a PVD unit that can be retro-fitted onto an existing strip line; e.g. a Colorcoat® or a CAPL line, and coat without reduction in line operating speed. With the current requirements of the technology this unit requires an estimated €30m investment.

On examination of the potential applications of the technology an opportunity exists for providing a competitive product into the construction and possible automotive market sectors whilst providing additional benefits of releasing some galvanised steel capacity for delivery to an expectant market.

TSE's initial view of the technology is in the coating of strip steel with zinc and magnesium based coating that can compete with its anti-corrosion range of hot dipped products such as Galvitite® and Magizinc®. The idea is being sold on the idea that there are significant line speed and performance improvements over conventional coating methods and chemistries, see Figure 20.



**Figure 20 - Graphical representation of PVD benefits [54]**

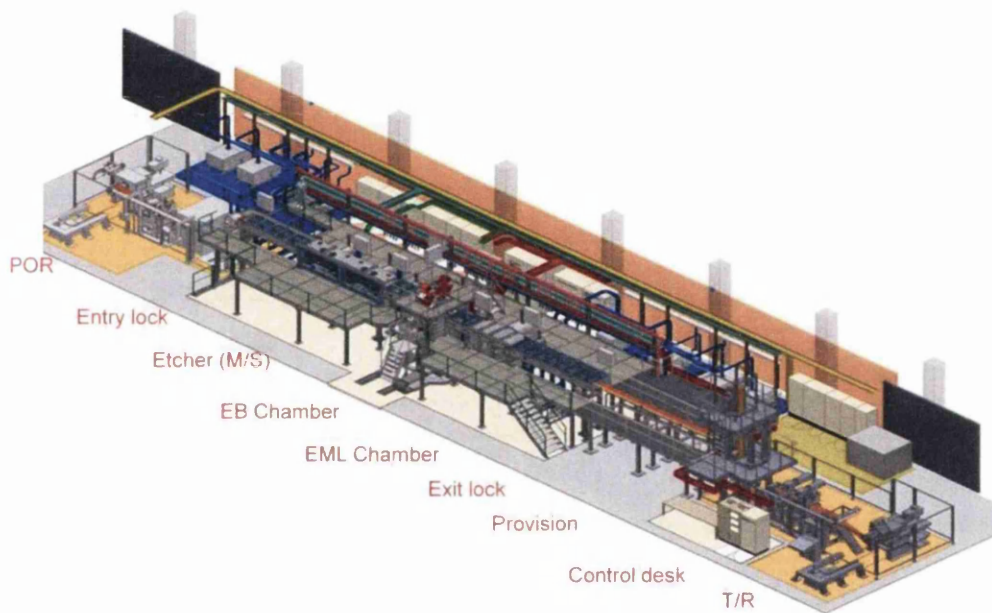
Early on in the development programme an opportunity arose to work collaboratively with another major player in the global steel manufacturing market, POSCO. At the time there were engineering solutions for the use of PVD to produce specialised coatings for steel strip or components, such as Jet and Electron beam, but these have limitations, or drawbacks. An agreement was made between TSE and POSCO to work together on the development of EML-PVD into a production scale technology with either company working on different areas of the development programme.

TSE has taken the lead with developing the evaporator technology and refining control systems to ensure the process run smoothly and consistently. POSCO have taken the lead in developing the line engineering to ensure coils of material can be passed through a vacuum system at production speeds.

After initially working with Corus on a drum type coater for the initial PVD coating investigations POSCO commissioned Von Ardenne to build a line size vacuum coater

capable of running 300mm width coil through a vacuum sufficient to produce PVD type coatings (pressures in the order of  $1 \times 10^{-3}$  mbar). The POSCO Pilot Line 200 (PPL200), see Figure 21, has been installed and is currently being commissioned for various evaporation methods including EML-PVD.

The PPL200 is being used to investigate the engineering solutions behind maintaining a sufficient vacuum at line speeds approaching the 300m/min (200m/min has been successfully completed [55]), see Figure 21.



**Figure 21 - Schematic of PPL200 [55]**

### 1.3.4.1 Industrialised processes

A closer, technical look at the current evolution of the technology is available later in this text but initially it is worth noting that the technology can operate at potentially unlimited speeds matching those possible on CAPL lines.

Using average figures of 200m/min line speed, strip width of 1.279m and 1.2mm gauge it has been shown that the PVD process can return £10m [56] to the business per annum, an

attractive prospect. There are also additional benefits in that the increased speed of work allows more of the Port Talbot (PT) slab to be processed through the PT Hot and Cold Mill.

### **1.3.4.2 PVD Process Steps**

In its most basic terms PVD involves the vapourisation of a source material or materials, whether these be elements, alloys or compounds, from a solid phase, usually but not exclusively through a molten liquid phase, into a gaseous phase before transfer and condensation onto a component or surface undergoing coating.

The steps therefore are a heating step, a channelling operation and the final condensation step that produces the required coating. The heating step is usually a very rapid, high energy density heating technique. A channelling step ensures the generated vapour cloud is directed towards the strip, increasing yield and decreasing operational costs. The condensation step requires movement of the component/strip to ensure fresh surface is exposed to the depositing atoms and controlling the way the coating forms.

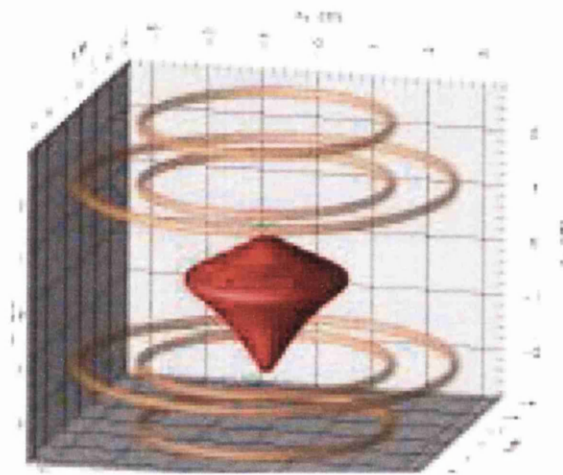
We will continue to look into these individual steps and the solutions that TSE are investigating to eliminate or reduce problems, or make potential use of these effects in possibly improving the final coating characteristics.

### **1.3.4.3 Evaporation and EML-PVD**

We have learned in a previous publication [57-59] that there are many different types of evaporation method each with its own benefits and drawbacks. For comparison we look at Jet PVD [52, 60, 61], a process where solid lumps of elemental metal, or alloy are added to a crucible before induction energy fields permeate through the walls of the crucible to heat the source. With certain elements of small atomic size they behave more aggressively towards the walls of the crucible, with aluminium being particularly

aggressive against anything other than boron-nitride [62]. This leads to the frequent replacement of expensive ceramic materials to maintain functionality.

To combat this TSE has looked at using an already existing technology of electromagnetic levitation to suspend a metallic droplet in a induction coil (radio frequency induced) electromagnetic field [59], see Figure 22. With sufficient AC frequency the eddy current forces induce eddy currents in the electron flows of the delocalised electrons in the levitated metal. These eddy currents result in Joule heating and rapid heating of the metal occurs eventually leading to melting and later, evaporation.



**Figure 22 – Schematic Model of Tata RD&T's Evaporation Droplet [63]**

When we are discussing evaporation rate of different elements, or alloys there are some interesting properties that need to be understood, properties that will restrict the formation of certain materials. The evaporation of a metal requires heating through the melting point (additional energy is required to overcome the latent heat of fusion) to the evaporation point where additional energy can be used to overcome the latent heat of vapourisation and also to increase the evaporation rate so that the vapour pressure of the gas is sufficient for production speeds. Graphs are available to determine the temperature required for certain metals to evaporate and the vapour pressures they release at those temperatures. They are altered slightly in PVD technology due to the process being

performed under very low pressures or low vacuum;  $\sim 1 \times 10^{-3}$  mbar. The working pressures are dictated by the mean-free-path, the distance a gaseous atom can travel from evaporation to impact with another gaseous (non energetic; i.e. air) atom; this has to be greater than the distance from the evaporator to the strip otherwise energy is lost to the non-excited atom and coating adhesion and density is affected.

If we examine the working pressures and temperatures for these elements, see Figure 23, we can see that zinc and magnesium sit quite closely together and so at a temperature of approximately 800°C the vapour generated above the 33:33:33 zn:mg:al droplet will contain approximately 90% zinc atoms, 10% mg atoms and no aluminium atoms. A droplet of aluminium will need to be at  $\sim 1600^\circ\text{C}$  to achieve the same vapour pressure, put simply as a droplet of zinc at 500°C. Therefore elemental properties limit the alloys that can be laid down together by this technology, though there is no limit to the sequential elements that can be deposited and then diffusion annealed.

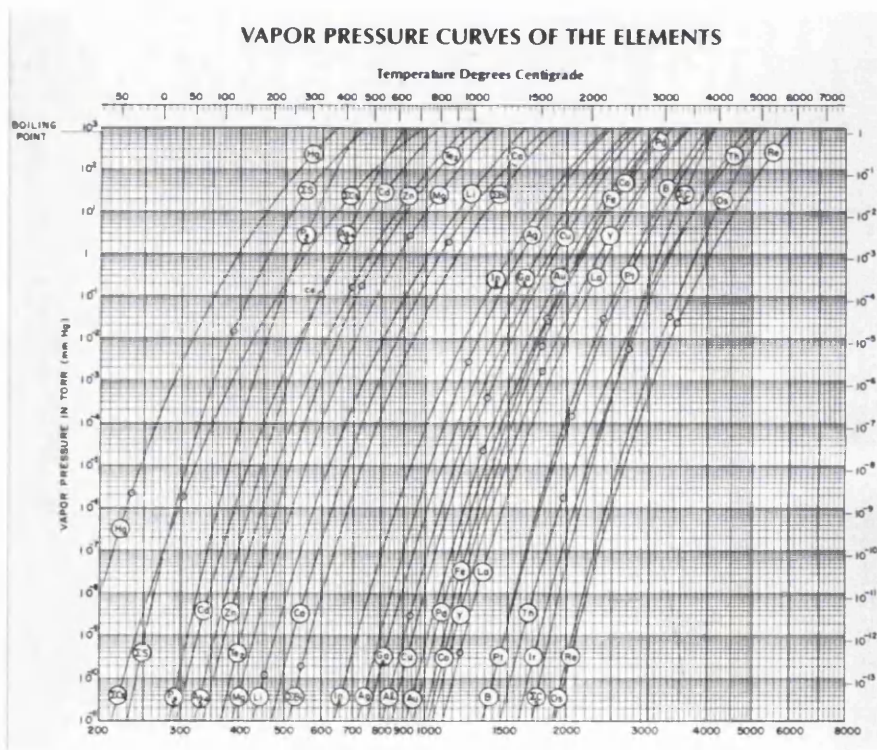


Figure 23 - Vapour pressure curves for some metallic elements [64]



#### **1.3.4.4 Possible benefits**

Two immediate benefits are recognised in this technology, one, that the droplet is levitated and so no contact exists with any crucible material and as such there is no replacement involved, saving cost. The second benefit is that the droplet can evaporate from its entire surface, increasing the possible production speed of the system.

During continuous production any system will need feeding with additional source metals or alloys. In closed systems such as Electron Beam and Jet PVD this requires provisions for the system to be topped up, outside of any vacuum or controlled atmosphere, or even to shut down the system completely. The Tata Steel system is being developed to use continuous wire feeding making it potentially possible for the system to run continuously for many production days.

It is not hard to imagine that the size of the droplet will reduce as the evaporation progresses, in so doing this also reduces the amount of energy the droplet requires from the induction coils, this in turn couples into the power system and can be read as a change in frequency. In so doing the system has an integral process control system, and so balancing the frequency of the power supply against feeding rate can make a stable, uniform evaporation rate.

#### **1.3.4.5 Possible problems**

One major hurdle to the technology being successfully implemented is controlling the stability of the metal droplet. It seems during the evaporation of the droplet (holding the droplet at energies sufficient for melting only does not show the phenomenon) that waves are induced into the surface of the droplet, either by the expulsion of the evaporating atoms or by the induction heating magnetic field fluctuations.

These waves, instead of being eliminated by the magnetic field forces pushing on the droplet seems to be reinforced by them, resulting in a turning moment. With higher and

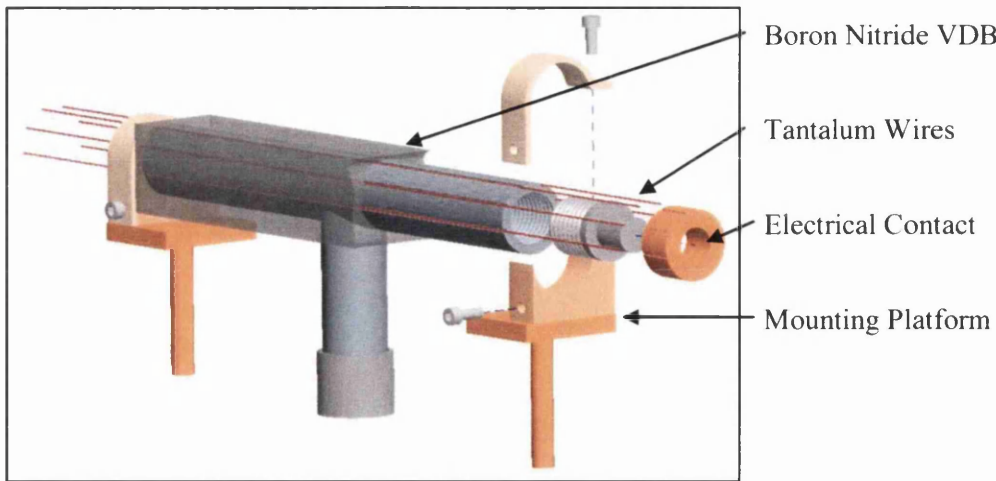
higher rates of heating (and obviously evaporation) the spinning becomes more severe and eventually results in sufficient force for the centrifugal forces to allow material to be thrown from the droplet hitting the walls of the containment tube. There is some investigation, however, in the use of boron nitride as a containment system around the droplet and possibly flooding the containment tube so that the walls stop any rotation, though this will limit the efficiency of the system and may be a last case fall back plan.

The idea scenario is that the droplet will be stabilised at high heating/evaporation rates. Tata Steel RD&T are investigating the use of strong permanent magnets and electromagnets in the system (together with the induction coil magnetic fields) to counteract the rotation forces.

#### **1.3.4.6 Channelling the vapour**

Once the vapour exists then the atoms need to be directed to the strip with the least amount of loss possible. The atoms travel supersonically, driven by impacts from those atoms being evaporated behind them. Each atom will travel on a line-of-sight vector and impact or impinge into any surface it comes into contact with. As the vapour requires channelling to the component there will likely be walls or surfaces before the component onto which condensation will be undesirable, such surfaces require heating to re-evaporate the atoms, or more accurately limit the amount of condensation on the surface.

Particular challenges exist in EML-PVD as the technology uses a vapour distribution box to channel the vapour to the widths found in CAPL products, the ultimate technological specification being 2m strip width. A schematic of the distribution box can be seen below showing the use of tantalum wires to create resistance heating so that ‘cold spots’ are eliminated, see Figure 24.



**Figure 24 - VDB with heating elements [63]**

Strip widths change frequently in TSE and methods for varying the coated width has to change in line with this, to this end this design has end plugs that can move into and out of the vapour distribution box (VDB). There is also some consideration being given to rotating the VDB so that the coated width is achieved without rendering the possibility for contaminated threads and expensive damage a real threat. This option also includes the possibility for automatic or more realistically semi-automatic changes in coated widths without the need to open the deposition chamber.

A consideration for the design of the VDB is whether or not there exists an electrical earthing system. Due to the high energy of the atoms in the vapour the excitation of atoms to ions with the required release of electrons is possible. When this occurs the electrons and ionized gas couples into the magnetic fields in the area around the induction coils and get accelerated. These ions impact the gaseous metallic atoms being evaporated creating a mixture of further excited atoms, ions and electrons and liberating light; this is a plasma. An electrically earthed VDB will cause the electrons and ions to be grounded, destroying the plasma and any potentially positive, or negative, effects it can have on the desired coating [65].

### 1.3.4.7 Condensation

Condensation is the pinnacle and the most important part of the whole operation. Much time and money can be wasted if the coating parameters are not as intended. External factors now become important such as the quality of the steel surface, both for cleanliness and surface topography, the control of strip speed, and the gauge; important for the cleaning step, the distance from the VDB, and the surface temperature.

### **1.3.4.8 Surface preparation**

One of the most important processing parameter to ensure when forming a vapour deposition coating is the cleanliness and preparation of the strip. In contrast to hot dipping where a metallic bond is formed between the steel substrate and the coating a PVD coating keys in to the substrate surface similar to how paint would key onto a rough surface better than a smooth surface albeit at an atomic level rather than macro scale.

Keying in points are etched into the surface of the strip by energetic particle impacts from a plasma. Atoms are knocked out of the surface to provide 'holes' where the depositing atoms can migrate to and nucleate the coating. It is very difficult to compare etching rates between techniques as the amount of material removed will obviously be very low and we have to look at the effect that poor etching performance dictates. Energetic coating particles, once adsorbed onto the surface, will travel to find the lowest energy position. Holes created by etching provide such low energy locations and the initial atoms have strong adhesion in these locations so the more nucleation points there are the stronger the coating will be adhered. Further energetic particles then migrate to build up crystals on top of these nucleation points.

Tata Steel's technology currently uses inverse magnetron sputtering to prepare the strip. This method uses closely couples magnetic dipoles to trap argon plasma generated by passing an electrical discharge through an argon gas flow. A magnet, sitting on the other side of the strip is used to pull some of the trapped plasma ions down onto the surface.

This technique has limitations in the gauge of the steel that it can clean due to the reduced magnetic permeability of the heavier gauge steel strip.

#### **1.3.4.9 Surface roughness**

An investigation is underway into the surface roughness effects that the uncoated strip steel has on the quality of the finished surface where it is thought that the coating will be affected by the peaks and troughs of the substrate due to shadowing during coating growth. Due to the deposition atoms arriving perpendicular to the strip (some deviation from absolutely perpendicular will arise from the engineering solution; i.e. nozzle diameter, nozzle length) a peak will be coated on the front face first, the peak momentarily and the back face secondary. This can lead to a grain boundary forming at the top of the peak though this is more likely to occur at limited surface energies where deposition atom mobility is reduced.

#### **1.3.4.10 Surface temperature**

We have discussed the fact that surface preparation is important in adhesion of the final coating, where together with etching surface energy, i.e. strip temperature, governs the amount of mobility of the adsorbed atoms on the surface. If the atoms cannot move to find the minimum energy location then they will not provide the adhesion that is required. As well as adhesion the surface energy is passed through the coating as it forms and governs the growth of the crystals. With sufficient energy, typically, for zinc based coatings, this is an approximate strip temperature of  $>50^{\circ}\text{C}$  (depends on the distance from evaporation source and the mean free path) adhesion is promoted and the coating builds up as a dense crystalline structure similar to those seen in electrogalvanised zinc coatings. Below these temperatures the coating will build up in skyscraper type grains called

columnar, but as in the analogy of a modern city the roads between the skyscrapers exposes the steel substrate for corrosive attack.

To avoid this, potentially the use of a continuous annealing line as a parent structure for a TSE PVD line will aid the process as the strip temperature can easily be controlled from the energy already input into the strip during the annealing process. These temperatures are typically in the region to initiate recrystallisation of ferrite grains (around 700°C) and so cooling would be required to achieve PVD coating growth temperatures (excess temperature will cause the PVD coating to melt and convert to a hot dipped type eutectic microstructure).

#### **1.3.4.11 Zinc-Magnesium**

As indicated above Tata Steel Europe Ltd. In 2007 launched a new hot dipped coating chemistry into the market place; MagiZinc®. This coating utilises an increased level of the grain refining element magnesium to modify the microstructure of zinc-aluminium, Galfan® type coatings, to provide an increased resistance to corrosive attack, compared to zinc only hot dipped galvanised products[46, 66-68].

This is the first of the modified zinc galvanised coatings to use elevated levels of magnesium to aid in the corrosion resistance lifetime. Another series of coatings is being investigated based on zinc and magnesium, eliminating aluminium altogether and possibly increasing the amount of magnesium.

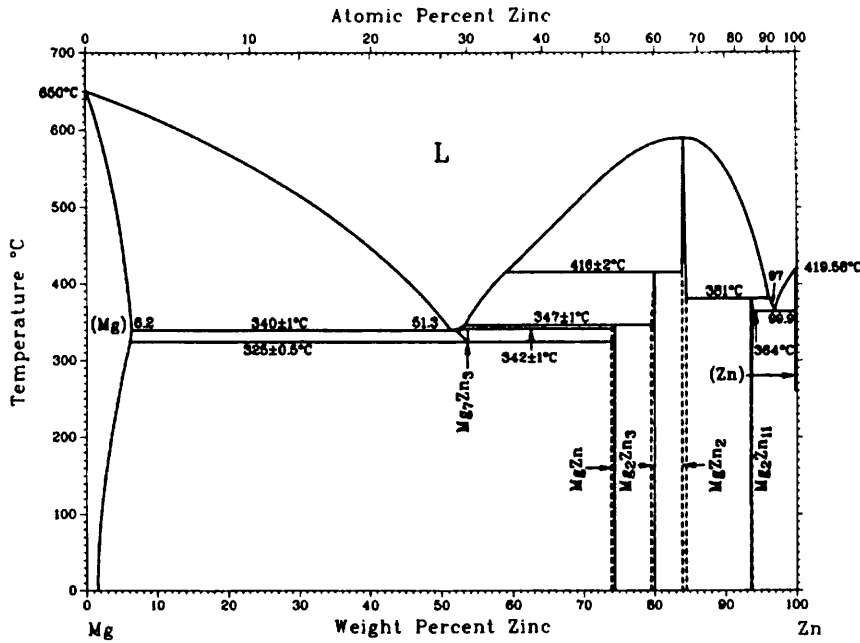
There is significant research both in the literature and ongoing in academia and in industry with many patents already existing describing single and multi-layered ZnMg coatings [52, 69-75].

#### 4.11.1 The corrosion chemistry of Zinc-Magnesium

There are many intermetallic compounds formed between zinc and magnesium as can be seen in the phase diagram, see Figure 25. Most of the work in the literature is concerned with the deposition of Mg in the range of 0-10 wt%. This, when fully inter-diffused, forms two intermetallic compounds,  $Mg_2Zn_{11}$  and  $MgZn_2$ , corresponding to the equilibrium phase diagram, see Figure 25.

Increased corrosion resistance is promoted by the increased alloying of magnesium increasing the electropositivity of the intermetallic, providing a differential in the corrosion driving forces between any formed ZnMg layer and any remaining Zn layer, or grains (the electrochemical potential difference occurs with  $Zn_{11}Mg_2$  and  $Zn_2Mg$ , with Mg dissolving out of these intermetallics to form corrosion products). It has been shown that having both intermetallics present in the coating layer promotes both fast Mg dissolution, from the Mg rich  $Zn_2Mg$  phase, to rapidly protect steel cut edges plus gradual dissolution, from the  $Zn_{11}Mg_2$  phase, and secondly to provide extended protection [72]. Table 3 shows the higher Mg concentrations possible by PVD deposition of ZnMg coatings, their relative speeds of Mg dissolution can therefore be postulated.

This is similar to differentials formed in adding aluminium into hot dipped galv products and creating a separation in the microstructure for primary and aluminium alloyed zinc phases.



**Figure 25 - The Binary Phase Diagram of Zinc & Magnesium [41]**

There is also significant discussion in the literature that the presence of ZnMg helps to modify the corrosion products formed by the corrosion of zinc in chloride containing accelerated corrosion testing [76]; evidence that does deviate from conditions in atmospheric corrosion but is still accepted by the majority of coated steel producers and their accepted, preferred testing methods of salt spray.

Zinc hydroxychloride ( $Zn_5Cl_2(OH)_8 \cdot H_2O$ ) also known as simonkolleite has been detected on ZnMg after corrosion testing together with  $Mg(OH)_2$  and, depending on the levels of dissolved  $CO_2$  in solution zinc hydroxycarbonates ( $Zn_4CO_3(OH)_6 \cdot H_2O$ ); though this is predicted more as a corrosion product of aluminium containing MagiZinc type coatings), and magnesium hydroxycarbonates (similar to  $Mg_5(CO_3)_4(OH)_2 \cdot H_2O$ ) [70].

Intermetallic	%Mg	%Zn
$Mg_2Zn_{11}$	6.3	93.7



MgZn <sub>2</sub>	15.7	84.3
Mg <sub>2</sub> Zn <sub>3</sub>	19.9	80.1
MgZn	27.1	72.9
Mg <sub>7</sub> Zn <sub>3</sub>	46.5	53.5

**Table 3 - ZnMg Intermetallic compositions**

## 1.4 Areas of research

It has been shown that nucleation rate and undercooling play an important role in the formation of a two phase microstructure in Zn-4.8wt% Al coatings [38]. Substrate gauge should also lower undercooling as thicker substrate gauges retain heat energy after exiting the hot dip coating bath, slowing the solidification process. This should have a marked difference on the two phase microstructure and the corrosion resistance properties of the coatings. Samples of 4.8wt%Al-zinc coatings have been produced in Tata Steel Colors on substrate gauges varying between 0.38mm and 1.00mm to determine the changes in the coating microstructures with respect to the reduction in undercooling. Corrosion testing will also determine the effect the changes in microstructure have on the coating's corrosion lifetime. The rate of metal loss and the mechanism for the metal loss was investigated using a combination of scanning electrochemical techniques and gravimetric mass loss analysis.

As shown in Table 2 there are many coating chemistries that are similar to the recently launched Tata Steel Europe metallic coating, MagiZinc®. This research looks to investigate changes in the alloying chemistry of the MZ coatings to see whether there are any potential benefits to slight increases or decrease to the alloying levels of the aluminium and magnesium levels in the coatings when we look at the microstructural changes and associated corrosion performance. The investigation utilised scanning

electrochemical techniques and gravimetric mass loss tests to determine comparative mass loss predictions and to investigate the mechanism for the mass loss.

To provide an indication on the next phase of development for the new coating technology of EML-PVD a requirement exists to investigate some of the first commercially attractive PVD coatings to the automotive market, namely those coatings based on zinc and magnesium that have been indicated to provide improved corrosion performance in salt spray testing, a basic qualification test for corrosion performance widely used in automotive materials testing. The PVD coatings were investigated for adhesion, comparing to the emerging hot dip coating benchmark coating MagiZinc. Corrosion mechanisms for cut-edge and the surface were investigated using scanning electrochemical techniques.

**Chapter 2**  
**Experimental Details**

## 2.0 Introduction

In the course of this work several methods were used to compare the samples' characteristics and properties.

Cross section and surface metallography were used to determine the metallic coating structure and factors associated with corrosion resistance i.e. amount of individual phases or layers present. Glow Discharge Optical Emission spectroscopy (GDOES) was used to investigate changes in composition as a function of depth. Interdiffusion of deposited elements from the PVD deposition technique was facilitated by means of the IR furnace of the Iwatani-Rhesca Hot-Dip simulator.

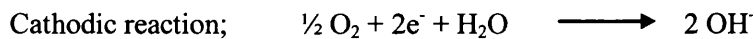
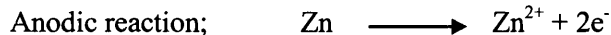
Corrosion evaluation tests used were the Scanning Vibrating Electrode Technique (SVET), cabinet tests including salt spray and humidity testing, and submerged mass loss investigations (mass loss determined by Inductively Coupled Plasma Optical Emission Spectroscopy - ICP-OES).

## 2.1 Scanning Vibrating Electrode Technique

The SVET is an evolution of an earlier technique called the Scanning Reference Electrode Technique (SRET) which has been used quite extensively in the examination of localised corrosion[8, 38, 77-79].

Put simply the SVET is a machine that controls the movement of a platinum microdisk electrode (the end of a 125µm diameter wire) through a region of electrolyte in which, if there is a corrosion phenomenon occurring, there is the migration of charged species. In the case of the iron/zinc galvanic couple, zinc has a higher electrode potential than iron and will therefore oxidise and release electrons, forming soluble  $Zn^{2+}$  cations, the electrons will move to the cathodic areas of the system. The migration of  $Zn^{2+}$  cations into solution, aided by the ionic strength of the electrolyte, is electrically balanced with

the counter reaction at the cathode which is the reduction of oxygen to form hydroxide anions, OH<sup>-</sup>.



The movement of the Pt disk through these charge regions stimulates the electrons in the wire and induces a signal; this is measured and converted, via a calibration step into current density and, via Faraday's Law, into mass loss.

### 2.1.1 Equipment Set-up

The system comprises many different elements, see Figure 26; a computer system for overall control and processing of the data, a 3-axis stepper motor controlled moving stage (capable of 2.5µm incremental movement). Obviously there is the microprobe; a Pt wire sheathed by a glass capillary, see Figure 27, a speaker (to which the probe is attached) housed in a shielding metal box; a lock-in amplifier that detects the Pt wire signal and sets the vibration frequency and amplitude of the speaker.

The sample needs to be immersed in electrolyte, therefore there needs to be a containment tank that is both inert to the electrolytes used (usually salt waters from 0.1% to 5%) and does not affect the electrical signals.

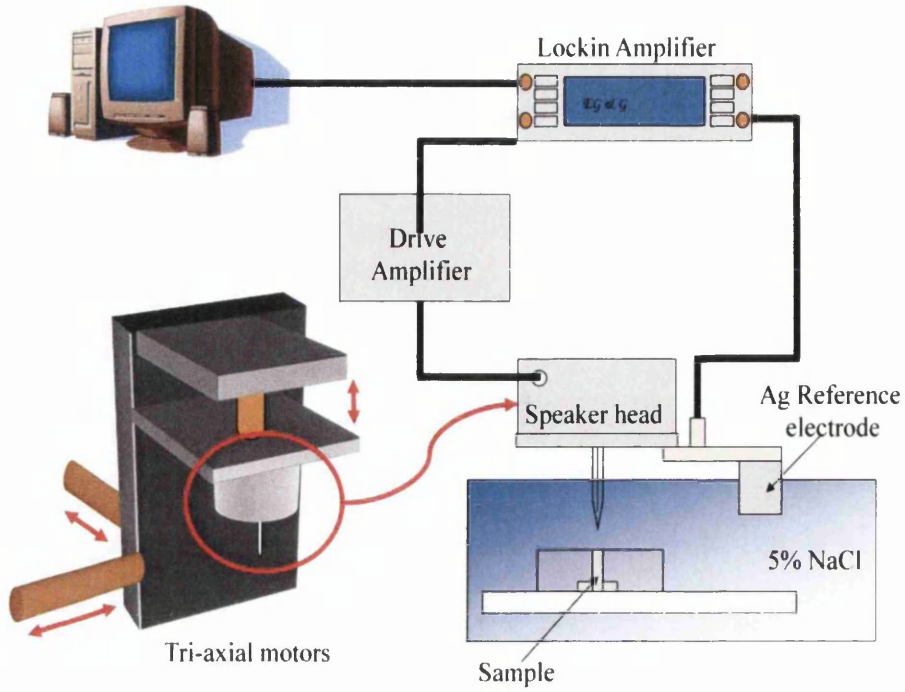


Figure 26 - SVET System Schematic [38]

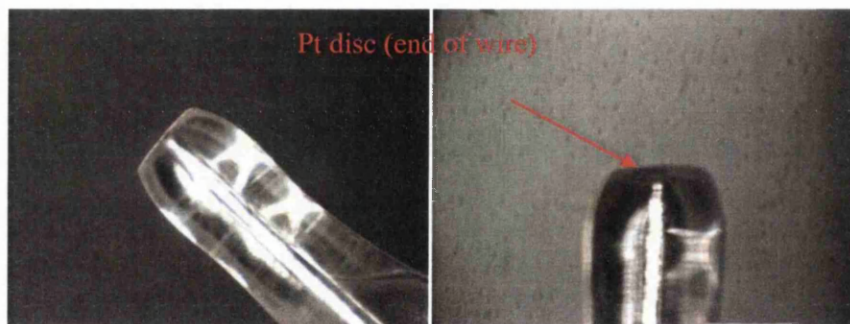


Figure 27 - SVET Microprobe

## 2.1.2 Experimental Theory

The vibration of the probe, in a region of current density, will create a signal proportional to  $A_{pp}$ , the peak to peak amplitude, the vibration frequency and the vibration distance, in the direction of vibration through the area of the current flux. As the distance from the surface, the probe vibration frequency and the probe oscillation are consistent the system

can detect, and more importantly compare and measure variations in the charge density as it scans the surface.

There is evidence that the current density above a point source gives a characteristic bell shape, see Figure 28 [80]. The intensity of the signal ( $F$ ) at any point from the point source, i.e. a distance  $x$  in the  $x$ -direction,  $y$  in the  $y$ -direction and  $z$  above the plane has been shown to be predicted by the following equation;

$$F = \frac{dE}{dz} = \frac{iz}{2\pi\kappa(x^2 + y^2 + z^2)^{1.5}} \quad [81]$$

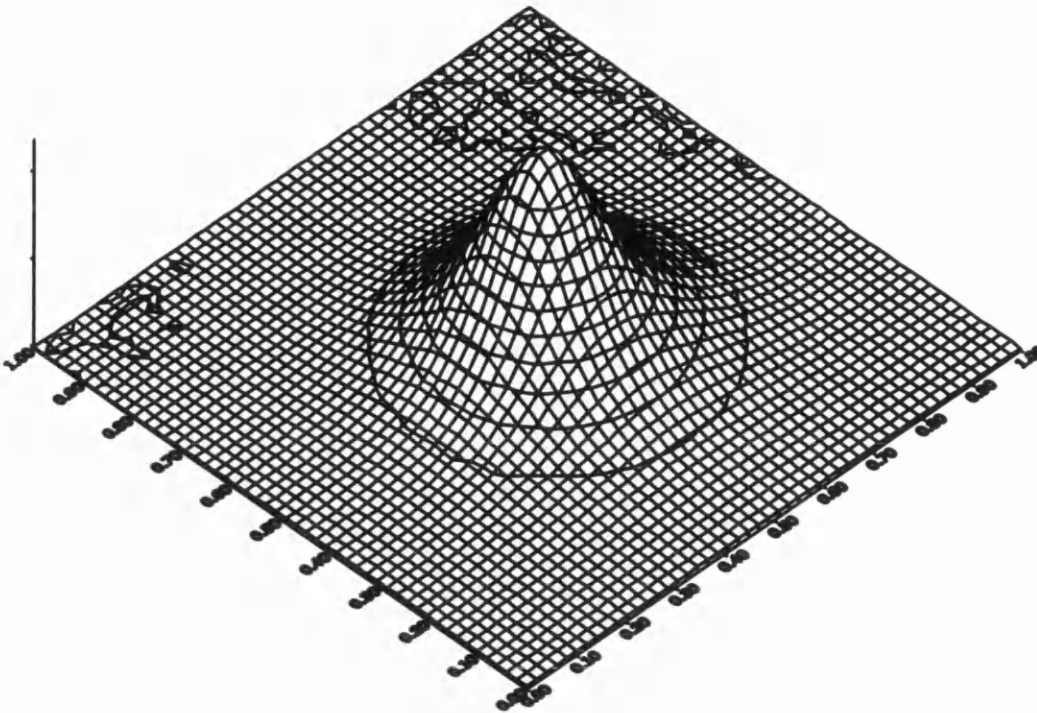
Where  $E$  is the electrical potential and  $\kappa$  is the conductivity of the electrolyte.

As can be seen in Figure 28 and can be seen from the equation (2.1) the maximum field strength can be predicted when  $x$  and  $y$  and  $z$  are 0, though the equation and indeed the SVET signal does not behave well when  $z=0$ ; i.e.

$$F_{max} = \frac{i}{2\pi\kappa z^2}$$

The SVET is usually scanned at a height of  $100\mu\text{m}$ , looking at the width of the bell curved response shows that the theoretical resolution of the SVET at this height is  $153\mu\text{m}$ . It has been seen that the measured width of the SVET bell curve at half maximum is  $0.26\text{mm}$ ; this is thought to be because of the limitations of the size of the  $125\mu\text{m}$  Pt wire in the SVET microprobe.

The vibration of the probe is controlled by using an electromagnetic driver, in the form of a simple speaker, through which a fixed signal frequency and voltage is passed. The voltage controls the vibration distance and the frequency controls the rate of vibration. Electromagnetic leakage from the loudspeaker can affect the



**Figure 28 - SVET scan over a point current source [2]**

SVET probe signal but housing the speaker system in a shielding box minimises any effect. For the purposes of this study the vibration frequency was set at 140Hz, and a drive voltage of 0.05 volts.

Previous work has shown that the vibration of the probe can be measured using strobe lighting so that individual positions of the probe at any point can be determined. The probe vibration amplitude at these settings has been measured at 30 $\mu$ m.



### 2.1.3 Theoretical assumptions and limitations

It is worth considering this because this lack of resolution, particularly when we consider the thickness of the coatings we will be examining are orders of magnitude smaller than the resolution, does result in the mass loss from the SVET scans being semi-quantitative. Also, considering the scan height there will be a decrease in the current density from being 100 $\mu\text{m}$  above the corrosion event, plus any small corrosion events whose current densities reach zero before the scan height (in the z axis) will never be seen, see Figure 29, these limitations restrict the SVET to being a semi-quantitative analysis tool.

It is worth noting that the limiting factors of the SVET occur for each scan being undertaken and as such the SVET is a good comparator tool. Indeed initial studies on the thinnest PVD coatings show responses in line with those expected.

The generated signal is inversely proportional to the square of the distance from the surface, this makes the control of height fundamental to providing comparable data. These factors have been taken into account within the control software of the system where topographical information from the sample surface can be captured so that the 100 $\mu\text{m}$  distance can be set.

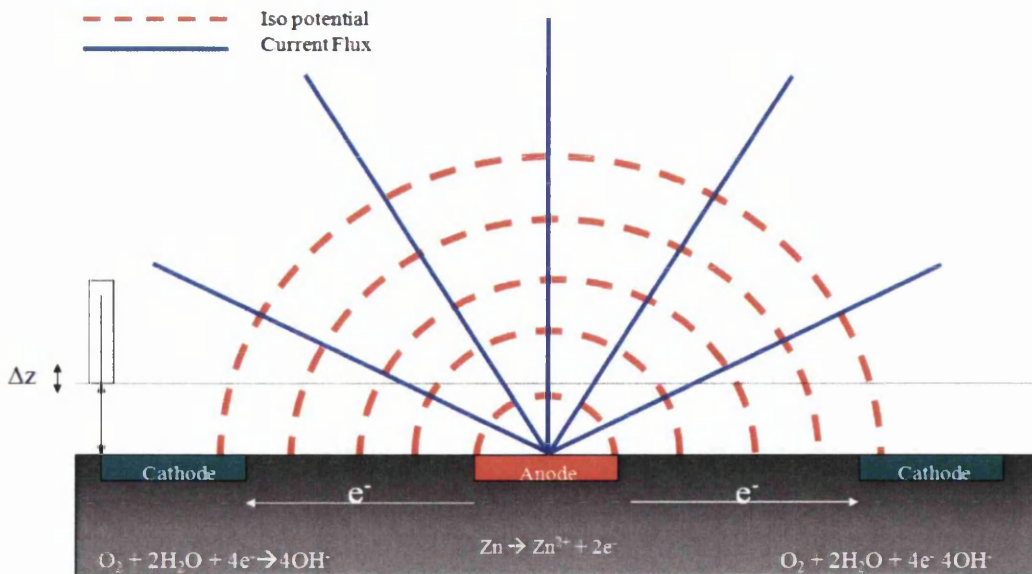


Figure 29 - Corrosion Cell Current Schematic [9]

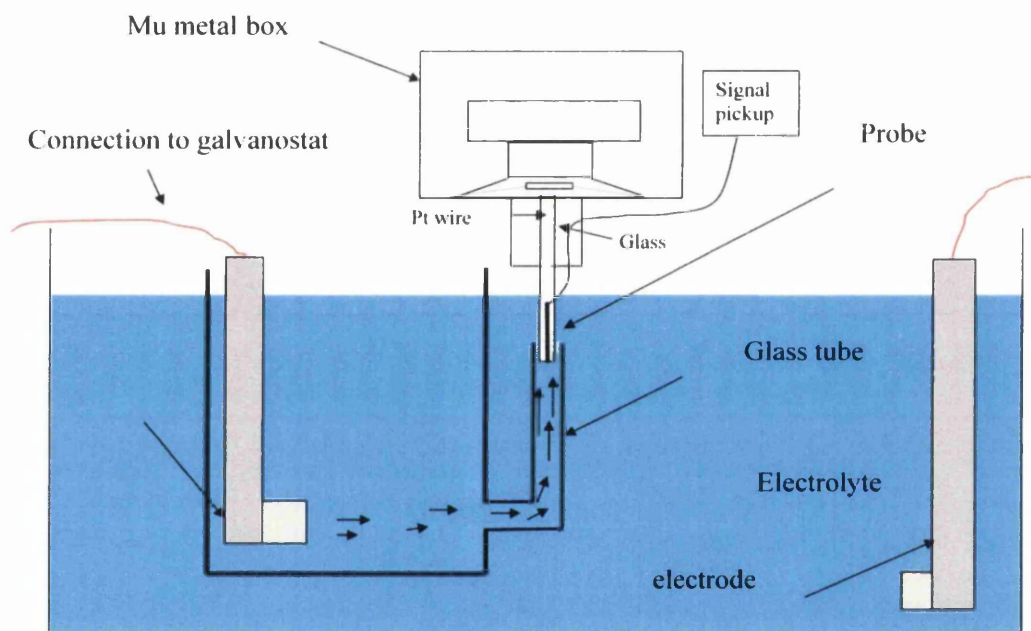
## 2.1.4 Equipment Calibration

The system is calibrated by measuring the maximum signal,  $F_{max}$ , returned when scanning over a point source that is supplying a constant current. The current can be provided accurately by a galvanostat through an embedded wire in a non-conducting plane, such as a metallographic resin mount. Scanning the area above the point source gives a characteristic bell shaped curve; see Figure 28, for each applied current. The maximum intensities can be plotted against the detected nanovolt signal to provide a calibration factor.

The usual calibration step is performed using a known cross-section charge localising calibration cell, see Figure 30. This calibration device uses a known internal diameter glass tube through which is passed a known current using a galvanostat. With the SVET probe inserted a minimum distance (approximately 10mm) into the tube the signal can be measured against the imposed current. The benefit of this approach is that the current has

been seen to be uniform across the diameter of the capillary tube and so scanning of over a point source, a timely step, is not required.

The imposed current should encapsulate the signal intensities that are likely to be seen in the scan, to this end a range of  $100\mu\text{A}$  ( $-50$  to  $+50\mu\text{A}$ ) is plotted against the observed signal to give calibration factor that the computer will use to convert the data ( $\text{nV}$ ) into  $\text{amps}/\text{m}^2$ , current density. Such a calibration plot can be seen in figure Figure 31. Calibration is usually performed before every scan and reassuringly returns a straight line plot, the slope of which is the calibration factor.



**Figure 30 - Schematic of Charge Localisation Calibration Step [38]**

SVET equipment is operated in a temperature controlled environment so that there are no thermal expansion issues that could affect the probe operating height. The baths have a sufficient surface area so that there is no barrier to oxygen diffusion,

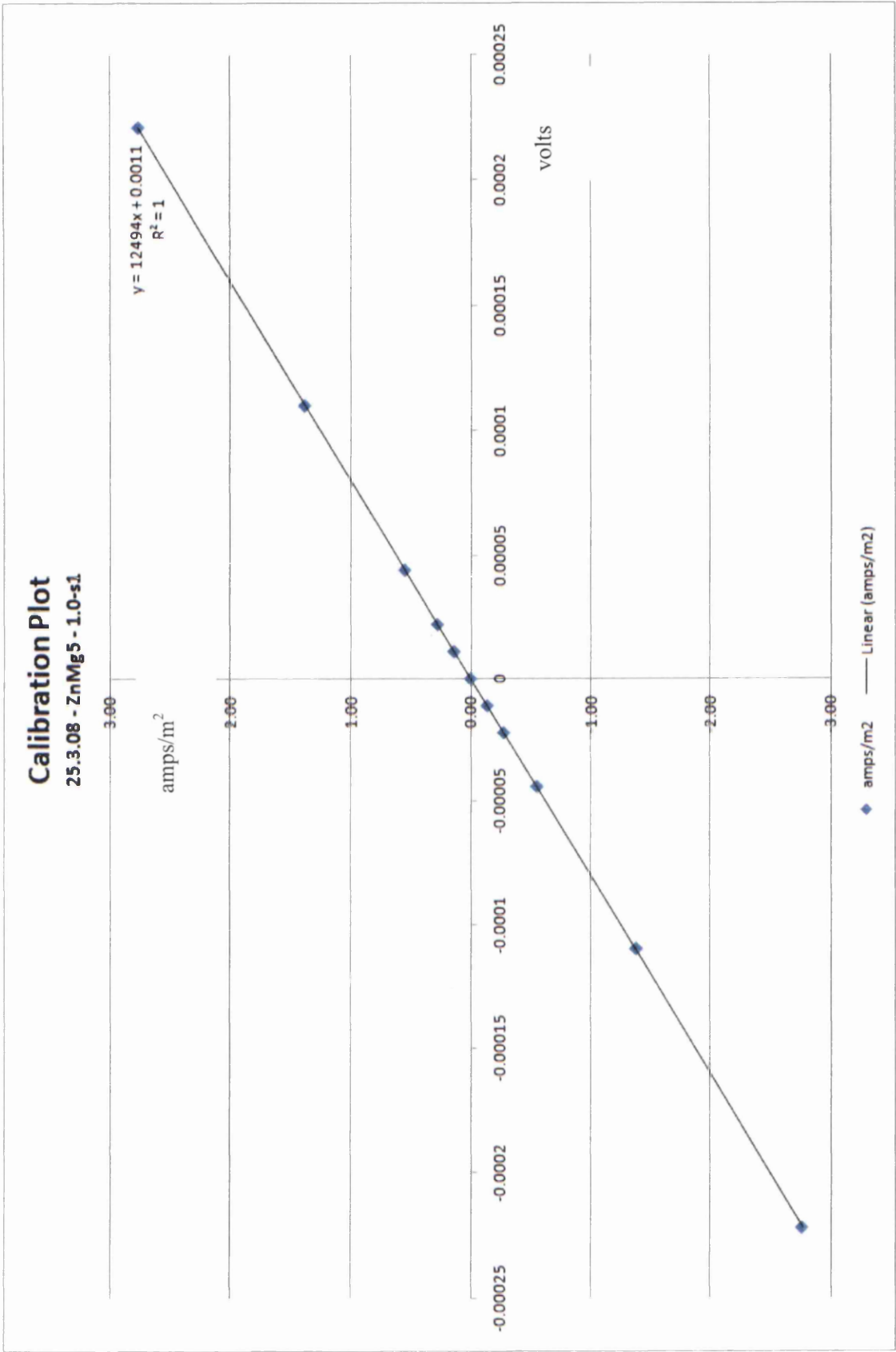


Figure 31 - A typical SVET calibration plot

and the length of time of the test is such that the electrolyte experiences very little in water vapour losses.

In all SVET tests the dissolved oxygen content was assumed to be  $2.8 \times 10^{-5} \text{ mol dm}^{-3}$  [82], the equilibrium concentration for air saturated water. Maintaining the SVET test tank open to the environment will ensure that the dissolved oxygen equilibrium is maintained ensuring oxygen losses from corrosion activity are replaced, and that there is no reduction in the rate of corrosion activity from supply of oxygen.

### **2.1.5 Sample Preparation**

Within the field of this study two types of sample investigation have been determined using the SVET, surface scans and cut-edge samples. Surface scans require an area of the sample to be identified and the extended area masked off to locate any corrosion activity within the area of investigation. The masking process uses a PTFE adhesive tape in which a square, usually  $1\text{cm}^2$ , section has been removed, the edges of tape must be ensured to adhere tightly to the sample surface so that no differential aeration corrosion mechanisms can proceed underneath the tape. It is essential that all other areas of the sample are sealed from the electrolyte. The SVET scan settings should ensure the probe is scanned as close to the edges of the tape.

Cut-edge samples have to be held vertically with the sides of the sample protected from the electrolyte. The best way of doing this is to mount the samples in a non-conducting resin such as a metallographic cold mounting resin. Selecting the correct grinding process and consumables is essential in returning a sample with sufficient flatness to be representative. The final polishing steps during metallographic preparation can use a polishing cloth with a certain 'lap', or fibre length. With thicker laps the fibres can extend and preferentially remove the softer parts of a cross section sample, such as a zinc

coating. This research has found that a woven silk cloth with minimal lap provides a sample with sufficient flatness.

It is worth noting that samples containing Mg, either by PVD deposition and to a lesser extent through conventional hot dipping have been seen to react significantly to conventional polishing fluids. To this end all planar grinding and polishing of cut-edge samples must be carried out using aliphatic hydrocarbon based lubricating fluids. This is not ideal as caution must be taken not to let the samples generate too much frictional heat as this can cause loss of adhesion between the resin and the sample, plus there are environmental implications associated with the run-off of organic liquid to waste.

Cut-edge samples scan areas are determined to cover the entire exposed surface of the sample and usually are in the order of 0.3mm x 23mm, with 35 data point in the x-axis and 92 data points in the y-axis.

Once the scan area has been set the software determines the integration distance for each data point in the x and y directions and moves sequentially through each x location before stepping to the next y location.

### **2.1.5.1 Height Scanning and Planar Interpolated modes**

As explained above the SVET probe is a platinum wire that is mounted by means of a glass push rod to a speaker that provides the vibration frequency. The importance of controlling the height from the sample has facilitated the need to develop a surface topography function within the SVET control system. The provision of a second speaker into the system provides a means of identification of the position in space of the sample surface by the use of a Wheatstone bridge, see Figure 32. When the probe is freely vibrating in air the two speakers are vibrating in unison, the resistances are equal and there is no difference in the impedance, ie.  $R_1/R_2 = R_x/R_3$ .

When the probe touches the surface the amplitude of the vibration is physically restricted, the coil is forced further into the magnetic core of the speaker and the inductance is altered generating a voltage. The resultant signal is detected by the lockin amplifier and can reliably detect probe displacements of  $2\mu\text{m}$  [83].

The position of the detected surface plane is recorded in the PC control software and the next data point is detected. The system automatically adds the selected scan height to the data points to construct a scan plane.

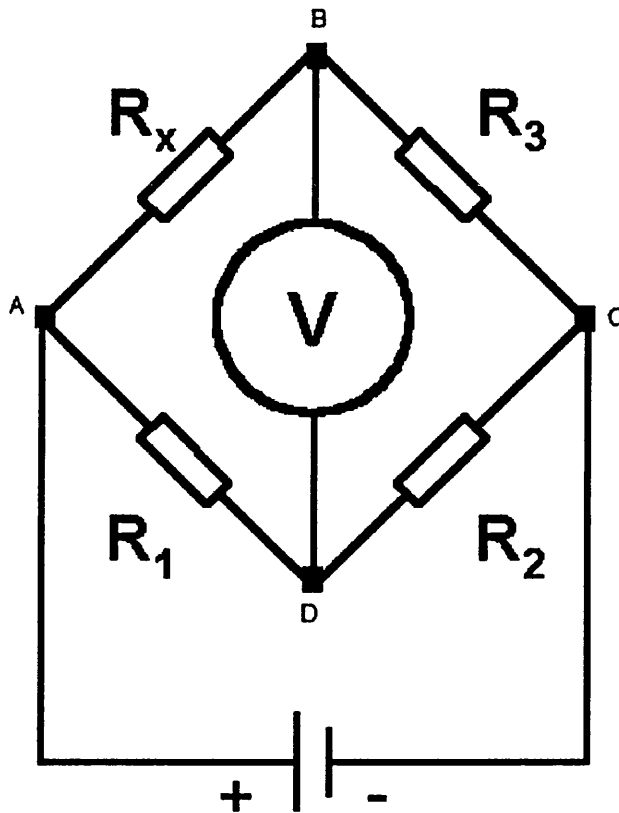


Figure 32 - Schematic of a Wheatstone Bridge [84]

### 2.1.6 Interpretation of data

The SVET control software provides a data point from the averaging of three measurements over one location. The software outputs an ASCII (can be opened with Excel via space delimited file import) file with the data expressed in nano-volts.

By use of the SVET Logfile Processor each data point is converted into volts and then, using the calibration factor, into current density (amps/m<sup>2</sup>). The current density can be thought of as a surface with peaks, assuming the lock-in amplifier has been set up in-phase, corresponding to anodic sites, and troughs to cathodic areas.

The use of a cartography package; Surfer<sup>®</sup> from Golden Software<sup>™</sup>, enables the user to utilise a trapezoidal algorithm to accurately determine the volume of current density<sup>8</sup> at the SVET resolution, combined with information on the time period between scans (for integration purposes), to evaluate the amount of positive and negative charge (cut and fill volume respectively) and return a value to the Logfile Processor. Using Faraday's law [85];

$$r = \frac{i}{nF}$$

where r is the zinc anode dissolution rate (moles/second),

i is the current (coulombs/second)

n is the number of electrons transferred (2 for Zinc) and

F is Faraday's constant (96,500 coulombs per mole).

With the predicted zinc dissolution rate and the known time frequency of the scans we can determine the amount of metal loss using the atomic mass of the element being liberated into solution. A 'Logfile processor' returns another ASCII datafile with each scan's total metallic loss. Relatively simple interrogation of these files can return a total metal loss from the duration of the scan.

---

<sup>8</sup> The trapezoidal algorithm is a more accurate method for determining the volume of a surface when the surface is mapped out with data points at a set spacing, compared to an averaging function. Obviously the lower the distance between data points the more accurate the calculation.



### 2.1.6.1 Mass loss data

The processed SVET data is exported as a list of scans with cut and fill volumes, mass losses, and mass losses per  $\text{m}^2$ . The cut and fill volumes are Surfer<sup>®</sup>'s estimations of the total anodic and cathodic current densities, Figure 33 and Figure 34 show how Surfer can illustrate the surface corrosion activity as a three dimensional visualisation. The cut and fill volumes should be equal to one another as the total current movement on the surface is balanced. It is rarely seen that the total anodic current and the total cathodic current will be equal to one another; this is likely to be due to the large size of the cathodic area, usually governed by the surface area of exposed steel. As explained above the SVET must intersect the iso-potential lines to generate a signal, in the cathodic areas these can remain quite close to the surface and hence we get an under-prediction for the total cathodic current density.

Examination of the mass loss per scan gives good mechanistic information of the metal loss for the duration of the test, i.e. is the metal loss uniform, or are their cathodic or anodic polarisation mechanisms occurring. Anodic and cathodic polarisation can be provided by adding inhibitors to the electrolyte and can aid in the study of passivation systems' effectiveness, or can be due to the build up of corrosion deposit on the surface, through precipitation, providing a barrier to oxygen diffusion, the usual rate determining step for SVET studies.

Mass loss per scan can be plotted to compare the rate of mass loss over the length of time of the scan. Total mass loss is the sum of the individual scan's mass loss values. The mass loss per  $\text{m}^2$  value is the determined automatically within the system from the calculated mass loss and the scan area. For cut-edge samples this is not representative of the mass loss per  $\text{m}^2$  as many data points will be scanned over the mounting resin, in this samples are normalised for the exposed cut edge distance. In comparative investigations

of sacrificial coatings then it is important to keep the gauge of the substrate consistent to maintain cathodic area exposure.

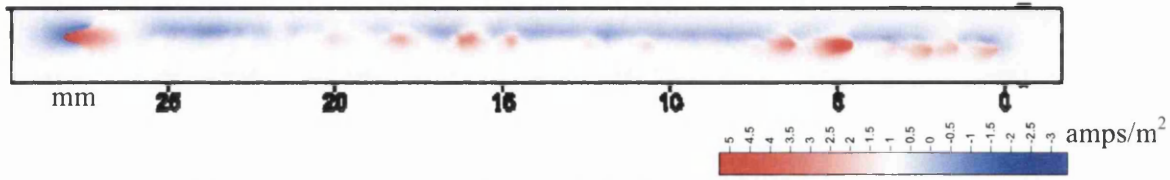


Figure 33 - Representative 2D cut-edge corrosion map

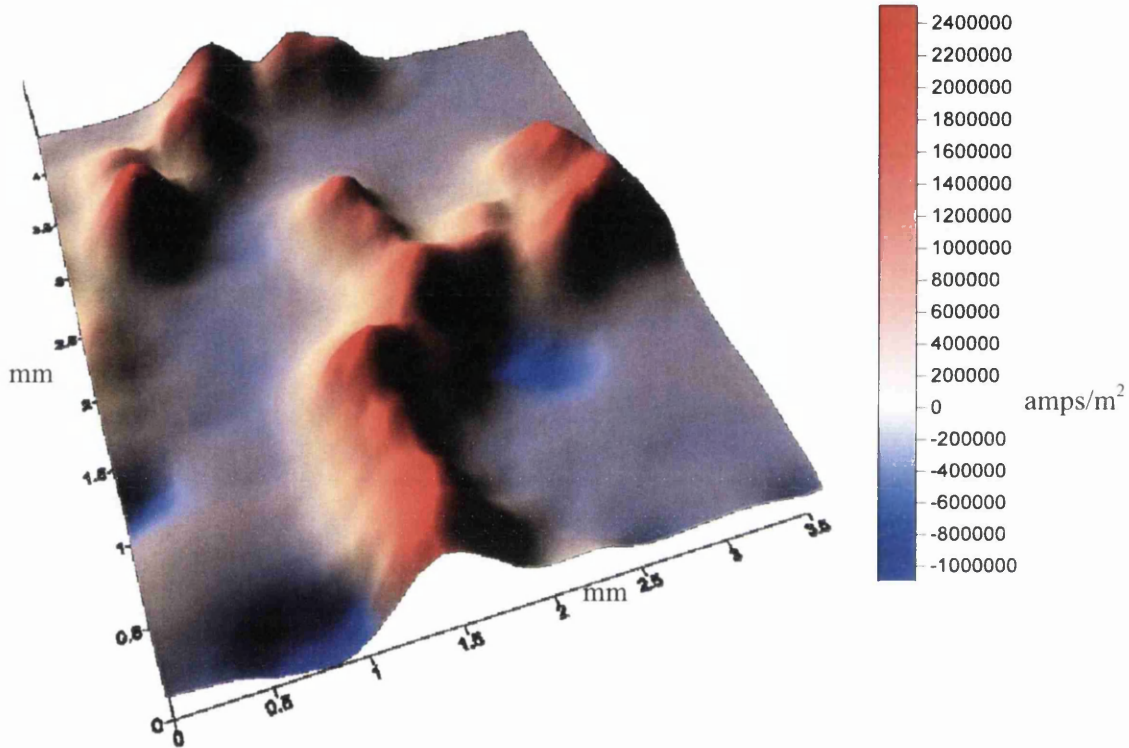


Figure 34 - 3D Surface Plot of Corrosion Activity

### 2.1.6.2 Residual anode analysis

Residual anode analysis is a method of characterising the activity of a sample under SVET investigation. The process has been used quite extensively to prepare graphical representations of the number of individual anodic sites that develop on a sample surface [86], and the length of time they are active.

Anodic sites are where zinc or other metallic ions are being liberated into the electrolyte. If an individual site is characterised as being a static anodic site for a sufficiently long

time it can be argued that the corrosion mechanism will resemble that of pitting corrosion, up to the maximum coating depth, or that an individual primary zinc dendrite is remaining active, giving mechanistic information about the potential lack of barrier protection from corrosion deposit precipitation.

A program has been developed within the scope of this research, developed using the same algorithm as the previous corrosion mechanism investigations, see Appendix A, but effectively makes use of Visual Basic™ within Microsoft Excel™ to accurately determine areas of anodic activity, to determine their position and track their movement, and to record and track their activity over the length of time of the test.

The program gives the user the functionality to select the threshold level at which point the system defines an anode. As this is a tool for analysing and comparing sets of data an anode has been classified as a data point that is the maximum among its 8 neighbouring data points and is also of an activity greater than  $1 \text{ amp/m}^2$ .

As we have seen above the resolution of the SVET within this research department is approximately 0.27mm, with data point spacing usually set at 0.2- 0.25mm. At this resolution level it is possible the local maximum attributable to a single anode can move slightly during the scanning process, and this movement can be also attributable to the movement of the active corrosion site along the surface. The program takes into account the movement of the anode sites and so anodic sites that move into one of the nearest 8 neighbours of a previous anode's location it is classified as the same anode and tracked under that anode's designation, or anode number. This is regarded as a step change over the old method.

The data is analysed and the duration of activity for each detected anode is determined. A typical 24 hour SVET scan is separated into 4 time slots of 0-6 hours, 6 to 12 hours, 12 to 18 hours and 18 to 24 hours, and the percentage of total anodes for each time slot represented graphically. An average of the intensity of the anodes over their lifetime can

be used with a residual anode intensity examination. Anodes with a high average intensity and with a significant lifetime of 18-24 hours can be considered as detrimental to the lifetime of the coating.

## **2.2 Cabinet testing**

As previously mentioned salt spray testing continues to be a standard test for corrosion resistance. The test duration is typically specified by the customer or the associated ASTM or BSi test specification. Common test durations are 1000hours, corresponding to approximately 40 days [87].

The test requires a cabinet of sufficient size to house the test panels, in which a fog of 5% NaCl is created by pumps and atomisation spray heads. Samples are usually examined daily for any evidence of red rust appearance (in the case of steel panels).

Other tests are available such as Prohesion involving exposing the sample under test to an aqueous solution containing 0.05% sodium chloride and 0.35 % ammonium sulphate. The test cycle consists of 1 hour exposure to salt mist at ambient temperature followed by 1 hour drying at 35°C.

## **2.3 GDOES**

Glow discharge Optical Emission Spectroscopy uses a glow discharge lamp to sputter the atoms on the surface of a test piece into an argon gas stream before excitation and quantification of the characteristic light emissions from the excited atoms [88]. The system seals a test piece against an o-ring and makes the test piece a cathode upon which the argon ions are attracted transferring sufficient energy to vapourise the surface atoms.

The system plots the intensity of the detected species against the test time to generate a graphical representation of the depth vs. composition, see Figure 35. By controlling the system variables, such as pressure and power, the sputtering rate can be maintained

during an investigation so that accurate comparisons of composition versus depth can be obtained.

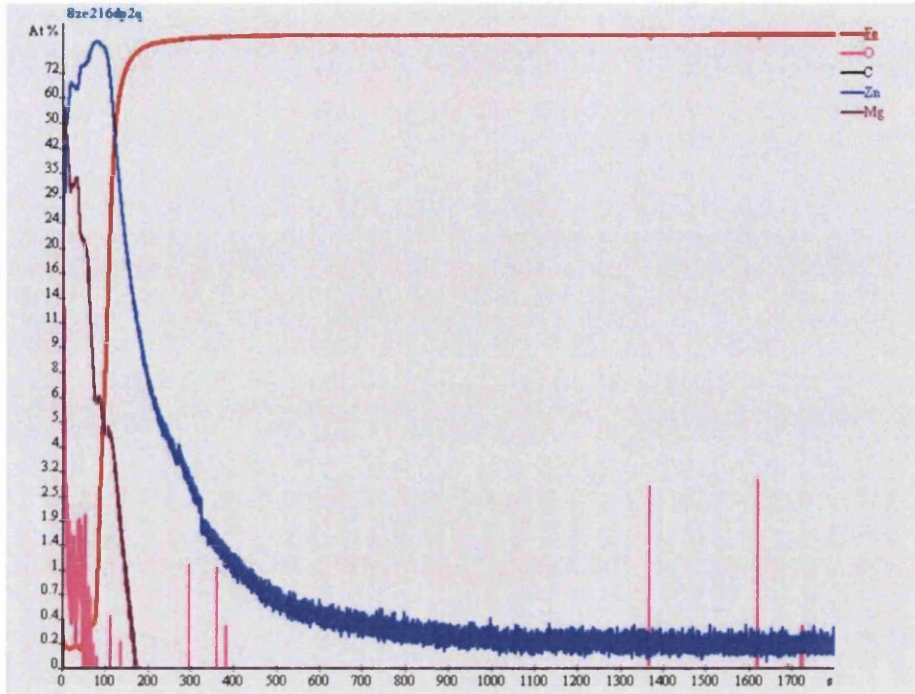


Figure 35 - GDOES analysis of 1.0Mg annealed at 250°C for 300secs

### 2.3.1 Interpretation of results

The raw data that generates the graph can be examined to determine the ratios of elements. In this study the ratio of zinc:magnesium has been determined to give an indication of the likely intermetallic species that has been produced through preparation or subsequent annealing of the coatings.

## 2.4 Depth profiling

Variations in the level of undercooling during solidification can promote changes in the microstructures of binary and ternary alloys. To accurately quantify the changes to the resultant microstructures analysis of percentage of phases is required as a function of depth. Polishing through the coating from surface to substrate interface provides the most accurate information on the coating microstructures providing the depth of the image

through the coating is monitored. A very efficient way of monitoring the amount of coating removal, and therefore the location of the image plane through the coating is through the use of a Vickers microhardness indenter [1, 9, 36].

The indents were made using a LECO M-400-G2 Hardness Tester, using 200g indent pressure and 10 second indent hold time. All measurements were made using a Reichart Polyvar microscope with calibrated graticule<sup>9</sup>. All measurements were made at x500 magnification, this equates to a resolution of 2µm per division of the graticule. All images were taken at x250 magnification, resulting in an imaged area of 0.12mm<sup>2</sup> (0.3mm x 0.4mm) for measurement of individual phases' surface area per image.

The measurement of the distance between the diagonal vertices of the indents can be used to determine the depth of the indent remaining, or more usefully the amount of coating that has been eroded from the polishing operation.

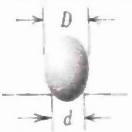



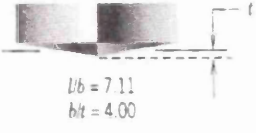

Vickers indents can be seen to produce square, pyramidal indents with opposite facets separated by 136°, see

Figure 36, 37 and 38.

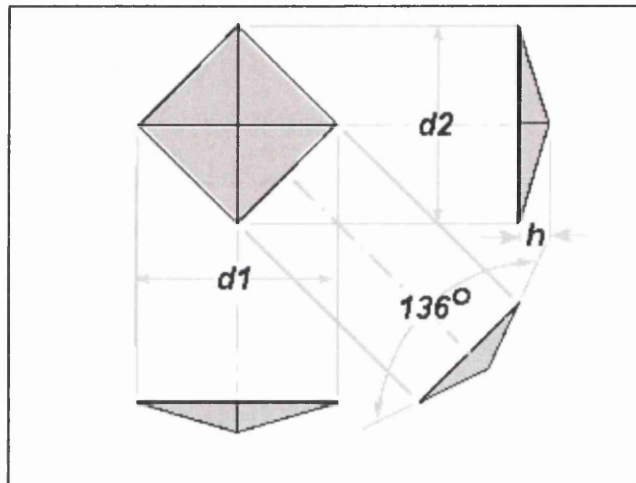
---

<sup>9</sup> The eyepiece graticule is calibrated against an UKAS accredited stage micrometer as instructed within Testing Solutions Wales QA procedure TSW/006 – Measurement and Recording of Microstructural Features and Grain Size Using the Polyvar Microscope and Associated Equipment. Records of the calibration are available.

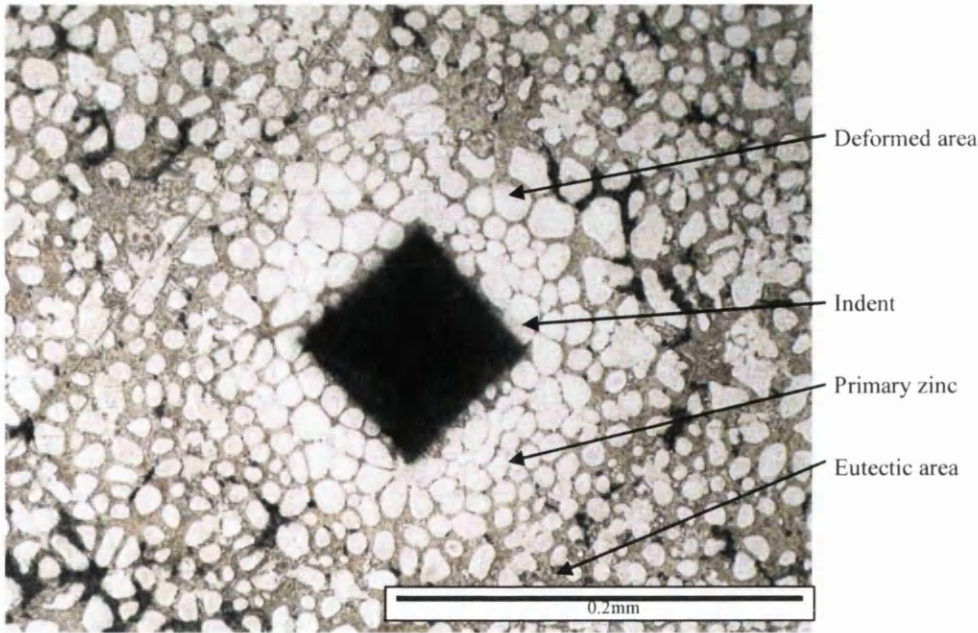
**Table 6.4** Hardness-Testing Techniques

Test	Indenter	Shape of Indentation	
		Side View	Top View
Brinell	10-mm sphere of steel or tungsten carbide		
Vickers microhardness	Diamond pyramid		
Knoop microhardness	Diamond pyramid		

**Figure 36 – Microhardness testing indenters [62, 89]**



**Figure 37 – Angles between faces on a Vickers Indenter [90]**



**Figure 38 - Vickers pyramidal indent in Zn-Mg-Al metallic coating**

A simple trigonometric analysis of the indent geometry tells us that the depth at the vertex, when the surrounding material is taken as the reference point can be calculated from;

$$d = \frac{d_1 + d_2}{2}, x = \text{side of square}$$

from Pythagoras' theorem;

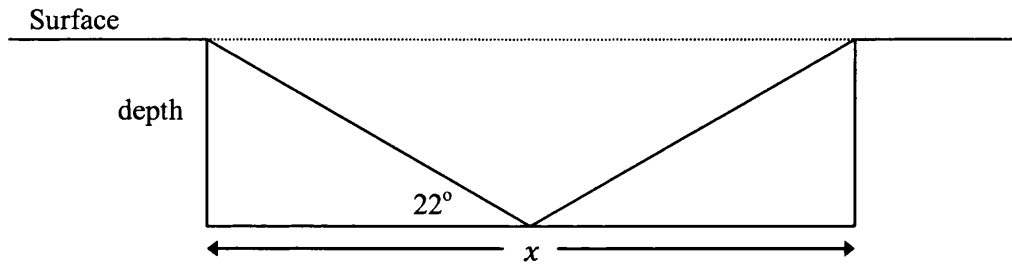
$$d^2 = x^2 + x^2 = 2x^2$$

re-arranging gives;

$$x = \frac{d}{\sqrt{2}}$$

A cross section of the indent, through the vertex and perpendicular to the sides of the square reveals;





$$\frac{\text{depth}}{x/2} = \tan(22^\circ)$$

Therefore;

$$\text{depth} \cdot \frac{2}{d/\sqrt{2}} = \tan(22^\circ)$$

Re-arranging gives;

$$\text{depth at vertex} = d \cdot \frac{\tan(22^\circ)}{2\sqrt{2}}$$

This formula was used to determine the depth of the remaining indent from the graticule measurement of the values of d1 and d2.

Areas immediately surrounding the indents have to be avoided due to the deformations imparted into the coating. These areas can be seen to show a microstructure that is expected at greater depths, see Figure 38.

### 2.4.1 Preparation of depth profiling samples

Each depth profiling sample was prepared from cutting a 20mm x 20mm sample from the parent material. In the case of organically coated samples the organic coating was softened by using methyl-ethyl ketone (MEK) and lifted from the surface. No contact was made on the metallic coating surface.

Each sample coupon was de-burred using a Struers Rotopol automatic polisher and 500 grit paper, then hot pressure mounted in Struers phenolic resin. Metallography was performed using a Struers DP-Dur woven silk polishing cloth and 1µmKemet Liquid Diamond Type K suspension. It is worth noting that polishing cloths of minimum nap; loose fibres in the cloth, as these will preferentially erode one side of the pyramidal indent<sup>10</sup> giving difficulties in defining the surface/indent edge and hence difficulties in accurately measuring diagonal distance.

## 2.4.2 Original method

A single indent method has been used quite effectively to characterise microstructures [1, 9, 36]. Figure 38 shows the deformations in the metallic coating microstructure as a result of the movement of material during the indent process. Following consideration of any non-planar polishing characteristics of the samples, and the distance from the indent where images become representative of the coating structure, it was considered that there were possible improvements to the methodology.

## 2.4.3 Improvements in the methodology

Bending stresses imposed into the sample during the guillotine process can cause the formation of a slight dome in the sample<sup>11</sup>. When the sample is polished the focussing of

---

<sup>10</sup> The long fibres of a napped cloth are bent during contact with the sample and resin mount. In the area of the indent the fibres are released into the pyramidal void and bend again upon hitting the opposite surface edge leading to a sharp edge 'upstream' of the cloth movement direction and a broad undefined edge opposite.

<sup>11</sup> The gap between the spring loaded sample holder and the shear edge of the guillotine leads to a slight downward bend at the edges of the sample, as each edge is cut in the same way this leads to the formation of a slight dome

the erosion at the top of the dome leads to rapid removal of material and very difficult to control depth profiling<sup>12</sup>.

It has been found that inverting the sample during the guillotining operation leads to the formation of a cup relative to the surface of interest. Once mounted this feature offers the sides of the sample piece as the first point of contact for polishing, thereby exposing the steel substrate at the edges of the sample before the metallic coating at the centre of the sample starts to be eroded. This slows the rate of erosion due to the increased hardness of the steel substrate compared to the zinc alloy coating thereby greatly improving the control of subsequent depth stages, see Figure 39a) and b).

Before polishing two indents are made in the surface, approximately 4mm apart<sup>13</sup>, in a suitable area, i.e. no surface deformations. The addition of a second indent allows for the determination of the range of depths at which the images are being taken. The size of each indent is measured before taking images of the surface to determine the depth of polishing. When a suitable incremental depth is confirmed the sample is ready for micrography.

Improvements to the subsequent image analysis are described below, see section 2.4.5.

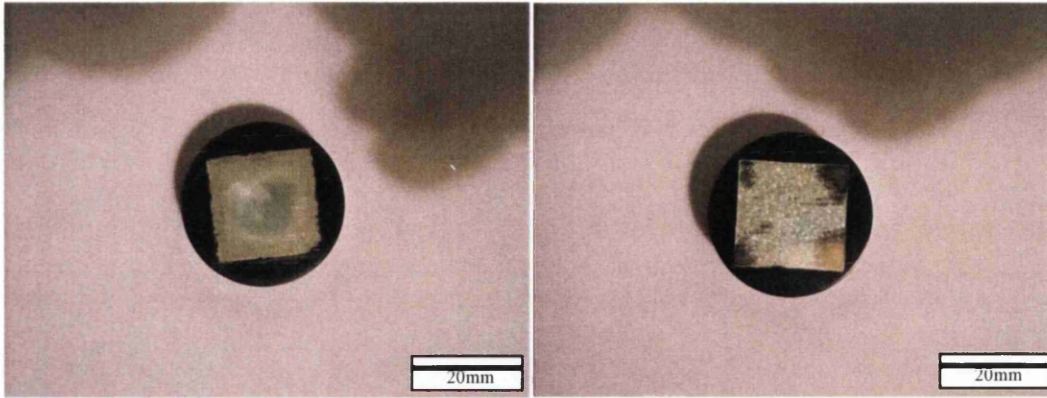
Images are taken between the two indents, away from the areas of deformation<sup>14</sup>, at incremental sample depths of 2-3 $\mu$ m until the substrate is reached.

---

<sup>12</sup> The sample metallic coating is very soft and erosion is virtually immediate even with minimal downward pressure on the sample.

<sup>13</sup> The sample is moved approximately 4mm in a single direction using a graduated micrometer attached to the stage of the microhardness indenter. Controlling the orientation of the indents relative to each other enables easier location of the indents during measurement. 4mm allows for 11 images to be taken with minimal overlap between images.

<sup>14</sup> Aligning the two indents in the x-direction of the microscope moving stage allows easy control of imaging between the two indent areas.



**Figure 39 – a) domed and b) cupped depth samples**

#### **2.4.4 Etchant development**

Metallic coated steels will look like a shiny surface under the microscope and hard to differentiate. Etching the surface with a suitable chemical can enable us to see the phases present in the coating.

In the original single indent method proposed in [1], Chromic acid,  $H_2CrO_{4(aq)}$  was used as the etchant following polishing<sup>15</sup>. Chromic acid is confirmed as a carcinogenic substance for humans [91] and was not available within Testing Solutions Wales (a Tata Steel Europe Ltd. subsidiary chemistry at the and materials engineering laboratory) at the time of doing this study.

As a suitable replacement a mixture of conventional inter-granular (Nital, 2ml concentrated nitric acid,  $HNO_3$ , in 100ml Ethanol) and tint etchants (Picral, 0.075g Picric

---

<sup>15</sup> Metallographic etching is essential to determine the differences in phases within a metallic coating. A tint etch can greatly aid in the visual separation of the phases present for subsequent image analysis.

acid<sup>16</sup> in 45ml of methanol) was combined to give an etchant with good phase separation and colouration properties.

The formulation used for this study is designated Nitpic, (0.1g Picric acid, 45ml Methanol and 0.5ml conc. Nitric acid) and was found to give good phase separation plus eutectic colouration, and uniform colouration of the primary zinc dendrites, see Figure 40.



**Figure 40 - polished & etched Galvalloy (ZA), 3 secs Nitpic etch**

### 2.4.5 Image analysis & data processing

For each consecutive polish the sizes of d1 and d2 from the two pyramidal indents are taken and entered the depth range calculated. Two images, selected for representation of the depth, and for best primary zinc phase / eutectic optical resolution, are analysed using a simple image processing program.

---

<sup>16</sup> Picric acid, 2,4,6-trinitrophenol, is not considered carcinogenic

The areas of primary zinc were selected using the 'Magic Wand' tool within the image manipulation program Paint.Net, a technique that automatically determines the boundary of an area of an image where nearby pixels exhibit the same or similar<sup>17</sup> appearance. This technique saves a great deal of time over the previous method of manually 'colouring in' the primary zinc areas. Once selected the primary zinc dendrites are coloured to excessively contrast them to the eutectic areas so that they can easily be detected by an image analysis program. Figure 41-Figure 43 show the steps required to colour the image so that the dendrites are easily visible.

It has been found that over-colouring the selected regions of primary zinc in black (RGB value 255,255,255) gives optimum sensitivity of the image measurement tool SigmaScan Pro (version 5) when determining the areas of interest. Each image is converted to a black and white image (as part of an automated function) and the intensity range 0 to 1 selected corresponding to fully 'black'.

SigmaScan Pro automatically returns values for the total number of dendrites and the size, in pixels, of each dendrite. A simple sum function of each dendrite's size returns the total number of pixels. Occasionally an image can have an area that is un-resolvable as eutectic or primary zinc, possibly through coating defects, should this happen the part the image is also 'coloured' and the percentage of the area determined in a similar way to the primary zinc areas.

---

<sup>17</sup> The degree of similarity can be selected within the program, usually about 30% variation in the RGB value determined the primary zinc phase boundary very well.



Figure 41 - original ZA image

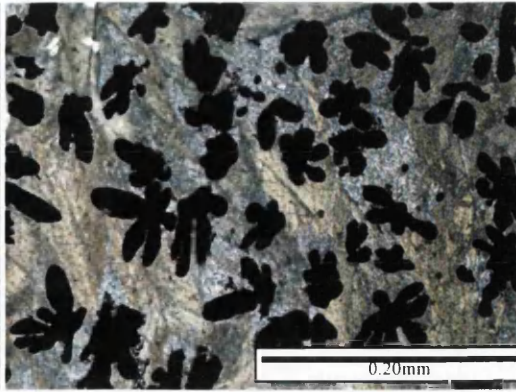


Figure 42 - dendrites coloured in

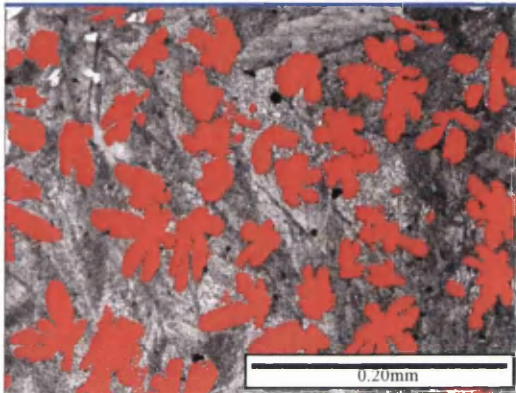


Figure 43 - Sigmascan detection

	A	B	C	D	E	F	G	H	I	J	K	L
36			442									
37			11214									
38			1610									
39			2302									
40			5716									
41			12171									
42			16773									
43			1649									
44			35393									
45			26557									
46			31189									
47			23636									
48			6727									
49			7431									
50			9645									
51			200									
52			57253									
53												
54												

Figure 44 - Sigmascan data

## 2.4.6 Measurement of primary zinc %

Each image captured is 1497 x 1160 pixels in total; the number of coloured pixels is taken from this total before calculating the percentage of primary zinc.

The date is collated with the depth determination from the indentation to give an accurate description of the morphology of the coating, see Figure 45.

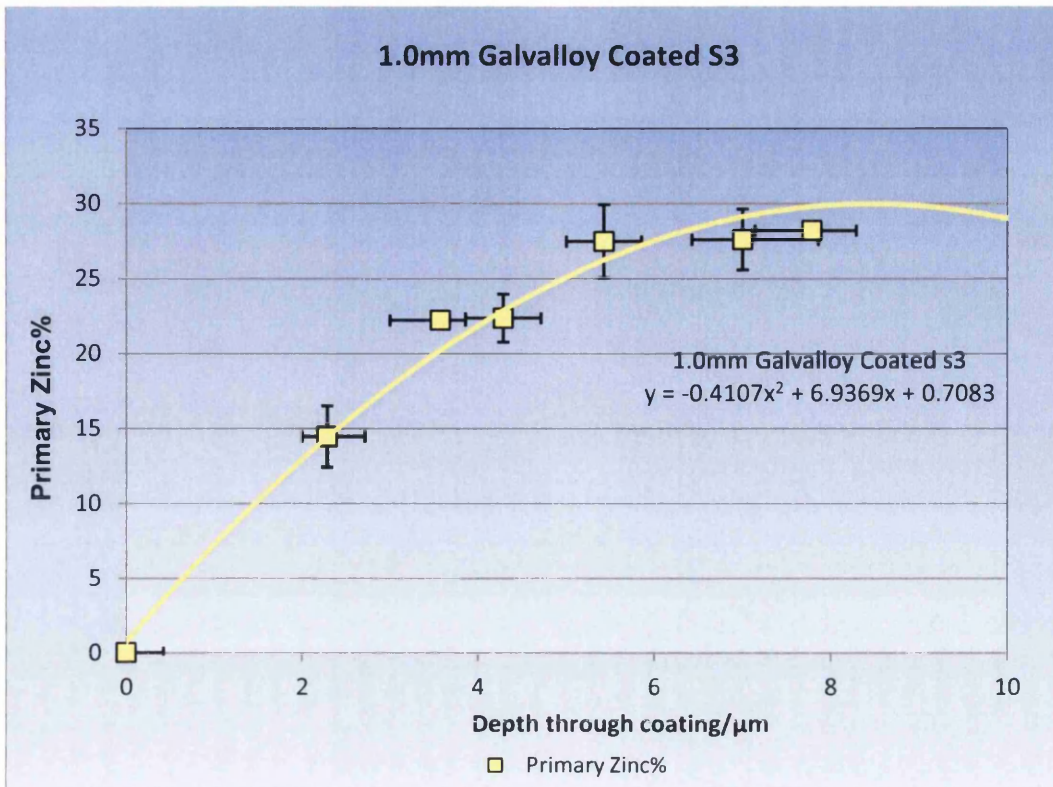


Figure 45 - example primary zinc depth profile

#### 2.4.7 Average number of dendrites per mm<sup>2</sup>

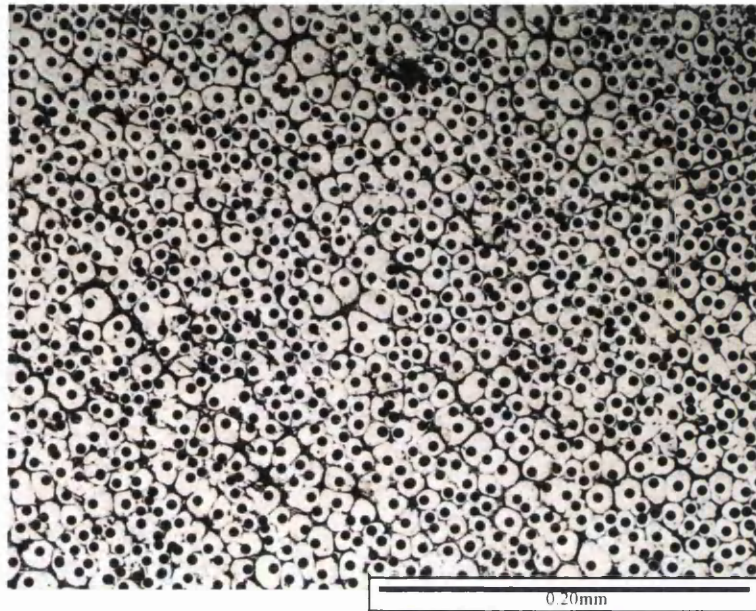
Calculations of dendrite number are taken from the area near the substrate coating interface so that the individual dendrites can be resolved more accurately<sup>18</sup>. Each depth micrograph image corresponds to 0.40mm x 0.31mm, a dendrite number can be expressed by normalising the individual dendrite count by the size of the image to obtain dendrites per mm<sup>2</sup>.

The dendrite count can usually be returned from the number of individual areas identified counted within a SigmaScan<sup>®</sup> image, see Figure 43, but in some cases the close proximity

<sup>18</sup> At areas away from the substrate-coating interface it is impossible to determine if areas of primary zinc are dendritic arms of the same dendrite. Only at the surface can the number of individual dendrites be determined accurately.



of neighbouring dendrite does not allow SigmaScan to resolve the individual dendrites. In cases such as this a backup counting process involves ‘painting’ individual dendrites within Paint.Net<sup>®</sup>, whilst simultaneously running a mouse click counting program such as OdoPlus<sup>®</sup>, see Figure 46.



**Figure 46 - MGZ42 Dendrite Count Image**

### **2.4.8 Average dendrite size**

As we are dealing with two dimensional images (parallel to the substrate) this is an expression of the cross sectional surface area through a dendrite. The total primary zinc percentage and the number of individual dendrites give an average dendrite size.

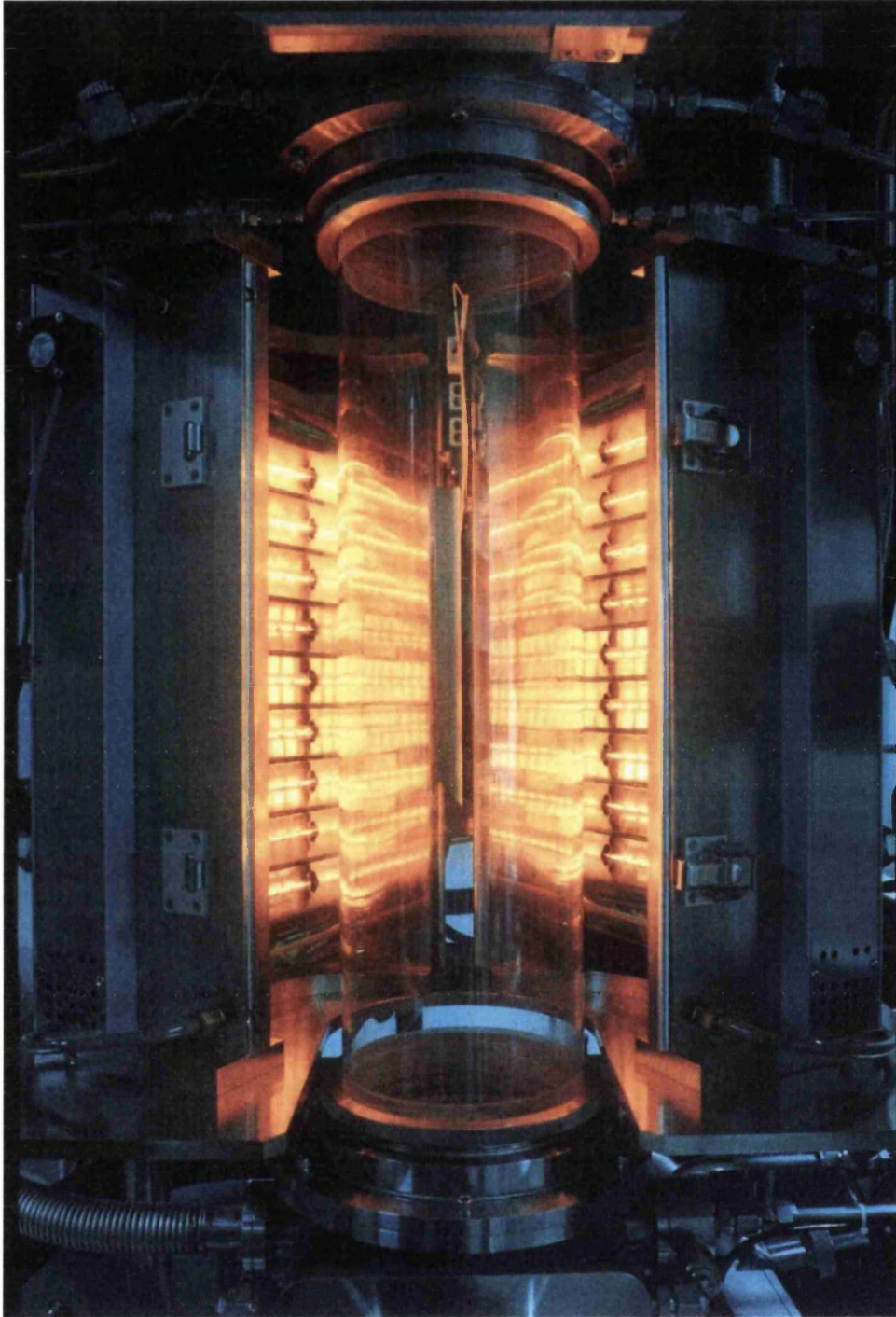
## **2.5 Hot Dip Simulator**

The Iwatani Rhesca Hot-Dip Simulator is a multi-stage, automatic, metallic coating system that can be used to generate laboratory scale samples comparable to those produced on metallic coating lines similar to Tata Steel’s Zodiac. The instrument has

been used successfully to produce metallic coated samples for previous research theses and papers including the investigation on the additions of magnesium into Galvalloy® [1] and the examination of different fluxes on post-galvanising of Zinc-aluminium alloys [92].

A small crucible allows for the preparation and melting of standard or research alloys before a sample coupon, heated in an atmosphere of choice, is lowered for coating. The system controls the coating thickness in a similar way to mass production equipment by physically moveable and flow controllable gas knives.

In this study the metallic coating functionality of the system was not required due to samples being prepared via pilot or production lines, though the annealing furnace, see Figure 47, designed to heat the samples to pre-coating temperatures, and to anneal zinc rich coatings to produce galvanneal, was used to heat the PVD samples in order to facilitate interdiffusion of the magnesium and zinc elemental layers.



**Figure 47 - IR heating/annealing furnace of the Rhesca Hot-Dip Simulator**

## 2.6 Immersed Mass Loss

As a comparison tool for the predicted mass loss determined by the SVET mass loss determinations can be conducted by immersion of the test specimen in the desired electrolyte. This investigative tool can be used to determine losses from cut-edge and surface losses.

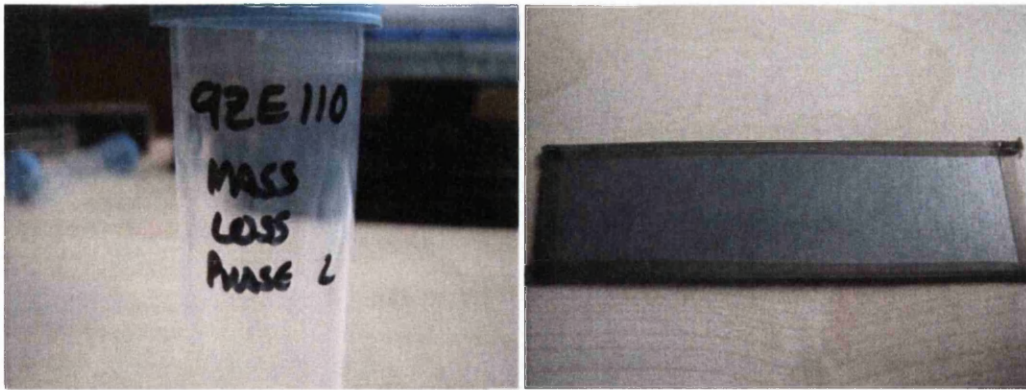
Cut-edge immersion mass loss is a test used for organically coated samples cut into approximately 15 x 50mm samples to fit into a test bottle, see Figure 48 and 49. The exposed cut-edge distance is measured to normalise the final results and the samples are weighed using an analytical balance with 0.1mg resolution. The samples are covered with suitable electrolyte and left to corrode for the required timescale. For short immersion durations multiples of the samples can be put together in the same sample tube. The samples are ultrasonically cleaned to remove any adherent corrosion deposit before being rinsed and drained and re-weighed.

For surface losses the sample coupons are sectioned to fit into a polypropylene test tube, the sample cut edges are sealed with SVET PTFE tape, the exposed surface area is measured and the samples are covered with electrolyte. After the required test duration<sup>19</sup> the samples are placed in an ultrasonic bath for 4 minutes to liberate any corrosion deposits from the surface into the electrolyte, the sample is removed and washed with DI water. The remaining electrolyte is acidified and the volume of the solution determined. The solutions are analysed against standard volumetric solutions, including a blank of acidified electrolyte, so that a mass loss can be calculated<sup>20</sup>.

---

<sup>19</sup> Within the field of this research samples have been exposed for durations of 24hours, 72 hours and 28 days, as required to compare with the SVET testing or the test requirement.

<sup>20</sup> Concentration (mg/l or ppm) x volume (ml) = mass of element lost from sample



**Figure 48 - Mass loss test tube    Figure 49 - Mass loss test specimen**

ICP-OES is a quantitative tool for determining the concentrations of elements in solution. In principle it is an argon gas stream that passes through a quartz torch assembly around which is an oscillating radio frequency generated by a radio frequency generating water cooled copper induction coil [93].

The generated radio frequency field is used to couple the argon ions produced by an electrical arc discharged into an argon gas stream. Ions are energised and accelerated by the RF field and collide with atoms of the gas stream producing significant heat. The test solution is aspirated into the gas stream<sup>21</sup> where the high temperatures cause the dissolved elements to emit characteristic wavelengths of light as excited electrons fall back to a lower energy state. The light emission is separated into its component wavelengths by suitable mono-chromator or optics, and can be measured using a suitable solid state detector, or a mass spectrometer. During the course of this study a Perkin-Elmer Optima 3X00 Series Axial ICP-OES. All ICP-OES certified calibration standards were sourced from Fisher Scientific.

---

<sup>21</sup> Care must be taken that the matrix (the solvent and dissolved material) should be consistent within the aqueous test specimens and calibration standards, i.e. test specimens of 0.1% NaCl and 5% NaCl should not be aspirated within the same test run as they may not deliver consistent amounts of material to the torch, invalidating the calibration.

## **Chapter 3**

### **Investigations into PVD Zinc Magnesium Coatings on Steel**

### **3.0 Introduction**

In order to be successful in the market place PVD coatings have to be of similar or improved performance or cost compared to hot dip products. Initial PVD results show that the coatings can offer increased corrosion performance at lower coating weights than traditional hot-dip galvanised products [94, 95].

This study was initiated to investigate the comparative performance of TSE's EMELY zinc magnesium coatings against the current benchmark hot dip galvanised product, MagiZinc<sup>®</sup>, in the standard SVET tests, and in the automotive standard tests of salt spray and humidity testing.

Currently a number of production methods and coating variables can deliver the optimum coating characteristics for a new TSE product. There is some evidence that the performance of the coating is improved by having a thin layer of ZnMg on top of a layer of zinc as the underlying non-alloyed zinc layer offers the ability to maintain adhesion to the steel substrate upon deformation, whereas a single brittle zinc-magnesium layer would delaminate [10]. There is extensive literature on the performance of coatings made by various methods [57, 61, 62, 96-100] but information on the sequential deposition or PVD Mg onto PVD Zn and simultaneous, or co-deposition of ZnMg as a homogeneous layer is quite limited.

### **3.1 Samples and sample quality**

Samples were received of PVD Mg on PVD Zn, in two different coating compositions on 0.3mm gauge steel, roughly A4 size, 2 panels each. One sample was produced on the 11<sup>th</sup> October 2007; designation 1.5Mg, and the second produced on the 15<sup>th</sup> October 2007, designation 1.0Mg. Each sample was produced by initial deposition of pure Zn followed by a period of about 30 minutes to allow for strip cool down, followed by secondary

deposition of a pure Mg layer. Table 4 shows the physical characteristics of the coating and layers determined from optical microscopy of representative areas of the coating.

Sample	1.0Mg	1.5Mg
Zn thickness / $\mu\text{m}$	3.25	4.25
Mg thickness / $\mu\text{m}$	0.75	3
Zn $\text{g}/\text{m}^2$	23.205	30.345
Mg $\text{g}/\text{m}^3$	1.3035	5.214
Coating %Mg (if homogeneous)	5.6	17.2
MgZn <sub>2</sub> :Zn ratio	1 : 14.5	6.1 : 1

**Table 4 - Coating composition determined by optical microscopy**

In the development of the EMELY process the original idea was the rapid production of aluminium coated steels that could be substituted into the packaging market, whilst the development partners POSCO would examine the production of zinc-magnesium coatings. The technical challenges of producing aluminium coatings resulted in the refocusing of the European activities and switching to the production of zinc-magnesium coatings also as a market entry process [101]. The increased vapourisation rate of zinc came with a problem that would limit the amount of work that could be carried out on the initial samples, namely that the increased volatility of zinc would mean that there was a significant amount of zinc vapour in the test chamber from overspray, zinc which did not hit the condensing strip steel surface. The over sprayed zinc would redeposit itself on the strip steel surface after the surface has been plasma etched, resulting in a decrease in activation energy of the surface when the surface reached the spray zone, the special separation of these zones can be seen in Figure 50. This would prove detrimental to the adhesion of the zinc surface to the strip steel.



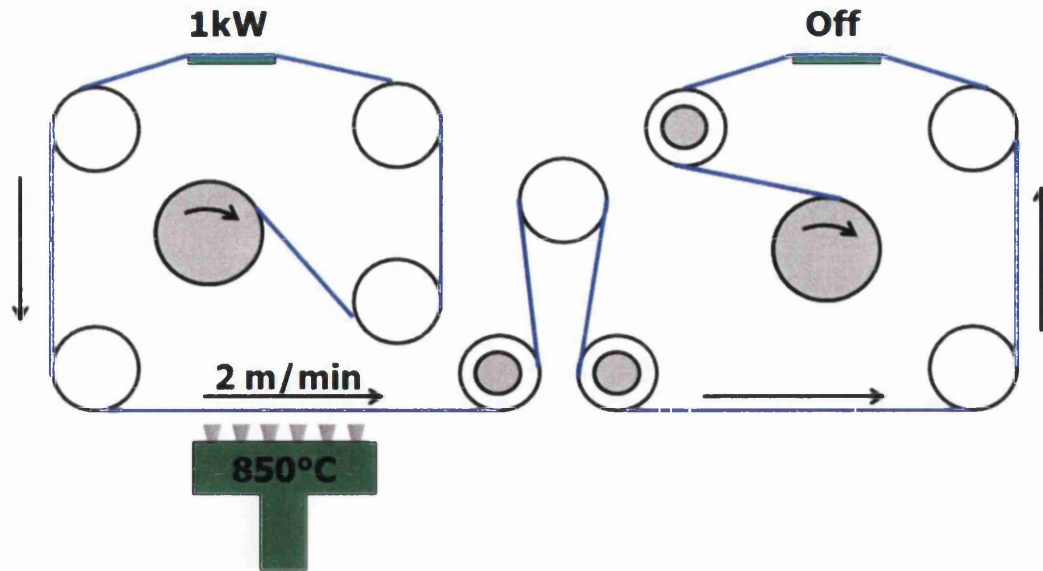


Figure 50 - Schematic of EML-PVD [63]

The surface quality of the samples was considered poor, see Figure 51a) and b); it is considered that the surface of the sample is coming into contact with the underside of the already coiled coating resulting in scratches in the direction of rolling. The surface is PVD coated Mg which has been seen to have little scratch adhesion.

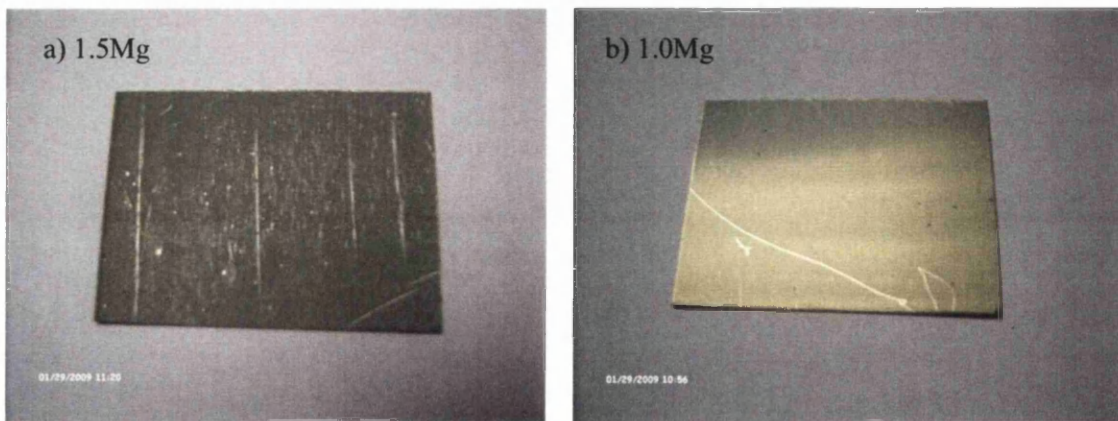
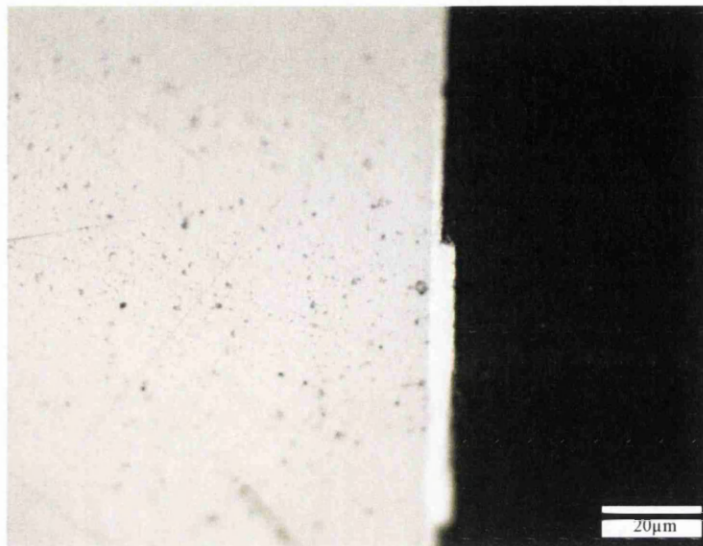


Figure 51 - Typical sections from a) 1.5Mg and b) 1.0Mg

Together with surface scratches there are numerous droplets caused by imperfections in the coating process. Cold spots and unstable evaporation can cause droplets to be emitted

from the VDB which will impinge on the substrate and get rolled down on coiling; an example of this can be seen in Figure 52.



**Figure 52 - zinc droplet rolled flat during production**

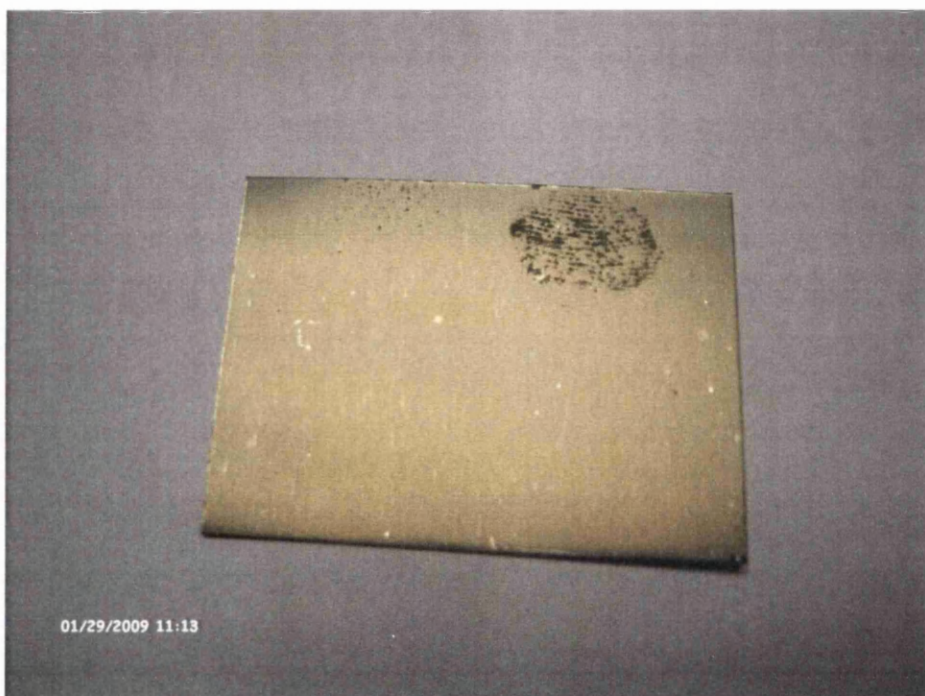
### **3.2 Metallography of reactive samples**

The reactivity of the pure magnesium on the surface requires careful metallographic preparation in order to repeatably obtain a reliable micrograph. The most reliable process has proven to be the use of a diamond cut off wheel on a Struers Accustom 5 automatic cut off machine using Water-free cutting fluid instead of the usual inhibited water based fluid.

A backup process required identification due to problems with the recirculation pump of the Accutom that uses conventional abrasive wheels. The technique uses the water-free cut off fluid that provides cooling during the Accutom 5 operation as the coolant and material removal fluid on the abrasive wheels. The only issue with using this technique is that the abrasive papers quickly become overloaded with ground material and need replacing due to the fact that limited amount of cutting fluid can be used as it cannot enter the normal water drainage system.

Once planar grinding is complete the sample can be fine polished in a similar way from both planar grinding/cutting techniques using woven silk polishing wheels and 6 $\mu$ m and 1 $\mu$ m diamond suspensions in aliphatic hydrocarbons consecutively.

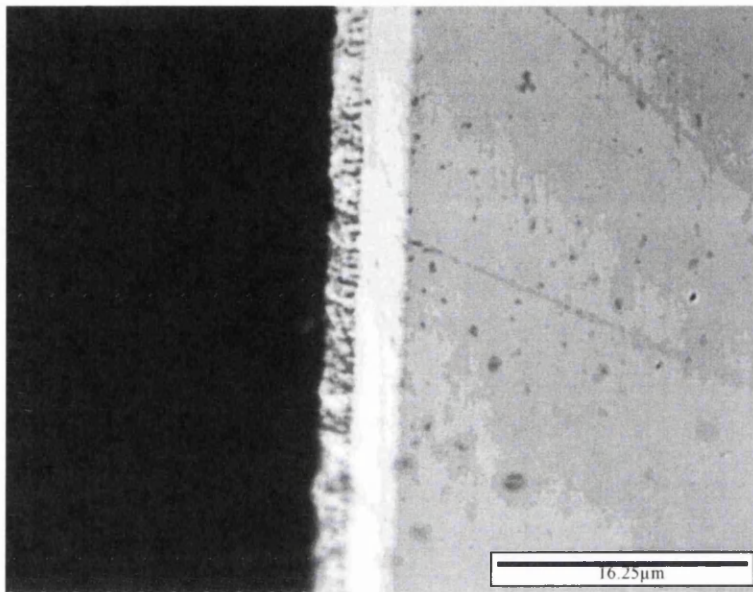
The mounting resin used is EpoFix, a 24hr cure epoxy resin supplied by Struers Ltd. Each sample requires cleaning with iso-propanol after sectioning to remove any surface oils that can cause the resin to pull away from surface during curing. Care must also be taken not to touch the samples with a bare hand as finger marks will develop as shown in Figure 53.



**Figure 53 - finger mark from reactions with Mg on surface of 1.0Mg**

### **3.3 Microstructural investigation**

The samples were delivered with very little information apart from a production date and an outline of the expected coating composition. The coatings show two distinct areas comprising the Mg rich phase and the Zn rich phase, see Figure 54.



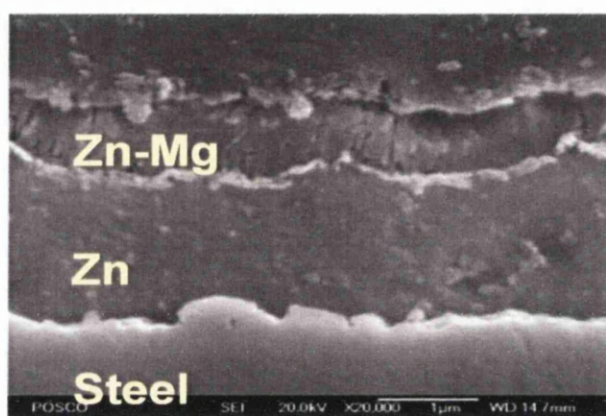
**Figure 54 - As received 1.5Mg sample microstructure**

It can be seen in this image that there is a clear interface between the pure zinc coating and the deposited magnesium coating above. It also shows that the secondary magnesium deposition layer seems to have a columnar structure, showing that the surface energy of the zinc layer was insufficient to promote dense layer construction. Consequences of reduced Mg mobility will be limited intermetallic formation between zinc and magnesium and possible lower adhesion, promoting the lower scratch adhesion of the magnesium layer and delamination upon forming.

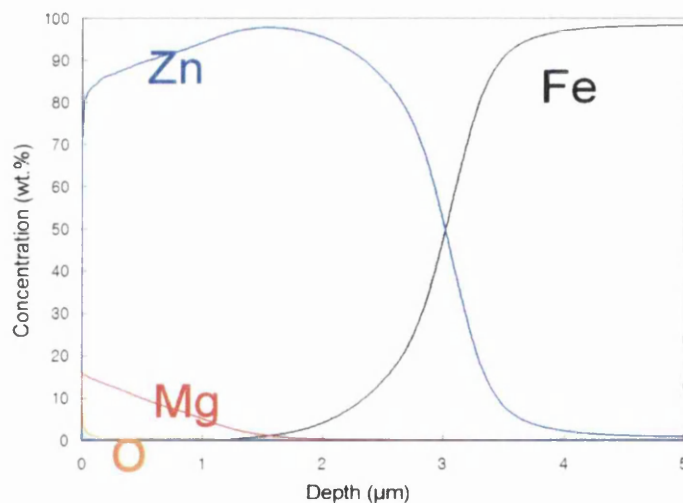
### **3.4 SEM & EPMA**

Scanning electron microscopy has been used to examine closer details of the coatings plus also, Electron Probe Micro-analysis (EPMA) has been used to examine elemental compositions and determine elemental profiles through the coating.

Linescan analysis is a function within SEM-EDX analysis that scans along a pre-set path and identifies the percentage of an element along that path by the intensity of those secondary electrons which are characteristic of that element. Below are a series of images showing the location of elements through a section of the coating 1.5Mg after annealing for 300 seconds at 300°C, see Figure 55 and Figure 56.



**Figure 55 – Secondary Electron Image (SEM) of annealed 1.5Mg coating**



**Figure 56 – SEM Linescan analysis of annealed 1.5Mg from coating surface into substrate**

### 3.5 Diffusion Annealing Investigation

Based on the evidence in the optical and EPMA linescan analysis the two distinct layers of Mg and Zn remain in the samples with a small area of interdiffusion in the Zn/Mg interface. The interdiffusion of Mg into the Zn layer can provide some interesting information on the formation of intermetallic compounds. In TSE investigations so far it has been identified that once magnesium diffusion reaches the steel surface then delamination of the coating is promoted. There is no body of work defining the intermetallic compounds responsible for this delamination phenomenon, and so a diffusion annealing study was initiated to try and identify what may be occurring.

Initially samples were sectioned into small enough sections (40mm x 30mm) to permit sufficient time and temperature combination to investigate both magnesium diffusion rates, and possibly provide some idea of annealing processing conditions if two layer PVD deposition followed by interdiffusion proves to be the desired processing route for a PVD CAPL ZnMg product.

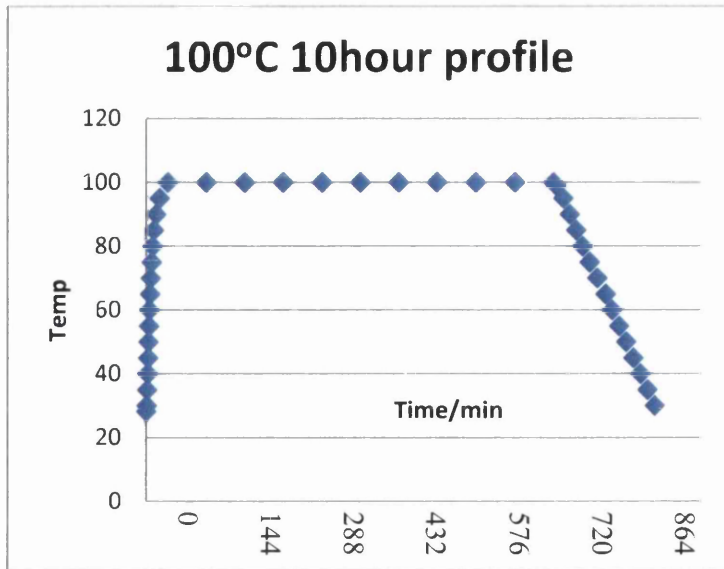
Table 5 shows the combinations of time and temperature selected. There is evidence in the literature that temperatures between 100°C and 300°C are required for diffusion of the Mg layer to progress, though this is dependent on the thickness of the Zn layer [95]. Initial dwell times of 1 hour to 10 hours for the lowest temperatures were selected for the initial investigation, and to provide sufficiently slow cooling to obtain equilibrium intermetallic compound formation.

	100°C	150°C	200°C	250°C	300°C
1 hour	x	x	x	x	x
2 hour	x	x	x	x	x
4 hour	x	x	x	x	
6 hour	x	x	x		
8 hour	x	x		x – annealed	
10 hour	x			x – annealed and sectioned	

**Table 5 - Initial diffusion annealing parameters**

Initially a suitable size glass dessicator was used after purging with dry argon and sealed to prevent gas loss. A Camlab Carbolite PF30 (200) electrically heated oven was used as a heating source. Each annealing temperature heating and cooling cycle was recorded and a temperature profile constructed, for the temperatures inside the dessicator; this will take out any effect on the heat capacity of the apparatus.

All temperatures were recorded on a calibrated Fluke® digital thermometer with K-type thermocouple, resulting in a profile similar to Figure 57.



**Figure 57 - Example lab diffusion annealing profile**

Further diffusion analysis work has used the hot dip simulator to anneal at lower time durations. The hot dip simulator requires the sample to have a K-type thermocouple spot welded onto the surface to control the heating furnace. This also provides constant data output throughout the length of the annealing cycle, the data can be plotted to give a representative heating profile, as in Figure 58.

	150°C	200°C	250°C	300°C	350°C
30 secs	✓				✓
300 secs	✓	✓	✓	✓	✓

**Table 6 - Initial sample annealing cycles**



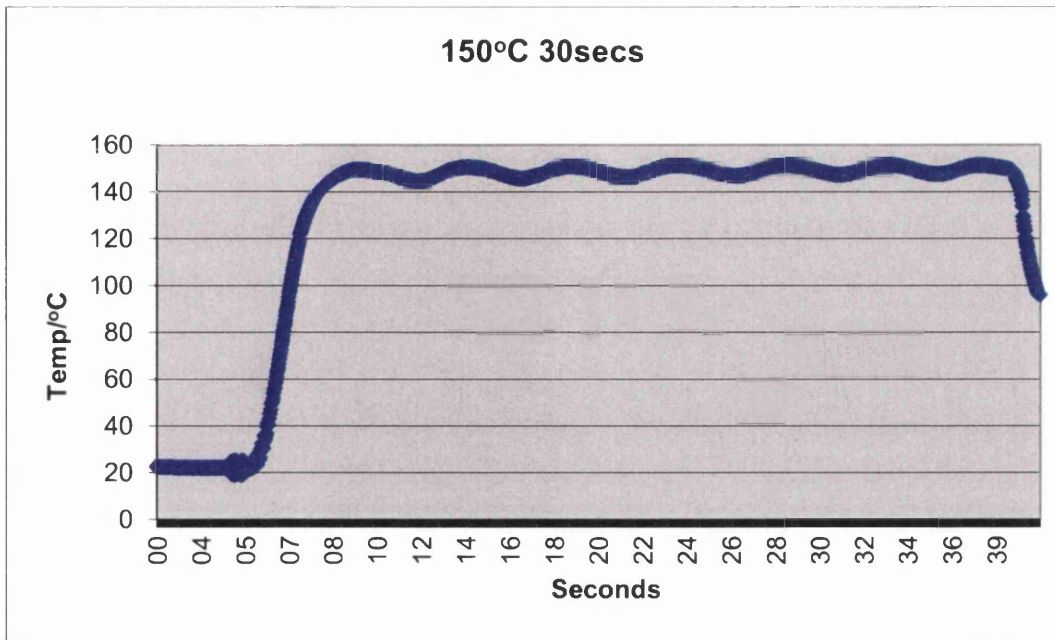
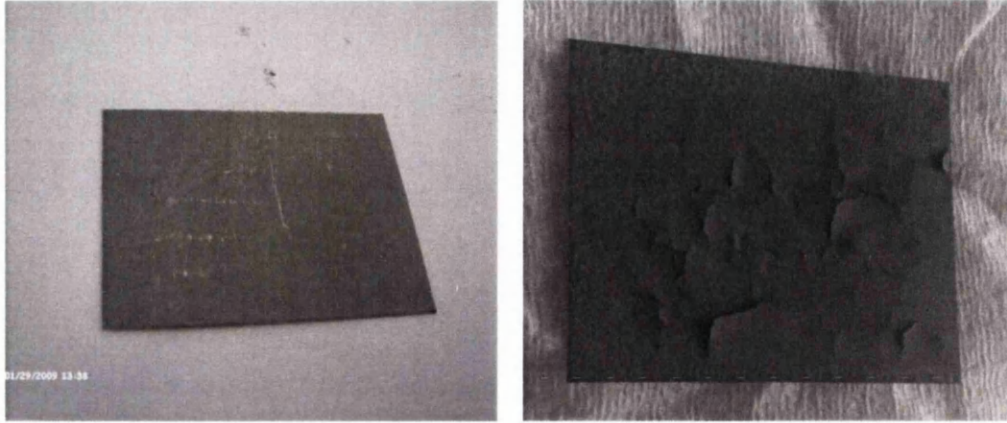


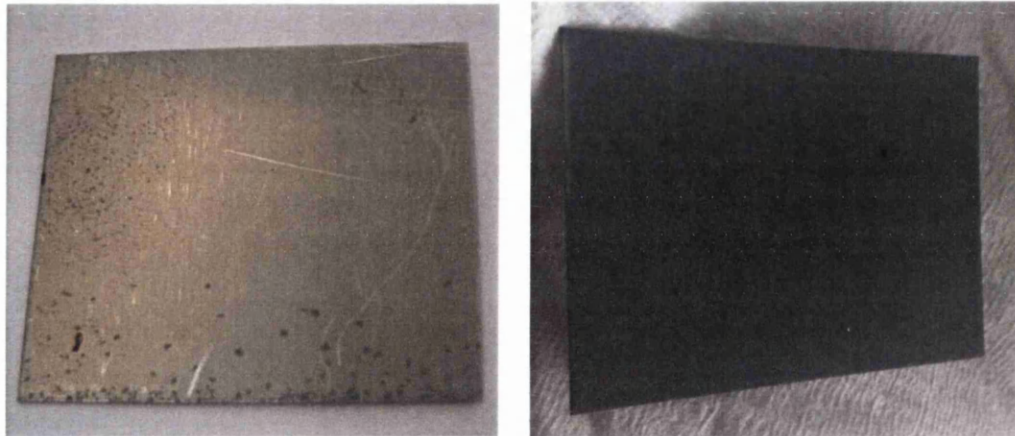
Figure 58 - Typical HDS annealing profile

### 3.5.1 Microstructural changes

Delamination has occurred in the 1.5Mg sample but not the 1.0Mg sample exposed to the same annealing conditions. Figure 59 a) and b) and Figure 60 a) and b) show the difference in the coating appearance before and after annealing at these conditions.

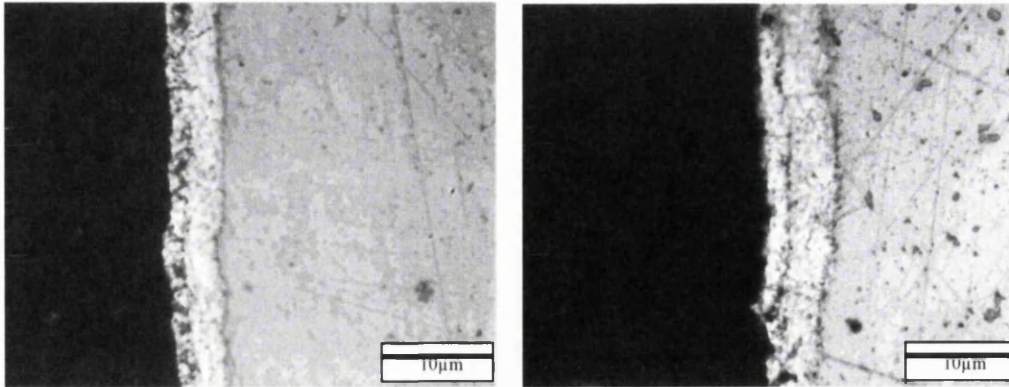


**Figure 59 – a) 1.5Mg as received and b) after 300°C for 120 mins**

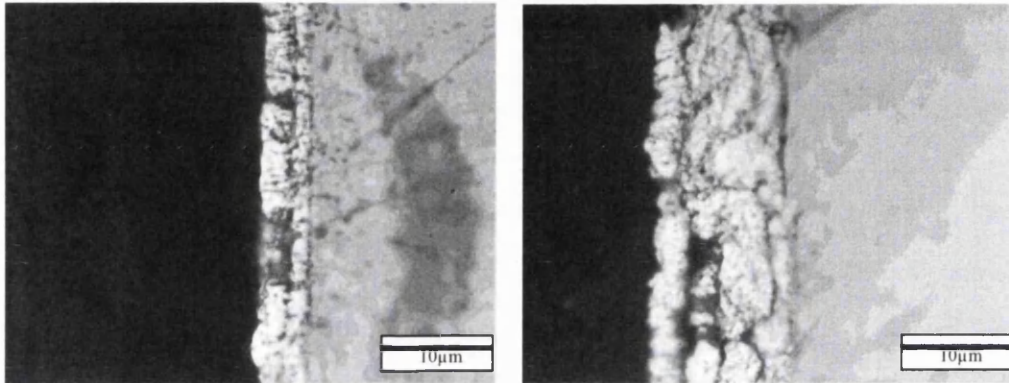


**Figure 60 – a) 1.0Mg as received and b) after 300°C for 120 mins**

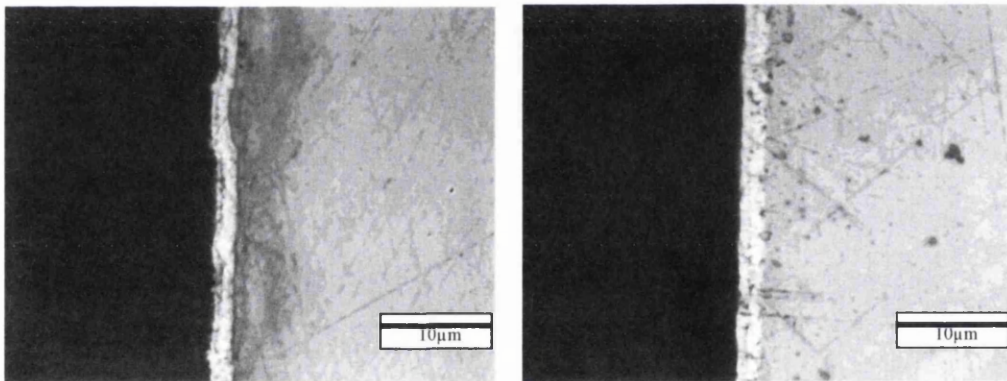
These samples and those identified in Table 5 have been examined for microstructural changes, see figures 61 to 64a) and b). There appears to be significant changes on heating above 100°C. As can be seen from the micrographs below there is significant increase in growth of the coating, further determination is required to determine if this is due to ZnMg intermetallic formation, or whether it is partially due to FeZn intermetallic formation. The 2 hours @ 300°C sample was completely de-adhered from the substrate.



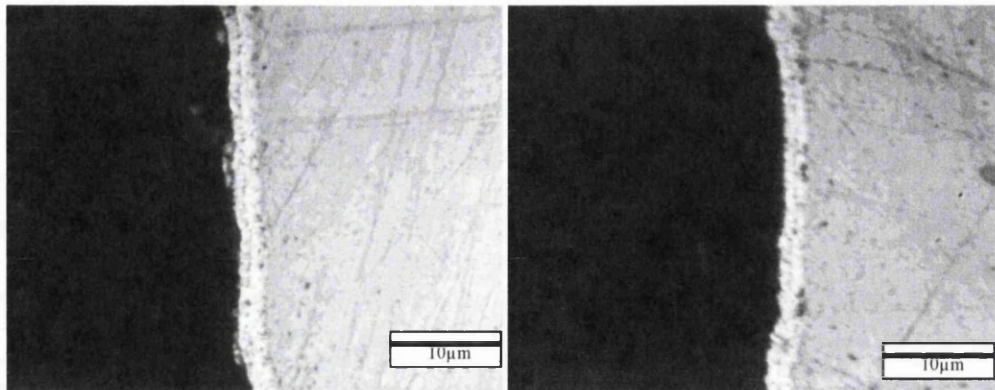
**Figure 61 – 1.5Mg, a) 100°C for 600 mins and b) 150°C for 480 mins**



**Figure 62- 1.5Mg, a) 200°C for 360mins and b) 250°C for 240 mins**



**Figure 63 - 1.0Mg, a) 100°C for 600 mins and b) 150°C for 480 mins**



**Figure 64 - 1.0Mg, a) 200°C for 360 mins and b) 250°C for 240 mins**

It can be seen that there is a great deal of difference in the behaviour of the two coatings. Additional EPMA analysis will confirm if this is due to the reduction in Mg composition, and, together with XRD analysis, that the amount of Mg available in the 1.0Mg sample is sufficient to produce a thin coating of  $Zn_2Mg$  and limit further diffusion.

### 3.6 X-ray Diffraction

X-ray diffraction scans of the annealed samples have been completed and the spectral peaks identified, see Figure 65 and Figure 66. The spectral peaks are compared to reference standards, see Table 7, and the intermetallic phases present within the samples determined. Table 8 shows the detected intermetallic phases for the zinc magnesium PVD system as annealing temperature increases.

1.0Mg	JCPDS Ref	00-004-0381	03-065-120	00-39-0951	01-087-0722	
	Species	Zinc	$MgZn_2$	$Mg_{32}(Al,Zn)_{49}$	Iron	
1.5Mg	JCPDS Ref	00-001-1238	0-001-1211,3	00-045-184,4	01-087-0731	01-087-0713
	Species	Zinc	$MgZn_2$	$FeZn_{10.98}$	$MgZn$	Zinc

**Table 7 – XRD Determination of Intermetallic Phases**

	100°C	150°C	200°C	250°C	300°C
1.0Mg	Zn, MgZn <sub>2</sub>	Zn, MgZn <sub>2</sub>	Zn, MgZn <sub>2</sub>	Zn, MgZn <sub>2</sub>	Zn, MgZn <sub>2</sub> , Mg <sub>32</sub> (Al,Zn) <sub>49</sub>
1.5Mg	Zn, MgZn <sub>2</sub>	Zn, MgZn <sub>2</sub>	Zn, MgZn <sub>2</sub>	MgZn <sub>2</sub> , MgZn	MgZn <sub>2</sub> , FeZn <sub>10.98</sub>

**Table 8 – intermetallic phases detected after diffusion**

From the data it can be seen that the diffusion of magnesium into the zinc layer generates the ZnMg<sub>2</sub> phase as indicated in the equilibrium phase diagram as a stable intermetallic compound. The samples do show that the increased loading of magnesium in the 1.5Mg samples show that production of MgZn is achieved at higher diffusion temperatures.

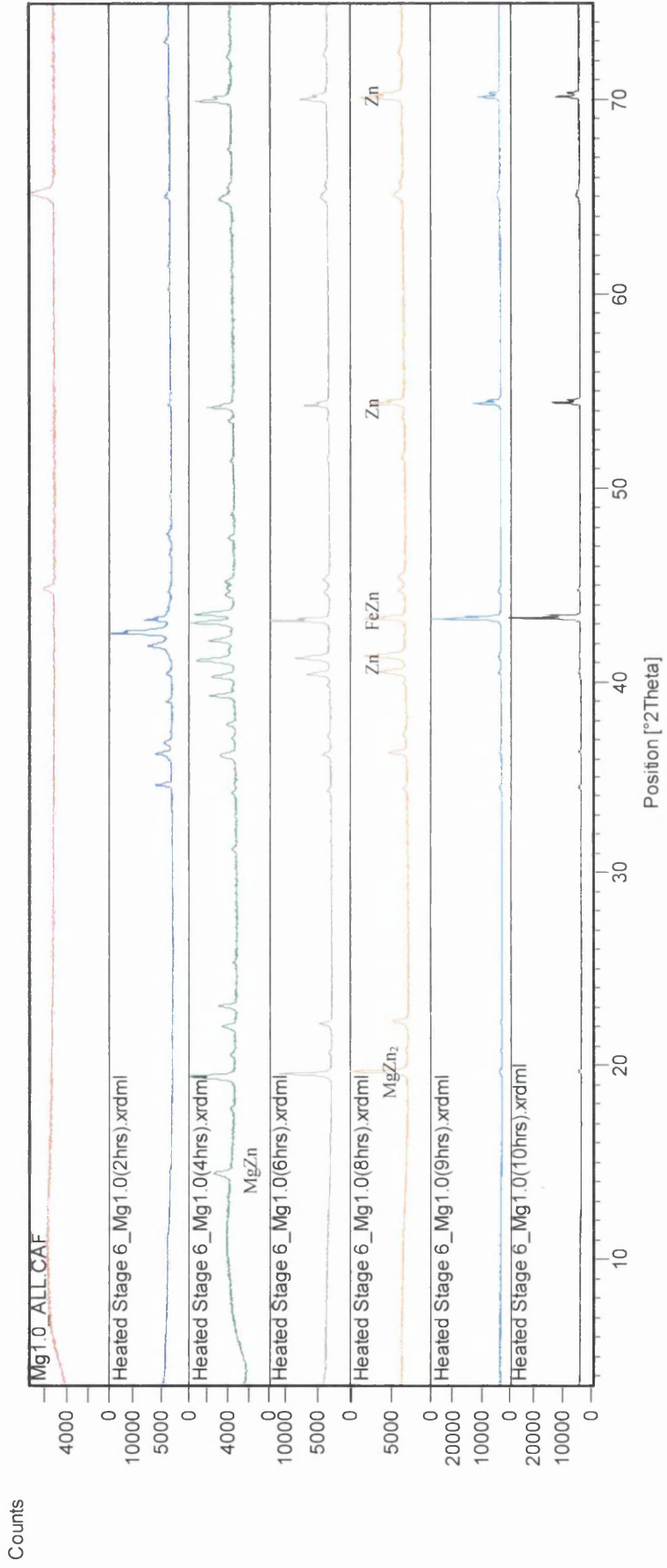


Figure 65 - X-ray diffraction data for all Mg<sub>1.0</sub> samples

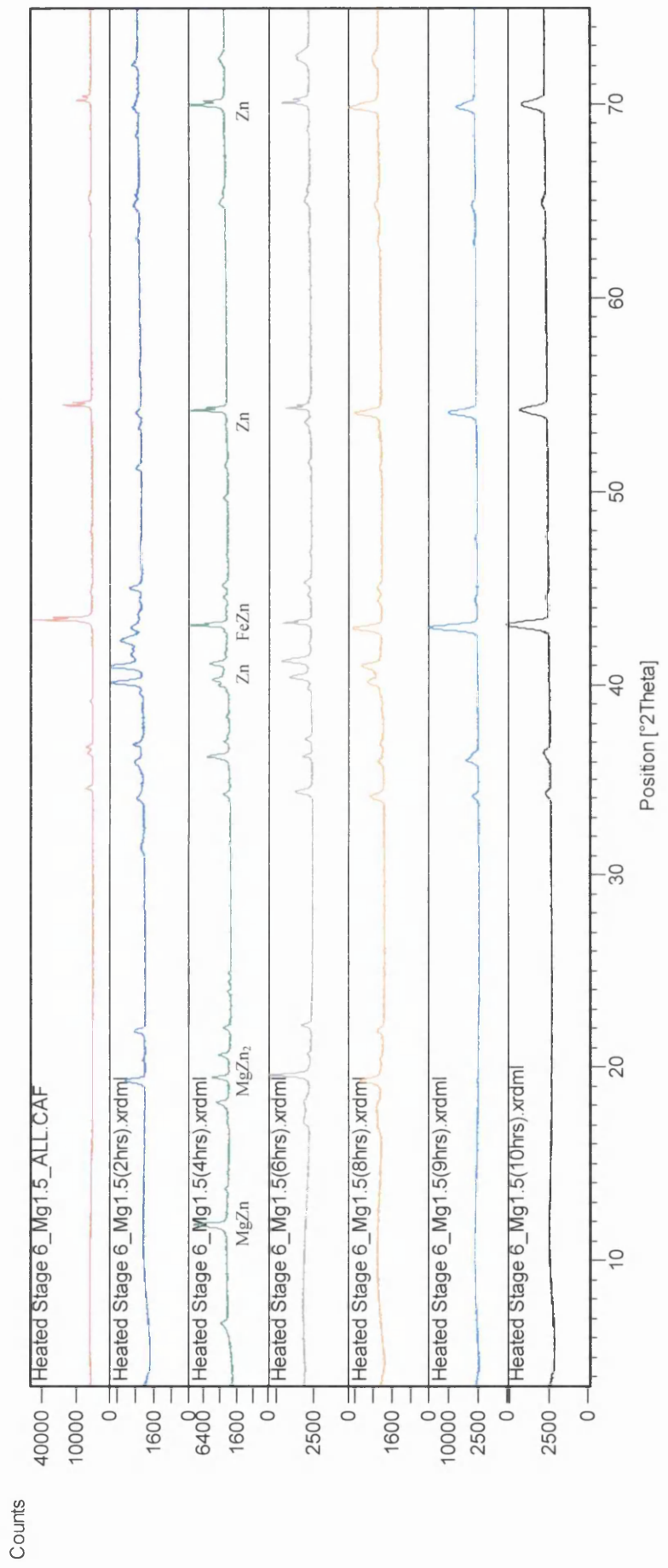


Figure 66 - X-ray diffraction data of Mg<sub>1.5</sub> samples

### 3.7 Coating Hardness

Inherent with intermetallic formation is the increase in hardness of the material, associated with the formation of a ceramic type compound. Using a Vickers microhardness indenter with 10g weight applied the coating hardness has been found to increase dramatically after annealing, see Figure 67. The increase in hardness can be attributed to the production of hard intermetallic phases and can have a marked effect on the formability of the coating.

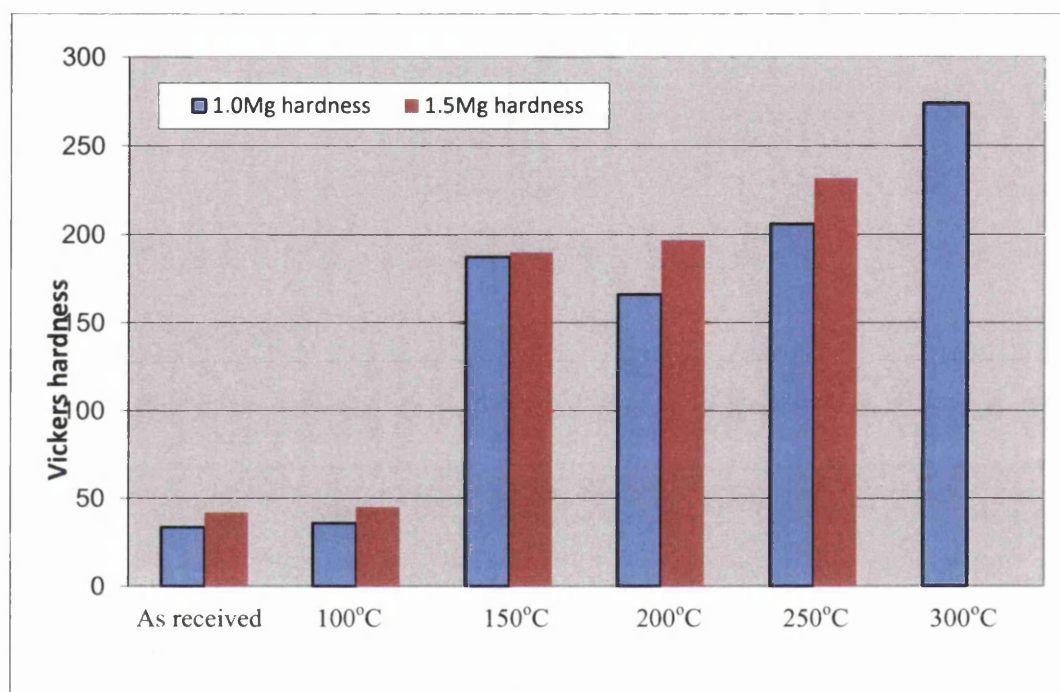


Figure 67 - hardness changes of 1.0Mg with annealing

### 3.8 Erichsen dome testing

Deforming a sample can provide information on the formability of the coating, a less formable coating will tend to show areas of delamination. An Erichsen tester is a standard formability test method that holds a sample in a fixed location and then a hemispherical ram is forced into the sample so that the sample surface is raised up to a pre-determined height. Areas of compression and tension exist in the coating and so good information on the behaviour of the coating system can be assessed [67].

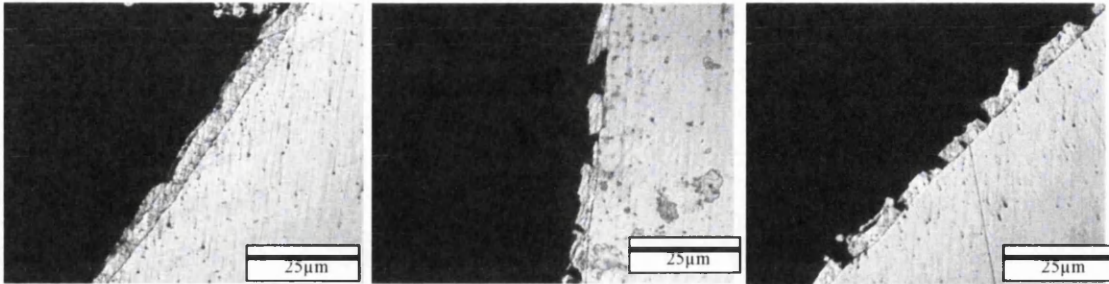


Each sample and a benchmarking sample (0.8mm gauge MZ140) have been tested at 5.0mm dome height. The height part of the test is more of a measure of the formability of the substrate but it does show, under microstructural investigation, if the coating can tolerate the movement of the substrate underneath, i.e. is the metallic bond sufficiently strong to withstand these forces.

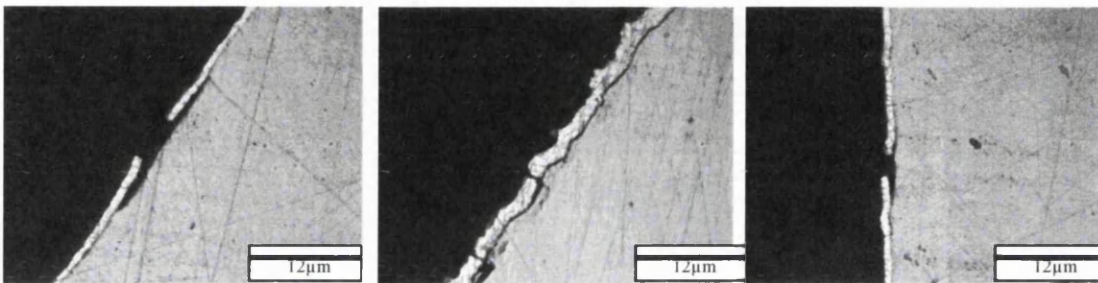
In its current form the PVD coating should be the most formable; the dense Zn layer will deform in much the same way as hot dip galv. The magnesium layer above is showing columnar structure and so will likely break up easily and flow with the zinc layer underneath. The major test for the PVD coatings is if they can tolerate the movement of the substrate due to the metallic bonding being limited to the degree of etching on preparation of the sample.

When forming coatings there are compressive and tensile forces acting at different areas of the dome. When the dome starts to lift the substrate bends up compressing the coating, this can cause delamination of the coating showing up as voids at the coating/substrate interface. The stretching of the material as the dome is lifted causes tensile forces that will thin a very formable coating so that no breaks in the coating occur, a less formable coating will show cracks. The formability of MZ140 ( $140\text{g/m}^2$  MZ) has been used to compare with the PVD coatings.

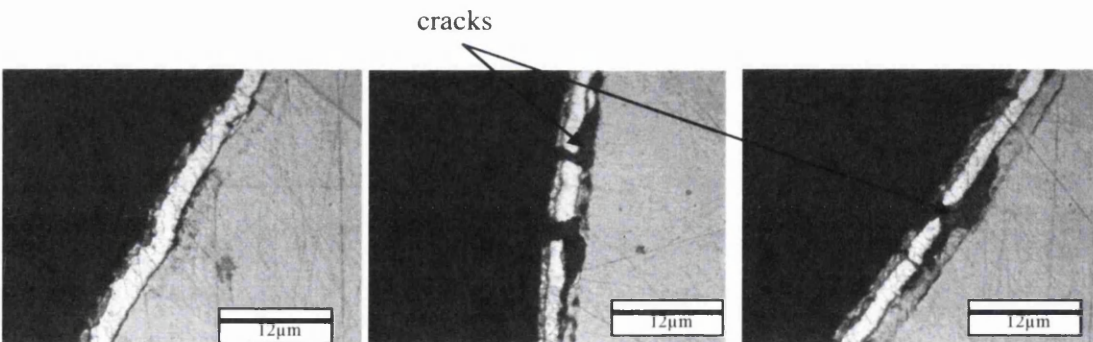
-70 a) to c) show a series of cross section images taken from the base, approximately half way up the dome height and the top of domes. There is extensive cracking of the coating from approximately half way up the coating. Similar performance is seen in the thinner coatings (lighter coating weights).



**Figure 68 - MZ140 a) bottom, b) side and c) top**



**Figure 69 1.0Mg a) bottom, b) side and c) top**



**Figure 70 1.5Mg a) bottom, b) side and c) top**

It can be seen from the microstructures that there is vastly different behaviour in the PVD coatings to the hot dipped MagiZinc<sup>®</sup> coating. At the bottom of the dome there is significant delamination from the compressive stresses whilst in the areas of maximum tensile stresses there is further, more significant delamination and cracking of the coating. It is worth noting that there appears to be significant flow of the Zn coating layer and evidence of necking before cracking. The side and top of the 1.5Mg sample show some

deformation of the substrate, possibly showing the limits of formability of the substrate, due to the decreased gauge.

### 3.9 GDOES Analysis

Initially the laboratory annealed samples were analysed by Electron Probe Micro-Analysis (EPMA) also called Energy Dispersive X-Ray Fluorescence (EDX), this was found to have some good information but also was quite difficult to interpret due to the problems of X-ray penetration into the sample and beam spot size causing de-resolution of the sharp interfaces observed optically. The HDS annealed samples have been analysed in STC for a more definitive determination of the diffusion of the Mg.

An example GDOES profile can be seen in Figure 71, the atomic percentage levels returned can be examined to determine the percentage of undiffused magnesium (minus any oxide present),  $MgZn_2$  intermetallic; as seen in the XRD analysis to be the most stable phase, and combined zinc and iron-zinc intermetallic species. Figure 72 to Figure 77 show the analysis of GDOES data to resolve the percentages of non-diffused Mg,  $MgZn_2$  and remaining zinc. GDOES data is returned as a function of time in seconds, the conditions for the analysis were kept constant so that the time versus depth relationship was consistent.

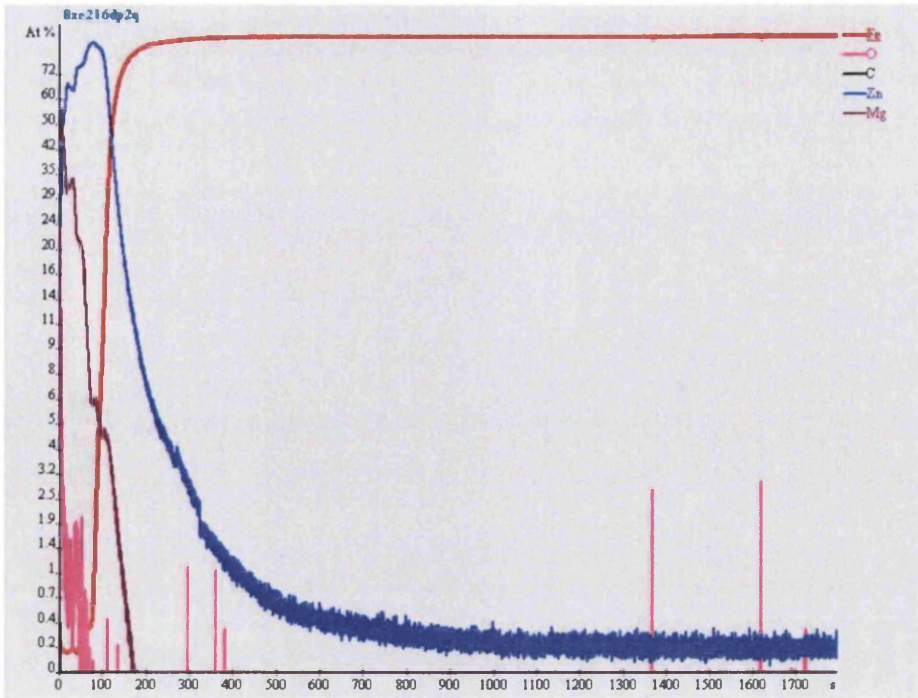


Figure 71 - GDOES analysis of 1.0Mg sample annealed at 250oC for 300 seconds

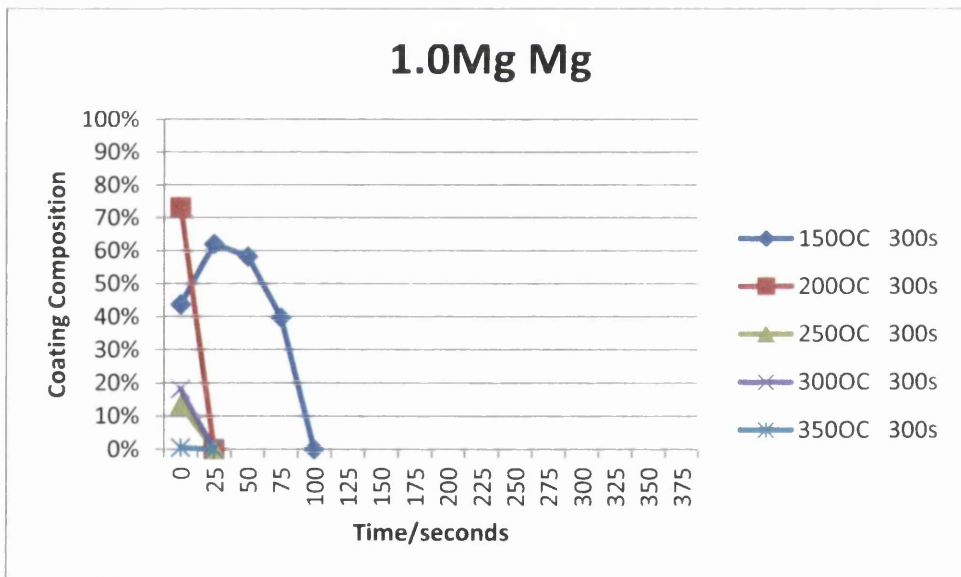


Figure 72 - Free Mg in 1.0Mg Annealed Samples

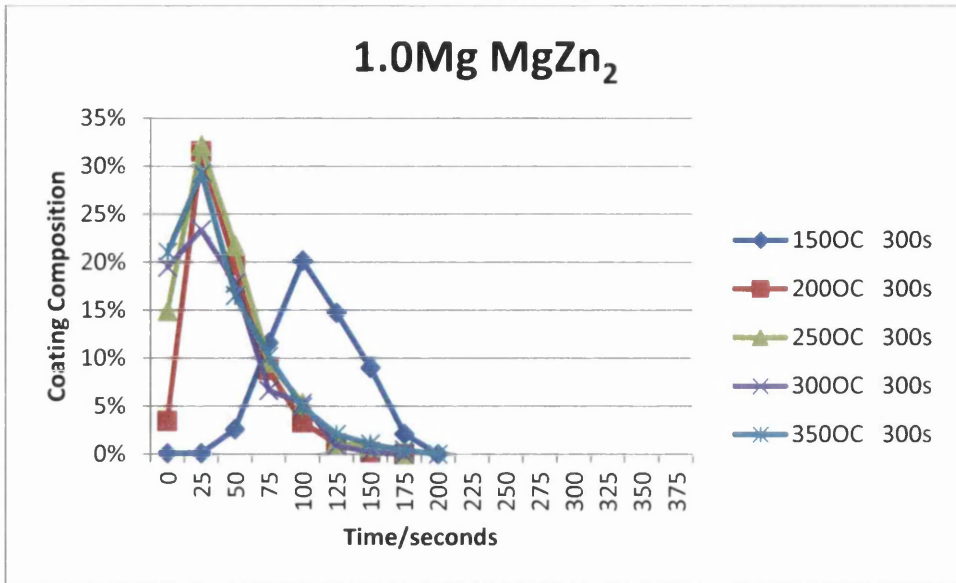


Figure 73 - MgZn<sub>2</sub> Content in 1.0Mg Annealed Samples

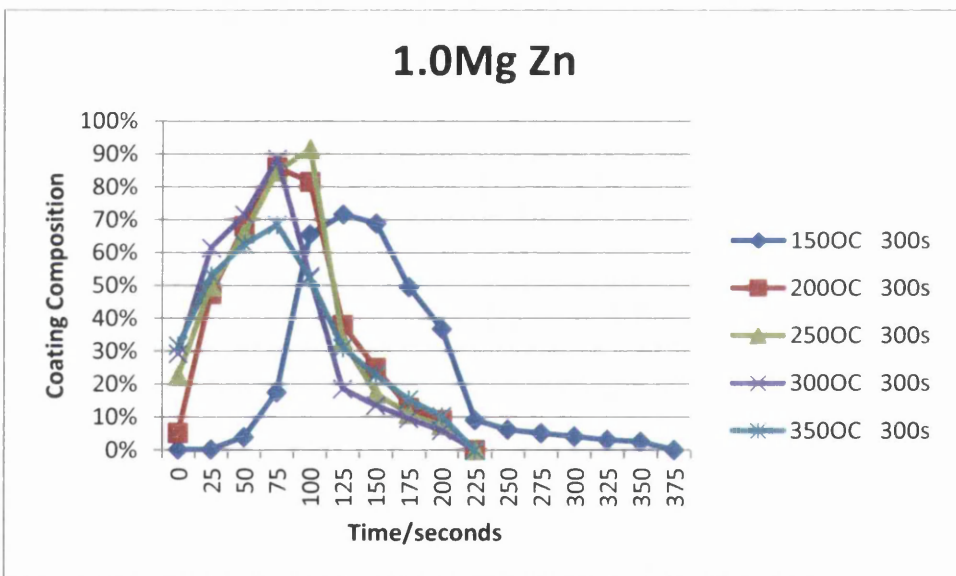


Figure 74 - Zn & Fe-Zn in 1.0Mg Annealed Samples

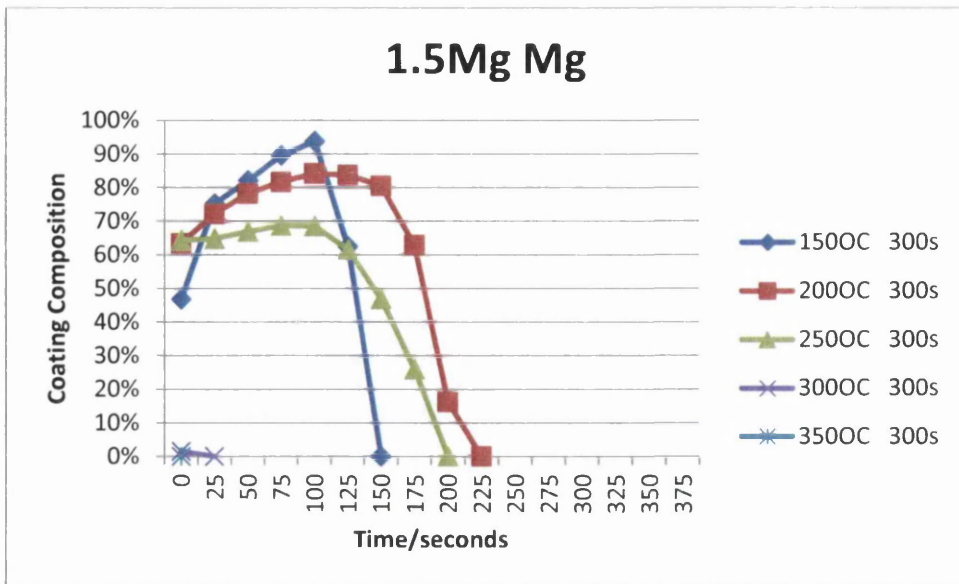


Figure 75- Free Mg in 1.5Mg Annealed Samples

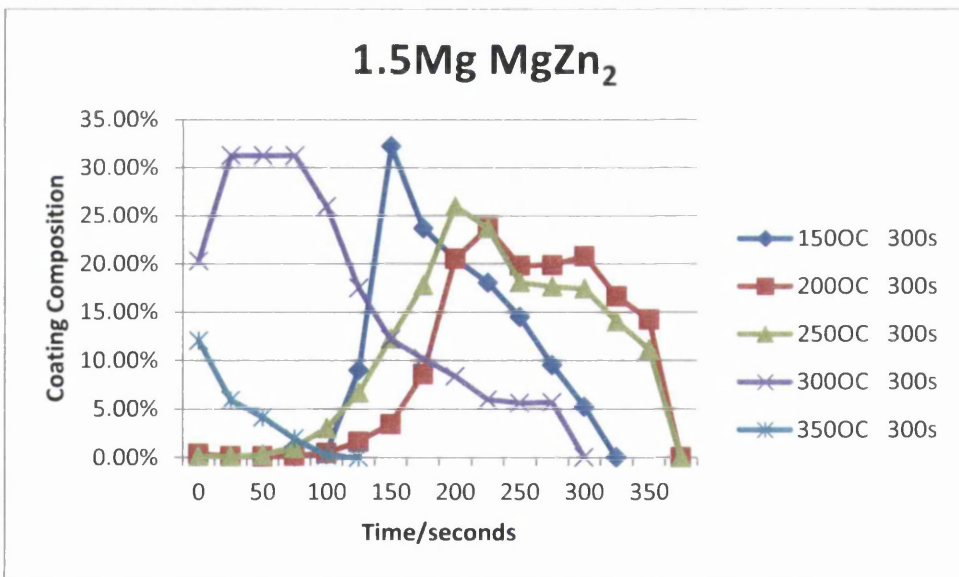
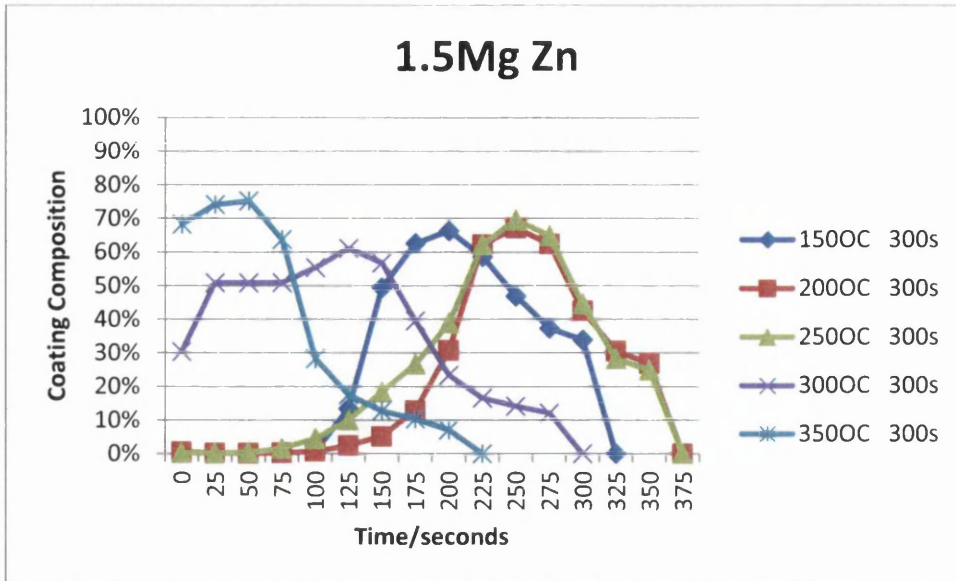


Figure 76 - MgZn<sub>2</sub> Content in 1.5Mg Annealed Samples



**Figure 77 - Zn & Fe-Zn in 1.5Mg Annealed Samples**

We can see from the GDOES analysis that the diffusion of magnesium into zinc is fully complete, i.e. no free magnesium remains, at 350°C for the 1.0Mg samples and at 300°C for the 1.5Mg samples. The production of MgZn<sub>2</sub> intermetallic phase can be seen to move to greater depths in the 1.5Mg samples compared to the 1.0Mg samples, though the amount of MgZn<sub>2</sub> seen is consistent between the two samples at around 30-35% of the coating maximum.

We can see that 150°C provides enough energy for the production of intermetallic phase but the rate of diffusion is too slow to allow the full interdiffusion of the magnesium layer within the 300 second annealing cycle. The 1.5Mg 350°C is showing less production MgZn<sub>2</sub> due to the full diffusion of iron to the surface of the coating.

### 3.10 Corrosion testing

SVET studies of the as received coatings show some interesting surface activity and reactions with the electrolyte (0.1% NaCl).

### 3.10.1 Surface Corrosion

Initial investigative work on the surface corrosion of 1.0Mg and 1.5Mg, using SVET and 0.1% NaCl generated results as expected; the corrosion was extreme at the start, due to the presence of reactive, elemental magnesium, even giving rise to the formation of hydrogen according to the reaction;

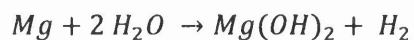
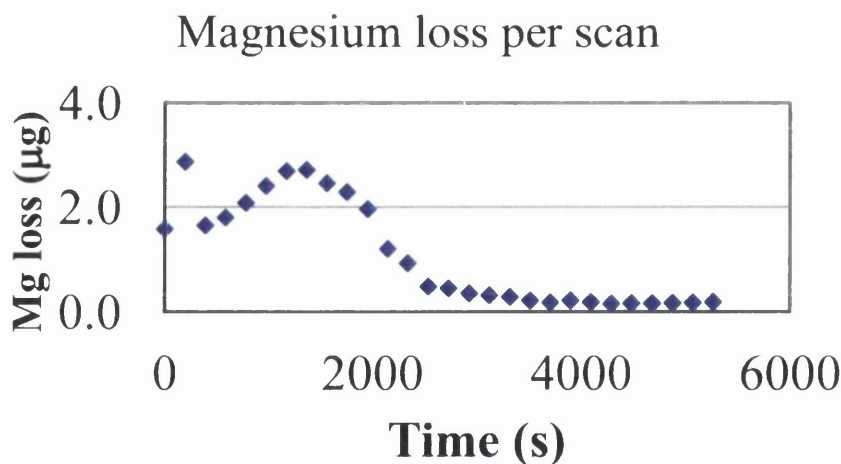


Figure 78 shows a mass loss graph for magnesium during a surface scan of 1.5Mg, calculated from Faraday's law, as section 2.1.6. The trend shows a point of inflection after approximately 8 minutes of immersion corresponding to the decrease in anodic activity for the free surface magnesium. It is thought that two effects could be occurring, that either the anodes are becoming increasingly smaller and more difficult to detect with this technique, that the corrosion is no longer localised enough for detection by the SVET.



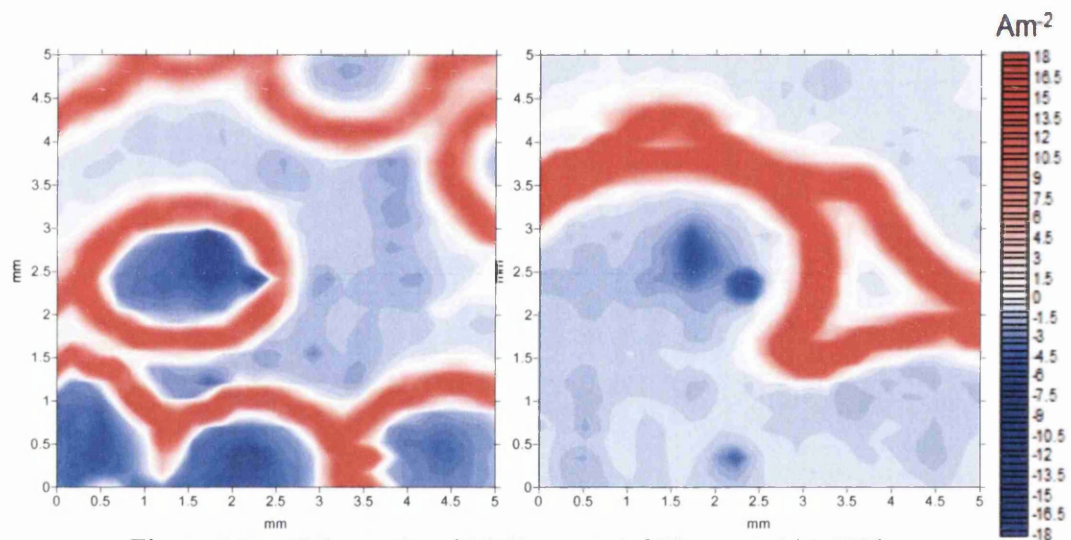
**Figure 78 - Mg mass loss 1.5Mg (surface)**

Along with the rapid removal of reactive magnesium from the surface there was some interesting corrosion activity on the surface with the formation of strongly anodic sites



that propagate through the magnesium layer as a series of anodic fronts from each initial anode, a number of scans can be seen in figure 79 a) and b), showing the movement of these anodic fronts.

The high levels of corrosion activity was indicated visually by the formation of a temporary black corrosion deposit on the initial anode, followed by later dissolution, and the deposition of further black corrosion deposit on the movement of the anodic front. It is thought that the black corrosion deposit is finely divided and deposited Mg metal probably due to the reaction proceeding with such vigour that microscopic pieces of the coating are being lifted into solution before full dissolution.



**Figure 79 -1.5Mg surface SVET scans a) 975secs and b) 1755 secs**

We can see the early activity associated with the rapid loss of magnesium [86, 102] in the plots of the surface mass losses for the PVD samples, see Figure 80 to Figure 82. Higher annealing temperatures show a linear mass loss corresponding to the samples that show little or no surface magnesium from the GDOES analysis.

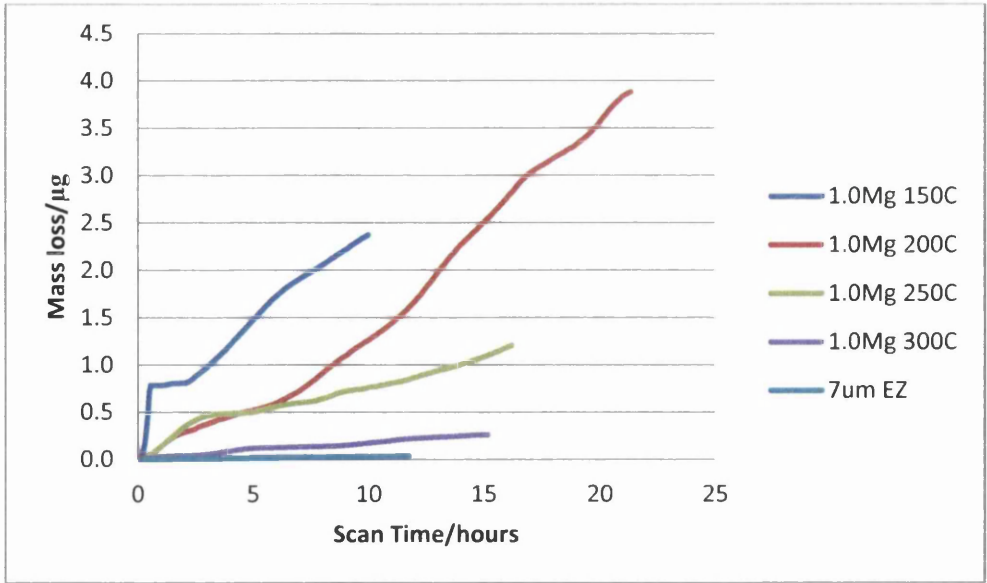


Figure 80 - Surface mass loss - 1.0Mg Samples

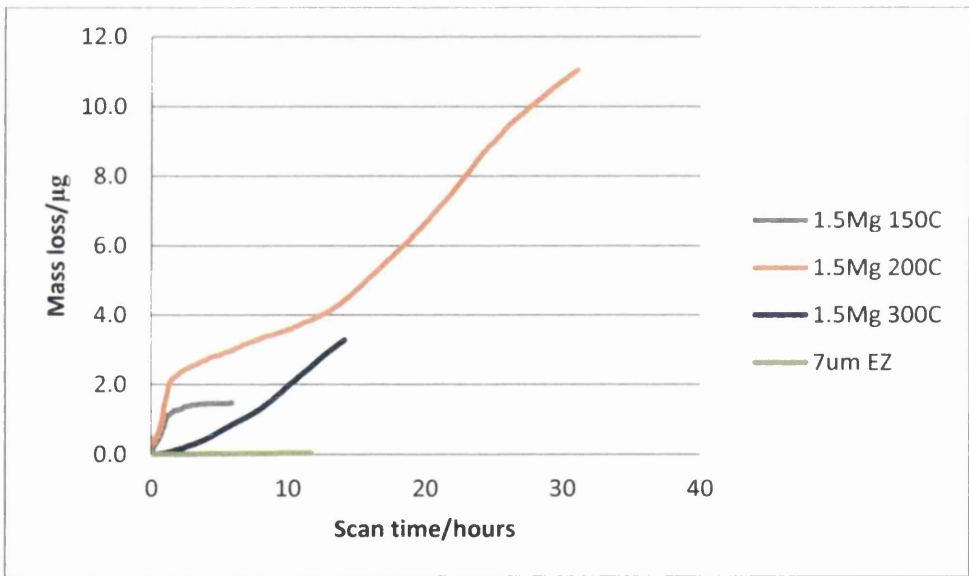
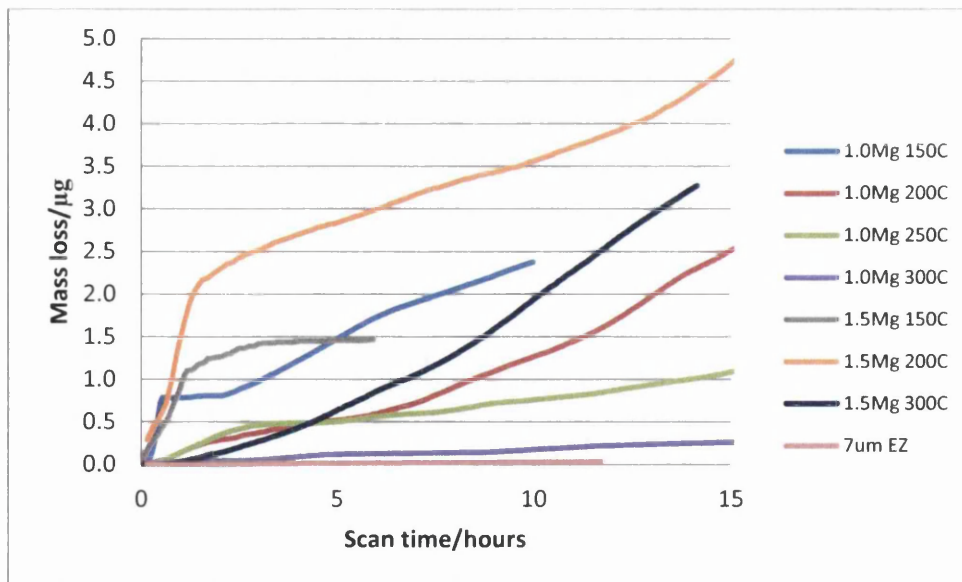


Figure 81 - Surface mass loss - 1.5Mg Samples



**Figure 82 - PVD Samples Surface Mass Loss**

From this information it can be seen that annealing temperatures of 250°C or above provide sufficient temperature to fully interdiffuse all of the Mg layer into the zinc layer. The best performing of the PVD samples are 1.0Mg annealed at 200, 250 and 300°C and 1.5Mg annealed at 300°C.

The trend lines for the corrosion losses give a measure of the corrosion rate, this can be calculated into lifetimes for the coatings as we know the coating weights, Table 9 shows the results. A sample of electrogalvanised zinc, EZ, was used as a surface corrosion benchmark sample as the electroplating process used to manufacture the coating generates a pure zinc layer, without any intermetallic phase on the substrate, or aluminium additions to the coating, giving a conventional production sample that is chemically identical to that of the PVD zinc coating.

Sample	Corrosion rate $\text{g/m}^2 \text{h}^{-1}$	Coating weight $\text{g/m}^2$	Lifetime (hours)
1.0Mg 200C	0.164	24.5	149.4
1.0Mg 250C	0.0763	24.5	321.2
1.0Mg 300C	0.0182	24.5	1346.6
1.5Mg 300C	0.1968	35.6	180.7
7 $\mu\text{m}$ EZ	0.0029	100.0	34,482.8

**Table 9 - Lifetimes for best performing coatings**

### 3.10.2 Cut-edge corrosion

Samples of the 0.31mm annealed samples were compared against 0.39mm gauge 275 $\text{g/m}^2$  hot dip galv. 20mm sections of the annealed samples were mounted in epoxy metallographic resin and polished to a flat surface using 1 $\mu\text{m}$  diamond suspension in an aliphatic hydrocarbon. All of the samples were tested using 0.1%NaCl solution and scanned continuously to investigate the metal loss. The metal losses can be plotted against scan time to determine a rate of corrosion loss per hour. The samples were compared against a sample of hot dig galvanised steel. We can see from Figure 83 and Figure 84 that for the 1.0Mg samples the 300 $^{\circ}\text{C}$  and the 150 $^{\circ}\text{C}$  annealing times produced coatings that behaved better than the benchmark sample, though for the 150 $^{\circ}\text{C}$  sample this is not following the trend of the samples and is thought to be due to the rapid reaction of undiffused magnesium moving away from the plane of the scan and out of the detection zone, i.e. the corrosion activity proceeded down the substrate/mounting resin interface.

All of the 1.5Mg samples performed better than the benchmark sample, corrosion losses are detailed in Table 10.

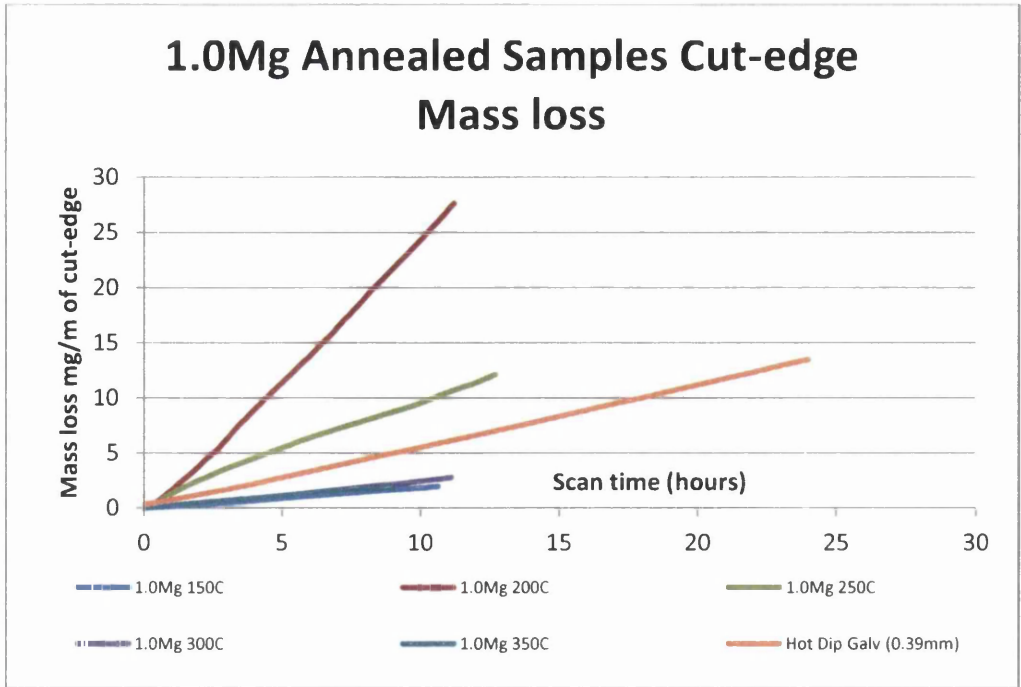


Figure 83 - Cut-edge losses from 1.0Mg Annealed Samples

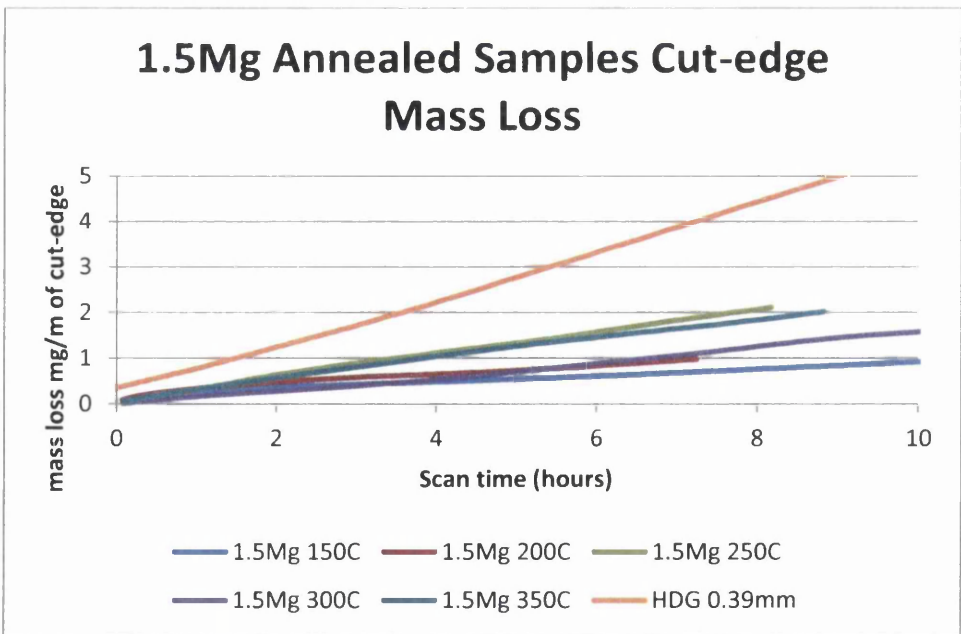


Figure 84 - Cut-edge losses from 1.5Mg Annealed Samples

Sample	Corrosion rate mg/m h <sup>-1</sup>
1.0Mg 150C	0.18
1.0Mg 200C	2.38
1.0Mg 250C	0.98
1.0Mg 300C	0.24
1.0Mg 350C	0.22
1.5Mg 150C	0.10
1.5Mg 200C	0.15
1.5Mg 250C	0.27
1.5Mg 300C	0.15
1.5Mg 350C	0.24
HDG 275gsm	0.56

**Table 10 - Cut edge corrosion rates for PVD Samples**

### 3.11 Cabinet Testing

The coated panels, as shown in Table 11 were tested according to TSW/103, which conforms to the ASTM B117 salt spray test. ASTM B117 uses a 5% sodium chloride solution (AnalaR grade), which is substantially free of nickel and copper and contains no more than 0.1% sodium iodide and 0.3% of total impurities. The pH of the salt solution is such that, when atomised at 35<sup>0</sup>C, the collected solution will be in the range of 6.5 – 7.2. The temperature of the spray chamber is maintained at 35<sup>0</sup>C (± 2<sup>0</sup>C). Fall out rates are such that 1.0 to 2.0ml/hr are collected in flasks, which have an 80cm<sup>2</sup> horizontal area.

Sample	Temp	Time	Surface
1.0Mg	150°C	300s	Flat
1.0Mg	150°C	300s	5.0mm Erichson Dome
1.0Mg	300°C	300s	Flat
1.0Mg	300°C	300s	5.0mm Erichson Dome
1.5Mg	150°C	300s	Flat
1.5Mg	150°C	300s	5.0mm Erichson Dome
1.5Mg	300°C	300s	Flat
1.5Mg	300°C	300s	5.0mm Erichson Dome

**Table 11 - PVD Salt Spray Samples**

The test was continuous for the duration of the entire agreed test period of 456 hours, except for routine inspection and recording of the coating appearance by images after every 24 hours. The samples were investigated for their red rust formation with the time for 5% red rust formation being the critical factor. Samples of GI275, MZ100 and EZ 7µm have been tested for comparison in both flat and domed format, Figure 85 and Figure 86, show the results.

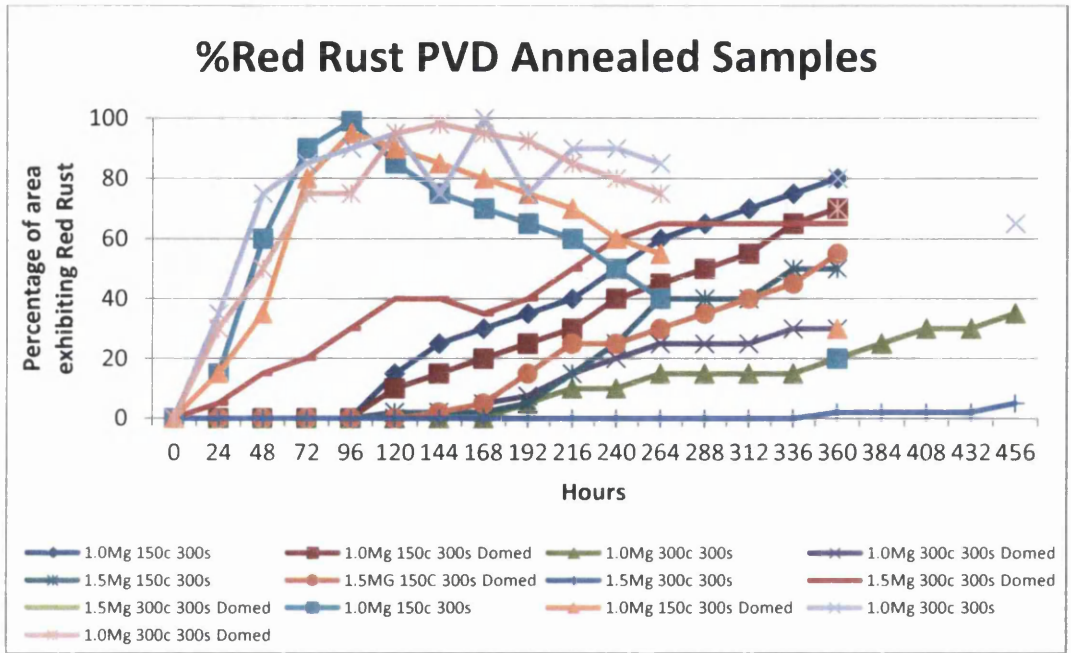


Figure 85 - %Red Rust PVD annealed Samples

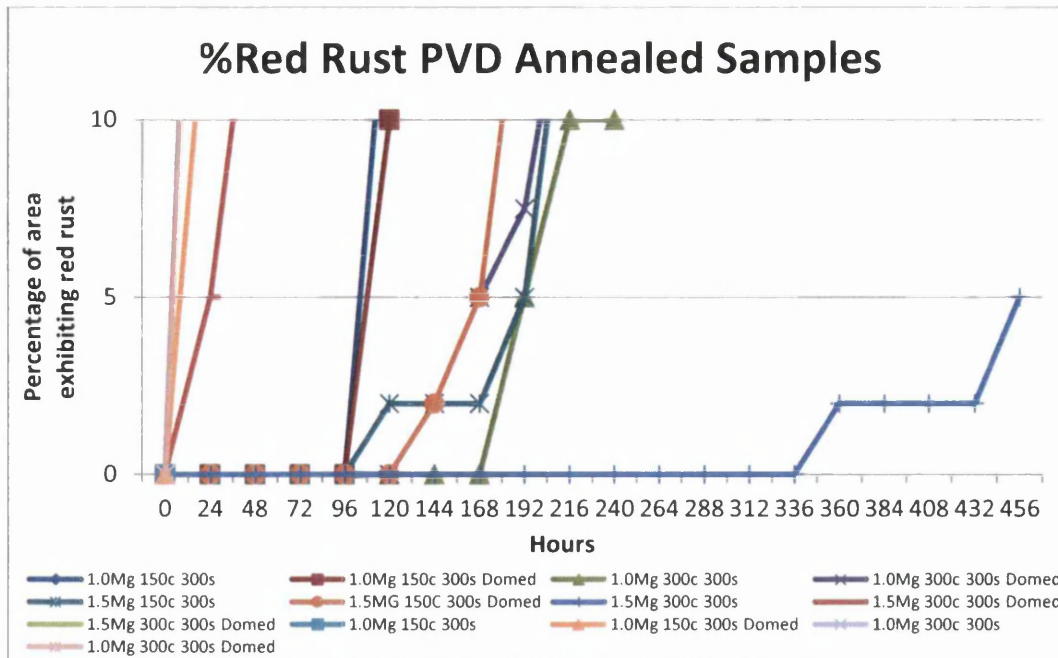


Figure 86 - %Red Rust PVD Samples (zoomed)

### 3.12 Discussion and conclusions

The PVD samples show very interesting corrosion activity, all of the samples tested showed a vigorous reaction when the surface is exposed to the chloride electrolyte, similar to the anodic ring mechanism seen in figures 79a) and b), and comparably poor mass loss results compared to a sample of EZ in surface SVET corrosion investigations, as seen in figures 80 and 81.

The salt spray results seemed to fall more in line with that expected and with some other findings in the literature, however it was interesting to see that the best performing coating, 1.5Mg annealed for 300°C for 300 seconds, whilst being the best coating as a flat panel, i.e. 456 hours to 5% red rust formation, was the worst performing coating as a formed sample. When we examine the coating characteristics this becomes evident from the extensive amount of intermetallic formation (the entire original magnesium layer has been interdiffused) which would limit the formability in line with the increased hardness that has been measured.



On salt spray the 1.0Mg annealed at 300°C performed similar in a way to the 1.5Mg coating annealed at 150°C, with the onset of red rust at 168 hours and 24 hours earlier for the domed samples, showing some degree of formability. The 1.5Mg sample shows some surface magnesium that has not been interdiffused as evidenced by the surface SVET corrosion testing. The 1.0Mg 300°C shows good corrosion losses in the surface SVET test. On cut-edge mass loss both of the samples outperform the benchmark sample.

PVD coatings are expensive to produce and so it is recommended that the coating characteristics in the thinner coating of 1.0Mg be used as a benchmark for further studies to examine if there are competitive solutions to the requirements of the coating for annealing. It is considered that the manufacturing of the coating on a strip processing line would be extremely challenging from an engineering viewpoint as the annealing times examined here would require furnace lengths similar to the annealing of strip steels not those found on conventional coating lines.

## **Chapter 4**

### **Influence of Steel Gauge on the Microstructure and Corrosion**

#### **Performance of Zinc Alloy Coated Steels**

**(Published paper)**

**Corrosion Science 52 (2010) 1853-1862**

**Sullivan J., Weirman C., Kennedy J. – Swansea University**

**Penney, D. - Corus Colors, Shotton Works**

## 4.0 Introduction

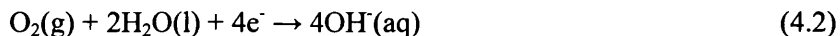
Zinc/Aluminium alloys are rapidly becoming the hot dipped galvanising coating material of choice for premium pre-painted steels within the steel industry due to their increased corrosion resistance over traditional hot dipped galvanised steel (HDG) [103].

Examples of such alloys are those based on aluminium compositions of 5%, known as Galfan, and higher aluminium content such as Galvalume at 55% Al and 1.5% Si. The aluminium in the structure promotes the formation of a two phase microstructure with primary zinc dendrites in a Zn/Al eutectic matrix for hypereutectic (<5% Al) systems whilst in hypoeutectic alloys (>5%) primary Al forms in a Zn/Al eutectic matrix [104].

The aluminium in the microstructure improves the corrosion resistance of the materials through formation of aluminium oxide that is a very adherent and protective barrier oxide [104]. The formation of a two phase microstructure also promotes preferential corrosion of the least noble phase that changes the corrosion mechanism and performance away from that of traditional Zn hot dipped galvanised steels containing around 0.2% Al [9].

Previous research has shown that cooling rate and coating thickness changes have dramatic effects on the microstructure and corrosion resistance of Zn/Al alloy coated steels [9, 38]. However, many different gauges of steel are used depending on the application within a building or automobile and presently no changes in processing conditions are applied to maintain similar microstructures for all gauges. This may be an issue if modifications introduced in the microstructures cause changes in cut edge corrosion behaviour when it comes to issuing warranties and lifetimes for the materials. Cut edge corrosion of these materials is primarily due to anodic Zn loss (4.1) with the cathodic reaction (4.2) supported on the steel substrate.





It is known from corrosion theory that as steel gauge increases, i.e. the cathodic area increases, the rate of cut edge zinc loss through anodic attack will increase as the reaction is predominantly cathodically controlled [105]. Suzuki has shown this to be the case for HDG with a fairly linear increase in Zn loss from the cut edge as steel gauge is increased with a drop in rate at thickness above 0.8 mm [106].

This body of research investigates the effect of steel gauge on the microstructure and cut edge corrosion resistance of Zn-4.8wt % Al alloy coatings compared with traditional Zn hot dipped materials (HDG). The cut edge corrosion performance of the alloy coated steels was assessed using the scanning vibrating electrode technique (SVET) that has proved very reliable in highlighting the corrosion mechanisms of galvanised steels and for predicting long term corrosion behaviour when compared with external weathering [38, 107].

## **4.1 Experimental**

### **4.1.1 Materials**

Samples of Zn-4.8 wt% Al coated steels with different steel substrate gauge thickness were obtained from Corus Colors at Shotton, Deeside, UK. All materials had an alloy coating weight of 100 gm<sup>-2</sup>. The materials also had 15 µm polyester organic coating on each side, this product is referred to as liner material in Tata Steel Colors. This polymer system contained no corrosion inhibitor so should not have influenced the corrosion behaviour of the alloy system dramatically and was consistent for all samples. The list of materials tested is outlined in Table 12.

Organic coating	Metallic coating	Metallic coating weight gm <sup>-2</sup>	Steel Substrate gauge/mm
15µm polyester	Zn-4.8wt% Al	100	0.38
15µm polyester	Zn-4.8wt% Al	100	0.60
15µm polyester	Zn-4.8wt% Al	100	0.80
15µm polyester	Zn-4.8wt% Al	100	1.00

**Table 12 - Zn-4.8wt% Al alloy coated steel sample details**

Samples of Hot dipped galvanised (HDG) steel on a variety of gauges was also provided from Corus Colors as reference material. This coating is predominantly pure Zn with a small alloy addition, 0.3 wt % Al, to prevent the formation of several brittle intermetallic phases during dipping. These samples had an identical organic coating thickness, the zinc coating weight and range of gauges were significantly different to the Zn-4.8wt% Al coated steels and this was due to the differences in production materials offered by the Corus Colors company. These materials are shown in Table 13. It should be noted that the aim of this investigation was to assess the effect of steel gauge on the corrosion trends of these materials rather than to directly compare the corrosion rates of Zn-4.8wt% Al and HDG coated steels. Thus, the difference in coating weight between the materials is not so important.

Organic coating	Metallic coating	Metallic coating weight gm <sup>-2</sup>	Steel Substrate gauge/mm
15µm polyester	Zn-0.3wt % Al	275	0.39
15µm polyester	Zn-0.3wt % Al	275	0.55
15µm polyester	Zn-0.3wt % Al	275	0.68
15µm polyester	Zn-0.3wt % Al	275	0.85

**Table 13 - HDG reference materials**

## **4.1.2 Metallographic investigation**

Samples of each Zn-4.8wt % Al material from Table 1 were guillotined into 20 x 20 mm coupons. The organic coating was first removed from the material by soaking in acetone and then the samples were mounted flat in phenolic mounting compound. In order to examine the microstructure of the alloy as a function of depth the samples were subjected to the depth profiling technique outlined in section 2.4.

## **4.1.3 Corrosion testing of Zn-4.8wt% Al and HDG coated steels**

### **4.1.4 Weight loss**

An initial assessment of coating performance with increasing steel gauge was carried out using a simple weight loss test. Samples of material from Table 12 and Table 13 were cut into 20x20 mm coupons thus providing a cut edge length of 80 mm. The samples were then individually weighed using a GMBH Sartorius laboratory balance (Germany) that had an accuracy to 0.0001 g.

The samples were then placed into individual containers and immersed in 0.1% NaCl in water for 144 hours. After this time the samples were exposed to ultrasonic cleaning in de-ionised water for 1 minute to remove loose corrosion products, removed, rinsed and dried. The sample was then weighed and the weight loss calculated.

## **4.1.5 Scanning Vibrating Electrode Technique (SVET) investigation into cut edge corrosion behaviour**

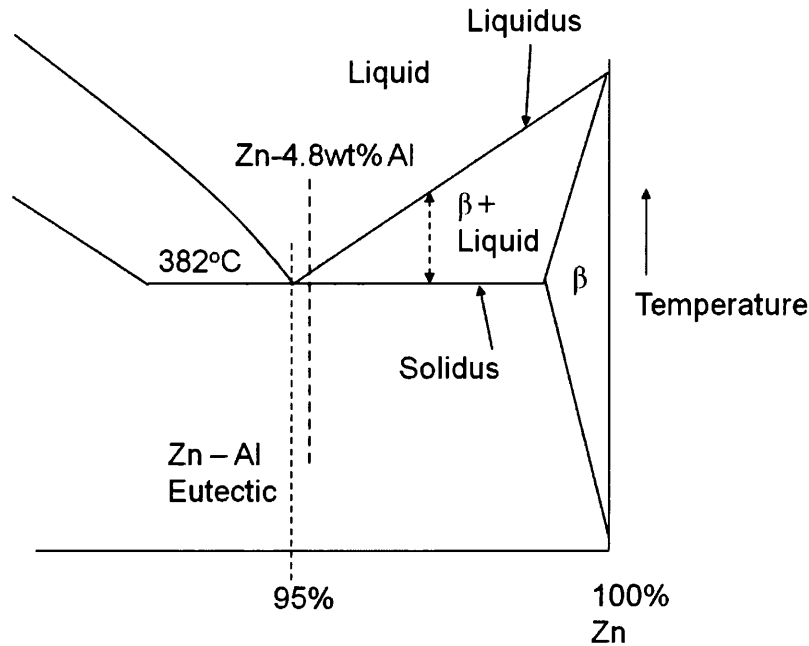
### **4.1.5.1 SVET sample preparation**

All samples from tables 12 and 13 were cut into 20x20 mm coupons and mounted in non-conductive resin to expose one length of cut edge. This edge was then polished flat and to a mirror finish using progressively finer emery papers and 1  $\mu\text{m}$  diamond slurry to ensure reproducible surfaces for SVET testing. The area scanned by the SVET was 20 mm along the cut edge and 2 mm perpendicular to this across the edge. The SVET probe made 80 measurements along the length of the cut edge and 20 measurements across the samples width generating a matrix of 1600 data points for each scan. The SVET tests were carried out in 0.1%NaCl solution and one scan was taken every hour for 24 hours and three repeat tests for each material were carried out. The dissolved oxygen concentration in bulk solution was assumed to be constant at  $2.8 \times 10^{-4} \text{ mol dm}^{-3}$  [108], the equilibrium concentration for air saturated water, and all tests were carried out at 25°C.

## **4.2 Results and discussion**

### **4.2.1 Solidification of the Zn-4.8wt% Al alloys.**

The Zn-4.8wt% Al alloy under investigation is hypereutectic lying just to the right of the eutectic point of 5 wt% Al in the Zn/Al equilibrium phase diagram as shown in the schematic in Figure 87.



**Figure 87 - Portion of the Zn/Al phase diagram showing the 4.8wt%Al region [104]**

On cooling from the liquid phase through the liquidus line nucleation of  $\beta$  crystals of primary Zn occurs at some undercooling below the liquidus temperature and the remaining liquid ahead of the solidification front becomes enriched in Al. As cooling proceeds the  $\beta$  crystals start to grow into a dendritic structure under practical cooling rates and when the remaining liquid reaches 5wt% Al it solidifies into a lamellar eutectic of alternating sheets of Zn and Al.

A rod eutectic can form but generally at very high cooling rates or with small additions of ternary elements such as Mg [36, 48, 109]. The final microstructure is therefore composed of primary zinc dendrites in a matrix of lamellar Zn/Al eutectic. The nucleation of the  $\beta$  primary zinc tends to occur on the steel substrate as this solid surface provides an energetically favourable site for heterogeneous nucleation. The dendrites then grow and branch upwards away from the steel and so there is a larger primary Zn volume fraction at the interface than at the surface where the coating is predominantly



eutectic. This is demonstrated in Figure 88 that shows the volume fraction of primary Zn as a function of depth for the four steel gauges investigated.

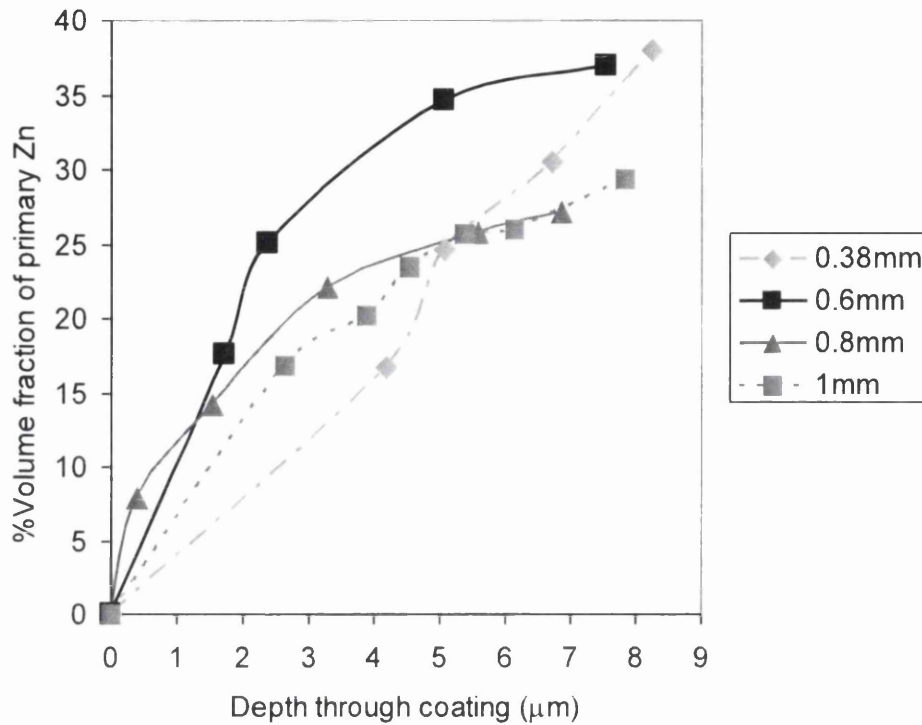


Figure 88 - Variation in volume fraction of primary Zn with depth with varying gauge

The Volume fraction is higher next to the coating/steel interface demonstrating this as the site for nucleation of the dendrites. All coatings had a thickness of approximately 8 µm.

All the materials show an increase in volume fraction with increasing depth through the coating suggesting that nucleation does indeed occur preferentially on the steel substrate.

The average volume fraction for all the materials is very similar and is shown in Table 14.

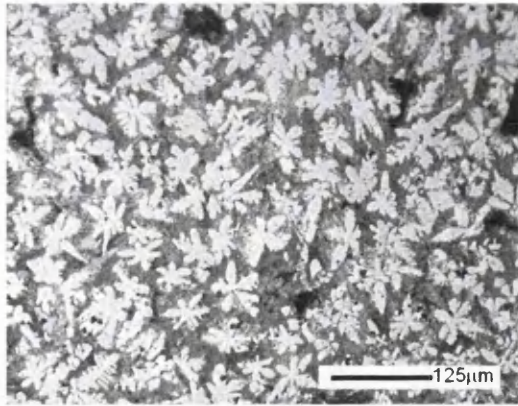
Steel gauge (mm)	Metallic Coating	Average Volume fraction %	Dendrite number mm <sup>-2</sup>	Average size of dendrite mm <sup>2</sup>
0.38	Zn-4.8wt% Al	29±3	456±51	1.2x10 <sup>-4</sup>
0.60	Zn-4.8wt% Al	22±3	226±15	1.9 x10 <sup>-4</sup>
0.80	Zn-4.8wt% Al	22±3	185±15	2.3 x10 <sup>-4</sup>
1.00	Zn-4.8wt% Al	24±3	164±15	2.9 x10 <sup>-4</sup>

**Table 14 - Average volume fraction of primary Zn and microstructural characteristics**

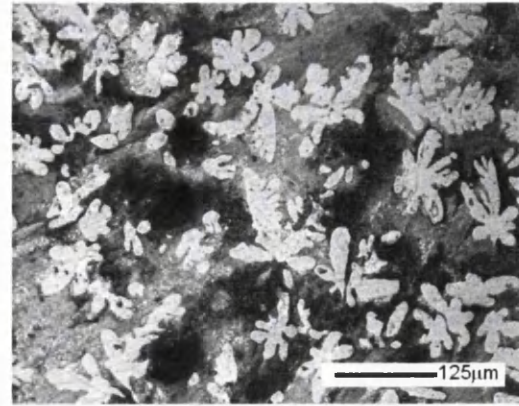
#### **4.2.1.1 Effect of steel gauge on the microstructure of Zn-4.8wt% Al alloy coatings.**

Figure 89 shows micrographs of the microstructure of each material just above the coating/substrate interface at a depth of approximately 8 μm. It is clear to see that there is a change in the microstructure from the thin to the thickest steel substrate gauge. Dendrites become less numerous and larger with increasing gauge due to slower cooling rate of the thicker steel substrates. On the thinnest gauge of 0.38 mm there are a higher number of smaller dendrites present and for the samples with increased steel gauge, the number of dendrites decreases but becomes larger.

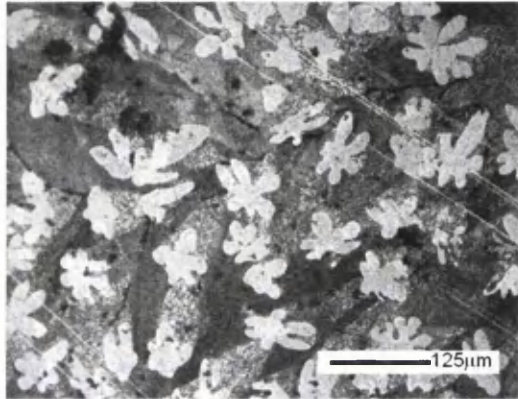
Table 14 shows the dendrite number per unit area for the different coated steel gauges. This highlights the change in the number of dendrites from 456±51 mm<sup>-2</sup> for the 0.38 mm gauge steel to 164±15 mm<sup>-2</sup> for the 1 mm gauge steel. The average dendrite size changes from 0.064 mm<sup>2</sup> to 0.146 mm<sup>2</sup> from the 0.38 mm to the 1 mm gauge steel. This change in microstructure is consistent with a change in cooling rate during the solidification of the alloy.



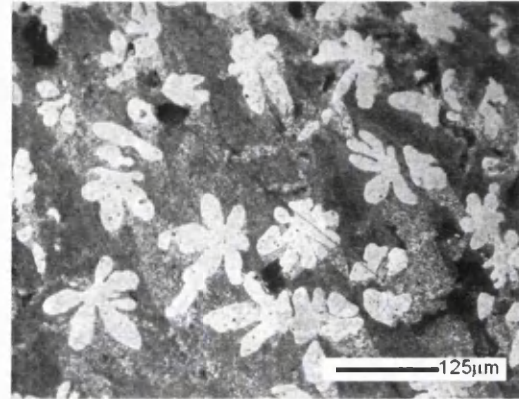
0.38mm gauge



0.60mm gauge



0.80mm gauge



1.00mm gauge

**Figure 89 - Microstructural changes in Zn-4.8wt% Al alloys with increasing substrate gauge (all images taken at 6µm through the coatings)**

In the process of hot dip galvanising, the steel substrate passes through a reducing furnace prior to dipping in order to remove any surface oxides so that the zinc alloy will wet and adhere to the steel. The steel substrate therefore enters the galvanising bath at a temperature of around 450°C. This temperature promotes reaction diffusion between the alloy and the substrate allowing the coating to stick. The steel then exits the bath through air knives that control the zinc alloy coating thickness.

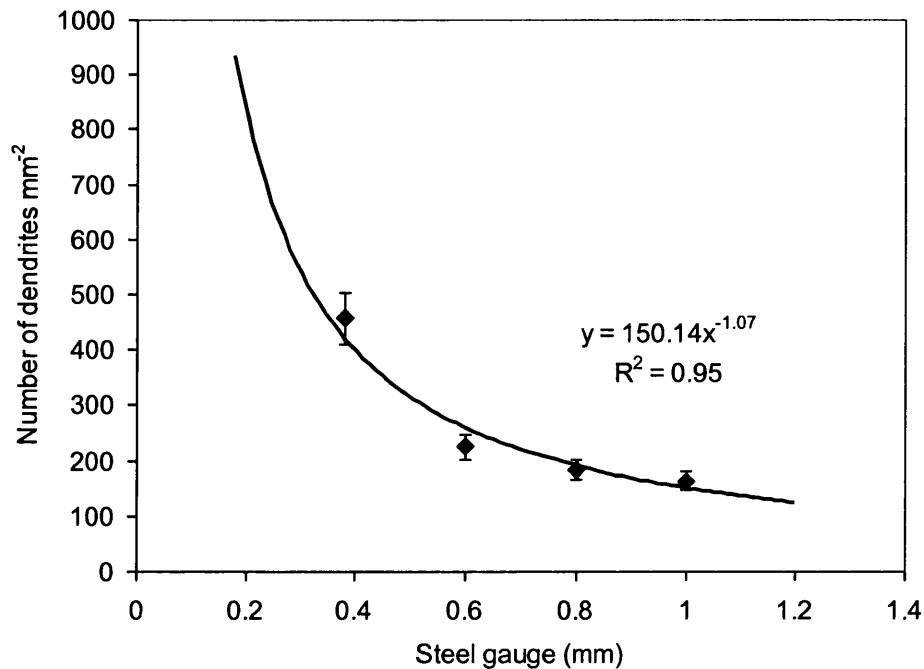
Solidification of the alloy initiates on exiting the knives and cooling rigs, situated 5-10m above the bath, are used to complete this solidification as the strip rises through the plant. In production of these samples the cooler was running at 45% of its total output for all the samples investigated. It appears from the microstructures observed here that the thicker

gauges of steel retain heat for longer on exiting the bath and thus promote a slower cooling rate leading to the formation of larger, less numerous dendrites. On the thinner steel gauges there is less retained heat so the cooling rate is faster leading to a greater nucleation rate thus producing smaller but more numerous dendrites. Figure 90 is graph of dendrite number per unit area for the different coated steel gauges. From this graph a power law relationship can be ascertained with reasonable fit with the data obtained.

The number of dendrites is an indirect measure of nucleation rate and the increasing steel gauge represents a decrease in cooling rate so these data show that as cooling rate decreases the nucleation rate of primary Zn also decreases. The power law relationship is shown in the equation;

$$D = 150.14 S^{-1.07}$$

where D is Dendrite number ( $\text{mm}^{-2}$ ) and S is the steel gauge (mm).



**Figure 90 - Number of primary Zn dendrites per unit area with varying gauge**

The increase in cooling rate on the thinner gauges samples will generate a larger degree of undercooling during solidification. This increased undercooling serves to reduce the free energy barrier to heterogeneous nucleation and also to reduce the critical radius for a nucleus to form and grow. This is shown in the equation

$$r^* = \frac{2\gamma_{SL}T_e}{L\Delta T} \quad [110]$$

where;

$r^*$  = Critical radius size of nuclei for growth

$\gamma_{SL}$  = Interfacial energy between Nuclei and Liquid

$T_e$  = Equilibrium freezing temperature

$L$  = Latent heat

$\Delta T$  = Amount of undercooling.

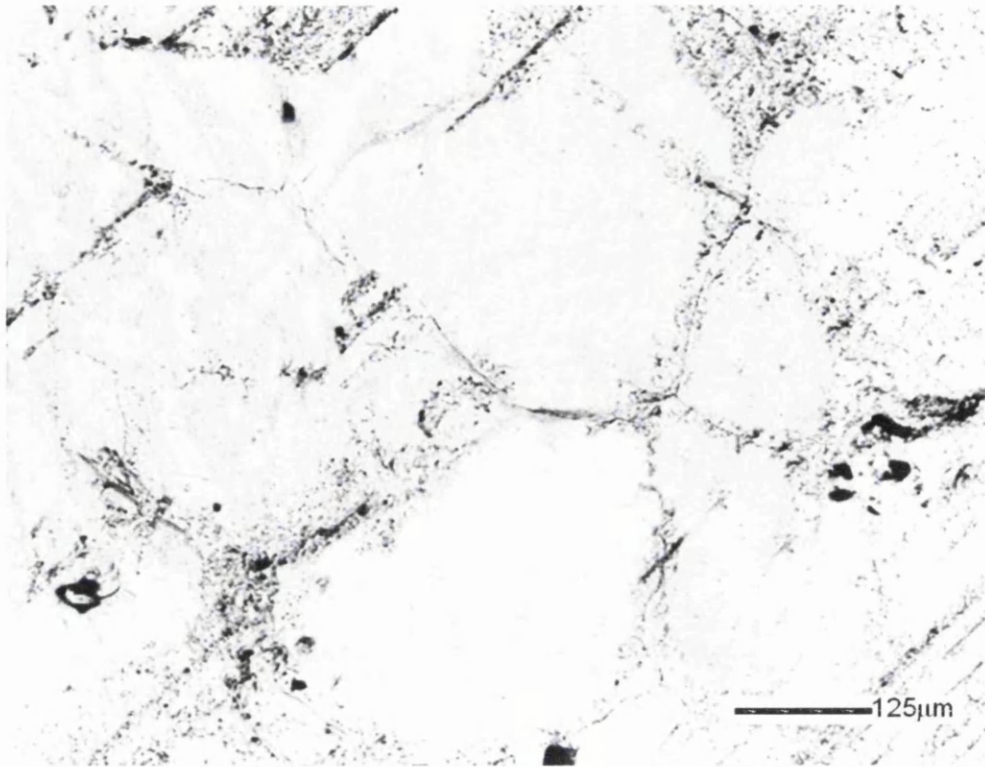
According to this equation the critical radius of nuclei needed to promote solidification and growth,  $r^*$ , becomes smaller as undercooling,  $\Delta T$ , becomes larger. Therefore as the cooling rate is increased, undercooling increases and the dendrites become more numerous as nucleation events are more favourable.

The size of the dendrites is also determined by the cooling rate as higher cooling rates reduce the time available for growth. Therefore the thinner gauges have more numerous but also smaller dendrites compared with the thicker gauges where larger, less numerous dendrites are formed.

#### 4.2.1.2 Microstructure of HDG coated materials.

The HDG samples used in this trial were dipped in a bath containing ~0.35 wt% Al with zero antimony and lead therefore giving a single phase microstructure. Hot dip galvanised (HDG) coatings are primarily composed of zinc. Small additions of aluminium (>0.13 wt%) are added to the galvanising bath in order to prevent the formation of several iron rich intermetallic phases at the coating / steel interface [104]. The aluminium promotes the formation of a  $\text{Fe}_2\text{Al}_3(\text{Zn})$  layer, often referred to as the inhibition layer. The layer increases the coating's formability, increases the lustre and reduces dross formation [104]. The inhibition layer is typically ~1  $\mu\text{m}$  thick however the thickness of this layer depends on factors such as bath temperature, steel temperature, aluminium levels in the bath and dwell time.

Thus, as the gauge of the steel was altered there were some increases in the grain size of the coating due to the reduced cooling rate on thicker gauges but they retained a single phase structure of almost pure Zn for almost the entirety of its thickness. An example micrograph of the single phase microstructure for HDG on 0.85 mm gauge steel taken at a depth of 6  $\mu\text{m}$  is shown in Figure 91.



**Figure 91- Microstructure of HDG on 0.85mm steel gauge (image taken at a depth of 6µm)**

#### **4.2.1.3 Cut edge corrosion of Zn-4.8wt% Al alloy and HDG coatings on various gauges of steel.**

It has been previously shown that for the corrosion rate of pure Zn coupled to Fe increases linearly in  $1 \text{ mol dm}^{-3}$  NaCl as the area of exposed Fe is increased [111]. Whitman and Russell have shown that when the galvanic current is limited by the rate of oxygen diffusion to the cathode, the rate of anodic dissolution of a less noble metal in a galvanic couple is directly proportional to the area of cathodic metal [112]. Suzuki has shown that in humid atmospheres the cut edge corrosion rate of HDG coatings increases linearly with steel gauge thickness up to gauges of 0.8 mm with a slight decrease in rate for higher gauges [106].

At the cut edge of coated steel a galvanic couple exists between the Zn based coating the Fe substrate. If the edge is covered by electrolyte and there is a supply of oxygen, the Fe will become cathodic with respect to the Zn which will undergo anodic dissolution. The Zn therefore cathodically polarises the Fe to a protective potential. Generally the rate of cut edge corrosion for coated steel will be controlled by the access of oxygen and water to the steel surface and so the cathodic reaction becomes the rate determining step in the system. If the area of exposed Fe increases i.e. as the steel gauge is increased, there is a larger free surface for cathodic reactions to take place and so the rate of anodic zinc dissolution will increase.

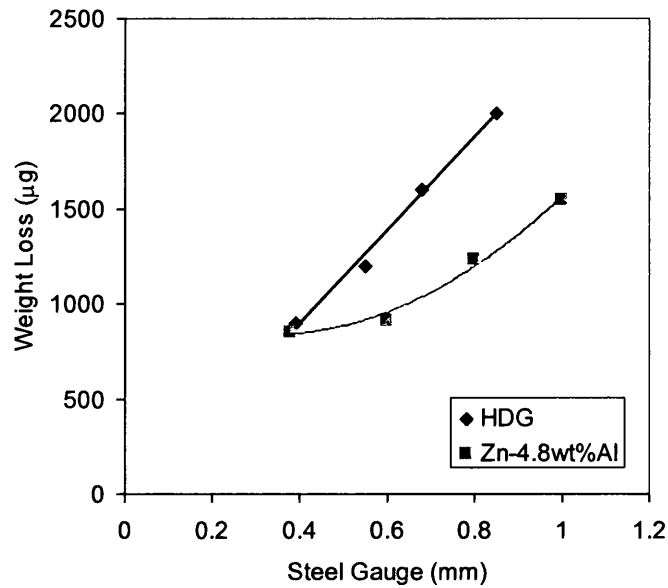
Furthermore it becomes more difficult for the thin zinc layer to polarise the increased area of steel and for zinc corrosion products to block or reduce this increased cathodic area thus contributing to the increased anodic Zn loss with increased steel gauge.

Figure 92 shows the results obtained from the weight loss experiments described in section 4.1.4. From the results it can be seen that the HDG samples indeed follow a linear trend of increasing zinc loss with increasing steel gauge as described above. However, the weight loss measured from the Zn-4.8wt% Al coated steels do not have a linear relationship over this gauge range but instead follow a polynomial relationship.

This suggests that the increasing cathodic area as steel gauge is increased is not the only factor that has determined the corrosion rate of the Zn alloy coating. It must be noted that these results do not provide a direct comparison of corrosion performance of the HDG and Zn-4.8wt% Al coatings as the coating weights of the two alloys were different.

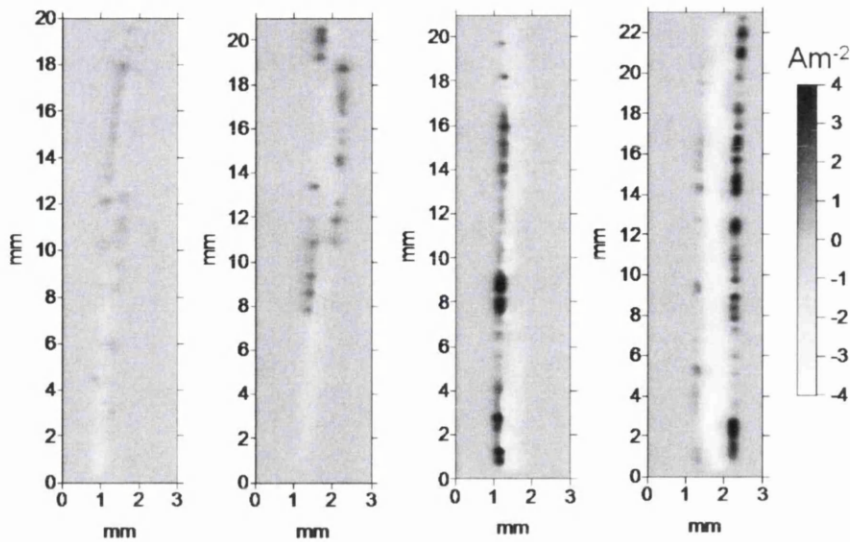
This investigation was purely to assess the trends in corrosion as the steel gauge was increased. However, the Zn-4.8wt% Al coatings corroded less than the HDG materials even though they had a lower coating weight and hence a larger ratio of cathode/anode, highlighting their inherent improvement in performance.





**Figure 92- Results obtained from mass loss experiments in 0.1% NaCl over 144 hours**

Figure 93 shows representative SVET iso-current corrosion obtained by scanning the cut edge of the Zn-4.8wt % Al samples. The maps show the corrosion activity taking place at hour 12 of the 24 hour test in 0.1% NaCl. The darker areas represent anodic sites with the light areas corresponding to cathodic activity. It can be seen from figure 93 that the anodic activity was focussed along the edges of the sample corresponding to the Zn-4.8wt% Al coatings with the steel substrate being cathodic and hence showing as light colours. Thus the Zn alloy coating is sacrificially protecting the steel. As the gauge was increased a corresponding increase in cathodic area was revealed by the SVET scans and also the anodic events had a greater intensity with the thicker gauges. A similar result was observed for the SVET data obtained for the cut edge corrosion of HDG samples with varying gauge.

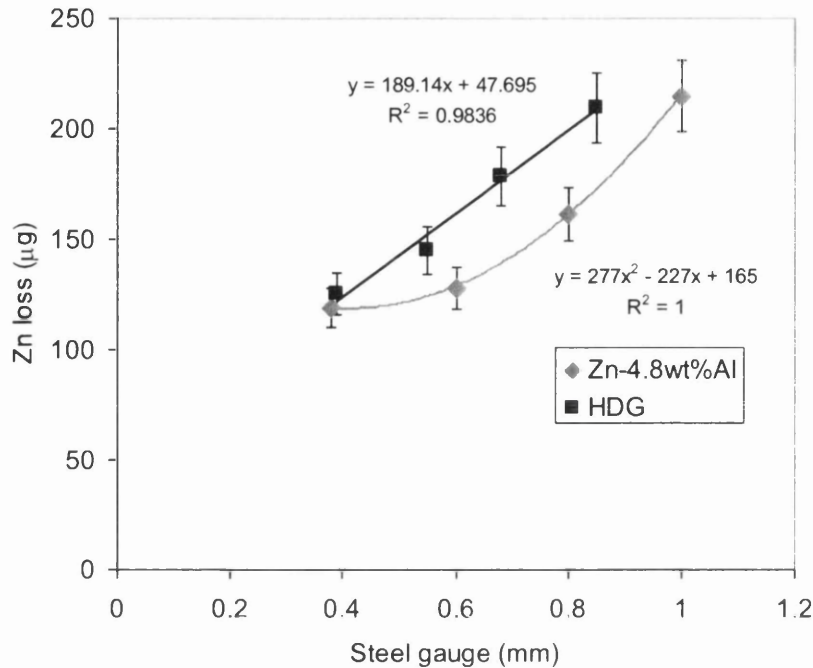


Steel Gauge = 0.39 mm      0.60 mm      0.80 mm      1.00 mm

**Figure 93- Representative SVET iso-current corrosion obtained by scanning the cut-edge of the Zn4.8wt% Al samples (the maps are hour 12 of the 24 hour test in 0.1% NaCl)**

Current density data obtained from the SVET may be converted using Faraday's law to give a semi quantitative measure of metal loss over the 24 hours as described in section 2.1.6.1. For these materials it was assumed that all corrosion activity represented Zn loss to simplify the calculations and because of the inherent lower wt% and corrosion activity of aluminium.

A number of previous investigations have shown that measuring Zn loss in this way to be useful in evaluating the performance of galvanised steels and the SVET data obtained compared favourably with external weathering of the materials [9, 36, 38]. The average SVET obtained Zn metal losses from the Zn-4.8wt % Al alloy and HDG coatings on various steel gauges are shown in Figure 94.



**Figure 94- Average SVET obtained metal losses (ug) from the Zn-4.8wt% Al alloy and HDG coatings on varying steel gauge after 24 hours**

From Figure 94 it can be seen that as the steel gauge increases the Zn loss also increases as expected with increasing cathodic area for both metallic coatings. Examination of these data showed that the HDG coated steels showed a linear increase in Zn loss with increasing steel gauge in line with theoretical predictions. For the Zn-4.8wt% Al alloy coated steel an increase in Zn loss with increasing steel gauge is also observed. However, this Zn loss is not directly proportional with increasing gauge thus differing from previous investigations and the HDG results.

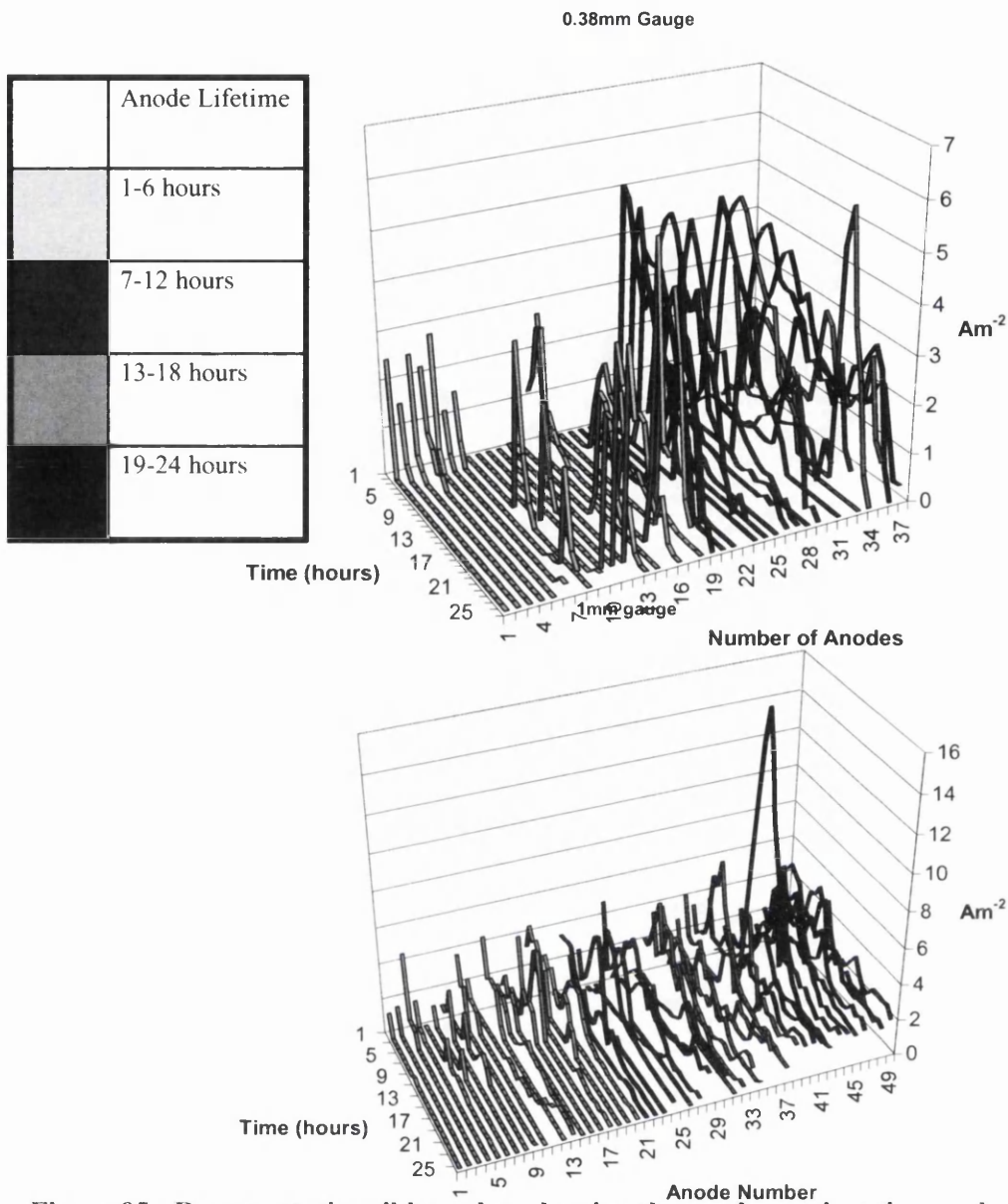
In fact there is a polynomial relationship for the Zn loss for the range of steel gauges investigated as shown in Figure 94. Thus, higher steel thicknesses led to greater Zn losses than may be anticipated from theory and from the performance of the HDG. The SVET Zn loss data therefore seems to confirm the observations from the weight loss

experiments. Therefore, the two phase microstructure of the Zn-4.8wt % Al alloy coatings must have an influence on the corrosion mechanism and rate in addition to the simple increase in cathodic steel area.

Zn-4.8wt % Al alloy coatings have been shown previously to corrode preferentially at the primary Zn dendrites [9, 107]. Interlamellar corrosion does occur [9] but the bulk Zn loss is due to attack of the primary Zn dendrites. Thus, control of the primary Zn phase is crucial in determining the corrosion rate of these alloys and factors such as alloy coating weight and ternary alloy additions have been previously investigated [36, 38].

It has been shown in section 4.2.1.1. that changing the steel gauge has a large influence on the microstructure of the final coating with thinner gauges having smaller but more numerous primary Zn dendrites than the thicker gauges. Thus, the morphology of the dendrites seems to have an influence on the corrosion rate of the material as well as the increased cathodic driving force of the increasing steel area.

The SVET data was further interrogated to assess the effect of the changes in microstructure. The SVET data was interrogated to assess the anode numbers, intensity and lifetime for both the HDG and Zn-4.8wt% Al coated steels using the software outlined in section 2.1.6.2. The software was set to record and monitor the lifetimes of anodic events that had intensities greater than  $1 \text{ Am}^{-2}$ . The results of this interrogation are shown in representative ribbon plots in Figure 95 for Zn-4.8wt% Al coatings on 0.38 mm gauge and 1 mm gauge steels. The ribbon plots show the number of active anodes over the 24 hours versus their intensity and lifetime in a 3D plot. Figure 95 shows that there are a greater number of anodes present for the 1 mm steel gauge sample, 49 compared with 37 for the 0.38 mm gauge steel, and most significantly more of these anodes persist for the longest time frame, 19-24 hours, suggesting that they are more damaging to the material.



**Figure 95 - Representative ribbon plots showing the anodes against time and anode intensity for Zn-4.8wt% Al alloy samples with 0.38mm and 1.0mm gauge**

Figure 96 a) and b) show the average intensity of anodes over the 24 hour experiment against their lifetime for the HDG and Zn-4.8wt%Al materials with varying gauge. It is clear from Figure 96 and Figure 97 that the anodes that live for longest had the highest average intensities over the time frame of the experiment and this suggests that they will therefore be more damaging to the coating.

Comparing these data from Figure 95 and Figure 96 shows that steels with thicker gauges have more long lived anodes that have high intensities and are therefore more significant

for the materials' corrosion rate. It is critical to look at the lifetime of these anodes as longer lived anodes will be more damaging than short lived anodes especially if they maintain a relatively high intensity. Figure 97 and Figure 98 show the percentage of anodes that are active for defined time frames, 0-6 hours, 7-12 hours, 13-18 hours and 19-24 hours for both metallic coatings on their various steel gauges. For HDG coated steels shown in Figure 97 it can be seen that the majority of anodes are either short lived, 1-6 hours, or long lived, 19-24 hours, with a smaller percentage covering the intermediate lifetimes.

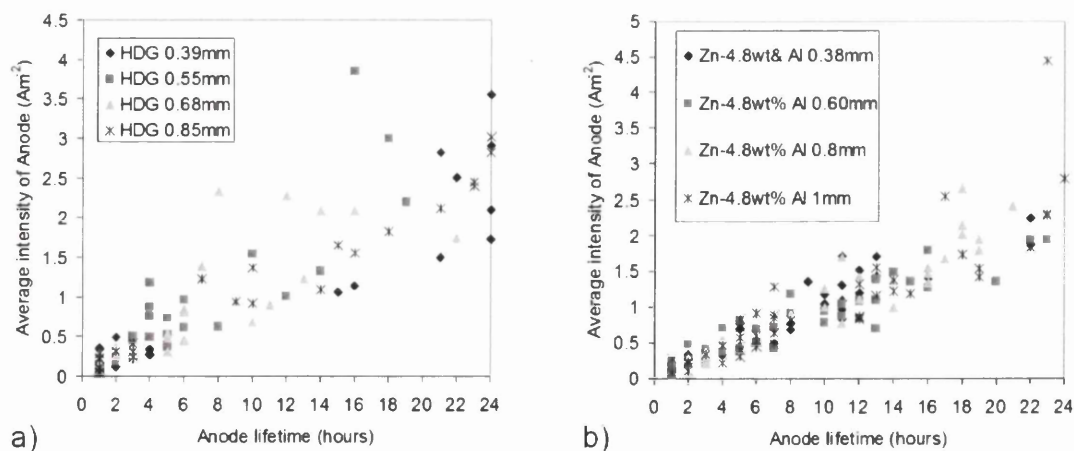
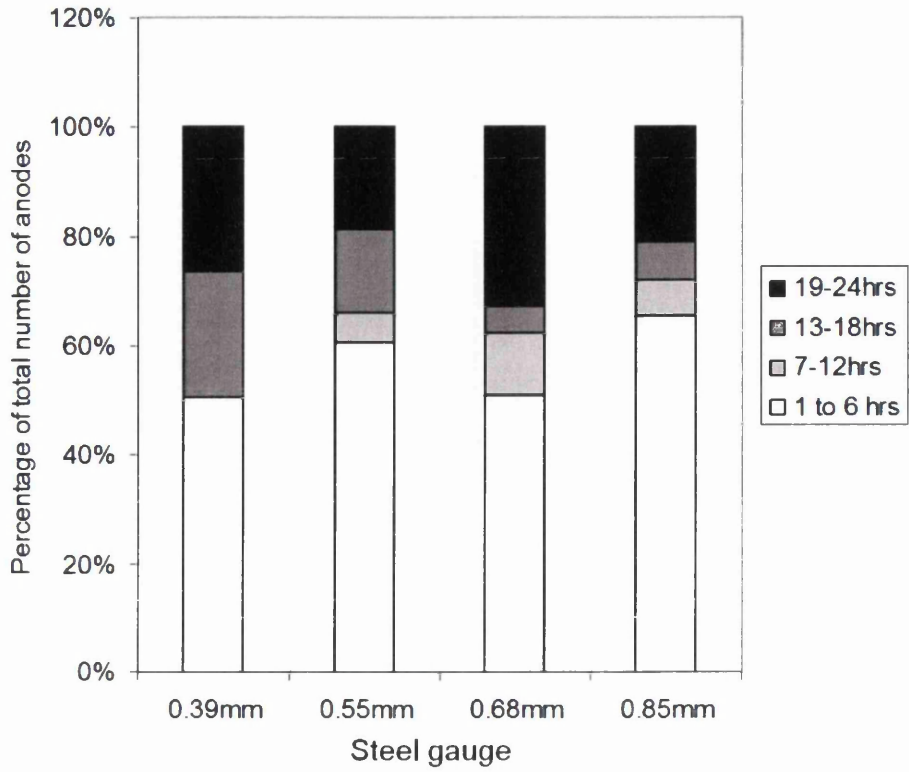
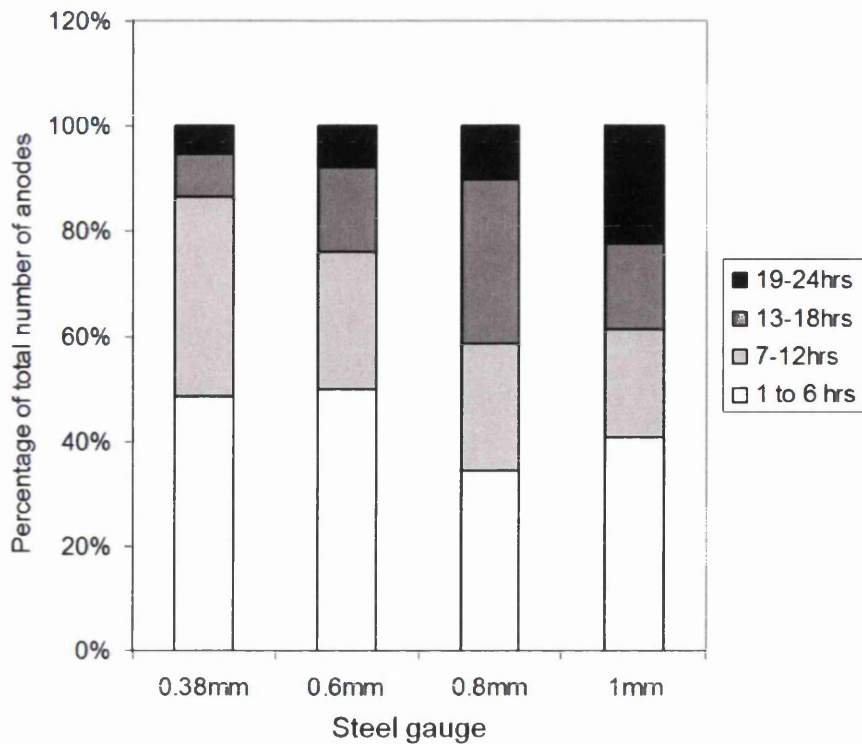


Figure 96 - Average intensity over the 24h experiment against their lifetime for a) HDG and b) Zn4.8wt% Al materials with varying gauge



**Figure 97 - Percentage of anodes that are active for defined time frames for HDG coated steel with various steel gauges**



**Figure 98 - Percentage of anodes that are active for defined time frames for Zn4.8wt% Al coated steel with various gauges**

On average 25% of the anodes have lifetimes that exceed 19 hours over the gauge range and it is these anodes that are the most damaging to the coating due to their persistent nature. There are no dramatic differences in the anode lifetimes for the HDG coated steels as the steel gauge is increased. For the Zn-4.8wt%Al coated steels shown in Figure 98, on average, across the gauge range, 12% of anodes have lifetimes exceeding 19 hours around half the value of HDG. This combined with generally lower anodic intensities as shown in Figure 96 a) and b) generally explain why the overall Zn loss was less for the Zn-4.8wt%Al coatings and is due to the protective action of the aluminium in the coating that forms a thin protective oxide barrier layer on the surface of the material resisting corrosive attack. Figure 98 also shows that for the Zn-4.8wt% Al coatings, as the steel

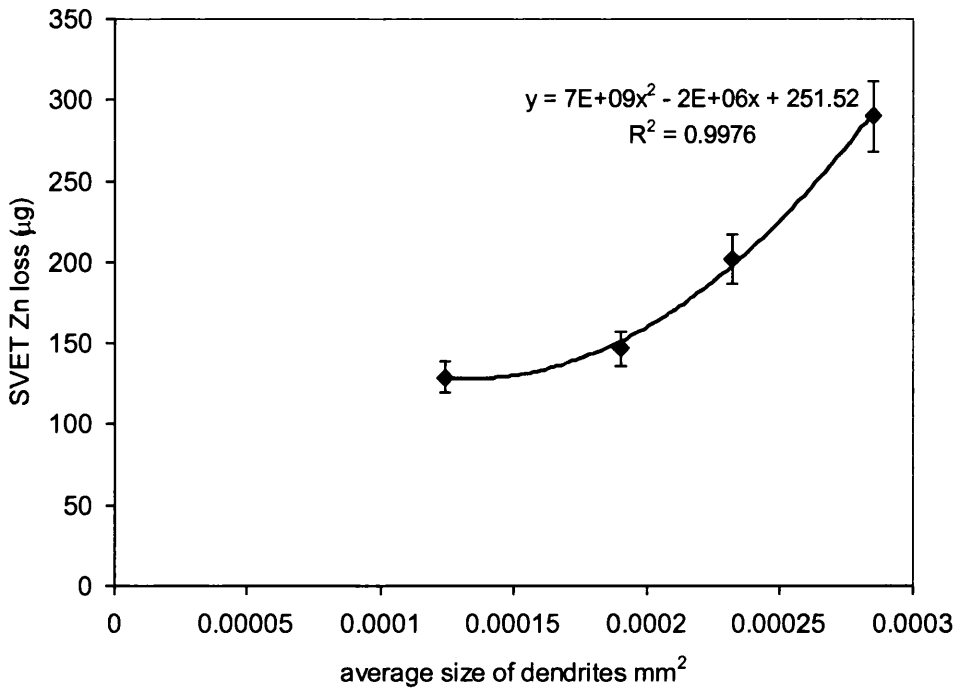


gauge increases the percentage of anodes that persist for the longest time period, 19-24 hours, also increases.

Therefore, as steel gauge increases the numbers of anodes that persist for the duration of the SVET scan increases, that leads to higher Zn loss and thus more damage to the coating. On the thickest gauge steel of 1 mm, the primary zinc dendrites are large and less numerous than on the thinner gauges as shown in Figure 89.

When an anode initiates on such a dendrite it will remain in this position until the dendrite has corroded and thus persist in this location longer than for smaller dendrites that will be consumed more rapidly. On the thinner gauge samples anodes will initiate and terminate more rapidly as the smaller dendrites are consumed. Energy must be used within the system to initiate new anodes. Thus, this microstructural effect seems to contribute to the increase in Zn loss as steel gauge increases. Not only is there the increased driving force of the larger steel cathodic area but also the microstructure produced on the thicker gauges supports more long lived corrosion events that are more damaging.

If the average size of primary zinc dendrite observed for the steel gauges is compared with the SVET zinc loss, Figure 99, then a polynomial trend is again observed thus suggesting that the microstructure does indeed have an influence on the relationship between zinc loss and steel gauge for the cut edge corrosion of Zn-4.8wt% Al alloy coated steels. The results suggest that it may be pertinent to increase the power to the fast coolers situated above the galvanising bath for thicker steel gauges coated with Zn-4.8wt% Al alloy. This will increase the cooling rate producing greater nucleation and growth of primary Zn dendrites which may then reduce the accelerated corrosion of the alloy with increasing gauge to a more linear trend as observed for HDG.



**Figure 99 - Comparison of the average size of primary zinc dendrites observed for the steel gauges against SVET measured zinc loss (µg) for Zn-4.8wt% Al coated steels.**

### 4.3 Conclusions

The cut edge corrosion of Zn coated steel is determined predominantly by the exposed area of steel, thus is cathodically driven. For HDG coated steels the rate of Zn loss from the cut edge increased linearly with increasing steel gauge for both weight loss measurements and SVET determined Zn loss as theory predicted. For Zn-4.8wt% Al coated steels the weight loss and SVET measured Zn loss followed a polynomial trend over the range of steel gauges.

This change in trend was a result of microstructural changes induced in the Zn-4.8wt% Al alloy coating as a result of a reduction in cooling rates with increasing steel gauge. This led to an increase in nucleation and reduced growth of primary Zn dendrites within the

microstructure. These primary Zn dendrites are the preferential corrosion sites for the alloy and interrogation of the SVET data showed that the larger dendrites associated with the thicker steel gauges produced more intense, long lived anodes than the small dendrites observed on the thinner steel samples.

A polynomial relationship was observed between the size of dendrites and SVET measured zinc loss that suggested that the microstructure changes had an influence on the rate of Zn loss in unison with the increased cathodic driving force of the steel gauge thus producing this polynomial relationship.

## **Chapter 5**

### **Microstructural investigation and Corrosion Performance of Zn, Zn-Al and Zn-Al-Mg coatings**

## 5.0 Introduction

HPS200 is the premium engineering product produced within Tata Steel Colors [4]. It comprises a sophisticated plastisol based organic coating on a Galvalloy coated steel substrate and can offer corrosion guarantees extending to 40 years [113].

Previous work has determined the grain refining properties of magnesium additions into Galvalloy and the subsequent improvement in cut-edge corrosion protection [36]. The alloying level of aluminium in galvalloy has been shown to vary with processing conditions and a combined change in corrosion performance has been identified [38]. Significant work has been undertaken to identify benefits in corrosion performance with respect to changing the aluminium and/or magnesium levels of the metallic alloys [39, 43, 114, 115].

Tata Steel Colors are investigating a new metallic coated product, MagiZinc that is a Zn-1.6wt% Al-1.6wt% Mg alloy that has been shown to provide increased corrosion performance compared to traditional galvanised coatings, typically Zn-0.15% Al [40, 116, 117].

Zn-1.6wt%Al-1.6wt%Mg has been shown to compose of primary zinc surrounded by a binary Zn-MgZn<sub>2</sub> eutectic phase and areas of ZnMg<sub>2</sub>/Zn lamellae eutectic with Al nodules. Magizinc offers increased corrosion protection through a combination of grain refinement and the reduction in the percentage of primary zinc phase, and from the delay of primary zinc dendrite corrosion from the initial corrosion of ZnMg<sub>2</sub> intermetallic species from the binary and ternary eutectic [118].

The mass production of hot dipped metallic coated steels uses molten metal baths through which the cleaned, de-oxidised strip steels are passed. The coated strip then passes through an area where the excess metallic coating is blown off to achieve the desired

coating weight before entering a cooling section where steam is blown on the surface to achieve the desired cooling rate [104].

Depending on the installation of the molten metal bath there can be the availability of separate molten bath equipment where alloying modifications can be prepared or through which trial material can be produced without affecting the mass production coating composition. Installations that have only one molten metal bath will require the addition of alloying elements or the dilution through the incorporation of additional zinc in order to modify the coating composition. This can have the effect of producing material that is non-standard, i.e. that sits between the ideal compositions of Zn-0.15wt%Al, or Zn-1.6wt%Al-1.6wt%Mg.

In magnesium containing coatings produced via molten metal immersion there is the tendency for the production of increased dross material due to the high affinity of magnesium for atmospheric oxygen. Dross particles are usually manually filtered from the molten metal bath and can therefore be incorporated into the coating during production in all but the most controlled processes. Dross particles can give rise to the increase in nucleation events during the cooling of the molten metallic coating and can affect the coating microstructure in a similar way to the surface spray of zinc dust that produces a minimised spangle Zn-0.15wt%Al coating [104].

This chapter investigates coatings that could be assumed to be non-standard, i.e. that sit between the Zn-0.15wt%Al and the Zn-1.6wt%Al-1.6wt%Mg and those that could be over alloyed in terms of the additions of Al and Mg to the molten bath up to approximately Zn-2wt%Al-2wt%Mg. The investigation has used cut-edge scanning vibrating electrode technique to investigate the corrosion losses and the mechanism of the corrosion losses of the range of samples. All samples have been produced on a 0.5mm gauge low carbon steel substrate. Immersed mass loss tests have examined the cut-edge gravimetric mass loss.

A Perkin-Elmer Optima 3X00 Axial ICP-OES has been used to determine the chemical composition of the coatings using a known area, acid digestion method and calibration standards sourced from Fisher Scientific.

Microstructural characterisation was performed using the depth profiling method described in section 2.4. All images were taken on a Reichart Polyvar optical microscope at x250 magnification, resulting in a 0.3mm x 0.4mm image (0.12mm<sup>2</sup> of coating characterised per image).

## 5.1 Comparison table

Several comparisons have been determined within the data set, see Table 15. Comparisons 1-3 refer to the effect of enhanced cooling on samples with similar alloy compositions.

Comparisons 7 and 8 examine the changes of alloy compositions when the cooling rate is kept consistent.

Comparisons 9 to 12 examine the effects of increasing the aluminium or magnesium content while keeping the cooling rate and other alloying additions at a similar level, for the two cooling conditions.

Where significant differences are seen we shall investigate in detail the microstructural and corrosion performance differences and examine the reasons why these differences occur.

	Sample ID	MGZ19	MGZ20	MGZ41	MGZ42	MGZ43	MGZ44	MGZ45	MGZ46	MGZ47	MGZ48	MGZ66	MGZ69	0.55mm HDG
Original values	Al %	0.7	0.98	1.63	1.6	1.7	1.72	1.67	1.67	1.37	1.35	1.2	1.2	0.3
	Mg %	0.08	0.09	0.52	0.53	1.14	1.19	1.84	1.845	1.93	1.9	1.2	1.2	0
	Fe %	0.4	0.43	0.16	0.16	0.11	0.11	0.09	0.14	0.11	0.1	0	0	0
	Zn %	98.82	98.5	97.69	97.71	97.05	96.98	96.4	96.345	96.59	96.65	97.6	97.6	97.3
	Speed	Fast	Slow	Fast	Slow	Slow	Fast	Fast	Slow	Slow	Fast	Fast	Slow	Slow
Comparison 1	Coating thickness / $\mu$ m	9.7	8.0	10.8	13.1	12.6	12.2	11.8	13.8	9.3	12.7	11.1	10.0	19.3
	Al	0.7	0.98	1.63	1.6	1.7	1.72	1.67	1.67	1.37	1.35	1.2	1.2	Fast v slow
	Mg	0.08	0.09	0.52	0.53	1.14	1.19	1.84	1.845	1.93	1.9	1.2	1.2	
	Fe	0.4	0.43	0.16	0.16	0.11	0.11	0.09	0.14	0.11	0.1	0	0	
	Zn	98.82	98.5	97.69	97.71	97.05	96.98	96.4	96.345	96.59	96.65	97.6	97.6	
Speed	Fast	Slow	Fast	Slow	Slow	Fast	Fast	Slow	Slow	Fast	Fast	Slow		
Comparison 2	Al	0.7	0.98	1.63	1.6	1.7	1.72	1.67	1.67	1.37	1.35	1.2	1.2	Fast v slow
	Mg	0.08	0.09	0.52	0.53	1.14	1.19	1.84	1.845	1.93	1.9	1.2	1.2	
	Fe	0.4	0.43	0.16	0.16	0.11	0.11	0.09	0.14	0.11	0.1	0	0	
	Zn	98.82	98.5	97.69	97.71	97.05	96.98	96.4	96.345	96.59	96.65	97.6	97.6	
	Speed	Fast	Slow	Fast	Slow	Slow	Fast	Fast	Slow	Slow	Fast	Fast	Slow	
Comparison 3	Al	0.7	0.98	1.63	1.6	1.7	1.72	1.67	1.67	1.37	1.35	1.2	1.2	Fast v slow
	Mg	0.08	0.09	0.52	0.53	1.14	1.19	1.84	1.845	1.93	1.9	1.2	1.2	
	Fe	0.4	0.43	0.16	0.16	0.11	0.11	0.09	0.14	0.11	0.1	0	0	
	Zn	98.82	98.5	97.69	97.71	97.05	96.98	96.4	96.345	96.59	96.65	97.6	97.6	
	Speed	Fast	Slow	Fast	Slow	Slow	Fast	Fast	Slow	Slow	Fast	Fast	Slow	
Comparison 7	Al	0.7	0.98	1.63	1.6	1.7	1.72	1.67	1.67	1.37	1.35	1.2	1.2	All Fasts
	Mg	0.08	0.09	0.52	0.53	1.14	1.19	1.84	1.845	1.93	1.9	1.2	1.2	
	Fe	0.4	0.43	0.16	0.16	0.11	0.11	0.09	0.14	0.11	0.1	0	0	
	Zn	98.82	98.5	97.69	97.71	97.05	96.98	96.4	96.345	96.59	96.65	97.6	97.6	
	Speed	Fast	Slow	Fast	Slow	Slow	Fast	Fast	Slow	Slow	Fast	Fast	Slow	
Comparison 8	Al	0.7	0.98	1.63	1.6	1.7	1.72	1.67	1.67	1.37	1.35	1.2	1.2	All slows
	Mg	0.08	0.09	0.52	0.53	1.14	1.19	1.84	1.845	1.93	1.9	1.2	1.2	
	Fe	0.4	0.43	0.16	0.16	0.11	0.11	0.09	0.14	0.11	0.1	0	0	
	Zn	98.82	98.5	97.69	97.71	97.05	96.98	96.4	96.345	96.59	96.65	97.6	97.6	
	Speed	Fast	Slow	Fast	Slow	Slow	Fast	Fast	Slow	Slow	Fast	Fast	Slow	
Comparison 9	Al	0.7	0.98	1.63	1.6	1.7	1.72	1.67	1.67	1.37	1.35	1.2	1.2	Same Al increasing Mg
	Mg	0.08	0.09	0.52	0.53	1.14	1.19	1.84	1.845	1.93	1.9	1.2	1.2	
	Fe	0.4	0.43	0.16	0.16	0.11	0.11	0.09	0.14	0.11	0.1	0	0	
	Zn	98.82	98.5	97.69	97.71	97.05	96.98	96.4	96.345	96.59	96.65	97.6	97.6	
	Speed	Fast	Slow	Fast	Slow	Slow	Fast	Fast	Slow	Slow	Fast	Fast	Slow	
Comparison 10	Al	0.7	0.98	1.63	1.6	1.7	1.72	1.67	1.67	1.37	1.35	1.2	1.2	Same Al increasing Mg
	Mg	0.08	0.09	0.52	0.53	1.14	1.19	1.84	1.845	1.93	1.9	1.2	1.2	
	Fe	0.4	0.43	0.16	0.16	0.11	0.11	0.09	0.14	0.11	0.1	0	0	
	Zn	98.82	98.5	97.69	97.71	97.05	96.98	96.4	96.345	96.59	96.65	97.6	97.6	
	Speed	Fast	Slow	Fast	Slow	Slow	Fast	Fast	Slow	Slow	Fast	Fast	Slow	
Comparison 11	Al	0.7	0.98	1.63	1.6	1.7	1.72	1.67	1.67	1.37	1.35	1.2	1.2	Same Mg increasing Al
	Mg	0.08	0.09	0.52	0.53	1.14	1.19	1.84	1.845	1.93	1.9	1.2	1.2	
	Fe	0.4	0.43	0.16	0.16	0.11	0.11	0.09	0.14	0.11	0.1	0	0	
	Zn	98.82	98.5	97.69	97.71	97.05	96.98	96.4	96.345	96.59	96.65	97.6	97.6	
	Speed	Fast	Slow	Fast	Slow	Slow	Fast	Fast	Slow	Slow	Fast	Fast	Slow	
Comparison 12	Al	0.7	0.98	1.63	1.6	1.7	1.72	1.67	1.67	1.37	1.35	1.2	1.2	Same Mg increasing Al
	Mg	0.08	0.09	0.52	0.53	1.14	1.19	1.84	1.845	1.93	1.9	1.2	1.2	
	Fe	0.4	0.43	0.16	0.16	0.11	0.11	0.09	0.14	0.11	0.1	0	0	
	Zn	98.82	98.5	97.69	97.71	97.05	96.98	96.4	96.345	96.59	96.65	97.6	97.6	
	Speed	Fast	Slow	Fast	Slow	Slow	Fast	Fast	Slow	Slow	Fast	Fast	Slow	

Table 15 - Comparison table for the MGZ Sample Set

## 5.2 Dendrite analysis

Depth profiling was performed on multiples of each sample to determine the growth curve and the dendrite number, see Table 16. Average primary zinc% is calculated from averaging the predicted zinc contents for the depth of the coating.



	Average primary zinc%	Interface Primary zinc%	Average dendrites per image
MGZ19	94.5	99.6	43
MGZ20	95.4	99.3	41
MGZ41	70.2	92.1	388
MGZ42	70.7	94.70	382.5
MGZ43	61.8	89.83	561.5
MGZ44	44.7	85.15	919.5
MGZ45	42.0	84.14	256
MGZ46	40.0	86.26	1074
MGZ47	29.6	77.07	61.5
MGZ48	52.1	80.78	150
MGZ66	63.9	85.61	124.5
MGZ69	63.0	86.94	44.5
	Average Dendrite size (mm <sup>2</sup> )	Average Dendrite volume (mm <sup>3</sup> x 1000)	Dendrite Number
MGZ19	0.0028	10.68	354
MGZ20	0.0029	9.22	342
MGZ41	0.0003	0.93	3229
MGZ42	0.0003	1.22	3188
MGZ43	0.0002	0.65	4679
MGZ44	0.0001	0.27	7663
MGZ45	0.0004	0.93	2133
MGZ46	0.0001	0.23	8950
MGZ47	0.0015	2.19	513
MGZ48	0.0006	2.21	1250
MGZ66	0.0008	2.77	1038
MGZ69	0.0023	0.68	371

**Table 16 - Dendrite analysis information MGZ samples**

A plot of the average primary zinc% shows the effect that magnesium and aluminium additions have on the microstructure, see Figure 100. We can clearly see the dependency that the primary zinc% has on the aluminium level.

We can also see in Figure 101 that the trend of dendrite number follows the trend of the total magnesium addition, showing that the alloying additions are increasing the nucleation rate, possibly from the incorporation of small intermetallic particles acting as nucleation points, or from an increased undercooling ahead of the solidification front, from an increase in constitutional supercooling in the higher alloyed coatings producing a

larger number of small nuclei. Figure 102 shows the corresponding inverse relationship on dendrite volume.

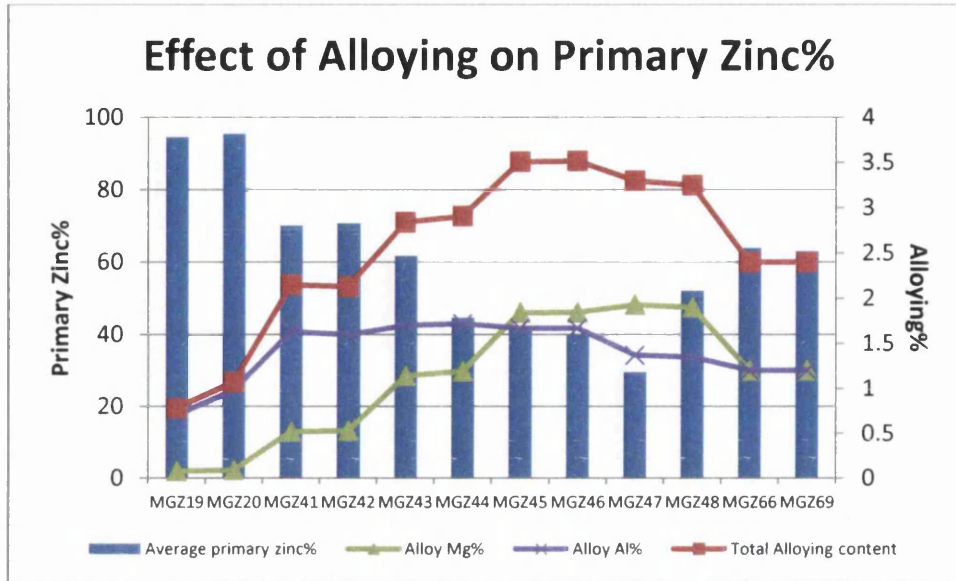


Figure 100 - Primary zinc% as a function of alloying level

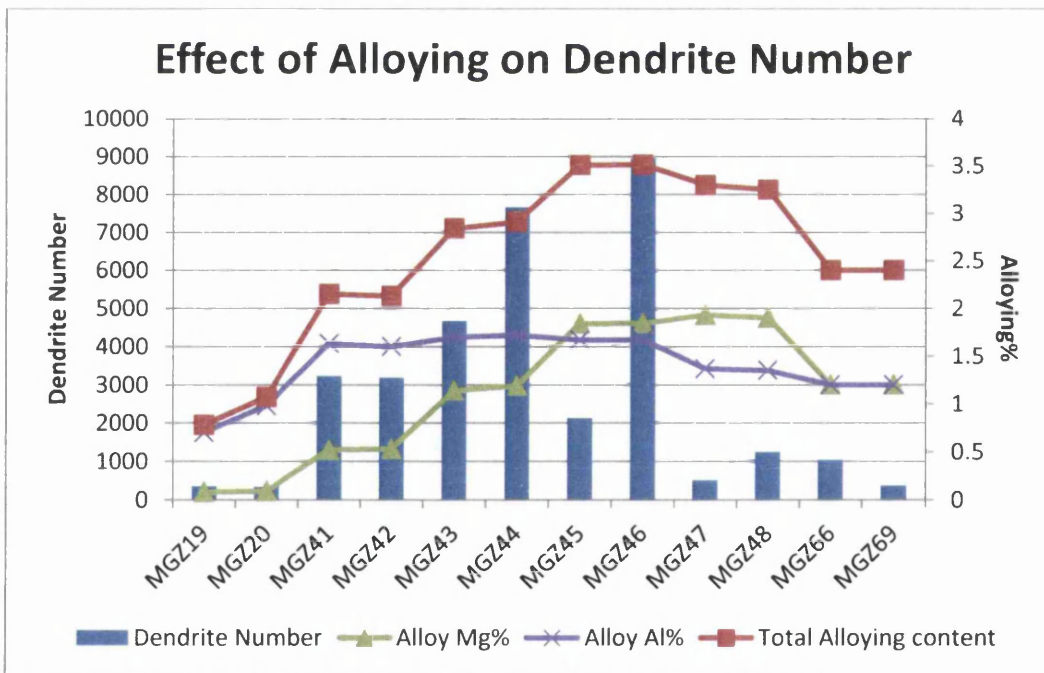


Figure 101 - Effect of alloying on dendrite number

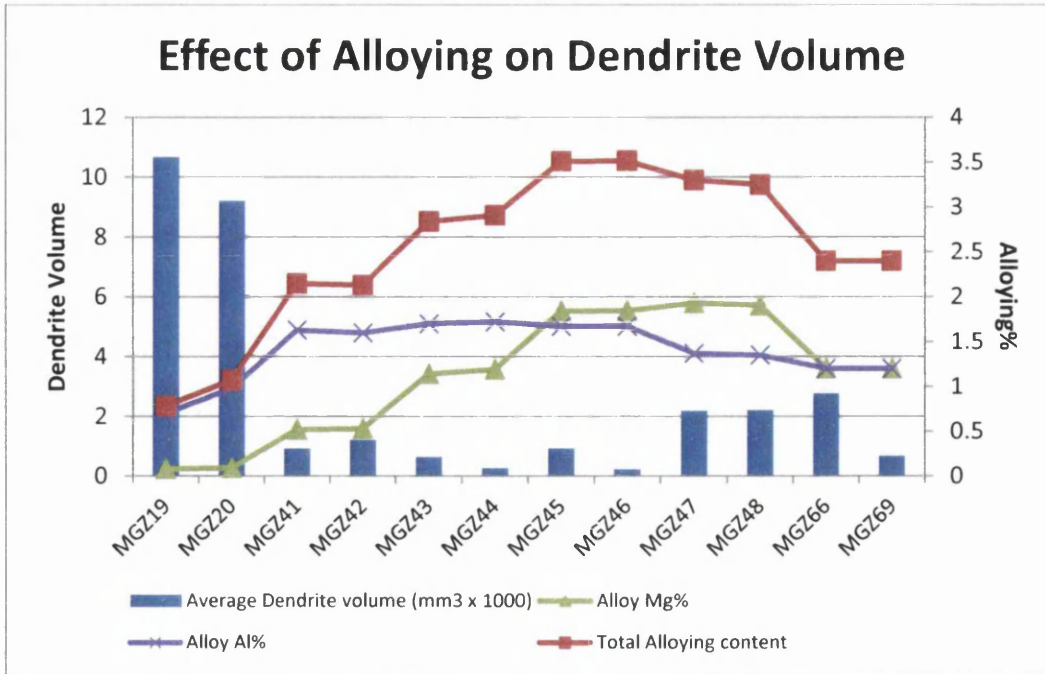


Figure 102 - Effect of Alloying Level on Dendrite Volume

### 5.3 Growth curve analysis

We will examine the growth curves within each comparison data set but we can summarise the factors of each of the growth curves in a table, see Table 17. Where  $c = 0$  the growth curve passes through the origin of the graph, depicting that the surface observable primary zinc% was 0, i.e. only eutectic phase could be seen at the surface.

$y = ax^2 + bx + c$	$a$	$b$	$c$
MGZ19	-0.2148	3.7387	83.208
MGZ20	-0.2828	4.811	80.16
MGZ41	-1.4433	23.588	0
MGZ42	-1.2533	21.865	0
MGZ43	-0.8316	17.025	0
MGZ44	-0.3072	10.153	0
MGZ45	0.3755	4.4031	0
MGZ46	0.2029	4.687	0
MGZ47	0.1187	5.6533	0
MGZ48	-0.4792	12.21	0
MGZ66	-1.205	20.564	0
MGZ69	-1.2514	21.163	0

Table 17 - MGZ Growth Curve Coefficients

## 5.4 Corrosion performance

Figure 103 to Figure 105 show the comparisons between the predicted cut-edge mass loss corrosion test from SVET analysis, and immersion mass loss results, and the variables in the coating alloying levels and microstructural features. In Figure 104 it can be seen that there is a strong inverse relationship between the primary zinc% and the mass loss figures. Previous findings have also established that the primary zinc dendrite becomes the site of anodic losses following initiation of the corrosion from the  $MgZn_2$  phases in the eutectic [118, 119]. A reduction in the primary zinc phase will therefore lead to an increase in the nucleation points for corrosion within the eutectic phase adjacent to a primary zinc dendrite.

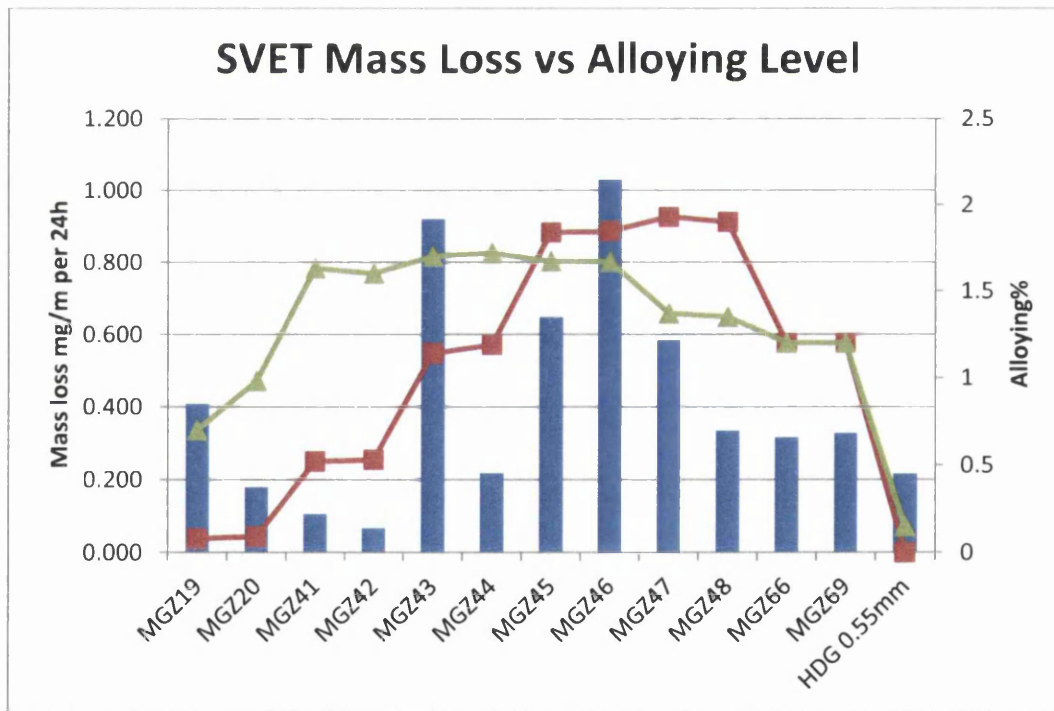


Figure 103 - Mass loss v Alloying Level Comparison

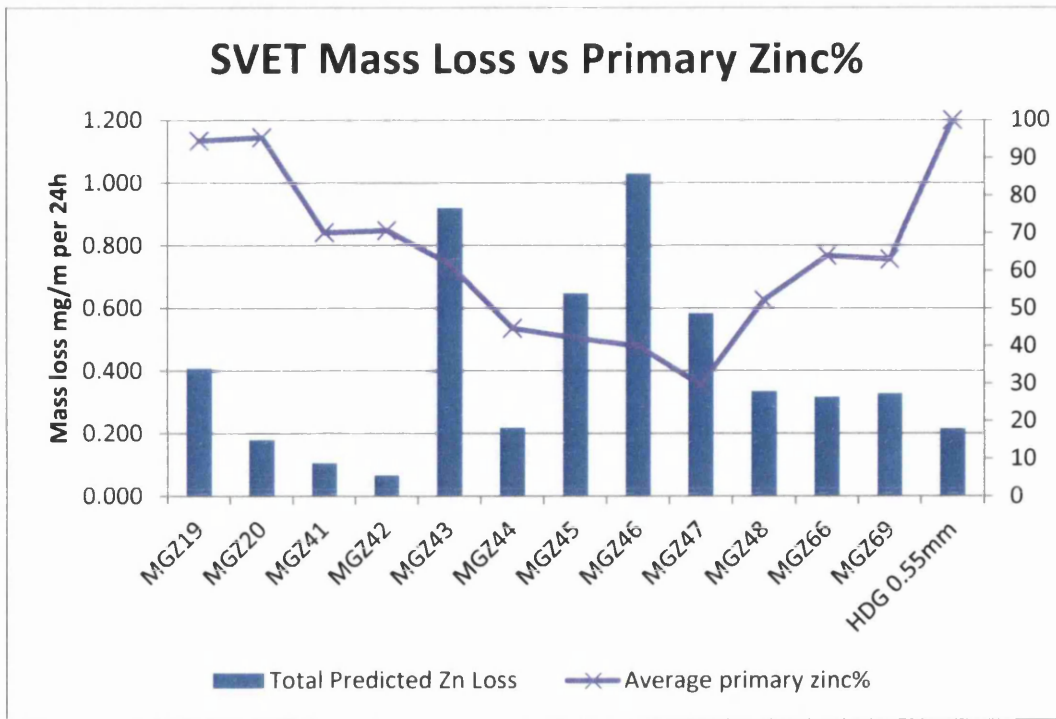


Figure 104 - Total SVET Mass Loss vs. Primary Zinc%

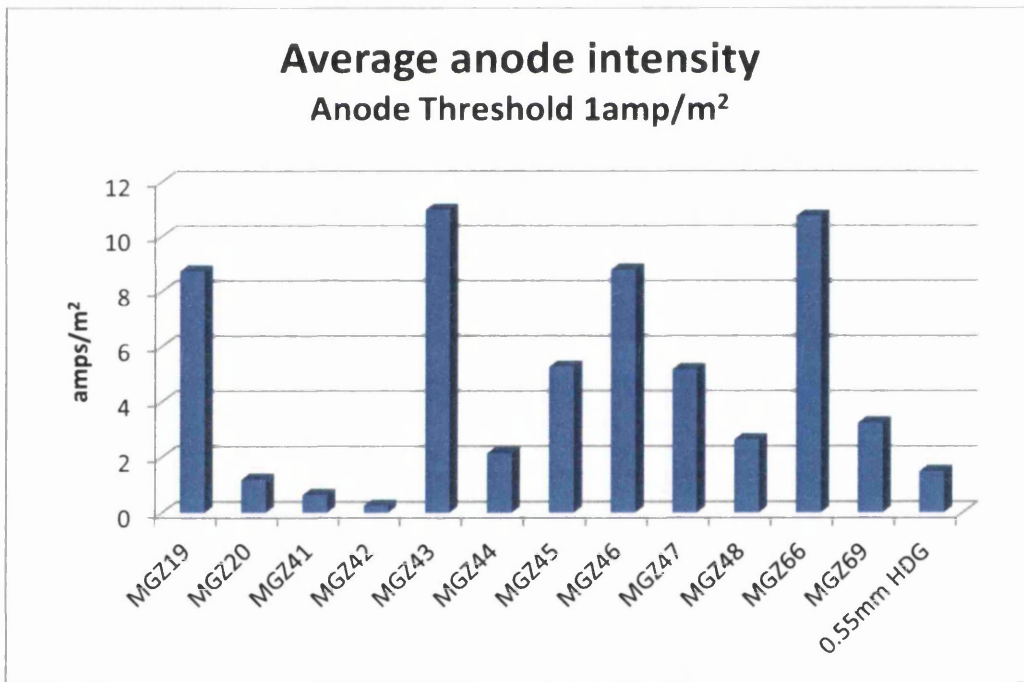


Figure 105 - Average Anode Intensities - MGZ Samples

Figure 107 a comparison of the predicted mass loss data determined from the SVET against the gravimetric mass loss determined. Each scan has been normalised for the length of the cut-edge exposed during the test and compared in values of total mass loss per meter of cut edge per 24 hours. The data shows good a very good correlation to the SVET mass loss data to that determined via a gravimetric method.

# Residual Anode Analysis 1amp/m<sup>2</sup> Threshold level

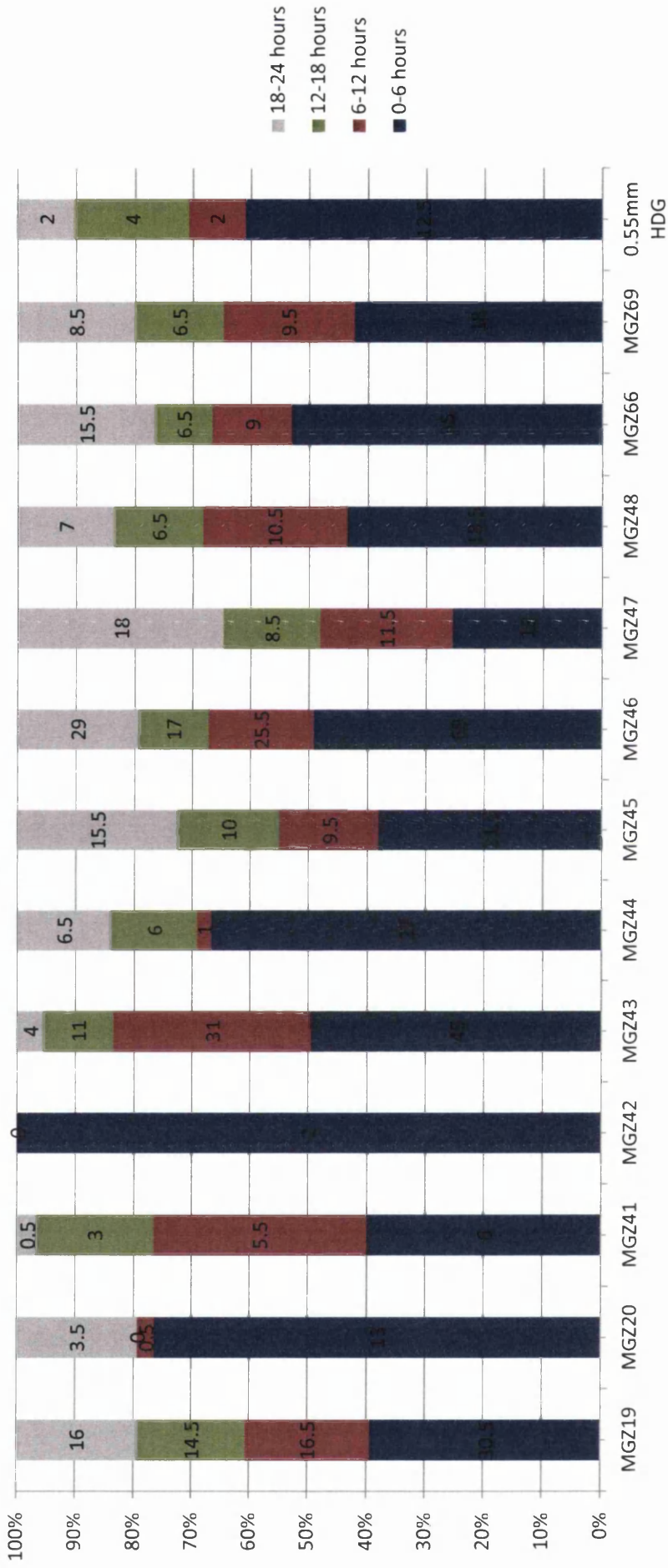


Figure 106 - Residual Anode Analysis MGZ Samples

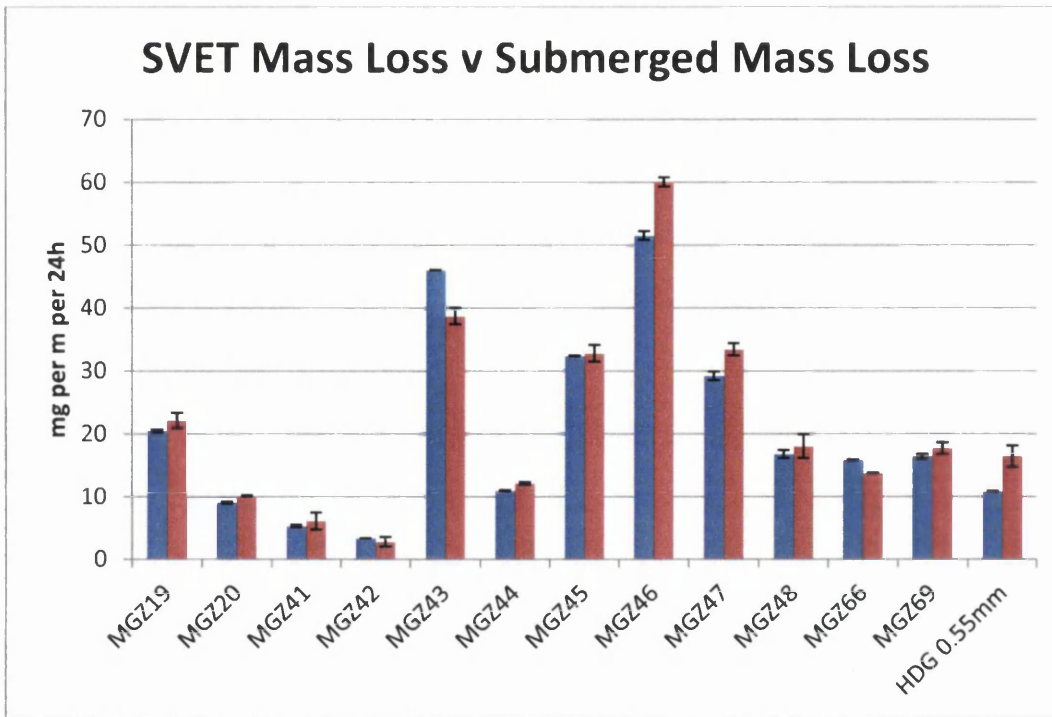
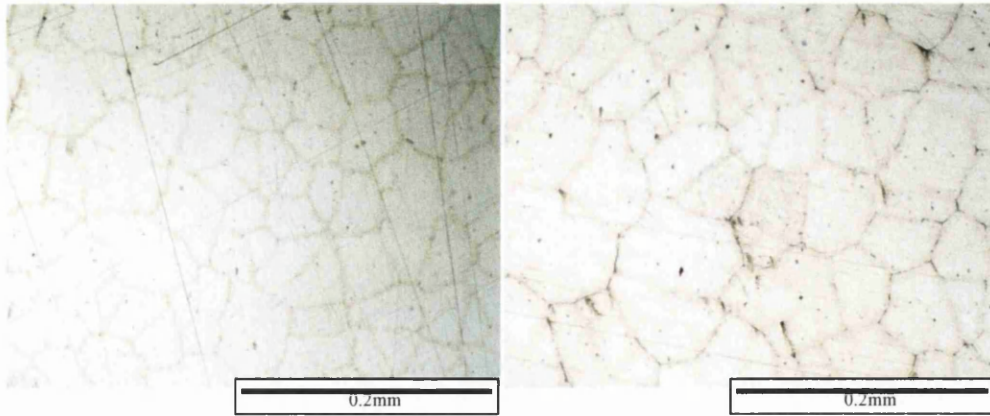


Figure 107 - Immersion mass loss comparison

## 5.5 Comparison 1 – Low alloying additions

MGZ19 and MGZ20 have very low alloying additions with a minimum zinc balance level of 98.5%. With the maximum solubility of aluminium in primary zinc of 1.14% then it is expected that the solidification will be cellular not dendritic as there is no solute rejection ahead of the solidification front and we will have a final microstructure similar to that of hot dip galv, see Figure 108 and 109 (both images taken at a depth of approximately  $8\mu\text{m}$ ), this is indeed what is seen, though the samples show different corrosion performance results with MGZ19 experiencing 226% more anodic losses than MGZ20.





**Figure 108 - MGZ19 micrograph**

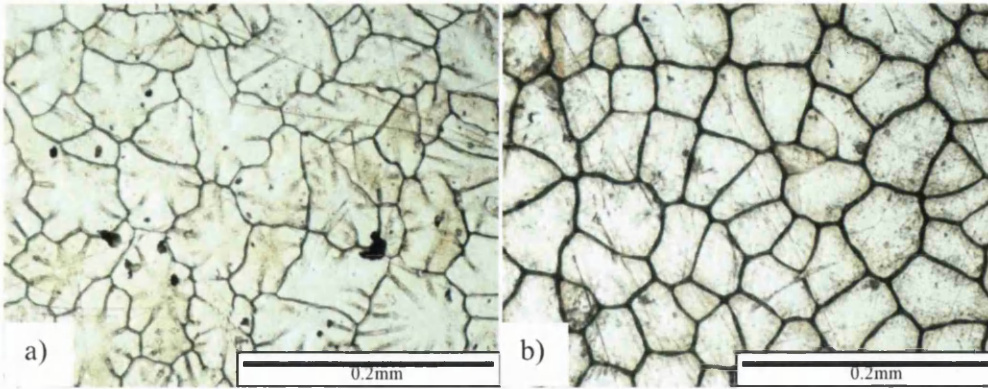
**Figure 109 - MGZ20 micrograph**

### 5.5.1 Microstructural characterisation

In examining the growth curve and the growth curve coefficients, see Table 17, we see that both samples show very similar primary zinc% curves, with little difference in the polynomial coefficients  $a$  and  $b$ , with a slight change in  $c$  signifying there is slightly more depression at the surface for MGZ20.

An overlaid average cell profile shows that the two coatings generate similar shape and size cells, although the increased coating thickness of the MGZ19 coating can be seen in the increased relative cell size. MGZ19 shows a calculated 5.5% of grain boundary compared to MGZ20 having 4.6%. This is an expected result considering the increased cooling rate. This has the effect of giving an overall increase in the volume of the MGZ19 cell, compared to a MGZ20 cell of 15.9%, even through the coating weight increases by 21.25%.

The average dendrite profile is also predicting the presence of significant amounts of primary zinc at the surface. Each sample can be regarded as shiny in appearance strengthen these finding, see Figure 110 a) and b).

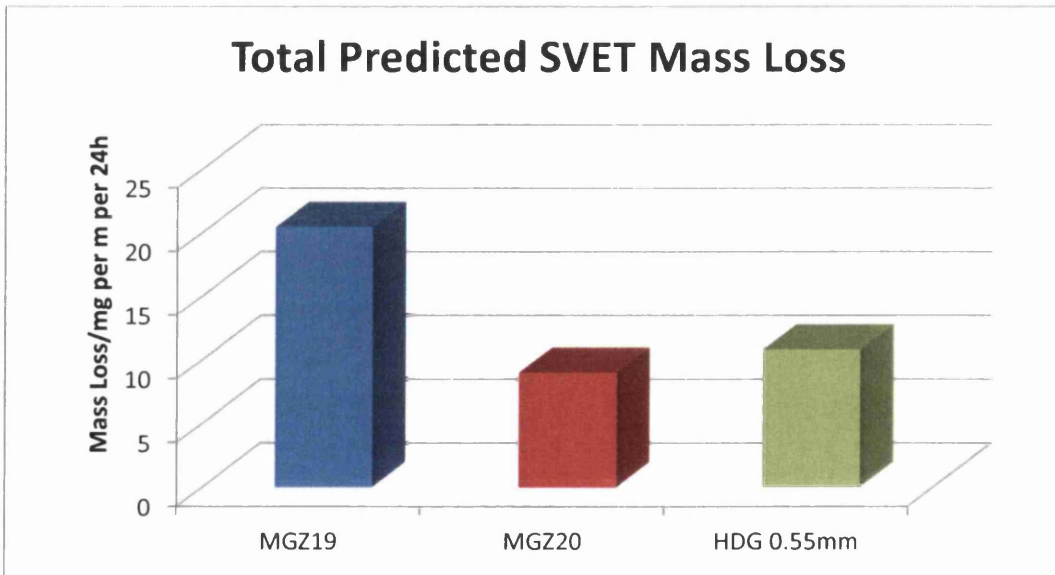


**Figure 110 - Surface appearance of a) MGZ19 and b) MGZ20**

### 5.5.2 Corrosion performance

MGZ20 shows very similar corrosion performance to the benchmark HDG sample. MGZ20 shows roughly half (44%) of the corrosion losses in a 24 hours period compared to MGZ19, see Figure 111.

MGZ19 shows an accelerating corrosion during the central hours of the SVET test, as can be seen in Figure 112, this is reflected in the residual anode analysis with MGZ19 having significant increases both in activity during the 6-18 hour period of the test, plus an increase in the total number of anodes in each of the SVET time quarters, see Figure 113.



**Figure 111 - Total Mass Loss - Comparison 1**

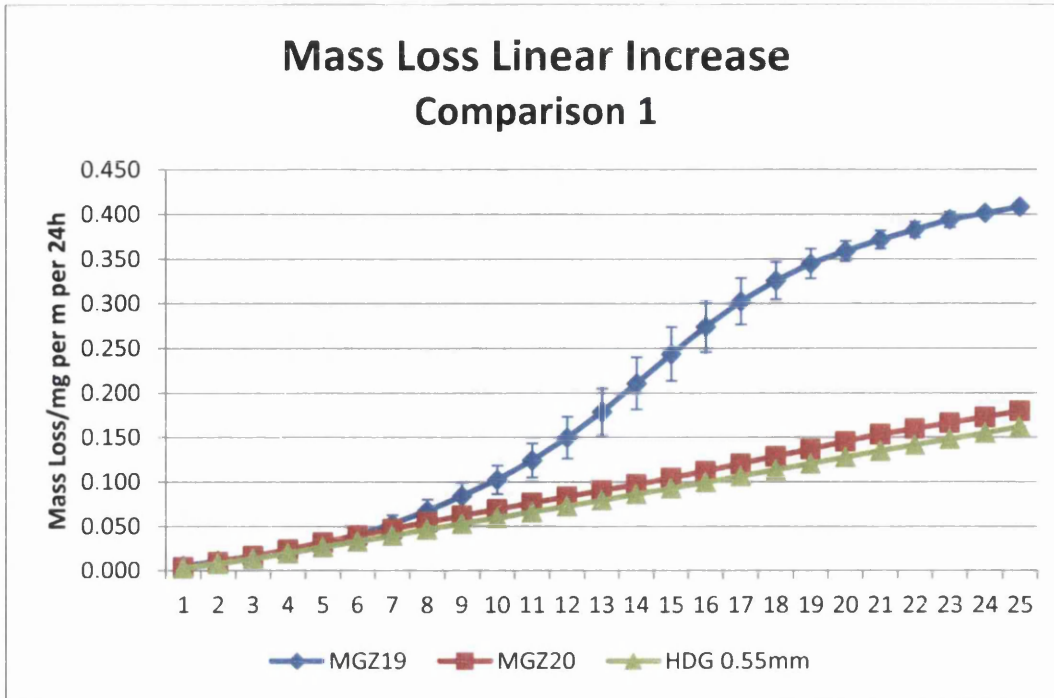


Figure 112 - Cumulative average mass loss per scan - Comparison 1

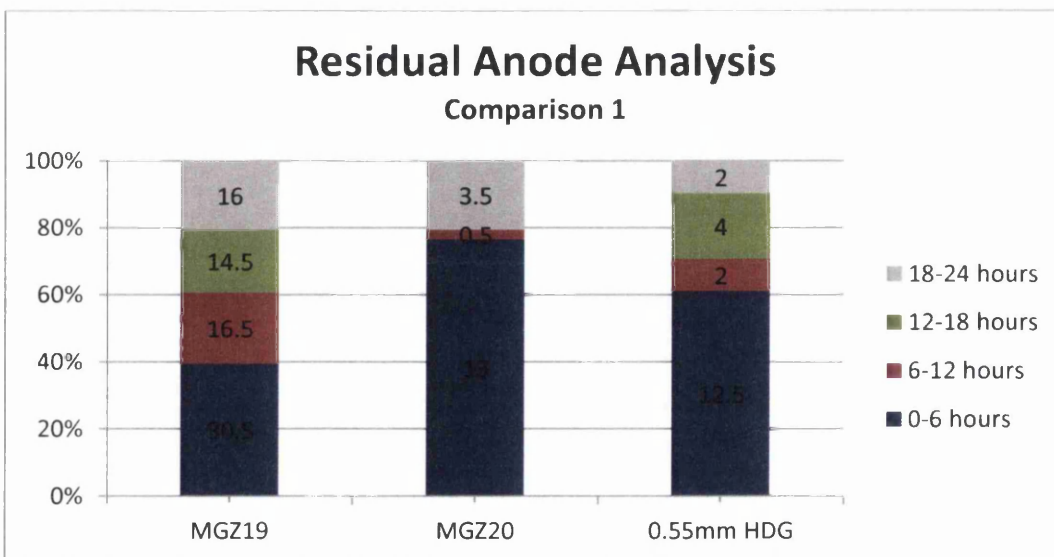


Figure 113 - Residual anode analysis data - Comparison 1

### 5.5.3 Comparison 1 results

The increase in activity is believed to be related to an increase in the amount of grain boundary areas that will be intersected during a cut-edge scan. Grain boundary sites will be areas where corrosive attack can initiate. The grain boundary depressions seen in Figure 110 a) and b) are formed from the contraction of the molten phase during solidification. Triple point depressions, where three eutectic cells converge can show the greatest depressions and have been shown to cause cracking in the metallic coating possibly extending through to the substrate [1]. A crack may still be evident in a cut-edge sample and could propagate into the plane of the coating when viewed in cross section. Without a crack the grain boundary depression is still an area where there are incomplete unit cells and atoms without the required number of nearest neighbours, providing corrosion initiation sites.

The results show that some consideration should small alloy additions to hot dip galv can have a marked reduction in the performance of the coatings if the processing conditions used to prepare the coating are not carefully considered. It is also worth noting that even in the case of MGZ20 the corrosion rate is only similar to, not better than the corrosion rate determined for hot dip galv. Therefore there appears to be no benefit in making small alloying additions to the hot dip galvanising bath chemistry.

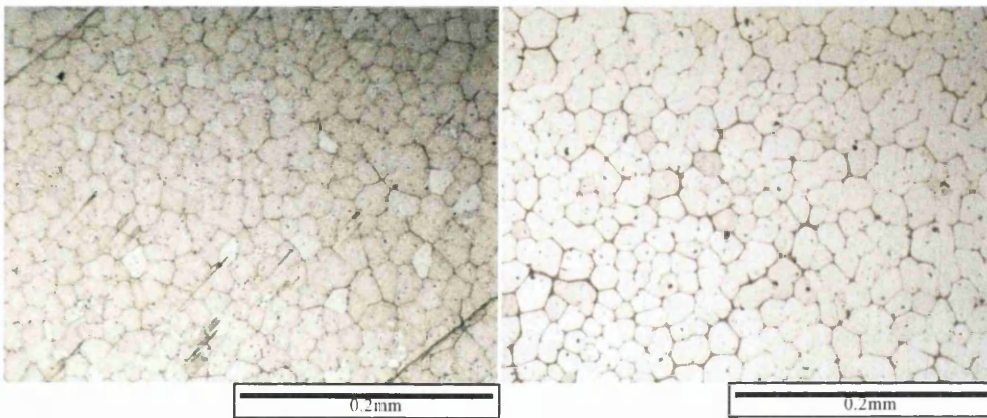
## 5.6 Comparison 2 – Low magnesium MagiZinc type coatings

MGZ41 and MGZ42 have been prepared to examine the effect of reduced a magnesium level in a MagiZinc<sup>®</sup> alloy. During the commercialisation of MagiZinc<sup>®</sup> the elements were added separately to the molten zinc bath and it was worth considering the impact on the coating should there be insufficient magnesium additions available to keep the desired chemistry, plus there may be benefits of reducing the total magnesium content should economic factors affect the price of raw materials.

## 5.6.1 Microstructural characterisation

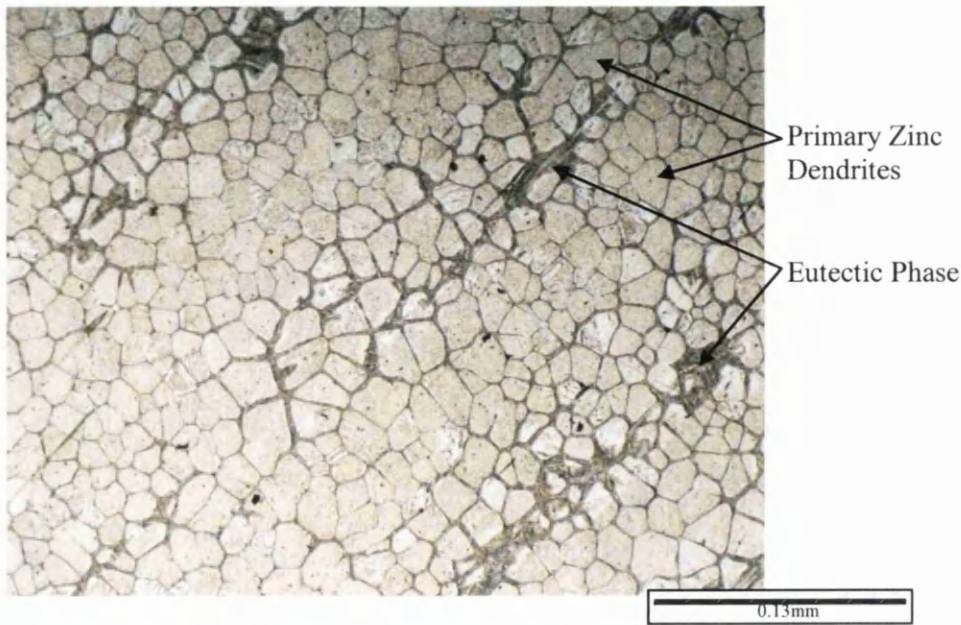
The data in Table 16 and Table 17 shows that the two coatings have similar microstructure. At the coating steel interface the two microstructures appear to be controlled by cellular dendrite growth and do not show the dendritic arm growth of the Galvalloy<sup>®</sup> type coatings previously examined, see Figure 114 and Figure 114 show the microstructures at a depth of approximately 8 $\mu$ m.

At the coating/substrate interface there is a decrease in the primary zinc%, see Figure 116, suggesting that there is a high nucleation rate of primary zinc dendrites and a uniform solidification front moving across the surface of the substrate. Neighbouring, growing dendrites form a region of eutectic phase between and under the cellular dendrites. Each dendrite grows towards the coating/air interface where it is covered with a thin eutectic phase.



**Figure 114 - MGZ41 Microstructure**

**Figure 115 - MGZ42 Microstructure**



**Figure 116 - MGZ41 near substrate interface**

MGZ42 cell volume is approximately 31% larger compared to the dendrite size of MGZ41.

The growth curves, see Figure 118 show that at the maximum primary zinc% at a depth of approximately  $8.5\mu\text{m}$  through the coating there is approximately 5% eutectic phase, this increases through to the coating/air interface. It has been shown by Sullivan et al [118] that the corrosion of the ternary zinc-aluminium-magnesium (ZAM) alloys proceed from initiation of a corrosion site within the  $\text{MgZn}_2$  lamellae in the binary and ternary eutectic regions, as in Figure 117. Sullivan et al have also seen that following the complete dissolution of the  $\text{MgZn}_2$  eutectic lamella the corrosion migrates to the primary zinc dendrites. Hausbrand et al have shown that the corrosion potential of  $\text{MgZn}_2$  is  $-0.92\text{V}$  (compared to standard hydrogen electrode) at near neutral pH's, which when compared to the zinc standard electrode potential of  $-0.76\text{V}$  strengthens the argument of the initiation of corrosion in the  $\text{MgZn}_2$  eutectic lamellae [41].

Figure 118 shows little difference in average dendrite width so it expected that there will be similar interconnectivity of neighbouring dendrites during cut edge corrosion investigations.

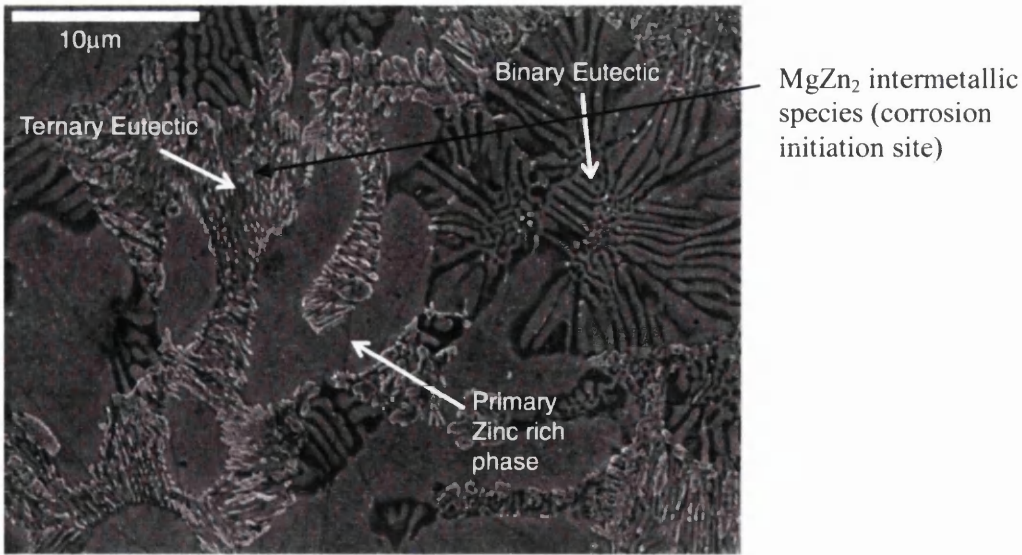


Figure 117 - SEM Image of MagiZinc alloy cross section [118]

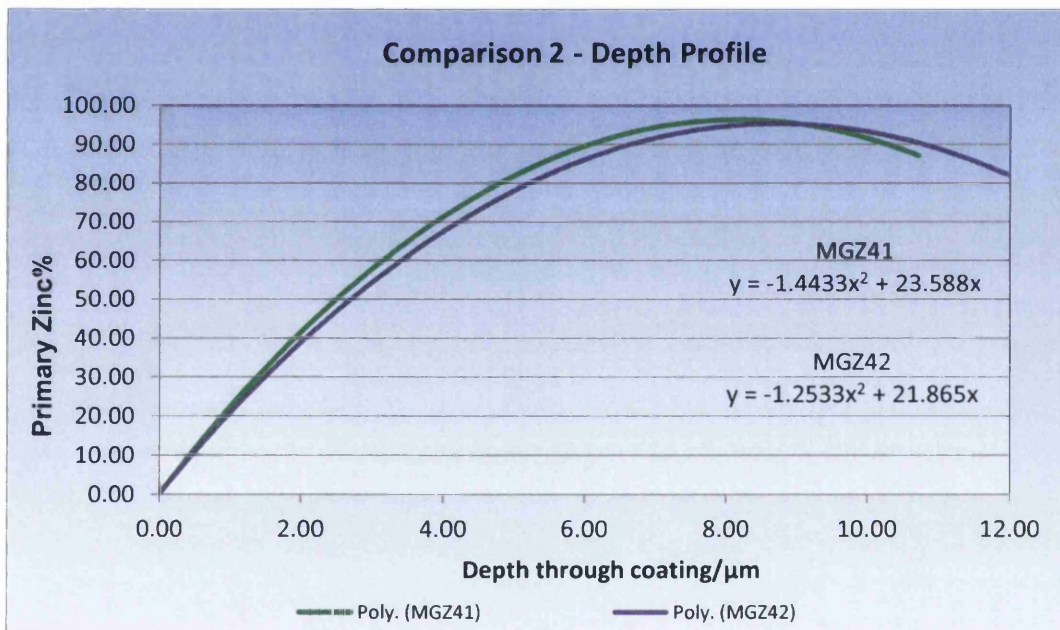


Figure 118 - Comparison 2 Primary Zinc% curves

## 5.6.2 Corrosion performance

Firstly the total predicted mass loss for both of the alloyed samples is less than that observed for the 0.5mm hot dip galv coating, see Figure 119.

With a threshold level of  $1\text{amp/m}^2$  very little activity can be seen in the residual anode analysis for MGZ42, see Figure 120, there are only 2 anodes that are greater than the threshold level and they both are active for less than 6 hours. Reducing the threshold level to  $0.5\text{amps/m}^2$  increases the number of detected anodes to 7, see Figure 121. MGZ41 can be seen to have anodic sites that are persist to longer timescales of 18-24 hours, see Figure 122, although the average intensity of the anodes is low at  $0.6\text{amps/m}^2$ . The overall behaviour is better than the 0.55mm galvanised benchmark sample.

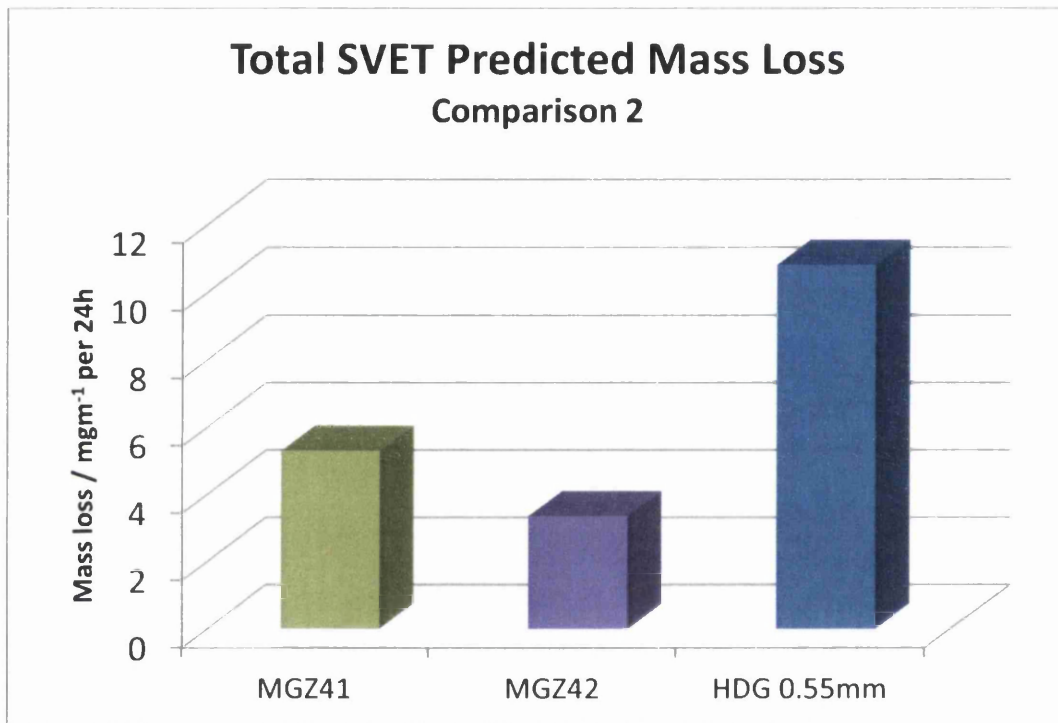
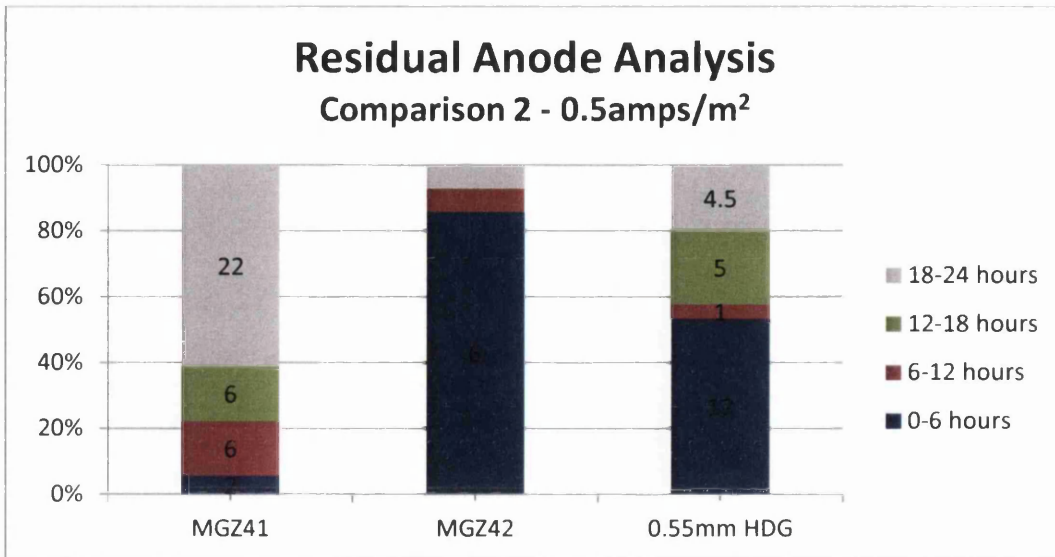
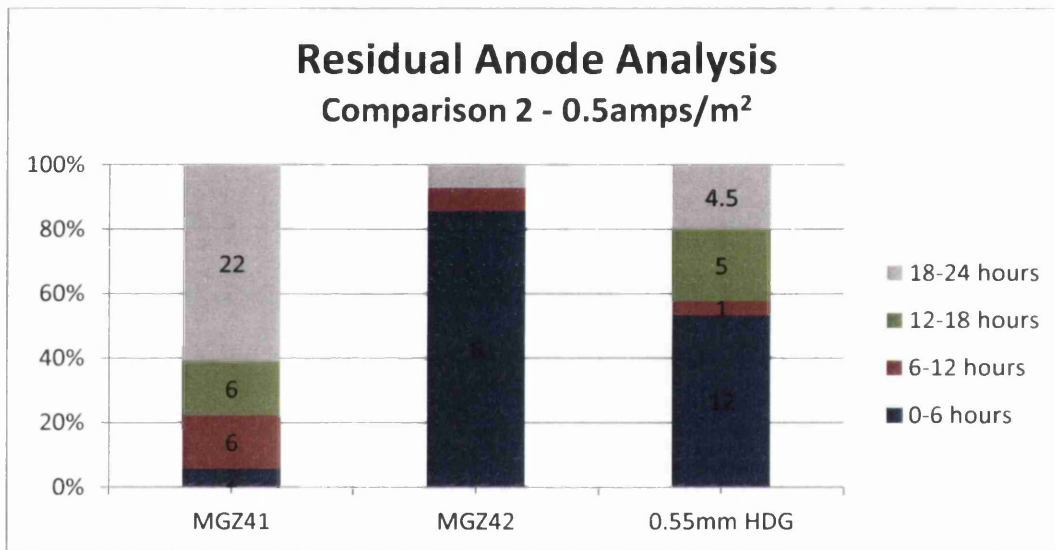


Figure 119 - Total mass loss Comparison 2

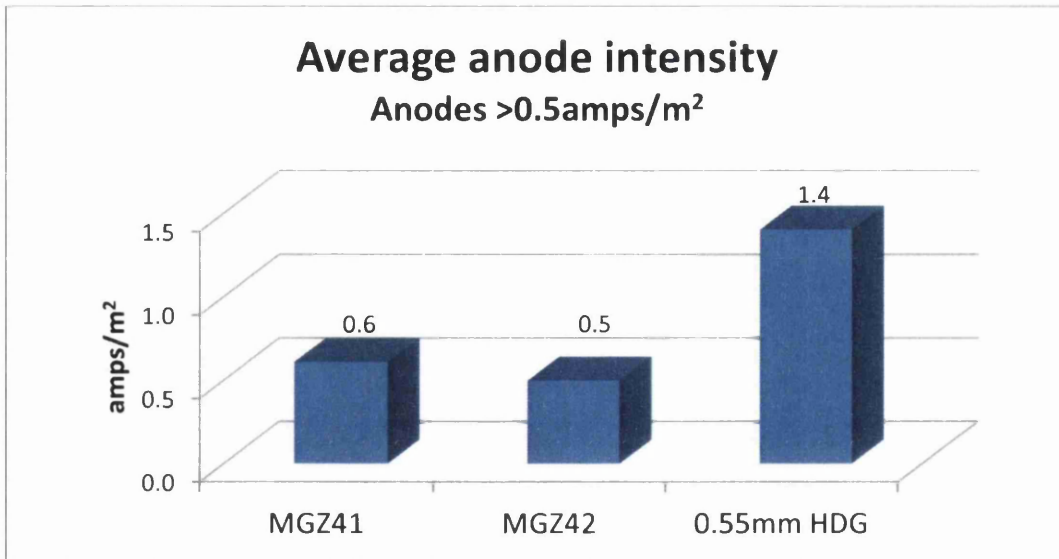




**Figure 120 – Residual anode analysis at 1.0amps/m<sup>2</sup> threshold**



**Figure 121 – Residual anode analysis at 0.5amps/m<sup>2</sup> threshold**



**Figure 122 - Anodes >0.5amps/m<sup>2</sup> Average Intensity**

The differences in the sample activities can clearly be seen if we examine a representative scan of the samples. Figure 123 shows the differences in the corrosion activity on the surface after 22 hours of immersion.

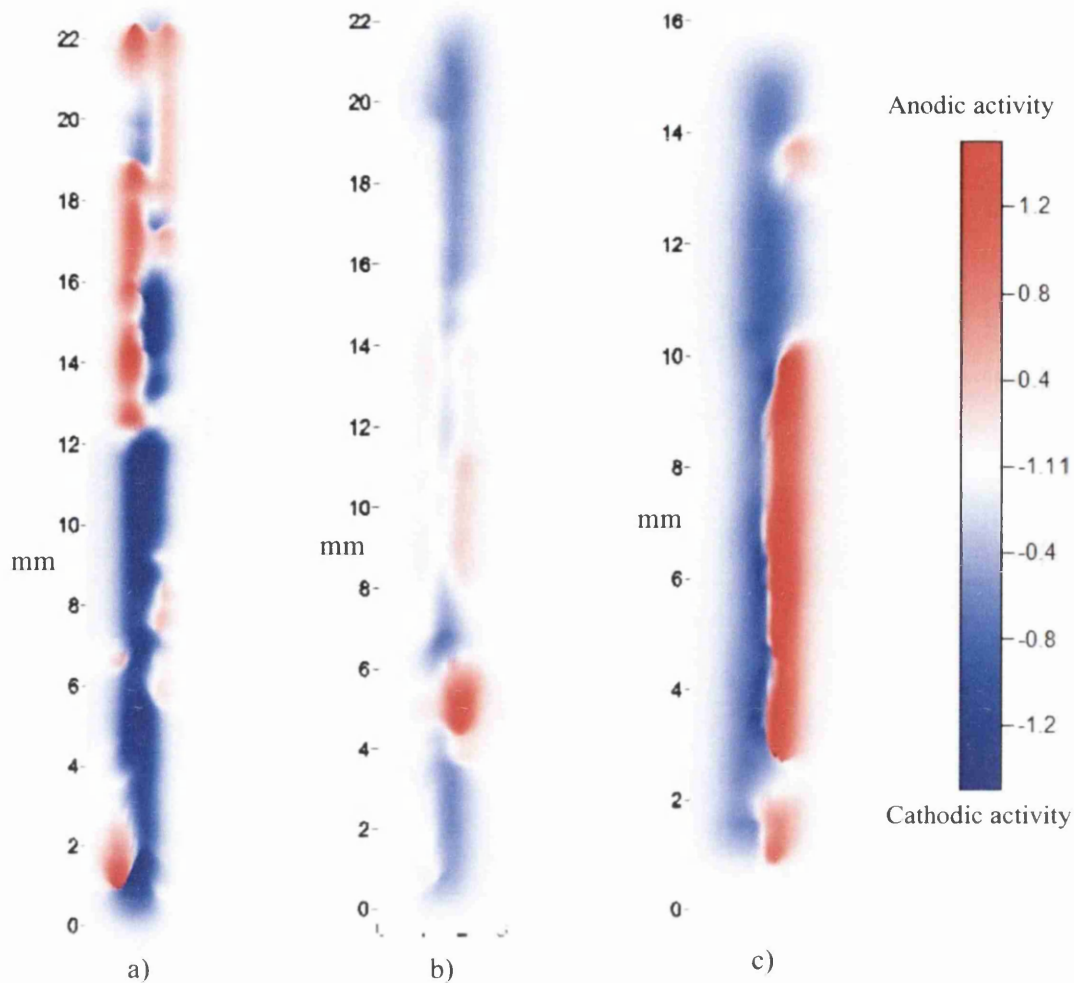


Figure 123 - SVET Scans after 22hours for a) MGZ41, b) MGZ42 and c) 0.55mm HDG

### 5.6.3 Comparison 2 Results

The increased SVET detected corrosion mass loss of MGZ41 compared to MGZ42, seen in figure 119, can be explained by the differences in the thicknesses of the two coatings. With the same level of steel substrate exposed the rate of corrosion is determined by the size of the cathode area. As MGZ41 has 30% less zinc coating thickness than MGZ42 the intensity of the corrosion seen by the SVET is proportionally increased. All sample data is normalised for the length of the sample piece, normalising for the thickness of the coating reduces the mass loss of MGZ41 to 0.077mg in 24hours (30% reduction from 0.11 mg/24h) suggests that the corrosion performance for the coatings is equal.

The microstructures of the two coatings seem to be relatively unaffected by the processing conditions used during their production, see Figure 114 and Figure 114. This could be due to the presence of intermetallic or dross particles within the molten bath providing additional nucleation sites and limiting the effect of increased nucleation rate for higher undercooling, or these particles are of sufficient size or chemistry to avoid dissolution and remain larger than the critical radius size for heterogeneous nucleation.

## 5.7 Comparison 3 – High alloying additions

MGZ43 and MGZ44 show marked differences in their microstructures and in their corrosion performance. We can see in Table 16 that there are large differences in the average primary zinc% and the dendrite count. MGZ43 also exhibits greater corrosion losses under SVET examination.

	Average primary zinc%	Interface Primary zinc%	Average dendrites per image
MGZ43	61.8	89.83	561.5
MGZ44	44.7	85.15	919.5
	Coating Thickness	Average Dendrite volume (mm <sup>3</sup> x 1000)	Dendrite Number
MGZ43	12.6	0.65	4679
MGZ44	12.2	0.27	7663

**Table 18 – microstructural characterisation of MGZ43 and MGZ44**

### 5.7.1 Microstructural characterisation

As can be seen from Figure 124 and Figure 125 the microstructures appear to form under cellular growth conditions, these images were taken at a depth of approximately 8µm.

MGZ43 shows increased zinc cell volume compared to MGZ44, equating to 240% growth in cell volume, see Table 18. There is an increased nucleation from that seen in section 5.6, but within this comparison set we see a marked difference in the dendrite

number between the two samples. The increased alloying content can be assumed to increase the concentration of solute elements ahead of the solidification front for the cells. With increased undercooling the diffusion of zinc atoms from the liquidus to the solidification front is therefore slowed limiting the growth of a cell, and hence giving a marked separation in the two coatings.

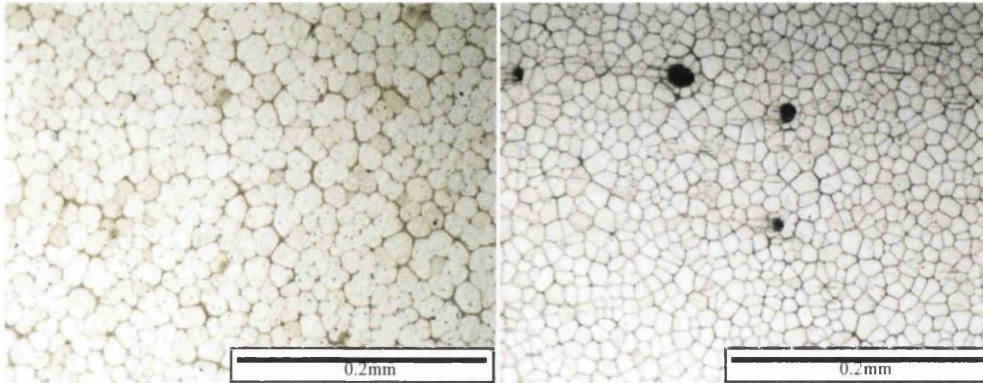


Figure 124 - MGZ43 Microstructure

Figure 125 - MGZ44 Microstructure

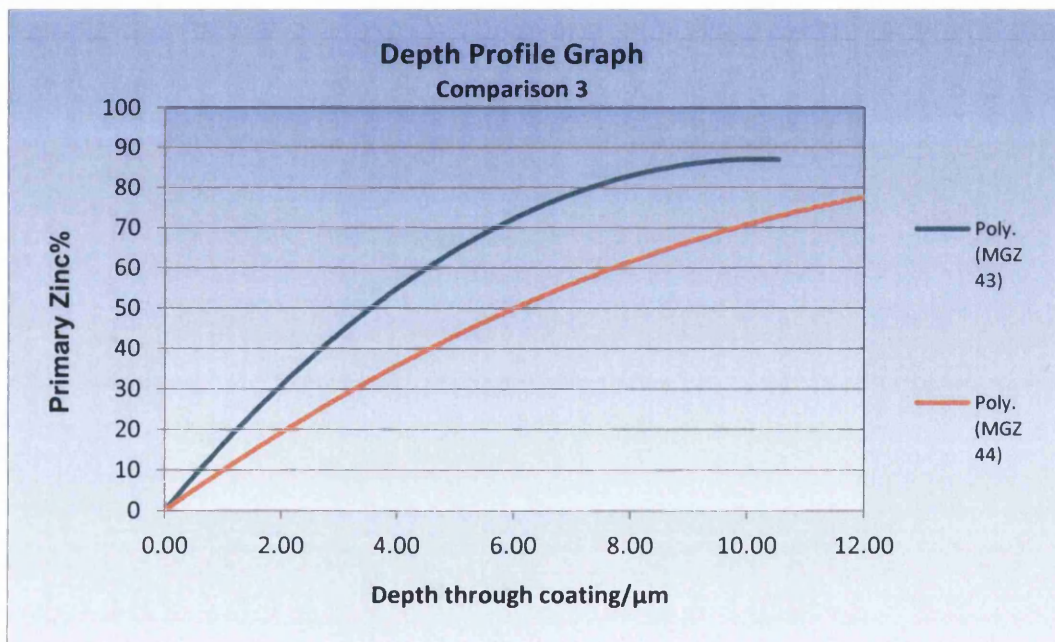


Figure 126 - Depth profile - Comparison 3

## 5.7.2 Corrosion Performance

The larger cell size of MGZ43 shows through in the mass loss examination of the samples, see Figure 127. The mechanism for the mass loss differences can be seen in the

longer lived anodes and higher average anode intensity for MGZ43, see Figure 128 and Figure 129. The corrosion mechanism highlighted in section 5.6 was determined for ternary ZAM alloys can be seen to bear more relevance here due to the increased average eutectic percentage (38.2% eutectic in MGZ43 and 55.3% eutectic in MGZ44). With increased undercooling of the MGZ44 there is an increased amount of zinc retained within the binary and ternary eutectic phases of the microstructure compared to MGZ43.

Figure 130 shows the elemental segregation in the primary, binary and ternary eutectic phases of production MagiZinc®. This has the effect of diluting the amount of intermetallic  $MgZn_2$  phase in the ternary eutectic and lowers the nucleation rate for the corrosion mechanism discussed in section 5.6. DeBruycker in Gent University has found the rapid cooling of ZAM alloy coatings can be seen to partition zinc into the ternary eutectic, as shown in Figure 130 and can promote the change in intermetallic phase of  $MgZn_2$  to  $Mg_2Zn_{11}$ .  $Mg_2Zn_{11}$  will have a lower electrode potential than  $MgZn_2$  and can also lead to a lowering of the nucleation rate for corrosion, although the mechanism for this corrosion rate will require additional investigation.

From Figure 130 and Figure 117 it can be seen that the binary eutectic is comprised of a lamellae structure of  $MgZn_2$  and Zn, whereas the ternary eutectic is comprised of  $MgZn_2$  and Zn with Al nodules [118]

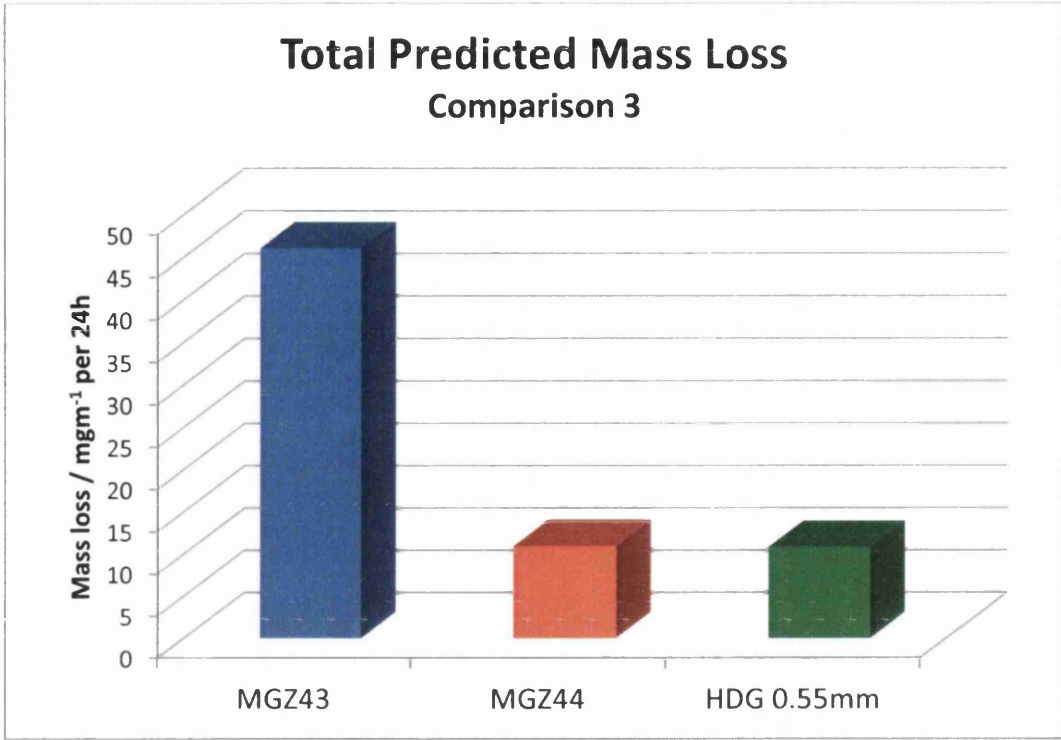


Figure 127 - Comparison 3 Mass Loss

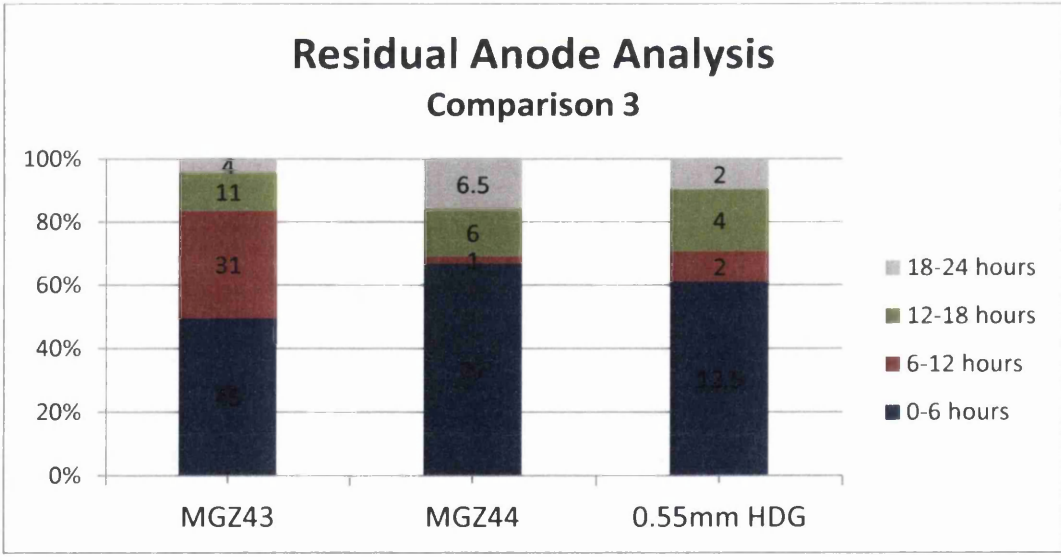


Figure 128 - Comparison 3 Residual Anode Analysis

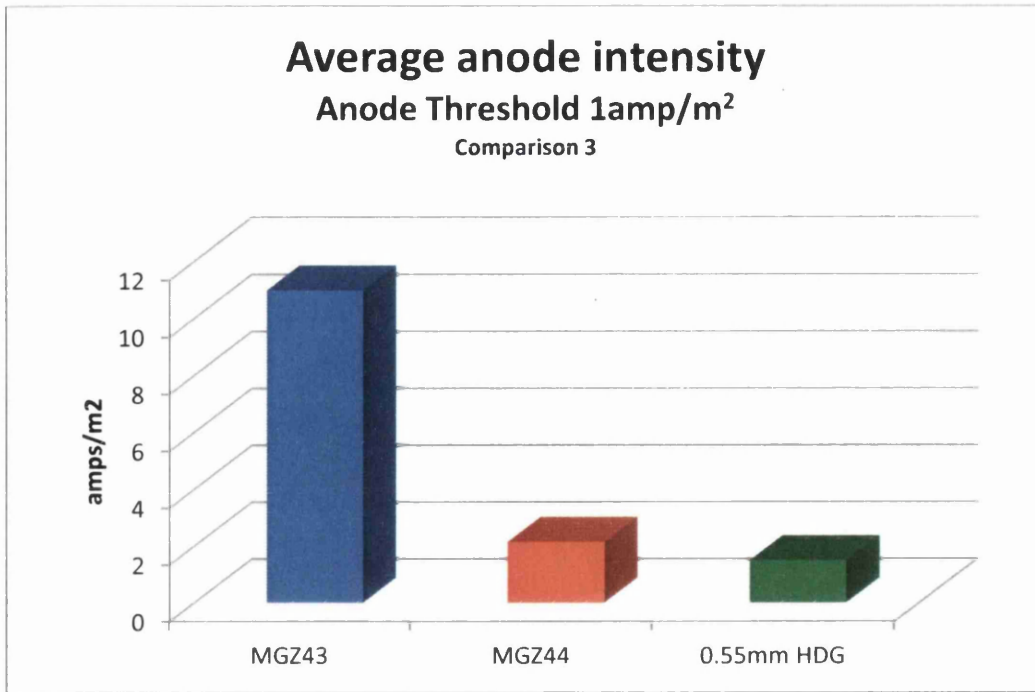


Figure 129 - Average anode intensity

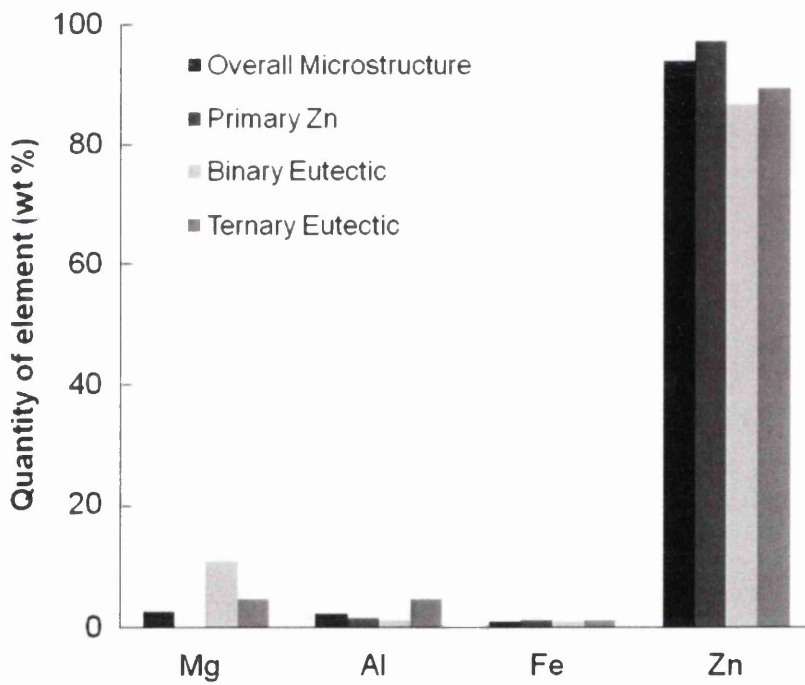


Figure 130 - Elemental partitioning in the phases of MagiZinc® [105]

## 5.8 Comparison 7 – Fast Cooled Sample Comparison



There are many changes to the alloying levels in this sample set but from keeping the processing conditions similar we can see the effect that alloying level has on the microstructure and corrosion performance of the coatings. Later we can go on to see the independent effect of alloying elements on the coating characteristics.

Within this comparison we will see there is a marked change in the coating microstructure and nucleation rate from varying coating chemistry with the greatest effect attributed to the magnesium additions.

Increasing alloy content has been seen in section 5.7 to affect the dendrite growth through the increased concentration gradient of solute atoms ahead of the solidification front of the growing dendrite. Figure 131 shows the inverse relationship of total alloying level and primary zinc%, for similar levels of undercooling. This is expected due to the overall alloying level increasing the percentage of binary and ternary eutectic phase therefore increasing the amount of  $MgZn_2$  phase and the likelihood of corrosion initiation from one of these more electrochemically active sites. Figure 132 shows the effect that increased alloying levels have on the effect of dendrite number. Figure 133 shows that for the highest alloyed sample MGZ45 the microstructure shows dendritic growth and significant eutectic surrounding each dendrite, Figure 133 and Figure 135 show the microstructure for MGZ66 and MGZ48, the fast cooled MagiZinc<sup>®</sup> alloy for comparison, all images are taken at a depth of approximately  $8\mu m$ .

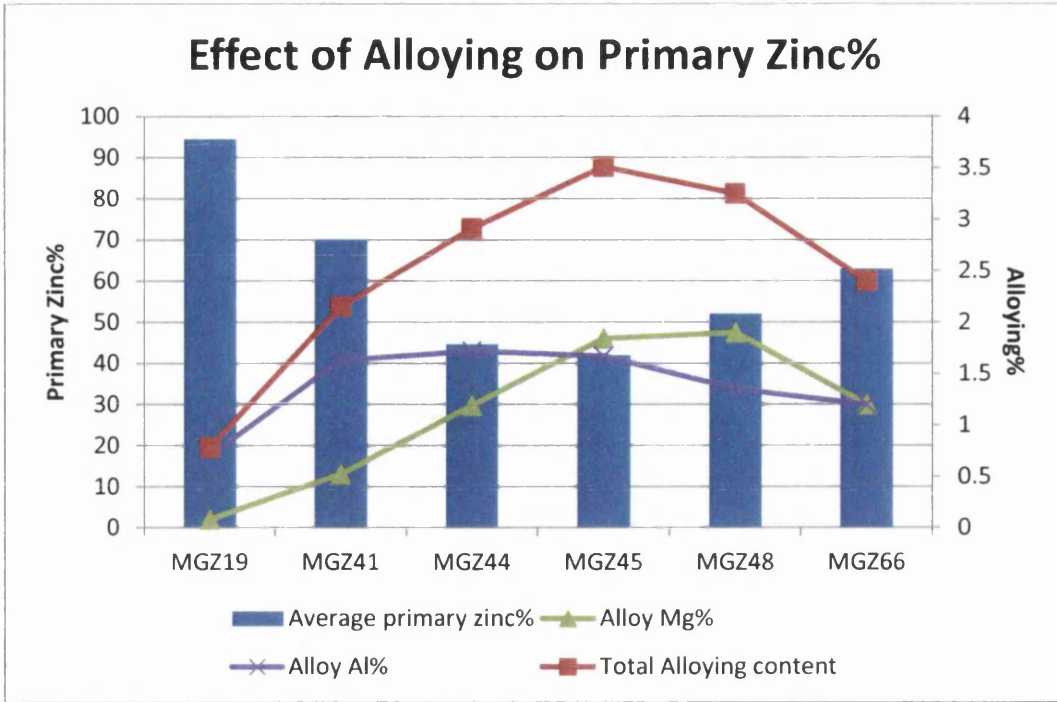


Figure 131 - Effect of Alloying Level on Primary Zinc%

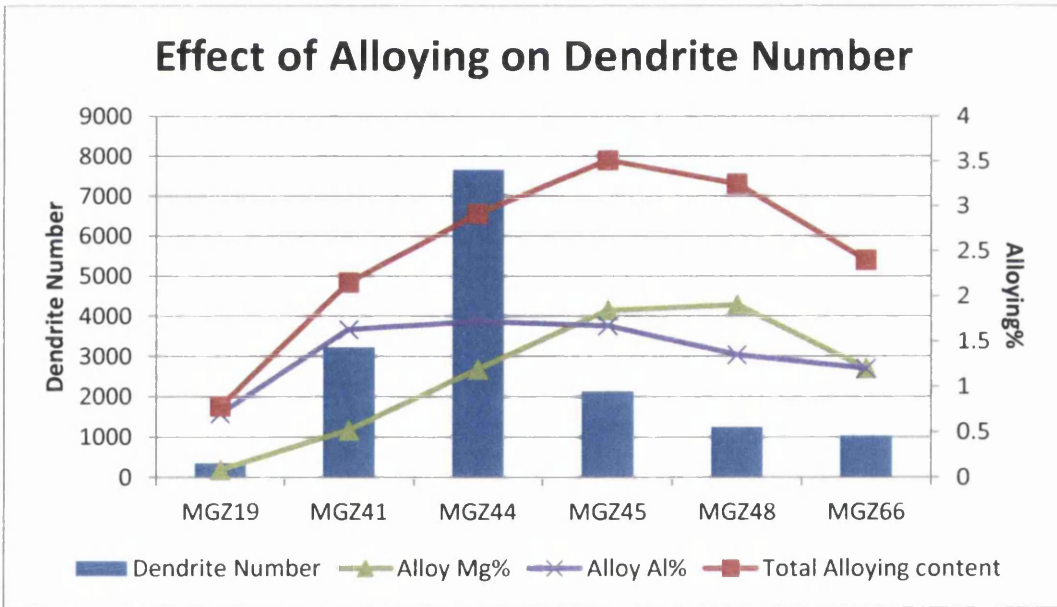
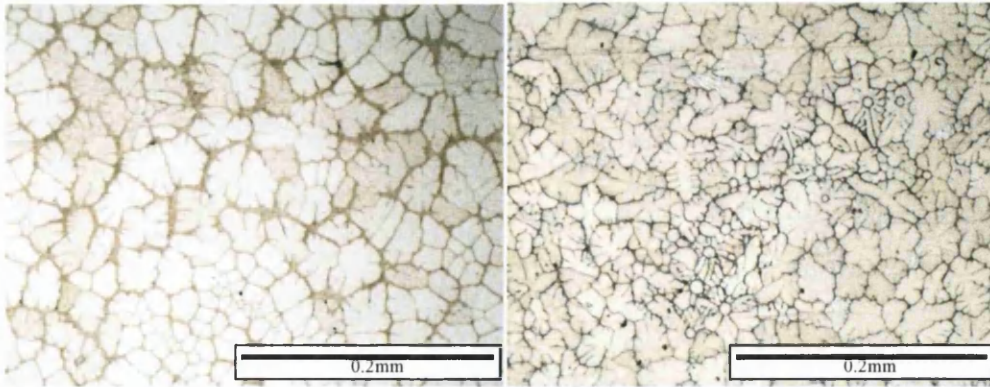
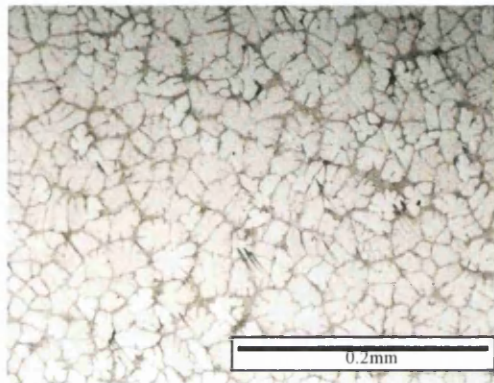


Figure 132 - Alloying effect on Dendrite Number



**Figure 133 - MGZ45 microstructure**

**Figure 134 - MGZ66 microstructure**

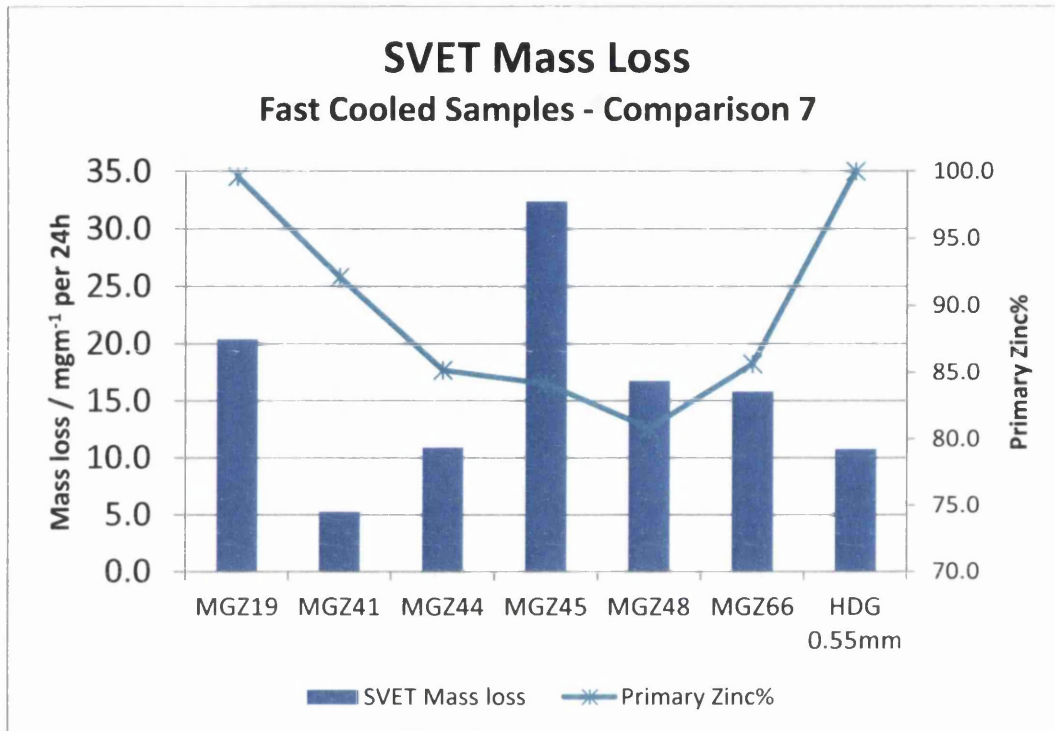


**Figure 135 - MGZ48 microstructure**

### 5.8.1 Corrosion performance

There is an inverse relationship for predicted SVET mass loss and the primary zinc%, see Figure 136. This adheres to the mechanism for the initiation of corrosion losses described in section 5.6. The marked increase in the zinc mass loss for the MGZ45 sample is related both to the increased magnesium level and the associated increase in expected  $MgZn_2$  intermetallic in the ternary eutectic phase offering an increased nucleation rate for corrosive attack, and the increase in dendrite size, compared to the cellular growth found in MGZ44. MGZ41 and MGZ44 show significantly less anodic zinc losses than both the benchmark sample of HDG and the MagiZinc<sup>®</sup> alloy chemistry of MGZ66.

MGZ48, see Figure 135, and MGZ44 have similar alloying level though the level of aluminium is higher in MGZ44 and in comparison the level of magnesium is higher in MGZ48. It is again expected that the increase in mass loss from the SVET study is due the increased loading of the ternary eutectic expected from the increase in magnesium alloying level.



**Figure 136 - SVET Mass Loss v Alloying Level**

MGZ66 shows an increased mass loss result compared to that determined for the benchmark sample of HDG for similar gauge. The increased corrosion protection for ZAM coatings tested under salt spray conditions is not identified here though that can be explained by the relatively short duration of the SVET test and the possible hindrance of generating protective corrosion deposits, similar to those found on ZAM coatings when tested in cyclic corrosion tests. Simonkolleite, zinchydroxychloride, has been detected on the corroded surfaces of ZAM coatings, together with Mg(OH)<sub>2</sub> with possible modification by carbonate species [70], it is thought that the continuous immersion in a chloride environment as used in the SVET test do not allow for the generation of

Mg(OH)<sub>2</sub> from the basic MgO surface oxide. The basic conditions of the Mg(OH)<sub>2</sub> species is require to produce the insoluble simonkollite and therefore the barrier protection it can offer does not retard the corrosion rate.

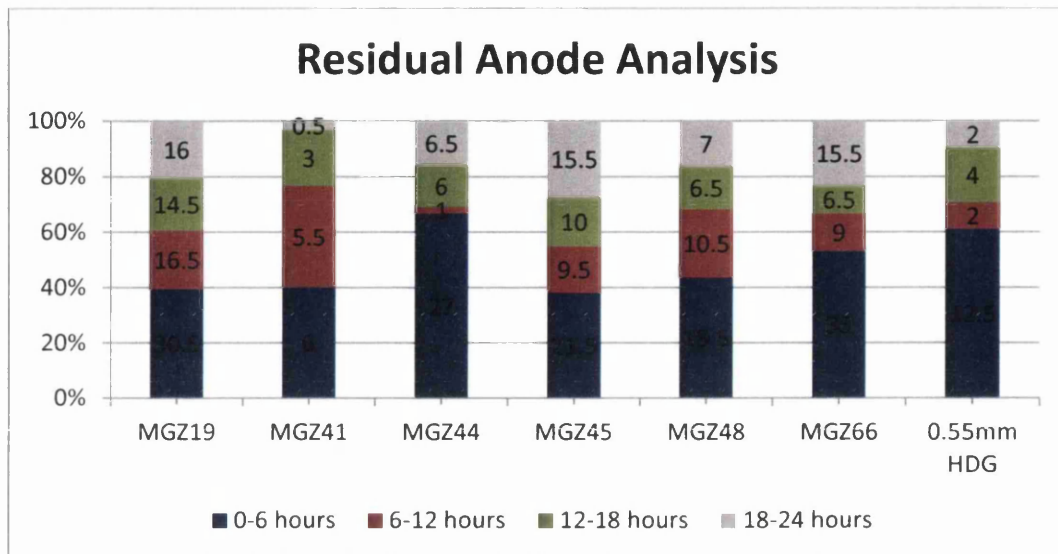


Figure 137 - Residual Anode Analysis

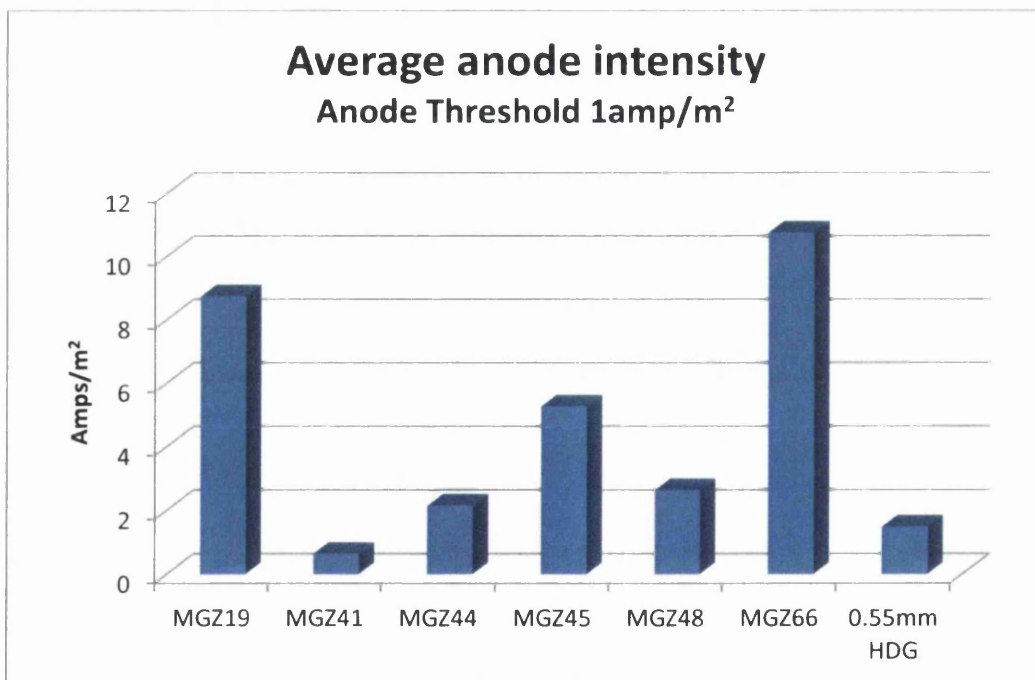


Figure 138 - Average anode intensity

## 5.9 Comparison 8 – Slow Cooled Samples

For the slow cooled samples a similar trend is seen in the average primary zinc% as was seen in the coatings with increased undercooling, see Figure 139. Lower undercooling will allow for increased diffusion of zinc atoms to the solidification front of a primary zinc cell or dendrite, and therefore coating microstructures will achieve closer approximations to an equilibrium cooled microstructure. We would expect to see higher primary zinc contents and possibly coarser eutectic phases [1]. This is what we see for the majority of the samples but in the case of the highest magnesium alloyed samples we see that lower undercooling reduces the amount of primary zinc phase that is measured in the microstructure compared to the fast cooled samples.

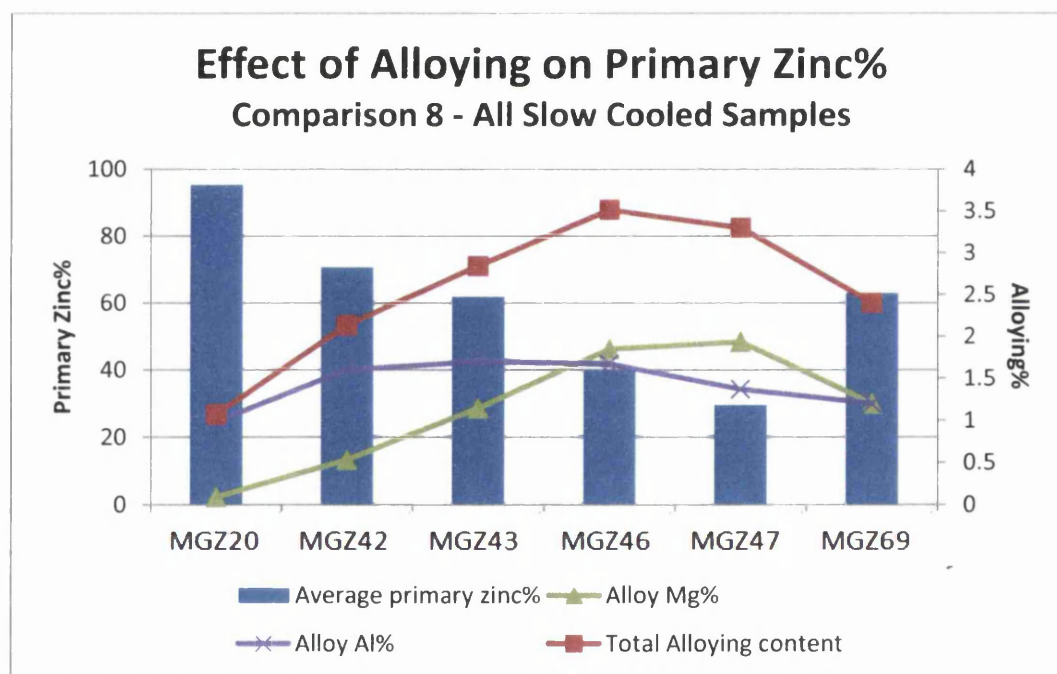


Figure 139 - Effect of Alloying Level on Primary Zinc

The microstructure of MGZ46 can be seen to be cellular in nature, see Figure 140, with coarse intercellular binary and ternary eutectic areas. The increased nucleation rate is proposed to be due to the presence of  $MgZn_2$  or dross particles acting as nucleation cells

(from the molten bath chemistry), or that due to the lower undercooling the diffusion on magnesium in the solute is such that the HCP primary zinc dendrites can nucleate the growth of HCP  $MgZn_2$  eutectic cell lamellae in the areas of constitutional supercooling ahead of the solidifying dendrite/solute interface. It can be seen that there is a considerable increase in the amounts of binary and ternary eutectic in the slow cooled MGZ47 sample, see Figure 140. This can attributed to the increased abundance of magnesium in the alloy, and an increased content of  $MgZn_2$  available to both binary and ternary eutectic phases.

The lower alloying level in MGZ69 coupled with the lower undercooling shows an extensive dendritic microstructure, see Figure 142, where there is a reduced ternary eutectic phase from the incorporation of the majority of the aluminium content in solid solution in the primary zinc dendrites and the surrounding binary eutectic. Ternary eutectic would be expected closer to the coating/air interface. All microstructures were taken at approximately  $8\mu m$  depth.

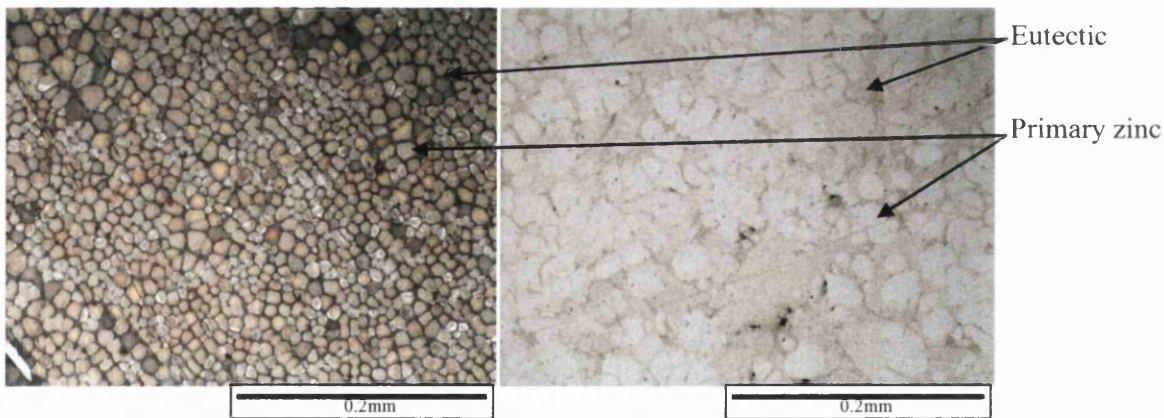


Figure 140 - MGZ46 Microstructure

Figure 141 - MGZ47 Microstructure

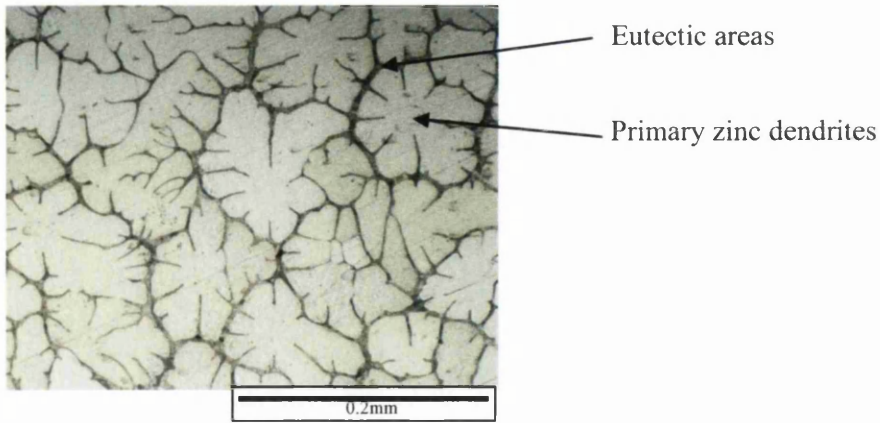


Figure 142 - MGZ69 Microstructure

### 5.9.1 Corrosion performance

The corrosion performance follows the same trends as the previous samples in that the relationship between the primary zinc and eutectic phase, see Figure 143. The slight deviations we see are due to the incorporation of more magnesium into the alloying chemistry and the expected increase of losses from the binary eutectic phase.

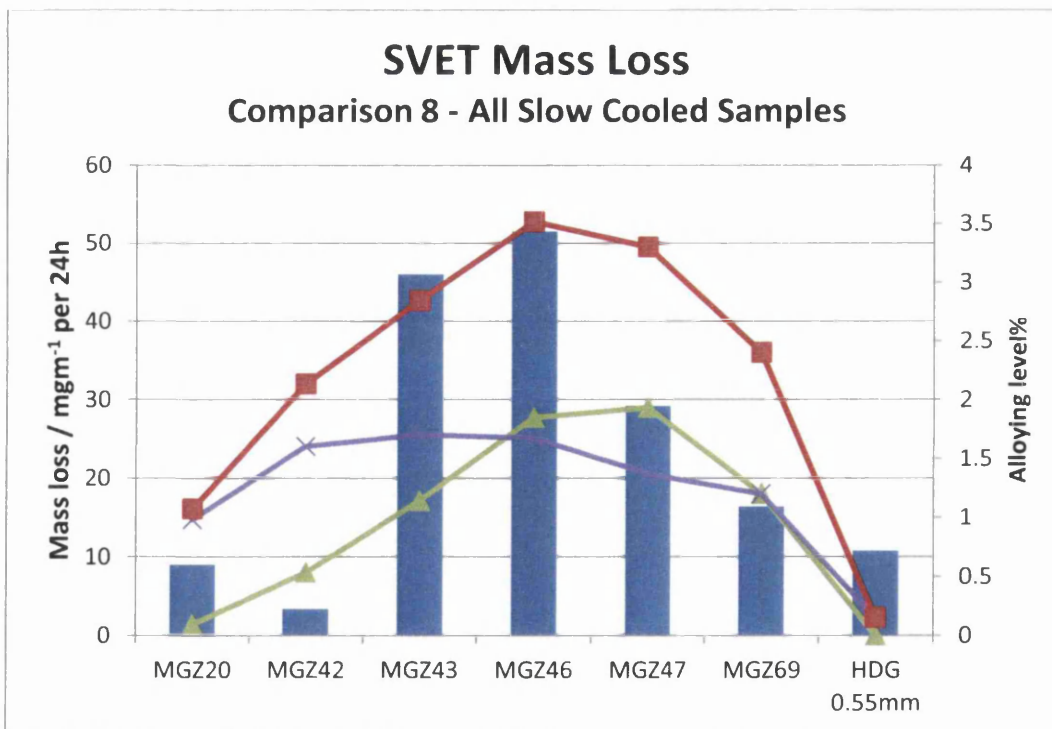


Figure 143 - Mass Loss Comparison 8

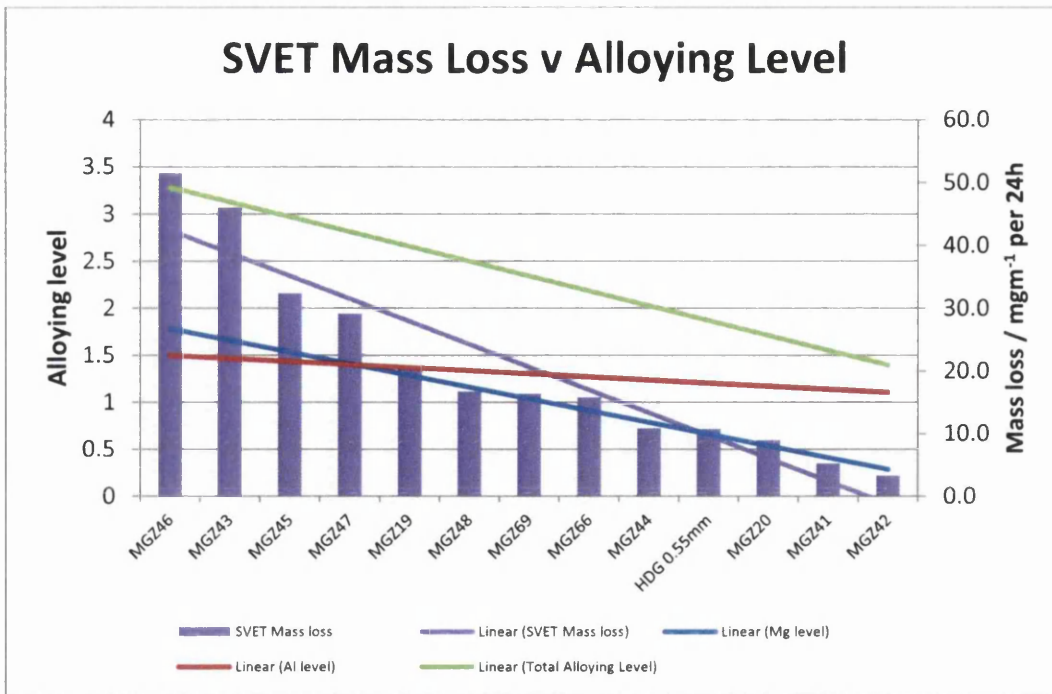


## 5.10 Overall Comparisons and Relationships – Comparisons 9-12

The previous sections have identified the principles that are governing the microstructure and, as a result of this the corrosion resistance differences between those comparisons. This section looks to identify if there are governing trends associated with the change in alloying level, both alloying of aluminium and magnesium and of total alloying level. Aluminium additions into zinc will create an increasing level of zinc-aluminium eutectic, further magnesium additions will increase the amount of eutectic for a consistent aluminium alloying level due to the depression of the eutectic temperature.

There is a strong relationship in the data set between the mass loss and the magnesium alloying levels. In Figure 144 we can see the trend lines for SVET mass loss and magnesium alloying level are similar showing a stronger dependency on the mass loss towards magnesium additions rather than the aluminium addition.

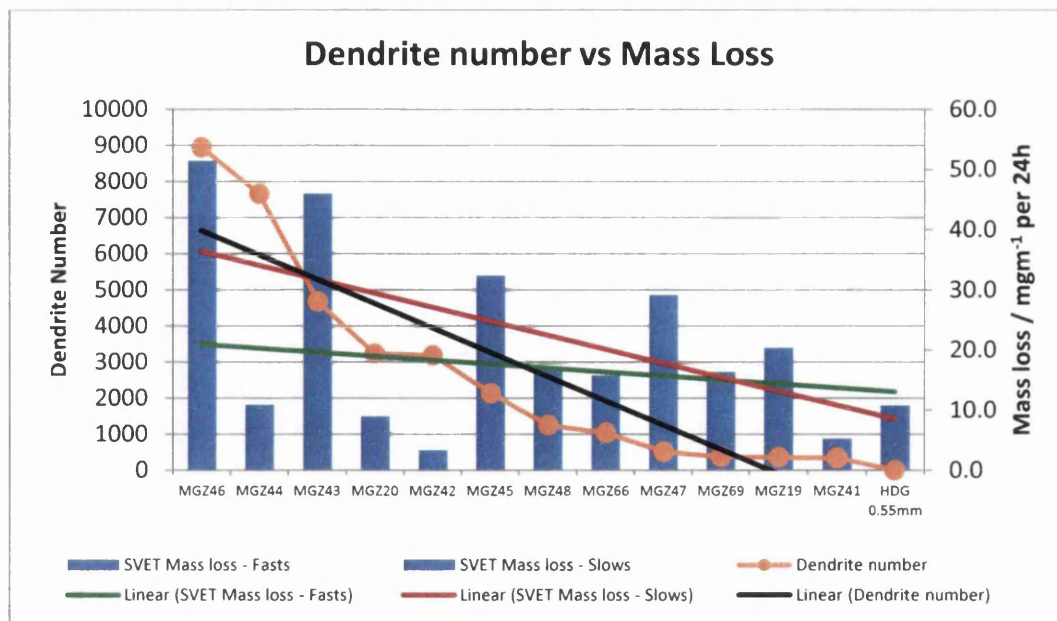
Plotting the data sets as a Pareto analysis, Figure 144 and Figure 145, or as an XY scatter graph, Figure 146 and Figure 147, and the plotting of linear trend lines can provide dependency information. Dependency of SVET mass loss to an elements' alloying level can be seen in the parallelism of the trend lines in Figure 144. Parallel trend lines show strong interdependency whilst trend lines that cross show limited dependency on the two data sets.



**Figure 144 - Mass loss to Alloying Level**

Figure 145 shows the relationships that have been determined between the predicted SVET mass loss for the fast and slow cooled samples, and how these can be related back to the changes to the dendrite number.

Figure 145 shows there is stronger dependency on the predicted mass loss for the slow cooled samples with the changes in dendrite number. The dependency is weaker than for the alloying level, see Figure 144, but a clear difference can be seen in the comparative dependencies of the fast and slow cooled SVET response to the dendrite number.



**Figure 145- Dendrite number vs. Mass loss**

An XY scatter graph of primary Zn% v alloying level can return a polynomial relationship. Not surprisingly there is a strong trend between primary Zn% and the alloying level, but separating out the primary Zn% against the levels of magnesium and aluminium separately shows that there is a greater dependency on the magnesium alloying level on the primary Zn% than aluminium alloying level, with 0.90 and 0.56 R<sup>2</sup> values respectively. This is considered to be due to the presence of Mg in both the binary and ternary eutectic phases.

The last interdependency that could be found in the data with a reasonable R<sup>2</sup> value is the relationship between the SVET mass loss and the alloying level. This is a useful relationship to have found because we can use the polynomial coefficients to determine the SVET mass loss for future alloying compositions. It is considered that the R<sup>2</sup> value could be increased with more repetitions per sample.

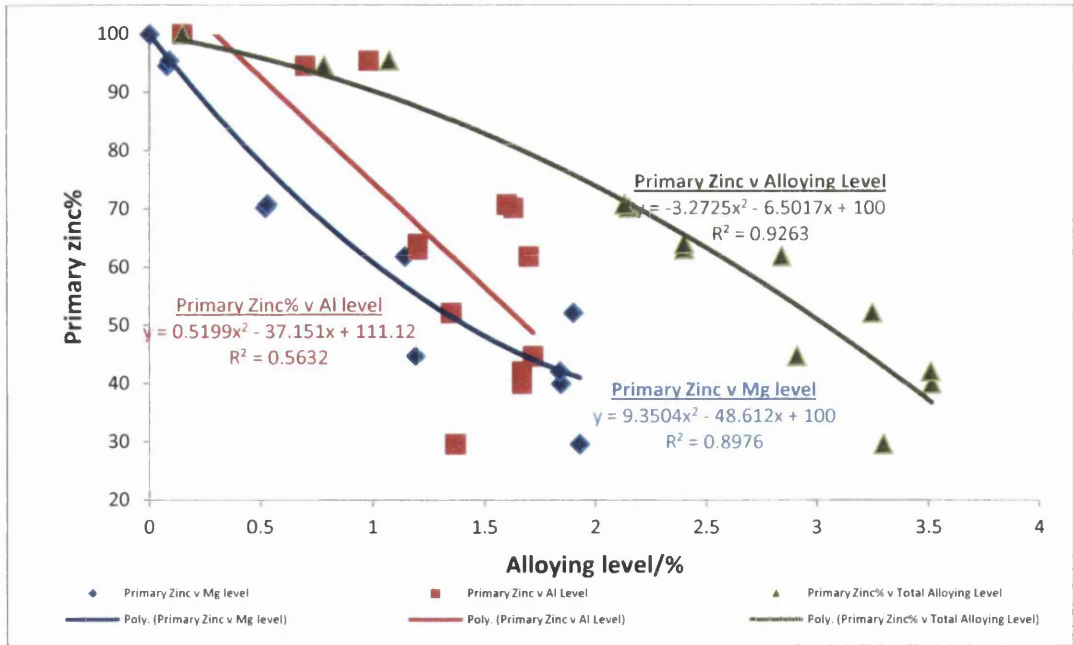


Figure 146 - Scatter graph of primary zinc% v alloying level

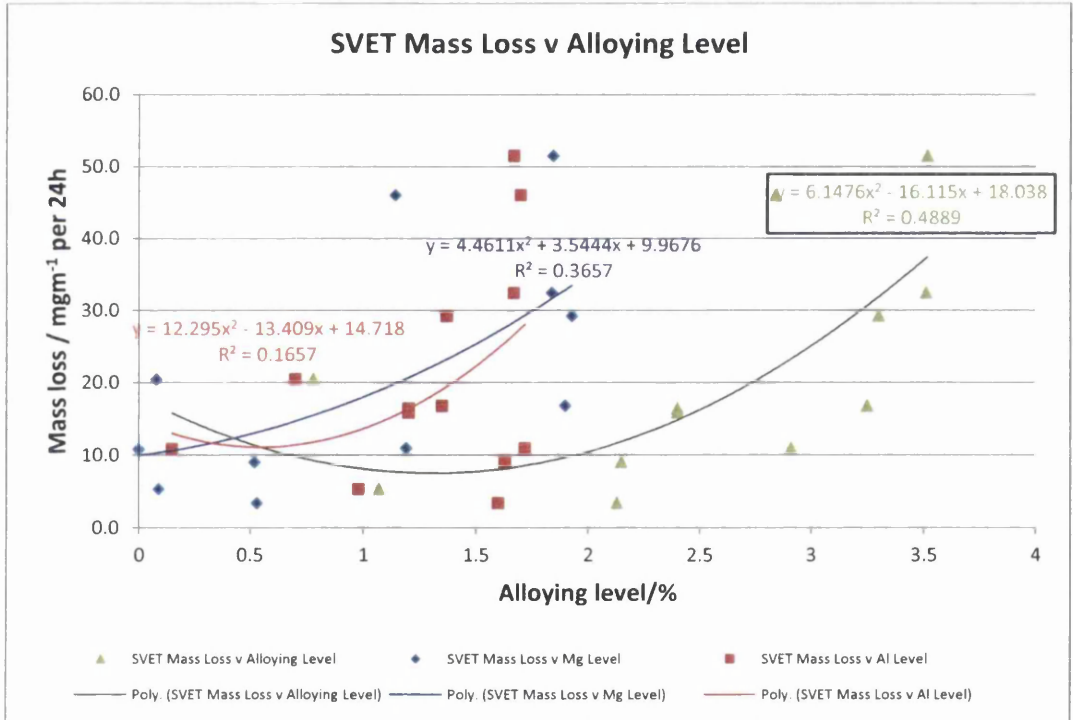


Figure 147 - Scatter graph of Mass Loss v Alloying Level

### 5.11 Results and discussion

We have seen that the microstructural characterisation is an extremely useful tool to define the microstructures of ternary alloy coatings on sheet steels. We have also seen

that for some chemistries of ZAM alloys the increase of decrease of undercooling has little effect on the changes in the coating microstructures, this is greatly dependent on the solubility levels of the alloying elements in the primary phase.

There are some interesting microstructural factors that play their part in defining the final cooled microstructure of a ZAM coating. Some of the factors that affect Zn-Al coatings, see section 4, do not apply when the coating microstructures exhibit binary and ternary eutectic phases.

The examination has found some useful interdependencies on alloying levels with microstructure generation and more importantly has defined a possible route for predicting the zinc mass losses observed via SVET when the coating alloy composition is know.

## **Chapter 6**

### **Investigation of Coated Steel Behaviour in High pH Environments**

## 6.0 Introduction

Coated steel products are widely used in the construction sector of the UK. The current UK market for coated steel is 800kt per annum, of which the majority is G275, hot dip galv (GI) of 275g/m<sup>2</sup> [44].

The development of the MagiZinc<sup>®</sup> (MZ) product has identified an opportunity for the replacement of hot dip galv products with a lower coating weight MZ product with similar corrosion resistance performance in standard tests [39, 68, 114].

There is significant work underway to prove the effectiveness of the lighter MZ coatings to the construction industry to allow confident entry into the market for this added value product [13]. As a business the opportunities for cost reduction can be realised from the reduction in the loading of zinc, an expensive commodity, see Figure 3. TSE have identified some financial benefit to the business in the replacement of G275 with MZ140, 140g/m<sup>2</sup>.

Although dispelled [120], the rumours that the available zinc reserves are drying up continue to impact on product development in the steel industry, and every effort is made to extend perceived reserves, but also to cut processing costs. Alongside the environmental pressures that perceived resource issues stimulate there is more legislative pressures on the reduction in the use of hazardous chemicals [121]. Tata Steel Ltd. continues to use chromate based passivation treatments on hot dip galv products in the construction market. Tata Steel Ltd., ahead of the introduction of the REACH guidelines<sup>22</sup>, is actively evaluating the performance of several chromate free passivation systems for the protection of zinc coated steels, including MagiZinc<sup>®</sup>, against white rust, zinc oxide, formation during the transport and storage phase of a construction solution.

---

<sup>22</sup> Registration, Evaluation, Authorisation & restriction of Chemicals (REACH), from 1<sup>st</sup> June 2007 a phased introduction of restrictions in the use of chemicals with the provision to harm human health.

Construction products such as composite floor decking and angle beads are used to support concrete structures, or to provide a mechanical support for cement plasters. The hardening of cement products is due to the reactions with water of the main components of calcium silicates,  $\text{CaO}\cdot\text{SiO}_2$ . During these reactions saturated calcium hydroxide is produced giving the high alkalinity. Saturated  $\text{Ca}(\text{OH})_2$  has been determined to be pH 12.7 [122-125].

The Pourbaix diagrams of zinc and magnesium show a difference in the activities of the two metals at the typical alkaline conditions found in fresh, wet cement mixtures. Magnesium is passive at this pH level and it is considered whether the alloying level in MagiZinc will translate into an increase in the comparative corrosion performance compared to hot dip galv. Also MgO is a basic oxide and could provide some barrier corrosion protection to the surface of the coating, in contrast to the hot dip Zn-0.15wt%Al coating which will have zinc and possibly aluminium oxides on the surface, both of which are amphoteric and will dissolve in saturated  $\text{Ca}(\text{OH})_2$  solution.



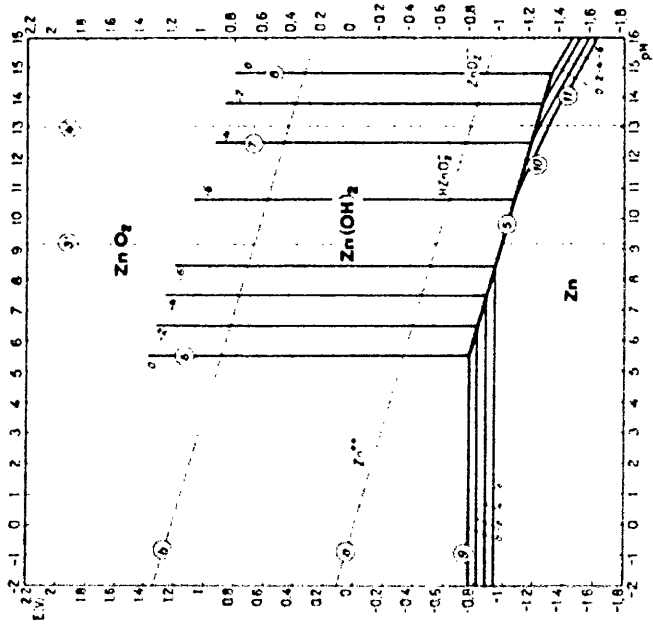


Figure 148 - Pourbaix diagram for Zinc [126]

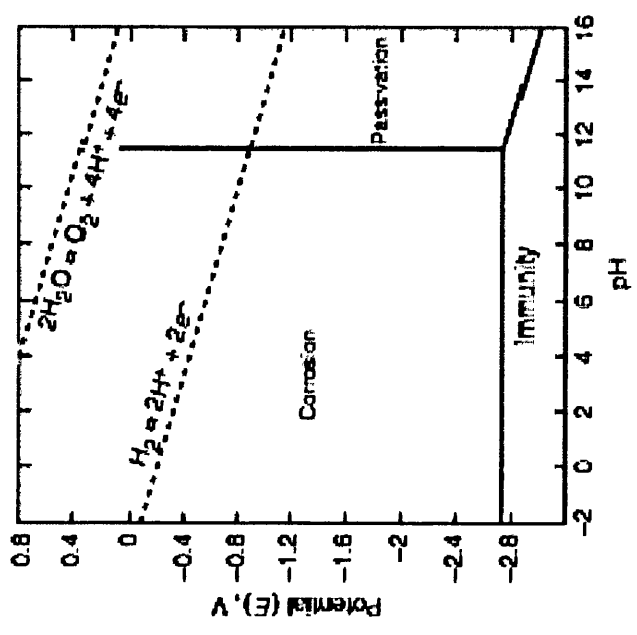
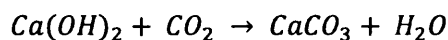


Figure 149 - Pourbaix Diagram of Mg [127]

## 6.1 Experimental Investigation

Several commercially available chrome free passivation systems have been compared using SVET and immersion mass loss tests to evaluate their corrosion resistance performance compared to industry standard chromate systems and oiling. There is evidence that the presence of calcium ions in solution can help retard the anodic dissolution of zinc alloys [128]. Because of this, and to increase the ‘real world’ comparison for the study it was decided to conduct the study using saturated calcium hydroxide solution. Calcium hydroxide solution rapidly reacts with atmospheric CO<sub>2</sub> to form calcium carbonate, CaCO<sub>3</sub> according to the reaction;



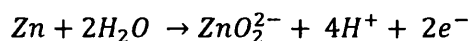
This reaction resulted in the formation of a white crust over the SVET bath which limited further solution neutralisation, excess un-dissolved Ca(OH)<sub>2</sub> was added to the SVET bath to limit the neutralisation resulting in a final solution pH of 12.2 after 24 hours test duration.

Immersion mass loss tests were conducted using fresh saturated calcium hydroxide solution. Samples of known exposed surface area were immersed for a period of 3 days, and a further 25 days. At the end of each time period the samples were ultrasonically shaken to remove any adherent corrosion deposit, the samples removed and rinsed and the solutions acidified and diluted to a known volume submission for analysis. Elemental analysis was carried out in Testing Solutions Wales (TSW), based in Port Talbot, a UKAS accredited laboratory. All testing was carried out in accordance with TSW/042 test procedure using a Perkin Elmer ICP-EOS analysis determined the metal content, and a mass loss per unit area calculated from the exposed surface area.

It was not prudent or possible in time allowed to perform SVET tests of 3 and 25 days to compare directly with the immersion mass loss investigation and so the mass loss in the duration of 3 days and the further 25 days was considered linear for the purposes of method comparison.

The mass loss experimental timescale was determined from the drying time for the high strength cement systems used in the associated study of cement covered or plastered, laboratory scale, composite floor deck and angle bead components [13]. 3 days is the hardening time for the cement system, and after 28 days the cement system is full cured. The reactions associated with these timescales can be simply considered to be the hydration of aluminium silicate and the liberation of calcium hydroxide within the first three days, with carbon dioxide absorption and conversion of solids calcium hydroxide to calcium carbonate

The Pourbaix diagram for zinc shows that the most favourable reaction is the production of the zincate ion,  $ZnO_2^{2-}$ , according to the reaction,



## 6.2 Sample Matrix

Sample id	Gauge	Coating	Coating Weight	Passivation	Product type	Description
9ZE133 s1	0.7	HDG	275	None	Investigative	HDG 0.7mm Z275 Cleaned Only
9ZE134 s1	0.7	HDG	275	5004	Sub - UK	HDG 0.7mm Z275 Passerite 5004
9ZE142 s1	0.7	HDG	275	NR6022	Current - UK	HDG 0.7mm Z275 NR6022
9ZE74	0.7	HDG	275	Oiled	Investigative	Z275 HDG 0.7mm Oiled
HDG 0.7mm Cr	0.7	HDG	275	Chromated	Current - UK	HDG 0.7mm Cr Zodiac
9ZE136 s1	1	HDG	275	5004	Sub - UK	HDG 1.0mm Z275 Passerite 5004
9ZE141 s1	1	HDG	275	NR6022	Current - UK	HDG 1.0mm Z275 NR6022
9ZE72	1	HDG	275	Oiled	Investigative	Z275 HDG 1.0mm Oiled
HDG 1.1mm Cr	1.1	HDG	275	Chromated	Current - UK	HDG 1.1mm Cr Zodiac
9ZE135 s1	2	HDG	275	NR6022	Current - UK	HDG 2.0mm Z275 NR6022
9ZE73	2	HDG	275	Oiled	Investigative	Z275 HDG 2.0mm Oiled
HDG 2.0mm Cr	2	HDG	275	Chromated	Current - UK	HDG Chromated 2.0mm Zodiac
9ZE75	0.63	MZ	140	5004	Sub - UK	MZ140 0.63mm Passerite 5004
9ZE101	0.74	MZ	350	Z801-16	Sub - IJ	MZ350 Z801-16 0.74mm Primecoat
9ZE137 s1	1	MZ	140	5010	Sub - UK	MZ140 1.0mm Passerite 5010
9ZE138 s1	1	MZ	140	None	Investigative	MZ140 1.0mm Clean Only
9ZE139 s1	1	MZ	140	5004	Sub - UK	MZ140 1.0mm Passerite 5004
9ZE140 s1	1	MZ	140	NR6022	Investigative	MZ140 1.0mm NR6022
9ZE76	1	MZ	140	Z801-16	Sub - IJ	MZ140 1.0mm Z801-16 Primecoat
9ZE77	1	MZ	140	None	Investigative	MZ140 1.0mm No passivation
9ZE104	1.48	MZ	140	Z801-16	Sub - IJ	MZ140 Z801-16 1.48mm Primecoat
9ZE103	1.48	MZ	200	Z801-16	Sub - IJ	MZ200 Z801-16 1.48mm Primecoat
9ZE110	1.48	MZ	275	Z801-16	Sub - IJ	MZ275 Z801-16 1.48mm Primecoat
9ZE109	1.48	MZ	350	Z801-16	Sub - IJ	MZ350 Z801-16 1.48mm Primecoat
9ZE107	1.5	MZ	275	Z801-16	Sub - IJ	MZ275 Z801-16 1.5mm Primecoat

**Table 19 - Sample Matrix High pH Investigation**

## 6.3 Passivation Systems

Okemcoat F1 NR6022 is the currently used chromate based passivation treatment used by TSSP-UK for their zinc coated products.

Henkel Passerite 5004 and 5010 are two chromate free passivation treatments currently in use by TSE in Ijmuiden, they are based on Ti, Mo, Mn phosphates and fluorides, with 5010 having the addition of a deep drawing assisting wax.

Coil Coating Technologies' Primecoat Z801-16 is currently in use by TSE in Ijmuiden.

## 6.4 Corrosion Test Results

TSE required a series of relatively quick corrosion tests to determine whether launching the MagiZinc® product would give any detrimental effects compared to the current market product of GI275, 275g/m<sup>2</sup>. SVET was requested to deliver the rapid investigation that the business demanded. The results presented here are the findings of the SVET study and the immersion mass loss analysis.

Figure 150 shows the overall conclusions of report detailing the mass losses from the 24 hours SVET study and the corresponding 3 days, and total 28 days of immersion mass loss. This graph shows that the selected choices of passivation treatment identified for the study have proven themselves to inhibit corrosive losses significantly better than those currently in use and those used in the sister plant in The Netherlands, within the conditions of this test regime. Both of the Henkel chemicals 5004 and 5010 show significantly better results than the standard chromate chemicals, at the coverage rate they were applied. TSE is recommended to work with Henkel the chemical manufacturer and supplier of the coated panels to broaden the scope of the investigation.

Figure 151 shows the SVET mass loss data. This graph shows a greater level of resolution than that possible in Figure 150 and it can be seen that in any 24 hour period the SVET determined mass losses do not exceed 1g/m<sup>2</sup>. Therefore the predicted minimum lifetime of the material in pH 12.7 solutions is an equivalent 70 days, before total metallic coating dissolution. This is longer than the specified cure time for the high strength cement material currently used in conjunction with TSE products.

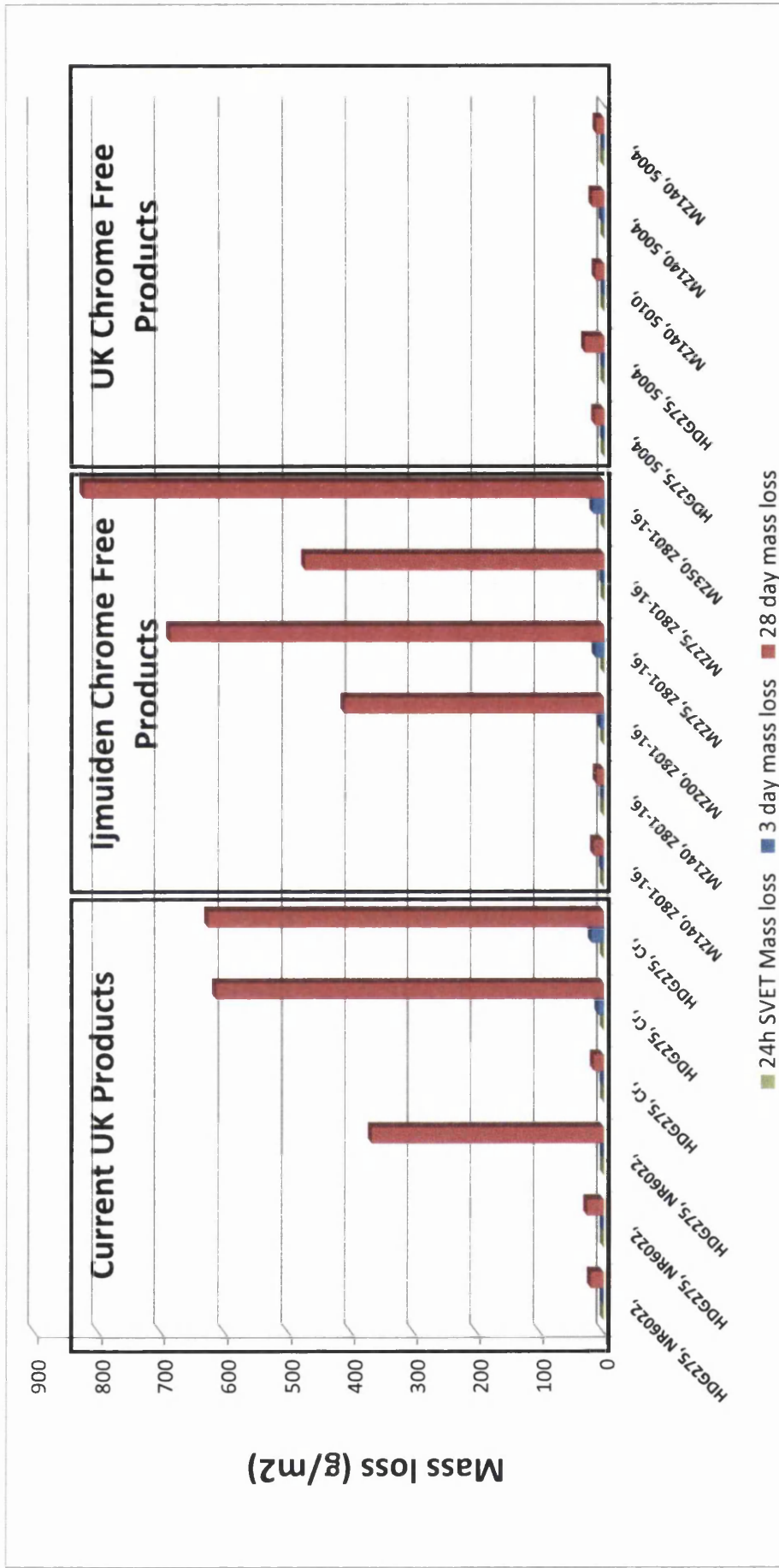


Figure 150 - Overall Comparison - Geographical Passivation Treatments

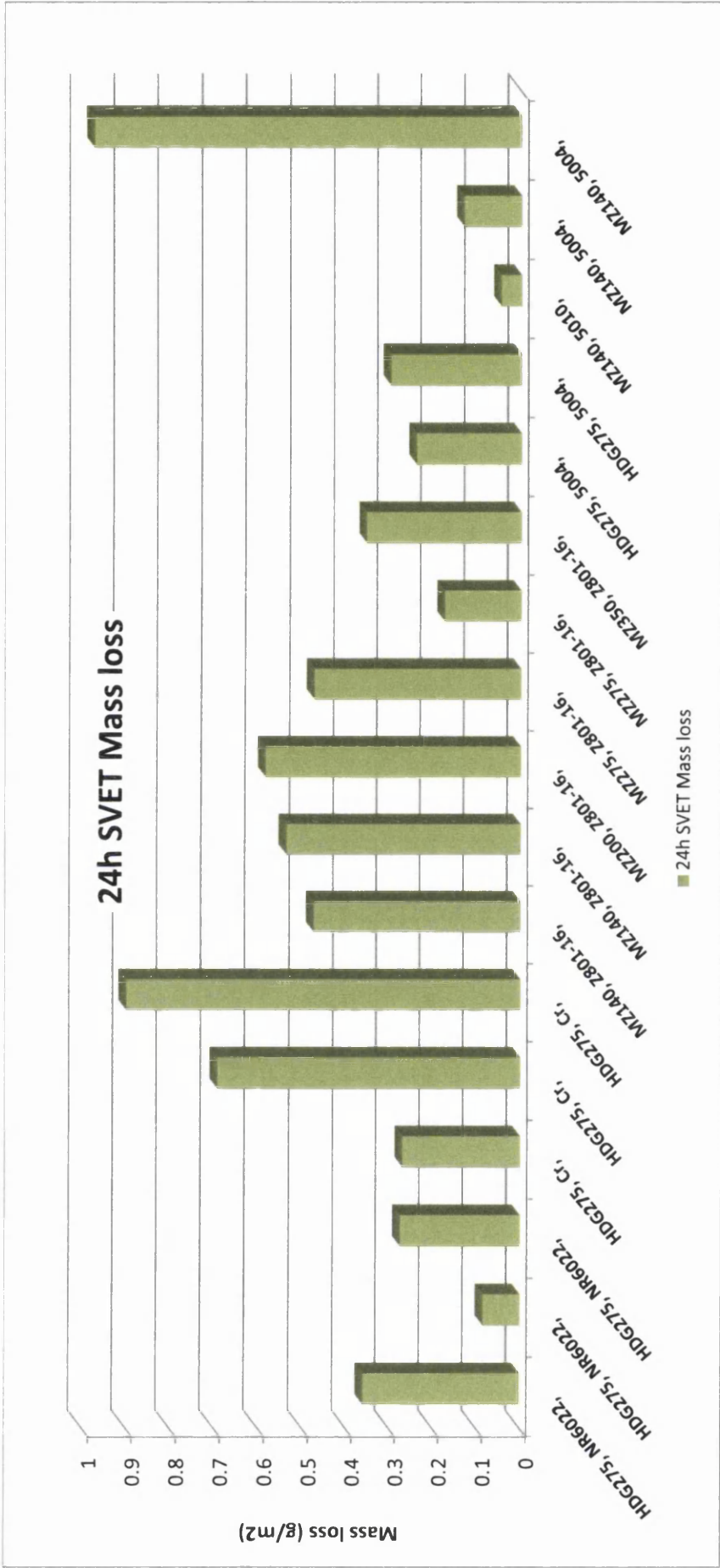


Figure 151 - 24 hours SVET Mass Loss Data – Arranged In Passivation Order

Figures Figure 152 to Figure 154 show the results of the ICP-OES analysis of the  $\text{Ca(OH)}_2$  solutions after immersion of the test samples for a period of 3 days and a further 25 days in fresh electrolyte. Total mass loss has been determined from the concentrations of magnesium, aluminium, zinc found in the electrolyte solutions. Figures Figure 153 and Figure 154, show the breakdown of the total immersion mass loss results into the elements contributing to the total mass loss.



### 3 & 28 Day Submerged Mass Loss Comparison

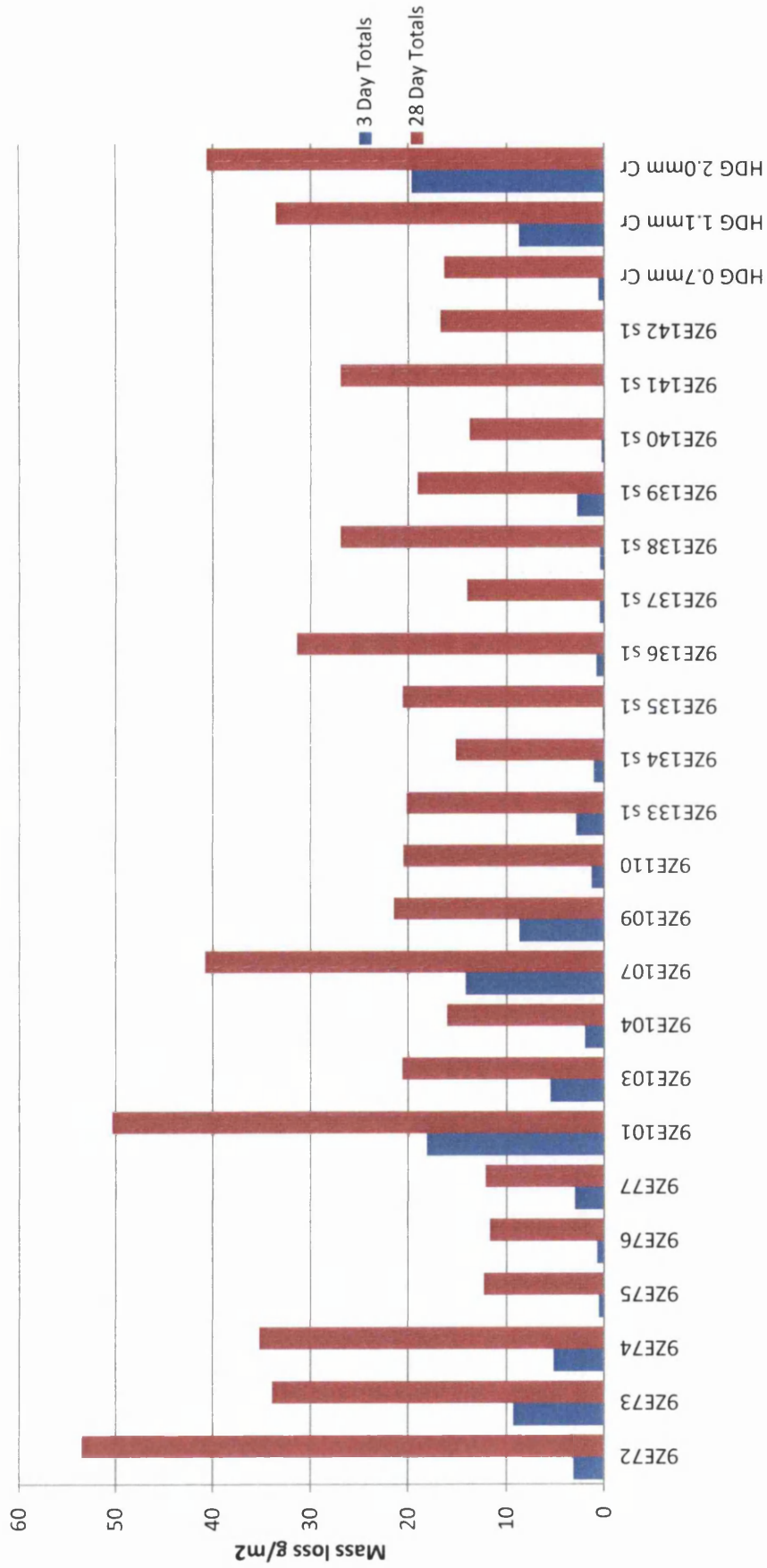


Figure 152 - Immersion Mass Loss Analysis

### 3 Day Mass Loss

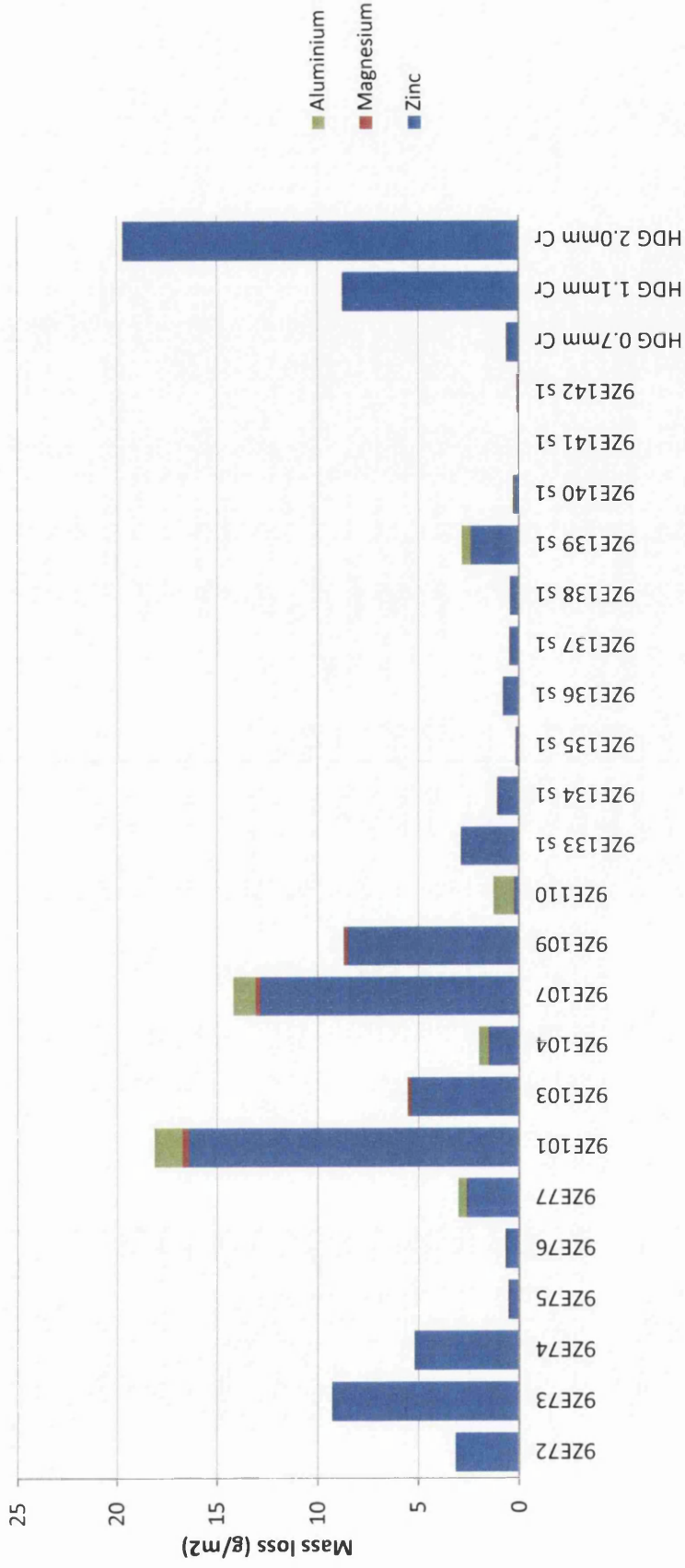


Figure 153 - Immersion Mass Loss Data - 3 Days Immersion

# 28 Day Mass Loss

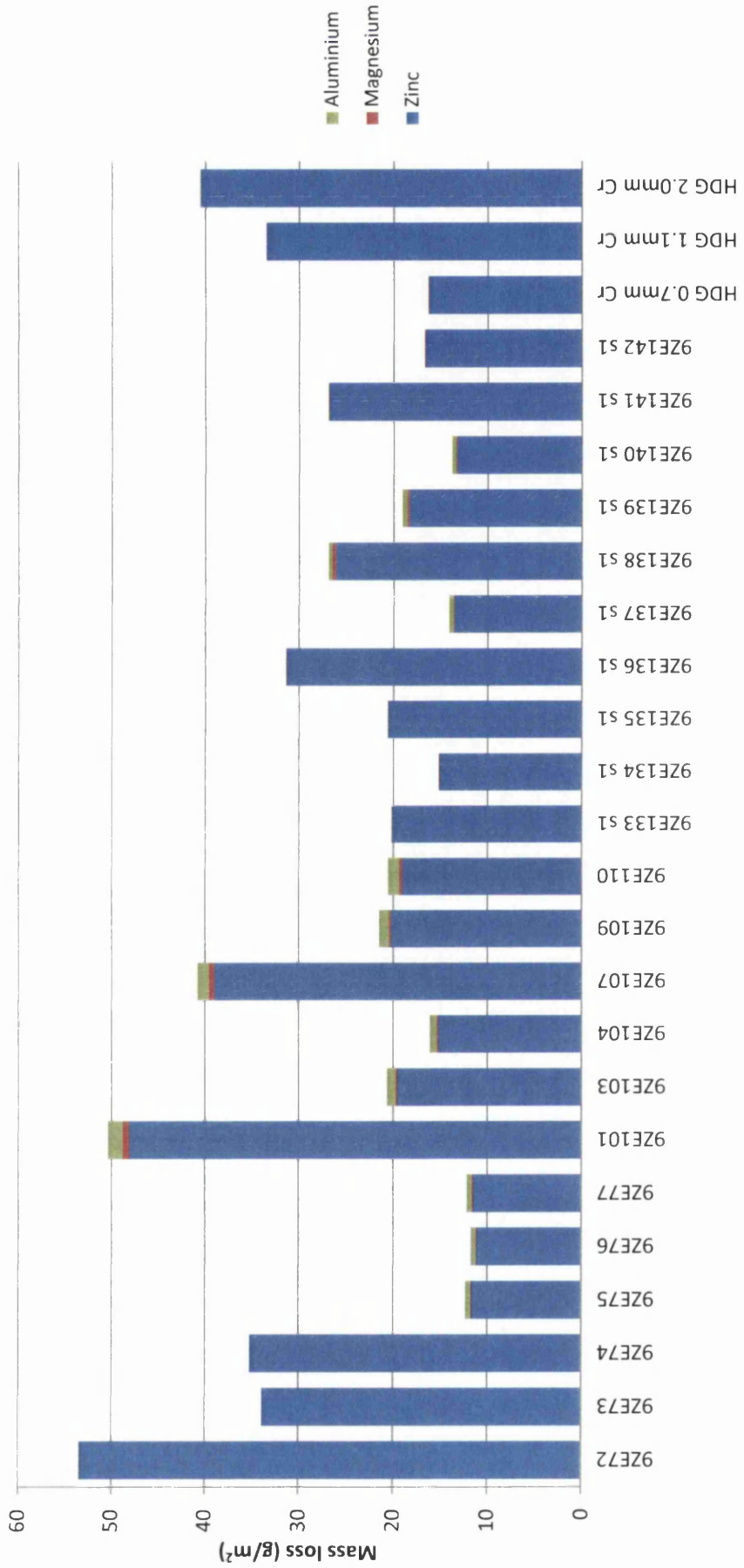


Figure 154 - Immersion Mass Loss Data - 28 Days Losses

Figure 155 shows the correlation of the SVET tests with the immersion mass loss tests and shows relatively good correlation considering the use of saturated calcium hydroxide solution within an SVET system had not been performed before, and was both technically challenging and an interesting health and safety concern.

Figure 156 is an analysis of the SVET data to show the split in the sample set between the two coating chemistries. It does show that there is a slight increase in the average losses from the MZ140 samples compared to the hot dip Zn-0.15wt%Al coating, though this is within the experimental error for the SVET equipment.

Figure 157 shows the residual anode analysis for the SVET scans of the data set and this shows that the overall level of intense anode activity (anodes over  $1 \text{ amp/m}^2$ ) was low.

Figure 158 shows the average anode intensity for any anodic areas over  $1 \text{ amp/m}^2$  was not altogether low, but the corresponding data in Figure 157 shows that for those anodes that were of an intense nature the length of activity was very short, <6 hours, though with the all corresponding low SVET mass loss data in Figure 6.4-b showing low levels of loss this is not considered detrimental to the integrity of the coating system.

# SVET - ICP-OES Comparison

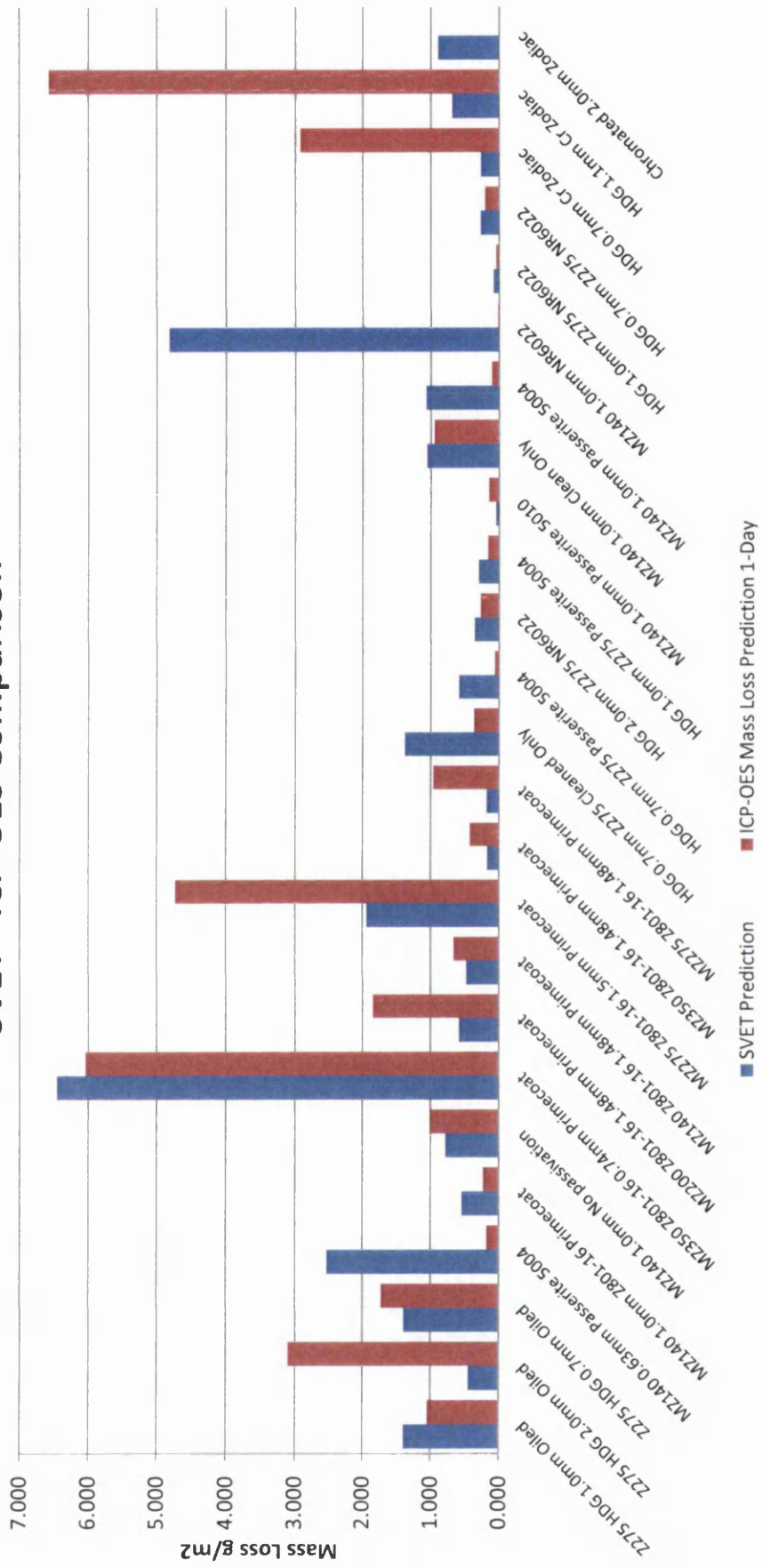


Figure 155 - Comparison of SVET Prediction to Immersion Mass Loss Data

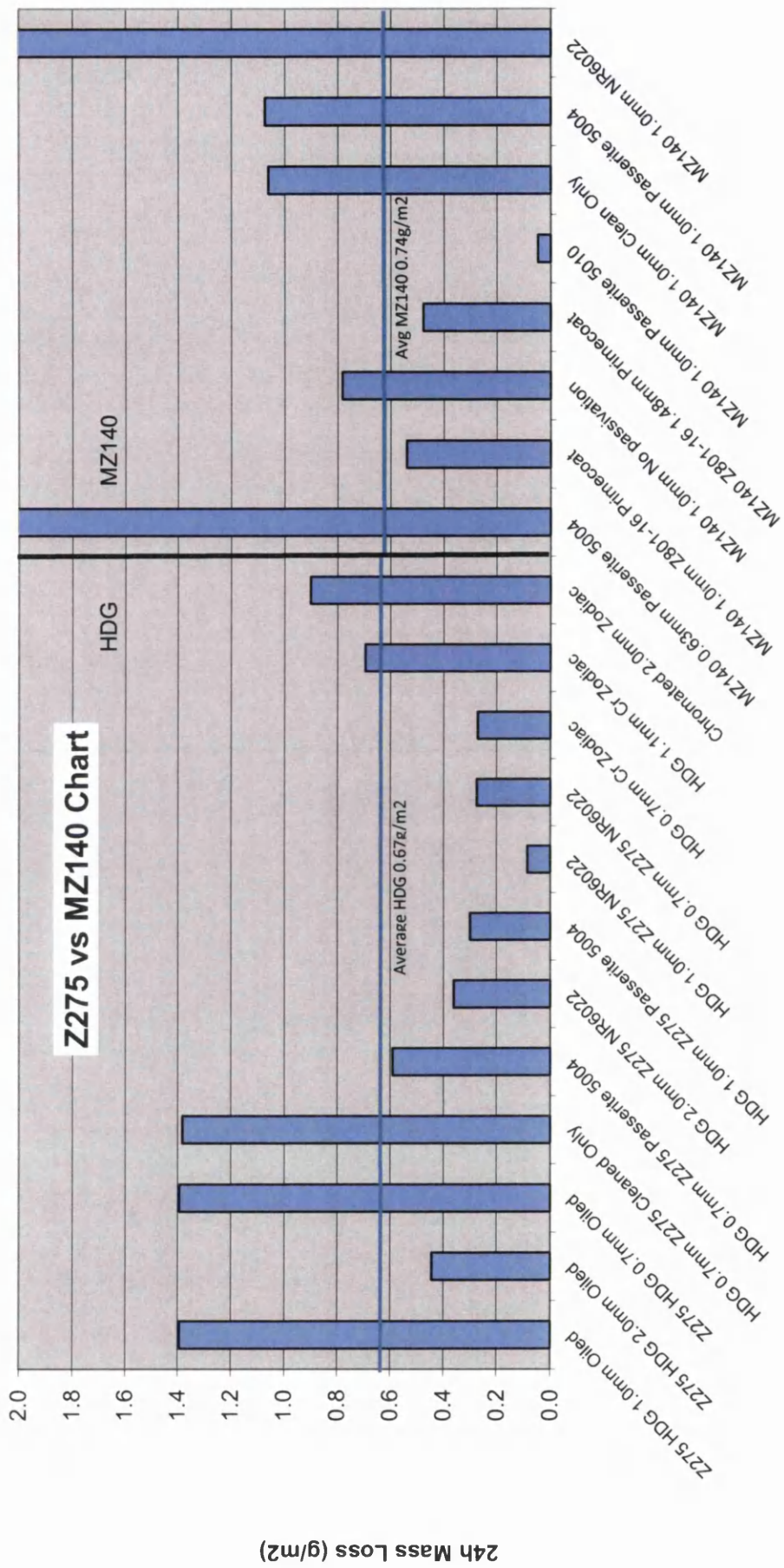


Figure 156 - SVET Data Comparison of HDG to MZ140

# Residual Anode Analysis

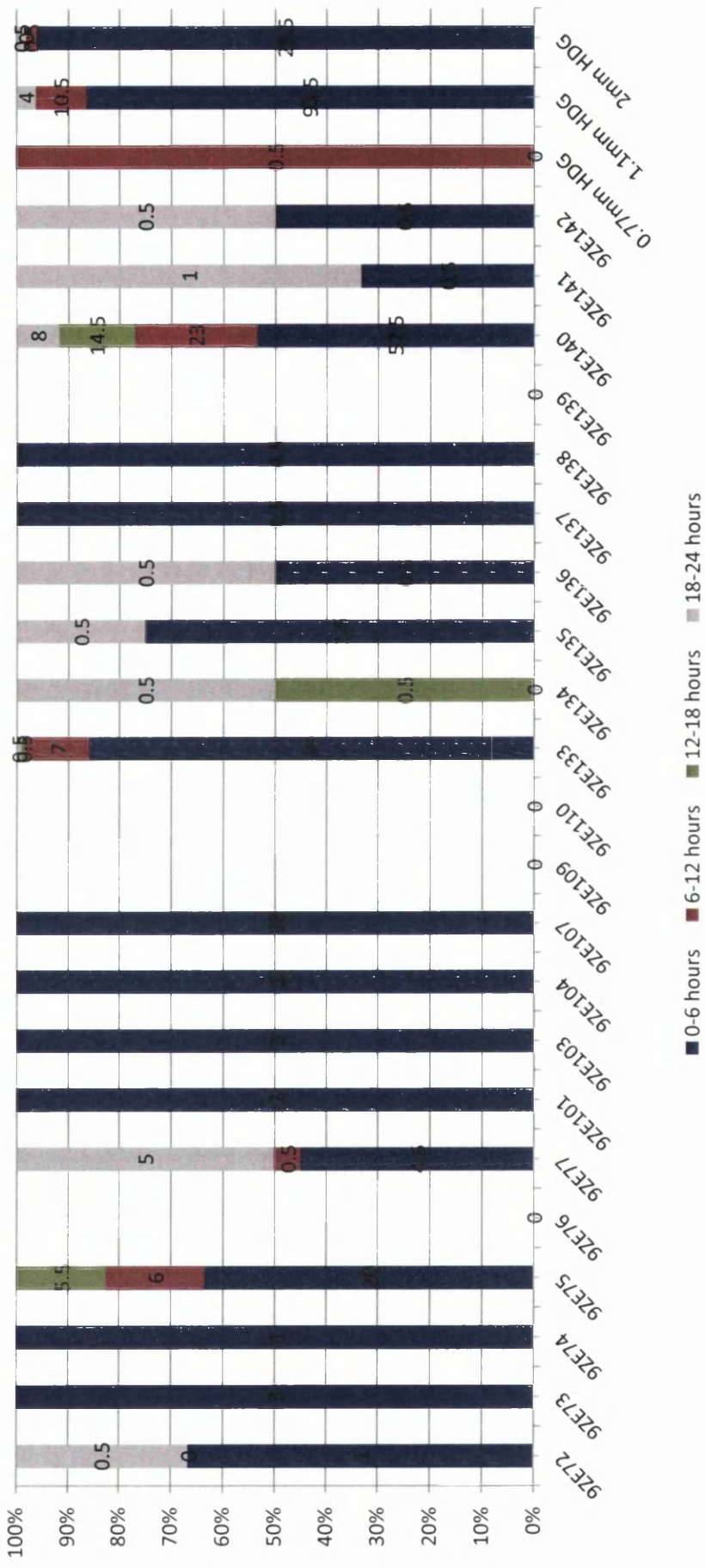
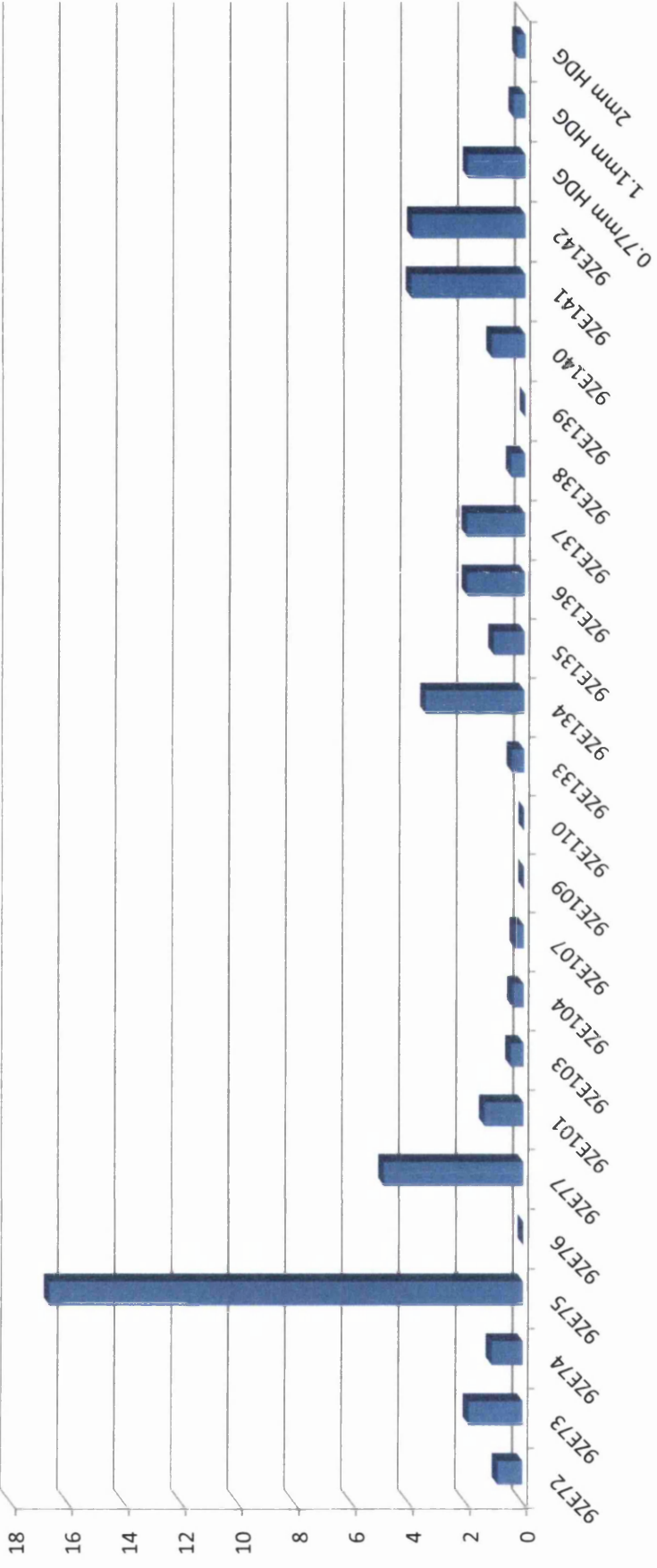


Figure 157 - Residual Anode Analysis

**Average anode intensity**  
**Anode Threshold 1amp/m<sup>2</sup>**



**Figure 158 - Average Anode Intensity**



## 6.5 Results and Discussion

These results have been broadcast to TSE Ltd. and show that the coatings, although active at the pH of the solution under test have returned mass loss results from SVET and from immersion mass loss that give a measure of reassurance that the coating weights will be satisfactory to protect the steel substrate, the engineering requirement for the product, though the length of the high pH environment.

TSE is now investigating the options that exist in the UK for the production of the newly developed ZAM coating. A team has been set up to study regulatory requirements like REACH that are driving forward the change to less potentially harmful chemical use. One of the initial areas of investigation is to understand the factors that affected Tata Steel's Ijmuiden plant in its introduction of non-chrome chemicals to the production route, and the effect that the customer saw in use. It is comforting to know that this brief study has enabled the potential removal of carcinogenic chemicals like hexavalent chromate away from people's working environments.

## **Chapter 7**

### **Discussion**

## 7.0 Discussion

Binary and ternary alloys continue to interest metallurgists and corrosion scientists and there are still many challenges as we strive towards the ultimate goal of efficiency, and conservation of resources. Questions like, what is the ideal mix of elements to make a super strong, super thin, super formable, super weldable steel, and how do we stop the environment undermining all our good work are questions that research strives to answer.

We have seen there are some indications of a move towards the latter with the results from the corrosion studies in this document. PVD continues to be an important technology that can generate the coatings of tomorrow. Using just two elements and a very new PVD technique that is still in development to this day we have seen results in accelerated corrosion tests of PVD coatings generated with just two selected elements that we can achieve results comparative to those of TSE's new automotive anti-corrosion coating, MagiZinc® with comparable coating thickness. If we can solve the engineering issues of production at speed and maintaining coating adhesion then the future is exciting for the coatings market.

From the analysis of the benchmark studies and the comparisons of the individual alloy chemistries or coating microstructures we can see that the alloy chemistries that have performed the best are the Zn-4.8wt%Al coatings from chapter 4, that outperform a thicker layer of Zn-0.15wt%Al at thinner gauges, i.e. more exposed cathodic area. The MGZ coatings MGZ19, MGZ20, MGZ41 and MGZ42 perform favourably compared to a thicker benchmark HDG sample. These four samples encapsulate the process conditions of two different alloy chemistries, therefore, Zn-(0.7-1)wt%Al-(0.1-0.5)wt%Mg may be a range of chemistries that can be used to provide a low alloyed alternative to hot dig galv, that can be processed at high and low undercooling conditions, and at approximately half the gauge of the GI275.

The results from the PVD samples show mixed results. In cut-edge corrosion testing in 0.1%NaCl, the samples composing a base layer of 4.25 $\mu$ m of PVD deposited zinc with 3 $\mu$ m of PVD deposited magnesium, annealed at a minimum temperature of 150°C for 300 seconds outperformed the benchmark Zn-0.15wt%Al sample. In the examination of surface corrosion the samples do not perform satisfactorily.

## **Chapter 8**

### **Conclusions**

## 8.0 Conclusions

The SVET test has proved itself to be a useful tool for the investigation of corrosion mechanisms and performance. Careful consideration should be made to how the immersion of test samples into electrolyte bears relevance to the corrosion mechanisms that materials exhibit in atmospheric exposure, or accelerated corrosion test cabinets.

Under development at Swansea is a flow cell that can refresh the electrolyte to avoid concentration effects, completely change the electrolyte for a different concentration, dope the electrolyte with inhibitors or remove the electrolyte from the test piece for a period of time so that factors such as humidity or dehydration can be investigated.

The comparative performance of the PVD materials in this research did not find a corresponding increase in corrosion resistance when tested under immersion conditions, for increasing Mg content. Salt spray testing has been seen to give a rapid increase in the performance of the PVD zinc coatings, and zinc coatings produced by conventional means (hot dipping and electro-galvanising) when Mg is deposited on the surface and diffusion annealed.

The PVD research is continuing within Tata Steel Europe and the quality of the samples under preparation are constantly improving. Factors such as formability are critical in the production of useable materials and the understanding of the parameters within the system employed in Tata Steel and their effect on the microstructure and mechanical properties of the formed coatings are becoming more understood. Since the production of the samples that were investigated with this piece of work the re-volatilisation of zinc onto the prepared strip, from the inner surfaces of the vacuum chamber, has been investigated, and solved. By lowering the average energy of the vapour species through earthing and subsequently eliminating any plasma this has the effect of increasing the vapour yield from reducing the amount of zinc that will re-evaporate from the coating.

The investigation of the variation in corrosion resistance of Galvalloy from changes in the microstructure, chapter 4, has shown that careful considerations should be given to the manufacturing process parameters for the whole product range. Larger, less numerous primary zinc dendrites have been shown to be detrimental to long term corrosion resistance through the increase in intensity of localised corrosion events extending to longer test lifetimes. Larger dendrites have been seen to develop through lowering of the degree of undercooling experienced by a coating from increase of the thermal mass of the steel substrate.

Chapter 5 demonstrated that significant changes in the microstructure can be expected with a change in alloying levels, for a consistent process condition. From the corrosion performance changes that have been defined through increases in dendrite volume and dendrite number in Galvalloy careful selection of the alloying levels of magnesium and aluminium will allow the generation of a finer microstructure, if the correct process parameters can be used.

We have seen from the initial study in chapter 6 that the change of passivation treatment chemical can have a great difference to the performance of the metallic coated steel system when exposed to elevated pH conditions. There appears to be little difference to the average corrosion resistance of the two metallic coating systems under investigation, 0.15%Al-Zn coating and the 1.6%-Mg-1.6%Al-Zn coating, MagiZinc.

## **Chapter 9**

### **Further Work**



## 9.0 Further work

### 9.1 ZnMg PVD

From the work presented in this study there is some interesting avenues of continued work in the study of PVD zinc and magnesium coatings. One coating has been identified that can give some useful benefits in corrosion resistance. It is worth identifying if annealing conditions exist that can achieve the same corrosion resistance and formability results but at lower annealing times, or higher annealing temperatures, or to determine processing conditions that can be used on a conventional coating line, if an EMELY type PVD coating installation becomes available as a retro-fit option. We have seen that there is a rapid increase in the hardness of the coatings with the formation of hard, brittle intermetallic species, and these may limit the use of any highly corrosion resistance coatings in the automotive market.

An interesting avenue for investigation would be to see if an element, or pre-treatment can be invented that can aid in the adhesion of the first atoms to hit the prepared strip surface, and to limit the diffusion of elements to the surface of the strip steel so that delamination is not promoted.

One of the opportunities that EMELY gives is the ability to co-deposit materials with a similar or usefully close vapour pressure at an isothermal temperature. The technology was not able to deliver samples of co-deposited zinc magnesium to check their corrosion performance in detail though they are expected to be similar to those of the fully inter-diffused PVD samples analysed. It would be worth investigating elements whose vapour pressure curves would allow for simultaneous deposition and properties that can offer an attractive market opportunity or technological advancement.

It is worth examining if the best of the PVD coatings prepared and examined in this project could be organically coated to determine their corrosion resistance as a finished

product. The rate of cathodic delamination is expected to reduce due to the presence of surface magnesium and basic magnesium oxides resisting the mechanism of cathodic delamination and the localised high pH created at the steel/coating interface.

### **9.1.1 MGZ development**

The results show, with some scatter, that there is a possible relationship between the alloying level of the coating chemistry and the expected mass loss during an SVET scan. Extending the sample set would hopefully reduce the scatter on this relationship and strengthen the model. This could be used to give an indication of the expected corrosion resistance from a quick production line check, within the confines of the processing conditions of the sample set. Extending the model to larger sample sets, incorporating different gauges and wider alloying ranges would be an inherent step towards achieving this.

### **9.1.2 High pH testing**

The investigation in a high pH environment should be continued for cross sectional analysis. Iron is certainly passive in this high pH environment so no additional incremental zinc mass loss rate would be expected for the exposure of the steel gauge but it is worth checking.

### **9.1.3 Residual anodes analysis**

Although full functional the programs are considered limited in its user interface plus the programs are also very inflexible in the analysis of data, in the respect of changes to scan variables.

Further work to the program can be considered to provide a 'Userform', a pop up window in which the number of scans could be selected, the threshold level, the location of data, and the common scan text. There can also be some development in the automatic data

analysis, some work has been carried out in the automatic analysis of data within the four 6 hour time slots that is usual for 24hour scans, though for total flexibility the user should be able to input the ranges required with the functionality that the scans interval is not always 1 hour. This does add some complexity to the program in that the scan time will need inputting to automatically calculate the scan where the requested time slots trip over.

Possible but difficult would also be the comparison between different scans. The initial step of automatically calculating the anode lifetimes within the requested time slots would pave the way for the programming of automatic comparison though this is considered likely to require a second program that would extract and analyse the residual anode output files.

Ultimately the algorithm and data analysis structure of the program should be written into the Logfile Processor currently used to calibrate and output useable data.

## References

- [1] J. Elvins, The relationship between the microstructure and corrosion resistance of galfan coated steels, in: Engineering Doctorate Center for Steel Technology, vol EngD, University of Wales, Swansea, Swansea, 2003.
- [2] D. J. Penney, The study of Galvalloy® coated steels using metallographic and scanning electrochemical techniques, in: Materials Research Centre, vol EngD, Swansea University, 2006.
- [3] F. Thebault, B. Vuillemin, R. Oltra, K. Ogle, C. Allely, *Electrochimica Acta* 53 (2008) 5226-5234.
- [4] Corus, Colorcoat HPS200®, 26th February 2007
- [5] Corus, Aludip (Hot-dip aluminium-silicon alloy coated steel), 12th July 2007
- [6] P. Jones, Corus Colors Information, in: Corus Ltd., 2007.
- [7] C. Ltd., Colorcoat HPS200®, in: 2004, p. 10.
- [8] S. Böhm, M. Challis, T. Heatley, D. A. Worsley, An Investigation of the Effects of Mg Levels on the Kinetics and Mechanisms of Cut-Edge Corrosion in Organically Coated Zinc Aluminium Alloy Galvanised Steels, in: Department of Materials Engineering, Swansea University, 2001.
- [9] J. Elvins, J. A. Spittle, D. A. Worsley, *Corrosion Science* 47 (2005) 2740-2759.
- [10] Corus-Posco, Zn-Mg Evaluation.pdf, in: 2006, p. 40.
- [11] S. R. Jones, Port Talbot: A Brief History, 5.1.2011,
- [12] C. S. P. UK, MagiZinc business case, in: 2010, p. 30.
- [13] K. Tinkham, Accelerated Corrosion Testing of MagiZinc in contact with Concrete and Plaster, in: Rotherham, 2010.
- [14] [www.kitco.com](http://www.kitco.com), 5 Year Zinc Spot Price, in: 5year\_zinc\_chart\_spot\_price.gif (Ed.) [www.phantasmix.com](http://www.phantasmix.com), 2011.
- [15] p. Ltd., Product health and safety data sheet 18, in: 2007, p. 3.
- [16] C. CSP-UK, Protected with strength - Solutions in Galvalite hot-dip galvanised steel, in: 2004.
- [17] A. Belghazi, S. Bohm, J. H. Sullivan, D. A. Worsley, *Corrosion Science* 44 (2002) 1639-1653.
- [18] M. Yaseen, H. E. Ashton, *Journal of Coatings Technology* 50 (1978) 50-59.
- [19] G. Fourlaris, Stainless Steels, in: Materials Research Centre, Swansea University, 2006.
- [20] P. Evans, Introduction to Steel Metallurgy, in: Tata Steel Europe Ltd., 2011.
- [21] E. Mattsson, Basic Corrosion Technology for Scientists and Engineers, The Institute of Materials, London, 1996, p. 204.
- [22] J. Elvins, The Relationship between the microstructure and corrosion resistance of galfan coated steels, in: Materials Research Center, vol EngD, Swansea University, Swansea, 2005, p. 141.
- [23] [www.tpub.com](http://www.tpub.com), Galvanic corrosion, in: g. corrosion.jpg (Ed.) 2011.
- [24] ASM International, ASM Handbook on DVD, in: M. I. Marek (Ed.) Fundamentals of Corrosion, vol 13, ASM International and The Dialog Corporation, 1999.
- [25] J. Tafel, *Z. Physik. Chem.* 50 (1905) 641.
- [26] D. Williams, Mechanistic Corrosion Studies in Organically Coated Galvanised Steels, in: Materials Engineering, vol EngD, University of Wales, Swansea, 2003, p. 240.
- [27] Wikipedia, Faraday's law of electrolysis, 19th April 2007,
- [28] N. D. Tomoshev, Theory of corrosion and protection in metals, Macmillan Company, New York Collier-Macmillan Limited, London, Moscow, 1966, p. 672.
- [29] C. Doctors, Poulitce Corrosion,
- [30] K. Bevan, F. H. Blekkenhorst, H. B. van Veldhuizen, Corrosion, corrosion mechanisms and durability of cladding materials for exterior applications, in: Corus RD&T, IJmuiden, 2003, p. 45.
- [31] C. doctors, Pitting Corrosion, 5 March 2007,
- [32] C. Evans, An Anecdotal History of the Galvanizing Industry, in: American Galvanizers Association, 1992, p. 12.
- [33] C. Doctors, Luigi Galvani (1737-1798), 3.2.2011,
- [34] F. Zhu, D. Persson, D. Thierry, *Corrosion* 57 (2000) 582-591.
- [35] A. K. Singh, G. Jha, S. Chakrabarti, Spangle formation on hot-dip galvanised steel sheet and its effects on corrosion-resistant properties, in: *Corrosion*, vol 59, 2003, pp. 189-197.
- [36] J. Elvins, J. A. Spittle, J. H. Sullivan, D. A. Worsley, *Corrosion Science* 50 (2008) 1650-1658.
- [37] N. C. Barnard, S. G. R. Brown, *Corrosion Science* 50 (2008) 2846-2857.
- [38] D. J. Penney, J. H. Sullivan, D. A. Worsley, *Corrosion Science* 49 (2007) 1321-1339.
- [39] T. Prosek, N. Larche, M. Vlot, F. Goodwin, D. Thierry, *Materials and Corrosion* 61 (2010) 412-421.

- [40] M. Dutta, A. K. Halder, S. B. Singh, *Surface and Coatings Technology* 205 (2010) 2578-2584.
- [41] R. Hausbrand, M. Stratmann, M. Rohwerder, *Corrosion Science* 51 (2009) 2107-2114.
- [42] K. Honda, H. Hatenaoka, H. Onozawa, Highly corrosion-resistant hot-dip galvanised steel product excellent in surface smoothness and formability and process for producing same, in: U. States (Ed.) Nippon Steel Corporation, United States, 2008, p. 13.
- [43] M. Vlot, M. Zuijderwijk, M. Toose, L. Elliott, R. Bleeker, T. Maalman, Hot dip ZnAlMg coatings, Microstructure and forming Properties, in: Corus RD&T, p. 6.
- [44] Corus, Magizinc Business Case, 23rd July 2010,
- [45] Corus, A UK appraisal of MagiZinc coated and painted products, 9th October 2009,
- [46] J. Hayden, Accelerated corrosion performance of Galfan, Galvalume and Hot Dip Galv, in: Corus RD&T, Rotherham, 2004, p. 5.
- [47] <http://www.corrosion-doctors.org/Definitions/Galvanizing.htm>, Galvanneal photomicrograph, 3 May 2007,
- [48] J. A. Spittle, *Materials Science and Technology* 11 (1977) 578-585.
- [49] F. Hinterberger, W. Maschek, J. Faderl, Influence of typical process parameters on the microstructure of galfan coatings, in: *Zinc-based Steel Coating Systems: Production and Performance*, vol The Minerals, Metals & Materials Society, 1998, 1998, pp. 281-292.
- [50] M. Zapponi, A. Quiroga, T. Perez, *Surface and Coatings Technology* 122 (1999) 18-20.
- [51] B. E. Sundquist, L. F. Mondolfo, *Trans A.I.M.E.* 221 (1961) 157.
- [52] B. Schuhmacher, C. Schwerdt, U. Seyfert, O. Zimmer, *Surface and Coatings Technology* 163-164 (2003) 703-709.
- [53] M. vlot, Product Development Plan ZnMg for Automotive, in: Corus RD&T, 2008, p. 6.
- [54] M. Goodenough, PVD Review Dec 2007, in: P. Team (Ed.) 2007.
- [55] M. Goodenough, PVD Team Meeting, in: P. Team (Ed.) IJmuiden, 2007.
- [56] A. Roberts, PVD Business Case and Line Loading - CSP-UK, in: P. R. Meeting (Ed.) Shotton, 2007.
- [57] C. Metzner, K. Goedicke, G. Hoetzsch, B. Scheffel, J.-P. Heinss, *Surface and Coatings Technology* 94-95 (1997) 663-668.
- [58] C. A. Weirman, Literature Review, in: Materials Research Department, 2007, p. 111.
- [59] L. Baptiste, N. v. Landschoot, G. Gleijm, J. S. v. Westrum, H. Velthuis, T.-Y. Kim, *Surface and Coatings Technology* 2007 (2007).
- [60] B. Schmitz, R. Colin, M. Economopoulos, "'Jet Vapor Deposition", a novel vacuum coating technique with superior properties', in: 1999.
- [61] B. Schmitz, *Steel Research* 72 (2001) 1-8.
- [62] D. M. Mattox, *Handbook of Physical Vapor Deposition (PVD) Processing: Film Formation, Adhesion, Surface Preparation and Contamination Control*, William Andrew, New York, 1998, p. 949.
- [63] L. Baptiste, LB Presentation in project meeting 18122007, in: P. E.-P. Team (Ed.) Corus, Gwangyang, Korea, 2007.
- [64] D. T. Hellman, Physical Vapor Deposition - Is it real, or is it PVD?, in: *Metal Finishing*, Colorado, pp. 50-55.
- [65] Y. Bohne, D. Manova, C. Blawert, M. Störmer, W. Dietzel, S. Mändl, *Nuclear Instruments and Methods in Physics Research Section B: Beam Interactions with Materials and Atoms* 257 (2007) 392-396.
- [66] S. Smith, Summary of resistance spot welding research on Corus Magizinc coating system, in: Corus RD&T, 2007, p. 38.
- [67] J. Hayden, S. Bohm, Magizinc coated with HPS200 Durability and adhesion, in: 2006.
- [68] T. Prosek, A. Nazurov, U. Bexell, D. Thierry, J. Serak, *Corrosion Science* 50 (2008) 2216-2231.
- [69] M. Morishita, K. Koyama, M. Murase, Y. Mori, *ISIJ International* 36 (1996) 714-719.
- [70] H. C. Hosking, M. A. Ström, P. H. Shipway, C. D. Rudd, *Corrosion Science* 49 (2007) 3669-3695.
- [71] K. Aragu, H. Shige, M. Iwai, T. Watase, Y. Kitou, Zn-Mg electroplated metal sheet and fabrication process thereof, in: U. S. Patent (Ed.) Kobe Steel Ltd. kobe, japan, United States, 2003, p. 16.
- [72] K. Shimogori, H. Satoh, M. Toyama, H. Shimoto, K. Ikeda, J. Kawahuku, S. Miyake, S. Nomura, H. Sakai, Zn-Mg alloy vapor deposition plated metals of high corrosion resistance, as well as method of producing them, in: U. S. Patent (Ed.) Kabushike Kaisha Kobe Seiko Sho, Kobe, Japan, 1991, p. 47.
- [73] Y. Fukui, M. Matsuno, H. Tanaka, T. Miono, K. Sakamoto, Y. Ariyoshi, M. Saito, Steel sheet coated with Zn-Mg binary coating layer excellent in corrosion resistance and manufacturing method thereof, in: U. S. Patent (Ed.) Nisshin Steel Co. Ltd., Tokyo, Japan, 1998, p. 19.
- [74] M. Morishita, K. Koyama, Y. Mori, *ISIJ International* 37 (1997) 55-58.

- [75] M. Morishita, K. Koyama, Y. Mori, *Materials Transactions* 38 (1997) 719-723.
- [76] P. Volovitch, C. Allely, K. Ogle, *Corrosion Science* 51 (2009) 1251-1262.
- [77] H. S. Isaacs, B. Vyas, *Electrochemical Corrosion Testing ASTM STP 727* (1981) 3-33.
- [78] A. M. P. Simoes, R. O. Carbonari, A. R. Di Sarli, B. del Amo, R. Romagnoli, *Corrosion Science* 53 (2010) 464-472.
- [79] R. M. Souto, Y. Gonzalez-Garcia, S. Gonzalez, *Corrosion Science* 50 (2007) 1637-1643.
- [80] J. H. Sullivan, H. N. McMurray, D. J. Penney, D. A. Worsley, Detection of current from a model pit using the scanning vibrating electrode technique (SVET), in: *Materials research centre, University of Wales Swansea, Swansea.*
- [81] H. S. Isaacs, M. P. Ryan, L. J. Oblonsky, *Mapping Currents at the Corroding Surface/Solution Interface*, in: *Brookhaven National Laboratory, Upton, New York, 1997, p. 17.*
- [82] H. N. McMurray, J. R. Searle, B. P. Wilson, The use of SVET for investigating changes in the corrosion mechanism induced by forming galvanised steel samples, in: *Engineering Doctorate Centre for Steel Technology, University of Wales, Swansea, Swansea, p. 9.*
- [83] H. N. McMurray, J. R. Searle, B. P. Wilson, The use of SVET for investigating changes in the corrosion mechanism induced by forming galvanised steel samples, in: *Eurocorr, Engineering Doctorate Centre for Steel Technology, University of Wales, Swansea, Queen Mary and Westfield College, London, 2000, p. 9.*
- [84] nrich.maths.org, The Wheatstone Bridge, in: *wheatstone.jpg (Ed.) 2011, p. Schematic of the Wheatstone Bridge.*
- [85] G. R. Holcomb, S. J. Bullard, B. S. J. Covino, S. D. Cramer, C. B. Cryer, G. E. McGill, *Electrochemical Aging of Thermal-Sprayed Zinc Anodes on Concrete*, in: *O. U. Albany Research Centre (Ed.) ASM International, 1996.*
- [86] G. Williams, H. N. McMurray, R. Grace, *Electrochimica Acta* 55 (2010) 7824-7833.
- [87] C. Doctors, *The Salt Spray Test*, 30th October 2007,
- [88] E. Belin-Ferre, *Surface Properties and Engineering of Complex Intermetallics*, *World Scientific Publishing Co., Singapore, 2010, p. 399.*
- [89] R. F. Bunshah, *Handbook of deposition technologies for films and coatings; Science, Technology and Applications*, in: *Noyes, New Jersey, Los Angeles, 1994, pp. 412-416.*
- [90] J. F. Shackelford, *Introduction to materials science for engineers*, *Macmillan Publishing Company, New York, 1992, p. 793.*
- [91] ScienceLab.com, *Material Safety Data Sheet Chromic Acid, 10% MSDS*, in: *Houston, 2010, p. 6.*
- [92] K. Bevan, *Zinc aluminium alloy batch galvanising of sheet steel assemblies*, in: *vol MRes, Swansea University, Swansea, 2008.*
- [93] R. Thomas, *Practical Guide to ICP-MS*, *Marcel Decker, New York, 2004, p. 309.*
- [94] L. Baptiste, *Extract from EML-PVD Surface Technology Conference Presentation - 01062006*, in: *2006.*
- [95] Posco, *Properties of Zn-Mg coatings*, in: *Gwangyang, Korea, 2006, p. Presentation.*
- [96] D. S. Rickerby, A. Matthews, *Advanced Surface Coatings: a Handbook of Surface Engineering*, *Chapman and Hall, New York, 1991, p. 368.*
- [97] K. L. Choy, *Progress in Materials Science* 48 (2003) 57-170.
- [98] Z. B. Zhao, B. A. Gillispie, J. R. Smith, *Surface and Coatings Technology* 200 (2006) 4746-4754.
- [99] I. L. Z. R. Organisation, *Continuous Hot-Dip Galvanising versus General (Batch) Galvanising*, 6th March 2011
- [100] H. O. Pierson, *Handbook of Chemical Vapour Deposition (CVD)*, *Noyes, New Jersey, 1992.*
- [101] M. Vlot, *Zn coatings by PVD on Emely: first coating weight series (1-8.5um)*, in: *Corus RD&T, IJmuiden, 2008, p. 32.*
- [102] M. Jonsson, D. Persson, D. Thierry, *Corrosion Science* 49 (2007) 1540-1558.
- [103] F. Goodwin, *Galfan Galvanising Alloy Technology ILZRO* (1984).
- [104] A. R. Marder, *Progress in Materials Science* 45 (2000) 191-271.
- [105] H. Dafydd, D. A. Worsley, H. N. McMurray, *Corrosion Science* 47 (2005) 3006-3018.
- [106] I. Suzuki, *Corrosion Resistant Coatings Technology*, *Marcel Dekker Publications, Monticello, NY., 1989.*
- [107] D. A. Worsley, H. N. McMurray, J. H. Sullivan, I. P. Williams, *Corrosion* 60 (2004) 437-448.
- [108] A. Bonnel, F. Dabosi, C. Delouis, M. Dupart, M. Kedam, B. Tribollet, *Journal of the Electrochemical Society* 130 (1983) 753-761.
- [109] P. A. Porot, N. Venham, R. D. Jones, J. A. Spittle, *Metallography* 20 (1987) 181-197.

- [110] D. A. Porter, K. E. Easterling, *Phase Transformations in Metals and Alloys*, Chapman and Hall, 2000.
- [111] M. J. Pryor, D. S. Keir, *Journal of the Electrochemical Society* 104 (1957) 269-275.
- [112] W. G. Whitman, R. P. Russell, *Industrial Engineering Chemistry* 16 (1924) 276-279.
- [113] Corus, Confidex®, 3rd February 2007
- [114] T. Prosek, A. Nazarov, D. Thierry, Role of magnesium in corrosion performance of Zn-Mg and Zn-Al-Mg alloy coatings in atmospheric conditions, in: *French Corrosion Institute*, p. 1.
- [115] A. P. Yadav, H. Katayama, K. Noda, H. Masuda, A. Nishikata, T. Tsuru, *Electrochimica Acta* 52 (2007) 2411-2422.
- [116] C. S. P. IJmuiden, Corus in IJmuiden launches MagiZinc: the next step in metallic coating, 23.6.2009
- [117] F. Mengueli, M. Zijderwijk, MagiZinc AHSS - 1st DVL2 Trial, in: *Tata Steel Europe RD&T, IJmuiden*, 2010, p. 21.
- [118] J. H. Sullivan, S. Mehraban, J. Elvins, In situ monitoring of the microstructural corrosion mechanisms of zinc-magnesium-aluminium alloys using time lapse microscopy, in: *Materials Research Centre, Swansea University, Swansea*, 2010, p. 25.
- [119] J. H. Sullivan, C. A. Weirman, J. Kennedy, D. J. Penney, *Corrosion Science* 52 (2010) 1853-1862.
- [120] [www.scienceinformer.com](http://www.scienceinformer.com), Zinc, 14th March 2011,
- [121] H. S. Executive, REACH Explained, 14th March 2011,
- [122] V. Rasanen, V. Penttala, *Cement and Concrete Research* 34 (2004) 813-820.
- [123] D. Shi-Gang, L. Chang-Jian, H. Rong-Gang, L. Lan-Qiang, D. Rong-Gui, *Electrochimica Acta* (2010) doi: 10.1016/j.electacta.2010.1008.1089.
- [124] T. Harrison, *The new concrete standards - getting started*, The Concrete Society, 2003, p. 20.
- [125] P. M. Lewis, O. Ennis, A. Kashif, W. A. Dickson, *International Journal of the Care of the Injured* 35 (2004) 982-985.
- [126] U. o. Cambridge, *Recycling of Metals*,
- [127] B. A. Shaw, *ASM International 13A - Corrosion* (2003) 692-697.
- [128] T. Prosek, D. Thierry, C. Taxen, J. Maixner, *Corrosion Science* 49 (2007) 2676-2693.

## **Appendix A – Residual Anode Programs**



## Residuals for SVET

Tedious but quite useful!!

- 1; Separate your calib grd files and srf maps into a new directory if you have not already done so (for a set of say 24 hours worth of scans)
- 2; Load up the first surfer map and set the colours to give you nice clear black anodes!
- 3; With the map highlighted go to the 'Map' tab and click 'digitise'
- 4; Move the cursor to the first anode you see and click; a red cross will appear on top of the anode and a new box will appear recording the X and Y position of that anode. Click on all the anodes you can see. When you are done mark them all with an easy wipe removable pen.
- 5; Save the .bln file with an appropriate name ('balls.bln' as an e.g.)
- 6; Click on the map and go to the 'Edit' tab and click on 'Properties'
- 7; In the general tab and under the input grid file information (there is a little folder shown) click on the folder and then select the second scan you are interested in.
- 8; You may need to adjust the scale on z to give nice clear black anodes.
- 9; Repeat step 3; this time though only digitise new anodes you have not identified before. Again mark them. You can now copy the new X and Y positions of the new anodes into 'balls.bln' from 5 above.
- 10; Save 'balls.bln' again (keeping the same name)
- 11; Repeat steps 6-10 for all 24 maps saving the edited 'balls.bln' each time.
- 12; When all is done and you have identified the X and Y positions of all active anodes firstly clean the screen on your PC! Then open up 'balls.bln' and in column C add zeros against all X and Y positions. Save the file AGAIN!
- 13; Under the 'Grid' tab click 'Residuals'. Double click on the grid file for the first scan. Then select the 'balls.bln' file. The residuals will then appear in column D
- 14; SAVE THE 'BALLS.BLN' FILE!!!!
- 15; Repeat 12-14 for all of the scans in your run saving the 'balls.bln' file at each stage.
- 16; When completed you can then save the final version of your 'balls.bln' file. Then save it in an xls format to open it in Excel.
- 17; Open in Excel. Firstly multiply all the data by minus one (so anodes appear positive) and then for clarity convert any negative numbers you have on the sheet to zeroes. You can now replace the zeros in column C with numbers for each anode.
- 18; Finally you can print the ribbon plot and then check into rehab. (make sure the ribbon comes out correctly with the anode number and time on X and Y and the current density on Z). There is quite a bit of analysis also possible more on which later!

## Residual Anodes program – Microsoft Excel 2003 Version (24 Scans)

```
Option Explicit

Sub import_files_into_workbook()
Attribute import_files_into_workbook.VB_ProcData.VB_Invoke_Func = " \n14"
'
' import_file_into_workbook Macro
'
Dim myfile As String
Dim mypath As String
Dim this_file As String
Dim target_file As String
Dim f As Integer
Dim scan_data As Variant
this_file = ActiveSheet.Name
mypath = ActiveWorkbook.Path & "\"
For f = 1 To 25
    If f <= 10 Then
        myfile = "text;" & mypath & this_file & "00" & (f - 1) & "calib.grd"
        target_file = this_file & "00" & (f - 1) & "calib"
    End If
    If f > 10 Then
        myfile = "text;" & mypath & this_file & "0" & (f - 1) & "calib.grd"
        target_file = this_file & "0" & (f - 1) & "calib"
    End If
'
ActiveSheet.Worksheets.Add
With ActiveSheet.QueryTables.Add(Connection:= _
    myfile _
    , Destination:=Range("$B$1"))
    .Name = target_file
    .FieldNames = True
    .RowNumbers = False
    .FillAdjacentFormulas = False
    .PreserveFormatting = True
```

```

.RefreshOnFileOpen = False
.RefreshStyle = xlInsertDeleteCells
.SavePassword = False
.SaveData = True
.AdjustColumnWidth = True
.RefreshPeriod = 0
.TextFilePromptOnRefresh = False
.TextFilePlatform = 850
.TextFileStartRow = 1
.TextFileParseType = xlDelimited
.TextFileTextQualifier = xlTextQualifierDoubleQuote
.TextFileConsecutiveDelimiter = True
.TextFileTabDelimiter = False
.TextFileSemicolonDelimiter = False
.TextFileCommaDelimiter = False
.TextFileSpaceDelimiter = True
.TextFileColumnDataTypes = Array(1, 1)
.TextFileTrailingMinusNumbers = True
.Refresh BackgroundQuery:=False

```

End With

Sheets.Select

Sheets(f).Move after:=Sheets(f + 1)

'Column("b:b").Select

Selection.Insert Shift:=xlToRight, CopyOrigin:=xlFormatFromLeftOrAbove

ActiveSheet.Name = target\_file

'select range of cells

'If f = 1 Then

'Set scan\_data = Application.InputBox("Please select cell range", "Cell Range Selection", "B6:AT91", , , , 8)

'last\_cell = Range.Find(8, "b{");

'End If

Next f

Dim c As Range

Dim i As Long

Dim shtcnt As Long

Dim column As Integer

```

Dim s As Variant

Dim anodecount As Integer

column = 0

anodecount = 1

Dim threshold_value As Single

Dim current_anode As Integer

Dim anode_done As Integer

If MsgBox("Residuals threshold value set to 1. Do you want to change this?", vbYesNo +
vbDefaultButton2, "Threshold Value OK?") = vbYes Then

    threshold_value = Application.InputBox("Please input new threshold value", "Threshold Value
Input", 1, , , , 1)

Else: threshold_value = 1

End If

For Each s In ActiveWorkbook.Sheets

Dim current_anode_range As Range

Dim current_anode_location As String

Dim cc As Range

        Worksheets(this_file).Cells(10, 1) = "Anode Number"

        Worksheets(this_file).Cells(10, 2) = "Initial Row"

        Worksheets(this_file).Cells(10, 3) = "Initial Column"

        Worksheets(this_file).Cells(10, 4) = "Initial Location"

        Worksheets(this_file).Cells(10, 5) = "Final Row"

        Worksheets(this_file).Cells(10, 6) = "Final Column"

        Worksheets(this_file).Cells(10, 7) = "Final Location"

s.Activate

    'If column = 1 Then

        '        scan_data = Application.InputBox("Please select cell range", "Cell Range Selection",
"b6:AT91", , , , , 8)

        'End If

If s.Name <> this_file Then

    i = 10

    Worksheets(this_file).Cells(i, column + 7) = ActiveSheet.Name

    i = i + 1

' Change the first value in the line below "0.value > 1". This will select threshold values of
whatever amps you require.

For Each c In Worksheets(s.Name).Range("b6:bz200")

```

```

If c.Value > threshold_value And c.Value > c.Offset(-1, -1).Value And c.Value > c.Offset(-1,
0).Value And c.Value > c.Offset(-1, 1).Value And c.Value > c.Offset(0, -1).Value And c.Value >
c.Offset(0, 1).Value And c.Value > c.Offset(1, -1).Value And c.Value > c.Offset(1, 0).Value And
c.Value >= c.Offset(1, 1).Value Then

```

```

    anode_done = 0

```

```

    With c.Interior

```

```

        .ColorIndex = 6

```

```

        .Pattern = xlSolid

```

```

    End With

```

```

    'current_anode_range = "c11:c" & anodecount

```

```

    'With Worksheets(this_file).Range(current_anode_count)

```

```

For Each cc In Worksheets(this_file).Range("b11:b" & anodecount + 11)

```

```

    If cc.Value <> 0 Then

```

```

        If Int(cc.Value) - Int(c.row) = 0 And Int(cc.Offset(0, 1).Value) - c.column = 0 Then

```

```

            Worksheets(this_file).Cells(cc.row, column + 7) = c.Value

```

```

            cc.Offset(0, 3) = Int(c.row)

```

```

            cc.Offset(0, 4) = Int(c.column)

```

```

            Worksheets(this_file).Cells(anodecount + 11, 7).Formula = "=address(b" & anodecount
+ 11 & ", c" & anodecount + 11 & ")"

```

```

            With Worksheets(this_file).Cells(cc.row, column + 7).Interior

```

```

                .ColorIndex = 6

```

```

                .Pattern = xlSolid

```

```

            End With

```

```

            anode_done = 1

```

```

        End If

```

```

If Int(cc.Value) - Int(c.row) = 0 And Abs(Int(cc.Offset(0, 1).Value) - c.column) = 1 Then

```

```

    Worksheets(this_file).Cells(cc.row, column + 7) = c.Value

```

```

    With Worksheets(this_file).Cells(cc.row, column + 7).Interior

```

```

        .ColorIndex = 6

```

```

        .Pattern = xlSolid

```

```

    End With

```

```

    cc.Offset(0, 3) = Int(c.row)

```

```

    cc.Offset(0, 4) = Int(c.column)

```

```

    Worksheets(this_file).Cells(anodecount + 11, 7).Formula = "=address(b" & anodecount + 11 & ",
c" & anodecount + 11 & ")"

```

```

    anode_done = 1

```

```

End If

```

```

If Abs(Int(cc.Value) - Int(c.row)) = 1 And Int(cc.Offset(0, 1).Value) - c.column = 0 Then
    Worksheets(this_file).Cells(cc.row, column + 7) = c.Value
    With Worksheets(this_file).Cells(cc.row, column + 7).Interior
        .ColorIndex = 6
        .Pattern = xlSolid
    End With
    cc.Offset(0, 3) = Int(c.row)
    cc.Offset(0, 4) = Int(c.column)
    anode_done = 1
    Worksheets(this_file).Cells(anodecount + 11, 7).Formula = "=address(b" & anodecount + 11 & ",
c" & anodecount + 11 & ")"
End If

```

```

If Abs(Int(cc.Value) - Int(c.row)) = 1 And Abs(Int(cc.Offset(0, 1).Value) - c.column) = 1 Then
    Worksheets(this_file).Cells(cc.row, column + 7) = c.Value
    With Worksheets(this_file).Cells(cc.row, column + 7).Interior
        .ColorIndex = 6
        .Pattern = xlSolid
    End With
    cc.Offset(0, 3) = Int(c.row)
    cc.Offset(0, 4) = Int(c.column)
    Worksheets(this_file).Cells(anodecount + 11, 7).Formula = "=address(b" & anodecount + 11 & ",
c" & anodecount + 11 & ")"
    anode_done = 1
End If
'Else
End If

```

```

Next cc

'Next cc

If anode_done = 0 Then
    Worksheets(this_file).Cells(anodecount + 11, 1) = anodecount
    Worksheets(this_file).Cells(anodecount + 11, 2) = Abs(Int(c.row))
    Worksheets(this_file).Cells(anodecount + 11, 3) = Abs(Int(c.column))
    Worksheets(this_file).Cells(anodecount + 11, 4).Formula = "=address(b" & anodecount + 11 & ",
c" & anodecount + 11 & ")"

```

```

Worksheets(this_file).Cells(anodecount + 11, 5) = Abs(Int(c.row))
Worksheets(this_file).Cells(anodecount + 11, 6) = Abs(Int(c.column))
Worksheets(this_file).Cells(anodecount + 11, 7).Formula = "=address(b" & anodecount + 11 & ",
c" & anodecount + 11 & ")"
Worksheets(this_file).Cells(anodecount + 11, column + 7) = c.Value
With Worksheets(this_file).Cells(anodecount + 11, column + 7).Interior
    .ColorIndex = 6
    .Pattern = xlSolid
End With
anodecount = anodecount + 1
End If

'End If
'Next cc

'If Worksheets(this_file).Cells(i, 3) = "" Then
'Else: End If

'Else: End If
'Worksheets(this_file).Cells(i, column + 3) = c.Value
i = i + 1
    Else
        i = i + 1
    End If

Next c

End If
column = column + 1
Next s
Worksheets(this_file).Activate
Cells.Select
Cells.EntireColumn.AutoFit
Cells.Select
    Selection.Copy
Cells.Select
    Selection.PasteSpecial Paste:=xlPasteValues, Operation:=xlNone, SkipBlanks _
:=False, Transpose:=False

```

```

Selection.Replace What:="$", Replacement:"", LookAt:=xlPart, _
    SearchOrder:=xlByRows, MatchCase:=False, SearchFormat:=False, _
    ReplaceFormat:=False
For Each c In Worksheets(this_file).Range("a10:dt20000")
Next c
' old sort by anode no. bit
    Rows("11:6557").Select
Selection.Sort Key1:=Range("A10"), Order1:=xlAscending, Key2:=Range("B10" _
    ), Order2:=xlAscending, Header:=xlGuess, OrderCustom:=1, MatchCase:= _
    False, Orientation:=xlTopToBottom, dataoption1:=xlSortNormal, DataOption2 _
    :=xlSortNormal

' end of sort by location bit
Dim my_residuals As Variant
anodecount = anodecount + 9
    Range("g11").Select

ActiveCell.FormulaR1C1 = "=if(rc[-2]<>0, ADDRESS(RC[-2],RC[-1]))"
'Range("D11").Select
my_residuals = "g11:g" & anodecount
Selection.AutoFill Destination:=Range(my_residuals)
'Range(my_residuals).Select

    Columns("b:c").Select
    Selection.NumberFormat = "0"
    Columns("e:f").Select
    Selection.NumberFormat = "0"
Columns("d:d").Select
Selection.Copy
Selection.PasteSpecial Paste:=xlPasteValues, Operation:=xlNone, SkipBlanks _
    :=False, Transpose:=False
Selection.Replace What:="$", Replacement:"", LookAt:=xlPart, _
    SearchOrder:=xlByRows, MatchCase:=False, SearchFormat:=False, _
    ReplaceFormat:=False
Columns("g:g").Select

```



```

Selection.Copy

Selection.PasteSpecial Paste:=xlPasteValues, Operation:=xlNone, SkipBlanks _
    :=False, Transpose:=False

Selection.Replace What:="$", Replacement:"", LookAt:=xlPart, _
    SearchOrder:=xlByRows, MatchCase:=False, SearchFormat:=False, _
    ReplaceFormat:=False

Columns("b:b").Select

Selection.ColumnWidth = 13

Dim final_info As Range

my_residuals = "h11:af" & anodecount

For Each final_info In Worksheets(this_file).Range(my_residuals)

    If final_info.Value = "" And Worksheets(this_file).Cells(final_info.row, 4).Value =
Worksheets(this_file).Cells(final_info.row, 7).Value Then

        final_info.Formula = "=" & Worksheets(this_file).Cells(10, final_info.column).Value & "!" &
Worksheets(this_file).Cells(final_info.row, 7).Value

    End If

    If final_info.Value = "" And Worksheets(this_file).Cells(final_info.row, 4).Value <>
Worksheets(this_file).Cells(final_info.row, 7).Value Then

        If final_info.column <= 20 Then

            final_info.Formula = "=" & Worksheets(this_file).Cells(10, final_info.column).Value & "!"
& Worksheets(this_file).Cells(final_info.row, 4).Value

        Else: final_info.Formula = "=" & Worksheets(this_file).Cells(10, final_info.column).Value &
"!" & Worksheets(this_file).Cells(final_info.row, 7).Value

        End If

    End If

End If

Next final_info

Columns("B:C").Select

Selection.EntireColumn.Hidden = True

Columns("E:F").Select

Selection.EntireColumn.Hidden = True

Worksheets(this_file).Range(my_residuals).Select

Selection.Copy

Selection.PasteSpecial Paste:=xlPasteValues, Operation:=xlNone, SkipBlanks _
    :=False, Transpose:=False

For Each final_info In Worksheets(this_file).Range(my_residuals)

    If final_info.Value < 0 Then

```

```

    final_info.Value = 0
End If
Next final_info

Worksheets(this_file).Rows("11:" & anodecount).Select
Selection.Sort Key1:=Range("A10"), Order1:=xlAscending, Order2:=xlAscending, Header:=xlGuess,
OrderCustom:=1, MatchCase:= _
    False, Orientation:=xlTopToBottom, dataoption1:=xlSortNormal, DataOption2 _
    :=xlSortNormal
Range(my_residuals).Select
Charts.Add
ActiveChart.ChartType = xl3DLine
ActiveChart.Name = "Residuals Graph"
ActiveChart.SetSourceData Source:=Sheets(this_file).Range(my_residuals) _
    , PlotBy:=xlRows
ActiveChart.Location Where:=xlLocationAsNewSheet
With ActiveChart
    .HasTitle = True
    .ChartTitle.Characters.Text = "Residuals Graph"
    .Axes(xlCategory).HasTitle = False
    .Axes(xlSeries).HasTitle = False
    .Axes(xlValue).HasTitle = False
End With

End Sub

```

## Residual Anodes Microsoft 2003 Version 100 Scans

Option Explicit

```
Sub import_files_into_workbook()  
,  
' import_file_into_workbook Macro  
,  
  
Dim myfile As String  
Dim mypath As String  
Dim this_file As String  
Dim target_file As String  
Dim f As Integer  
Dim scan_data As Variant  
  
this_file = ActiveSheet.Name  
mypath = ActiveWorkbook.Path & "\"  
  
For f = 1 To 100  
    If f <= 10 Then  
        myfile = "text;" & mypath & this_file & "00" & (f - 1) & "calib.grd"  
        target_file = this_file & "00" & (f - 1) & "calib"  
    End If  
  
    If f > 10 And f <> 100 Then  
        myfile = "text;" & mypath & this_file & "0" & (f - 1) & "calib.grd"  
        target_file = this_file & "0" & (f - 1) & "calib"  
    End If  
  
    If f = 100 Then  
        myfile = "text;" & mypath & this_file & "100" & "calib.grd"  
        target_file = this_file & "100" & "calib"  
    End If  
  
,  
  
ActiveWorkbook.Worksheets.Add  
  
With ActiveSheet.QueryTables.Add(Connection:= _  
    myfile _  
    , Destination:=Range("$B$1"))  
    .Name = target_file  
    .FieldNames = True  
    .RowNumbers = False
```

```

.FillAdjacentFormulas = False

.PreserveFormatting = True

.RefreshOnFileOpen = False

.RefreshStyle = xlInsertDeleteCells

.SavePassword = False

.SaveData = True

.AdjustColumnWidth = True

.RefreshPeriod = 0

.TextFilePromptOnRefresh = False

.TextFilePlatform = 850

.TextFileStartRow = 1

.TextFileParseType = xlDelimited

.TextFileTextQualifier = xlTextQualifierDoubleQuote

.TextFileConsecutiveDelimiter = True

.TextFileTabDelimiter = False

.TextFileSemicolonDelimiter = False

.TextFileCommaDelimiter = False

.TextFileSpaceDelimiter = True

.TextFileColumnDataTypes = Array(1, 1)

.TextFileTrailingMinusNumbers = True

.Refresh BackgroundQuery:=False

End With

Sheets.Select

Sheets(f).Move after:=Sheets(f + 1)

'Columns("b:b").Select

Selection.Insert Shift:=xlToRight, CopyOrigin:=xlFormatFromLeftOrAbove

ActiveSheet.Name = target_file

'select range of cells

'If f = 1 Then

'Set scan_data = Application.InputBox("Please select cell range", "Cell Range Selection",
"B6:AT91", , , , 8)

'last_cell = Range.Find(8, "b6")

'End If

Next f

Dim c As Range

Dim i As Long

```

```

Dim shtcnt As Long

Dim column As Integer

Dim s As Variant

Dim anodecount As Integer

column = 0

anodecount = 1

Dim threshold_value As Single

Dim current_anode As Integer

Dim anode_done As Integer

If MsgBox("Residuals threshold value set to 1. Do you want to change this?", vbYesNo +
vbDefaultButton2, "Threshold Value OK?") = vbYes Then

    threshold_value = Application.InputBox("Please input new threshold value", "Threshold Value
Input", 1, , , , 1)

Else: threshold_value = 1

End If

For Each s In ActiveWorkbook.Sheets

Dim current_anode_range As Range

Dim current_anode_location As String

Dim cc As Range

        Worksheets(this_file).Cells(10, 1) = "Anode Number"

        Worksheets(this_file).Cells(10, 2) = "Initial Row"

        Worksheets(this_file).Cells(10, 3) = "Initial Column"

        Worksheets(this_file).Cells(10, 4) = "Initial Location"

        Worksheets(this_file).Cells(10, 5) = "Final Row"

        Worksheets(this_file).Cells(10, 6) = "Final Column"

        Worksheets(this_file).Cells(10, 7) = "Final Location"

s.Activate

'If column = 1 Then

'
'    scan_data = Application.InputBox("Please select cell range", "Cell Range Selection",
"B6:AT91", , , , 8)

'End If

If s.Name <> this_file Then

i = 10

        Worksheets(this_file).Cells(i, column + 7) = ActiveSheet.Name

        i = i + 1

' change the first value in the line below "c.value > 1". this will select threshold values of
whatever amps you require.

```

```

For Each c In Worksheets(s.Name).Range("b6:bz200")

    If c.Value > threshold_value And c.Value > c.Offset(-1, -1).Value And c.Value > c.Offset(-
1, 0).Value And c.Value > c.Offset(-1, 1).Value And c.Value > c.Offset(0, -1).Value And c.Value >
c.Offset(0, 1).Value And c.Value > c.Offset(1, -1).Value And c.Value > c.Offset(1, 0).Value And c.Value
>= c.Offset(1, 1).Value Then

        anode_done = 0

        With c.Interior

            .ColorIndex = 6

            .Pattern = xlSolid

        End With

        'current_anode_range = "c11:c" & anodecount

        'With Worksheets(this_file).Range(current_anode_count)

        For Each cc In Worksheets(this_file).Range("b11:b" & anodecount + 11)

            If cc.Value <> 0 Then

                If Int(cc.Value) - Int(c.row) = 0 And Int(cc.Offset(0, 1).Value) - c.column = 0

Then

                    Worksheets(this_file).Cells(cc.row, column + 7) = c.Value

                    cc.Offset(0, 3) = Int(c.row)

                    cc.Offset(0, 4) = Int(c.column)

                    Worksheets(this_file).Cells(anodecount + 11, 7).Formula = "=address(b" &
anodecount + 11 & ", c" & anodecount + 11 & ")"

                    With Worksheets(this_file).Cells(cc.row, column + 7).Interior

                        .ColorIndex = 6

                        .Pattern = xlSolid

                    End With

                    anode_done = 1

                End If

                If Int(cc.Value) - Int(c.row) = 0 And Abs(Int(cc.Offset(0, 1).Value) -
c.column) = 1 Then

                    Worksheets(this_file).Cells(cc.row, column + 7) = c.Value

                    With Worksheets(this_file).Cells(cc.row, column + 7).Interior

                        .ColorIndex = 6

                        .Pattern = xlSolid

                    End With

                    cc.Offset(0, 3) = Int(c.row)

                    cc.Offset(0, 4) = Int(c.column)

                    Worksheets(this_file).Cells(anodecount + 11, 7).Formula = "=address(b" &
anodecount + 11 & ", c" & anodecount + 11 & ")"

```

```

        anode_done = 1
    End If
    If Abs(Int(cc.Value) - Int(c.row)) = 1 And Int(cc.Offset(0, 1).Value) -
c..column = 0 Then
        Worksheets(this_file).Cells(cc.row, column + 7) = c.Value
        With Worksheets(this_file).Cells(cc.row, column + 7).Interior
            .ColorIndex = 6
            .Pattern = xlSolid
        End With
        cc.Offset(0, 3) = Int(c.row)
        cc.Offset(0, 4) = Int(c.column)
        anode_done = 1
        Worksheets(this_file).Cells(anodecount + 11, 7).Formula = "=address(b" &
anodecount + 11 & ", c" & anodecount + 11 & ")"
    End If
    If Abs(Int(cc.Value) - Int(c.row)) = 1 And Abs(Int(cc.Offset(0, 1).Value) -
c..column) = 1 Then
        Worksheets(this_file).Cells(cc.row, column + 7) = c.Value
        With Worksheets(this_file).Cells(cc.row, column + 7).Interior
            .ColorIndex = 6
            .Pattern = xlSolid
        End With
        cc.Offset(0, 3) = Int(c.row)
        cc.Offset(0, 4) = Int(c.column)
        Worksheets(this_file).Cells(anodecount + 11, 7).Formula = "=address(b" &
anodecount + 11 & ", c" & anodecount + 11 & ")"
        anode_done = 1
    End If
    'Else
    End If

Next cc

'Next cc

If anode_done = 0 Then
    Worksheets(this_file).Cells(anodecount + 11, 1) = anodecount
    Worksheets(this_file).Cells(anodecount + 11, 2) = Abs(Int(c.row))
    Worksheets(this_file).Cells(anodecount + 11, 3) = Abs(Int(c.column))

```

```

        Worksheets(this_file).Cells(anodecount + 11, 4).Formula = "=address(b" &
anodecount + 11 & ", c" & anodecount + 11 & ")"

        Worksheets(this_file).Cells(anodecount + 11, 5) = Abs(Int(c.row))

        Worksheets(this_file).Cells(anodecount + 11, 6) = Abs(Int(c.column))

        Worksheets(this_file).Cells(anodecount + 11, 7).Formula = "=address(b" &
anodecount + 11 & ", c" & anodecount + 11 & ")"

        Worksheets(this_file).Cells(anodecount + 11, column + 7) = c.Value

                With Worksheets(this_file).Cells(anodecount + 11, column + 7).Interior

.ColorIndex = 6

.Pattern = xlSolid

                End With

        anodecount = anodecount + 1

    End If

'End If

'Next cc

        'If Worksheets(this_file).Cells(i, 3) = "" Then

        'Else: End If

'Else: End If

        'Worksheets(this_file).Cells(i, column + 3) = c.Value

        i = i + 1

Else

        i = i + 1

End If

Next c

End If

column = column + 1

Next s

Worksheets(this_file).Activate

Cells.Select

Cells.EntireColumn.AutoFit

Cells.Select

Selection.Copy

Cells.Select

Selection.PasteSpecial Paste:=xlPasteValues, Operation:=xlNone, SkipBlanks _

```



```

:=False, Transpose:=False
Selection.Replace What:="$", Replacement:"", LookAt:=xlPart, _
    SearchOrder:=xlByRows, MatchCase:=False, SearchFormat:=False, _
    ReplaceFormat:=False
For Each c In Worksheets(this_file).Range("a10:dt20000")
Next c
' old sort by anode no. bit
Rows("11:6557").Select
Selection.Sort Key1:=Range("A10"), Order1:=xlAscending, Key2:=Range("B10" _
    ), Order2:=xlAscending, Header:=xlGuess, OrderCustom:=1, MatchCase:= _
    False, Orientation:=xlTopToBottom, dataoption1:=xlSortNormal, DataOption2 _
    :=xlSortNormal

' end of sort by location bit
Dim my_residuals As Variant
anodecount = anodecount + 9
Range("g11").Select

ActiveCell.FormulaR1C1 = "=if(rc[-2]<>0, ADDRESS(RC[-2],RC[-1]))"
'Range("D11").Select
my_residuals = "g11:g" & anodecount
Selection.AutoFill Destination:=Range(my_residuals)
'Range(my_residuals).Select

Columns("b:c").Select
Selection.NumberFormat = "0"
Columns("e:f").Select
Selection.NumberFormat = "0"
Columns("d:d").Select
Selection.Copy
Selection.PasteSpecial Paste:=xlPasteValues, Operation:=xlNone, SkipBlanks _
    :=False, Transpose:=False
Selection.Replace What:="$", Replacement:"", LookAt:=xlPart, _
    SearchOrder:=xlByRows, MatchCase:=False, SearchFormat:=False, _
    ReplaceFormat:=False

```

```

Columns("g:g").Select
Selection.Copy
Selection.PasteSpecial Paste:=xlPasteValues, Operation:=xlNone, SkipBlanks _
:=False, Transpose:=False
Selection.Replace What:="$", Replacement:="", LookAt:=xlPart, _
SearchOrder:=xlByRows, MatchCase:=False, SearchFormat:=False, _
ReplaceFormat:=False
Columns("b:b").Select
Selection.ColumnWidth = 13

Dim final_info As Range
my_residuals = "h11:dc" & anodecount

For Each final_info In Worksheets(this_file).Range(my_residuals)

If final_info.Value = "" And Worksheets(this_file).Cells(final_info.row, 4).Value =
Worksheets(this_file).Cells(final_info.row, 7).Value Then

final_info.Formula = "=" & Worksheets(this_file).Cells(10, final_info.column).Value & "!" &
Worksheets(this_file).Cells(final_info.row, 7).Value

End If

If final_info.Value = "" And Worksheets(this_file).Cells(final_info.row, 4).Value <>
Worksheets(this_file).Cells(final_info.row, 7).Value Then

If final_info.column <= 20 Then

final_info.Formula = "=" & Worksheets(this_file).Cells(10, final_info.column).Value & "!"
& Worksheets(this_file).Cells(final_info.row, 4).Value

Else: final_info.Formula = "=" & Worksheets(this_file).Cells(10, final_info.column).Value &
"!" & Worksheets(this_file).Cells(final_info.row, 7).Value

End If

End If

Next final_info

Columns("B:C").Select
Selection.EntireColumn.Hidden = True

Columns("E:F").Select
Selection.EntireColumn.Hidden = True

Worksheets(this_file).Range(my_residuals).Select
Selection.Copy

Selection.PasteSpecial Paste:=xlPasteValues, Operation:=xlNone, SkipBlanks _
:=False, Transpose:=False

For Each final_info In Worksheets(this_file).Range(my_residuals)

```

```

If final_info.Value < 0 Then
    final_info.Value = 0
End If
Next final_info

Worksheets(this_file).Rows("11:" & anodecount).Select

Selection.Sort Key1:=Range("A10"), Order1:=xlAscending, Order2:=xlAscending, Header:=xlGuess,
OrderCustom:=1, MatchCase:= _
    False, Orientation:=xlTopToBottom, dataoption1:=xlSortNormal, DataOption2 _
    :=xlSortNormal

Range(my_residuals).Select

Charts.Add

ActiveChart.ChartType = xl3DLine

ActiveChart.Name = "Residuals Graph"

ActiveChart.SetSourceData Source:=Sheets(this_file).Range(my_residuals) _
    , PlotBy:=xlRows

ActiveChart.Location Where:=xlLocationAsNewSheet

With ActiveChart
    .HasTitle = True

    .ChartTitle.Characters.Text = "Residuals Graph"

    .Axes(xlCategory).HasTitle = False

    .Axes(xlSeries).HasTitle = False

    .Axes(xlValue).HasTitle = False
End With

End Sub

```